University of Kentucky

UKnowledge

Theses and Dissertations--Physiology   Physiology

2014

TRPA1 CHANNELS IN COCHLEAR SUPPORTING CELLS REGULATE HEARING SENSITIVITY AFTER NOISE EXPOSURE

Alejandra C. Velez-Ortega
University of Kentucky, bmalvel@yahoo.com

Right click to open a feedback form in a new tab to let us know how this document benefits you.

TRPA1 CHANNELS IN COCHLEAR SUPPORTING CELLS
REGULATE HEARING SENSITIVITY AFTER NOISE EXPOSURE

_____

DISSERTATION

_____

A dissertation submitted in partial fulfillment of the
requirements for the degree of Doctor of Philosophy in the
College of Medicine at the University of Kentucky

By
Alejandra Catalina Vélez-Ortega
Lexington, Kentucky

Director: Dr. Gregory I. Frolenkov, Associate Professor of Physiology

Lexington, Kentucky
2014

ABSTRACT

TRPA1 CHANNELS IN COCHLEAR SUPPORTING CELLS
REGULATE HEARING SENSITIVITY AFTER NOISE EXPOSURE

TRPA1 channels are sensors for noxious stimuli in a subset of nociceptive neurons. TRPA1 channels are also expressed in cells of the mammalian inner ear, but their function in this tissue remains unknown given that $Trpa1^{-/-}$ mice exhibit normal hearing, balance and sensory mechanotransduction. Here we show that non-sensory (supporting) cells of the hearing organ in the cochlea detect tissue damage via the activation of TRPA1 channels and subsequently modulate cochlear amplification through active cell-shape changes.

We found that cochlear supporting cells of wild type but not $Trpa1^{-/-}$ mice generate inward currents and robust long-lasting Ca^{2+} responses after stimulation with TRPA1 agonists. These Ca^{2+} responses often propagated between different types of supporting cells and were accompanied by prominent tissue displacements. The most prominent shape changes were observed in pillar cells which here we show possess Ca^{2+}-dependent contractile machinery. Increased oxidative stress following acoustic overstimulation leads to the generation of lipid peroxidation byproducts such as 4-hydroxynonenal (4-HNE) that could directly activate TRPA1. Therefore, we exposed mice to mild noise and found a longer-lasting inhibition of cochlear amplification in wild type than in $Trpa1^{-/-}$ mice.

Our results suggest that TRPA1-dependent changes in pillar cell shape can alter the tissue geometry and affect cochlear amplification. We believe this novel mechanism of cochlear regulation may protect or fine-tune the organ of Corti after noise exposure or other cochlear injuries.

KEYWORDS: Transient receptor potential A1 channel, cochlear supporting cells, reactive oxygen species, cochlear amplification, 4-hydroxynonenal

Alejandra Catalina Vélez-Ortega
Student's Signature

December 10, 2014
Date

TRPA1 CHANNELS IN COCHLEAR SUPPORTING CELLS
REGULATE HEARING SENSITIVITY AFTER NOISE EXPOSURE

By

Alejandra Catalina Vélez-Ortega

Dr. Gregory I. Frolenkov
Director of Dissertation

Dr. Bret N. Smith
Director of Graduate Studies

December 10, 2014
Date

To my father,

whose creativity kept my curiosity from fading

(a curiosity that now fuels a career in research).

PREFACE AND ACKNOWLEDGEMENTS

Almost 10 years ago, in a course for advanced English writing, I was asked to write an essay about the perfect career pattern for myself. I wrote about my passion for research and my desire to return to school to obtain a graduate degree. Now that I see 'the light at the end of the PhD tunnel', I am glad that I still feel the same level of passion and curiosity I felt 10 years ago. This further confirms my desire to pursue a career in research. Interestingly, back then I was absolutely convinced that "…*it (was) not part of my (career) scheme to create my own research group*". I did not feel I was creative enough or that I had the critical thinking required to develop my own research ideas. So, I went on and obtained a Master's degree and subsequently joined a PhD program, all while thinking that a career in academia was not the option for me.

I thank my advisor, Dr. Gregory I. Frolenkov, for his guidance throughout the development and execution of this research project. At occasions, my curiosity led me off track, but he always brought me back by providing a clear distinction between the main experiments that were required to test our hypothesis vs. the additional experiments that only provided extra support (or, as he called them, the 'icing on the cake'). Gregory often made me think like an independent investigator. For instance, he allowed me set up the imaging/electrophysiological system that was used for most experiments presented here. For about three months, I read countless manuals, made dozens of cable connections, calibrated and tested individual components, and configured the system's software. Gregory knew that by allowing me to do this I would be able to easily troubleshoot "technical problems" encountered during the experiments. Additionally, I knew the full capabilities of the system and therefore was able to plan experiments to take full advantage of them. This process indeed facilitated the standardization phase of new experiments. But most importantly, as Gregory knew and eventually told me, those 3

to apply to a PhD program in the University of Kentucky. Francesc is also one of the kindest people I have ever met and my time in his laboratory was incredibly enjoyable.

To my friends, far too many to mention individually (for which I am grateful for), I am thankful for the words of encouragement throughout this PhD process, the laughter shared over coffee dates, the long nights dancing, the expeditions and trips together, the willingness to lend an ear and serve as my pressure release valves, the early morning rides to the airport, the welcoming smile after a long work day, the delicious cakes, cupcakes, desserts and little doughnuts, the tolerance and support during my craziness over world-cup season, and the silly science-related jokes. All of you have made the past few years quite an interesting ride.

I am grateful to have the support from my family, both the family related through blood and the families through love and close friendships. My parents, brother and aunts in Colombia and my world traveler sister have given me nothing but freedom and encouragement after my decision to move to a different country to pursue a lifestyle of long working hours. I thank my host parents here in Lexington for their unconditional love and fun gatherings; and thank my in-laws in South Carolina for always welcoming me with warm hugs and the biggest smiles every time I visit them.

Lastly, I would like to thank my sweet and loving husband, Phillip Chase Hawkins. Chase brought a new meaning to music in my life. At times, Chase seems to know me better than I know myself. Without him by my side, this process would have been infinite times more stressful.

TABLE OF CONTENTS

LIST OF TABLES

LIST OF FIGURES

CHAPTER 1

An introduction to cochlear cell morphology and function

1.1 Overview of mammalian hearing

Air pressure sound waves that reach the *pinna* of the outer ear (a cartilaginous structure that protrudes on the side of the head) are reflected into the *ear canal* and toward the *tympanic membrane* (colloquially known as the *ear drum*) (Figure 1.1). When the tympanic membrane vibrates, it causes the movement of the chain of three small bones in the middle ear, known as *ossicles*. The ossicles are in charge of transmitting vibrations from the tympanic membrane to the *oval window* at the base of the cochlea in the inner ear. The oval window is significantly smaller than the tympanic membrane, resulting in a necessary large increase in force –given that the sound pressure waves now need to travel in a fluid-filled environment.

Sound waves reach the coiled cochlea and cause the vibration of the sensory epithelium contained within. This sensory epithelium rests on the *basilar membrane*, a membrane that gradually decreases in stiffness, but increases in size, from the base to the apex of the cochlea [1, 2]. Sound-induced vibrations of the sensory epithelium initiate traveling waves that resonate at specific regions of the basilar membrane depending on their frequency, with high frequencies toward the base and low frequencies toward the apex of the cochlea. And, as explained in greater detail in section 1.4, there are cells within the cochlear sensory epithelium that can transduce such tonotopically-arranged vibrations into neurotransmitter release and excitation of cochlear nerve afferent neurons.
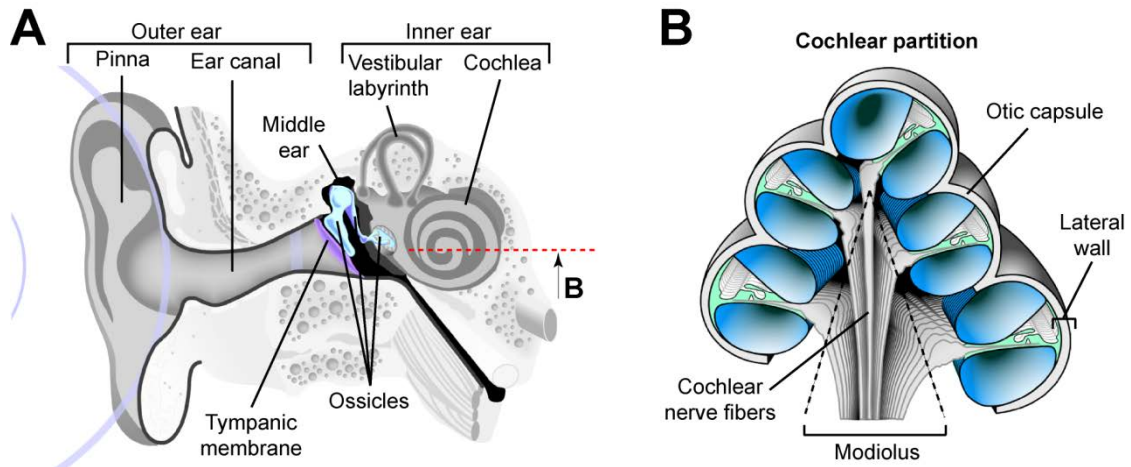
Figure 1.1†. Overview of the human ear

Modified from reference [3]. *A*, Diagram showing the main structures of the external, middle and inner ear with sound vibrations traveling through the ear canal. *B*, Cross-section of the cochlea (from a perpendicular plane positioned at the red dashed line in *A*) through the cochlear modiolus.

1.2 The cochlea

The bony structure in the middle of the cochlea, known as the *modiolus*, has a conical shape and it is filled with cell bodies and axons from cochlear nerve neurons. In a cochlear cross section, the modiolus constitutes the *medial* part of the cochlea while the outer shell localized to both sides is referred to as the *lateral wall* (Figure 1.1). The outermost layer of the lateral wall is the *otic capsule* made up of bone. The basilar membrane spans from the modiolus to the lateral wall, and its sites of insertion at each end are known as the *spiral limbus* (medial) and *spiral prominence* (lateral) (Figure 1.2). The spiral prominence spans the inner side of the otic capsule on the lateral wall. Several types of sensory and supporting cells rest on the basilar membrane, and they will be discussed in detail in sections 1.4 and 1.6.

A cross-section of the cochlea reveals the presence of three distinct compartments: *scala vestibuli*, *scala media* and *scala tympani* (Figure 1.2).

---

† All drawings and data figures in this dissertation are my original artwork and experimental results, unless otherwise stated.
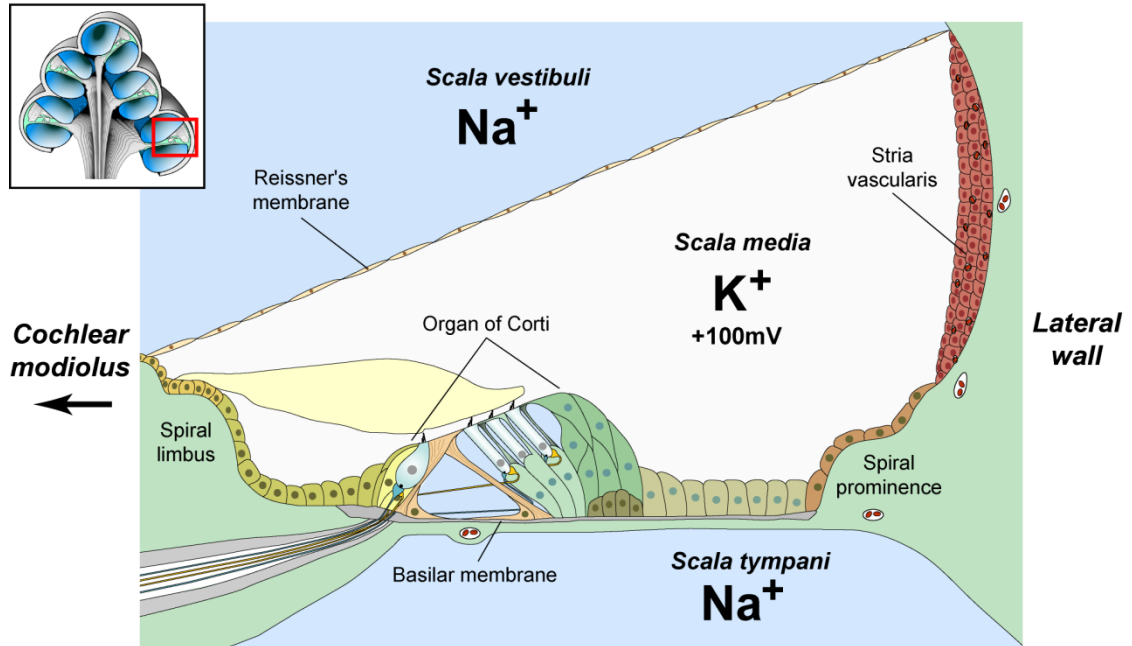
Figure 1.2. Diagram showing the three fluid compartments found in the mammalian cochlea

A small region in a cochlear partition (indicated by the red box in the *inset*) is shown at greater magnification. The scalae vestibuli and tympani are rich in Na^+ while the scala media is filled with an unusual extracellular fluid high in K^+ and a high extracellular potential. Labels pointing to the positions of the lateral wall and modiolus are shown as reference.

The scalae vestibuli and tympani contain *perilymph*, a Na^+-rich solution similar to the cerebrospinal fluid. In contrast, the scala media contains a K^+-rich solution that has an electric potential of about +80 to +120 mV (Figure 1.2) [1, 4]. The scalae media and vestibuli are separated by a thin epithelial layer known as the *Reissner's membrane*. Similarly, the sensory and supporting cells located above the basilar membrane are connected with tight junctions at their apical side and form a barrier known as the *reticular lamina*, which keeps the endolymph in the scala media separate from the perilymph in the scala tympani.

The *stria vascularis*, which rests on the spiral prominence and constitutes the inner layer of the lateral wall (Figure 1.2), is a highly vascularized tissue that contains three

layers of specialized epithelial cells in charge of pumping K+ ions into the endolymph to establish the positive extracellular potential.

1.3 The cochlear sensory epithelium

Several types of sensory and supporting cells compose the epithelium located over the basilar membrane (Figure 1.3). The sensory *hair cells* and the supporting cells in close proximity are known as the *organ of Corti* (Figure 1.2). A unique extracellular matrix structure, the *tectorial membrane*, extends from the medial region of the cochlea and covers the apical surface of the organ of Corti.

When sound vibrations cause the basilar membrane to move up and down, a shear force is produced between the hair cells and the tectorial membrane (Figure 1.4). This leads to the deflection of the mechanosensitive apparatus located on the surface of the hair cells (see section 1.4.1 for more details) [5, 6].
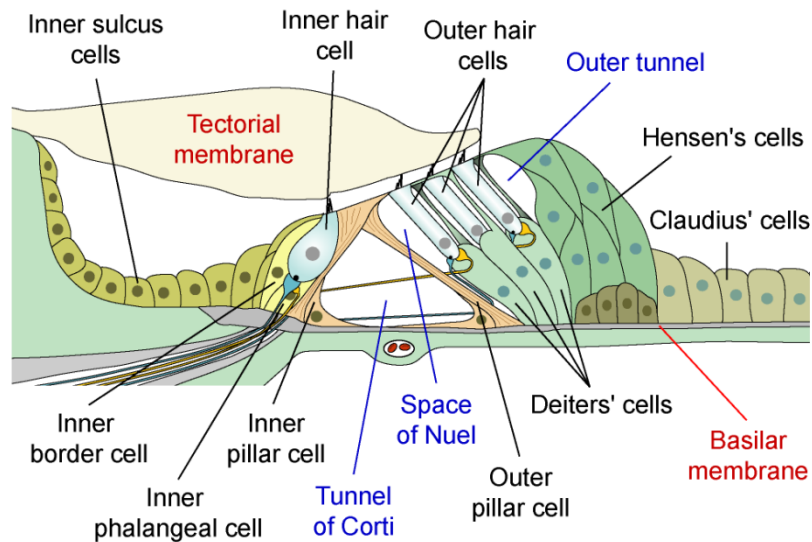
Figure 1.3. Diagram of the adult mammalian cochlear epithelium
Redrawn from reference [3]. Colored labels indicate the different types of sensory and supporting cells (black), extracellular membranes (red) and fluid-filled compartments (blue) present in the adult mammalian cochlear epithelium.

1.4 Cochlear sensory cells and mechano-electrical transduction

There are two types of sensory cells in the mammalian cochlea: *inner* and *outer hair cells*. They receive the name of *hair cells* due to the modified microvilli projections present on their apical surface, which have been inaccurately named as *stereocilia* (Figure 1.5). Hair cells are arranged in one row of inner hair cells (IHC) medially and three to four rows of outer hair cells (OHC) laterally (Figures 1.3 and 1.5A).

The stereocilia in the tallest row of OHC (but not IHC) are directly connected to the overlaying tectorial membrane and thus basilar membrane movements directly lead to OHC stereocilia bundle deflections (see inset in Figure 1.4B). In contrast, IHC stereocilia seem to get deflected by the fluid motion initiated with the basilar membrane vibrations.
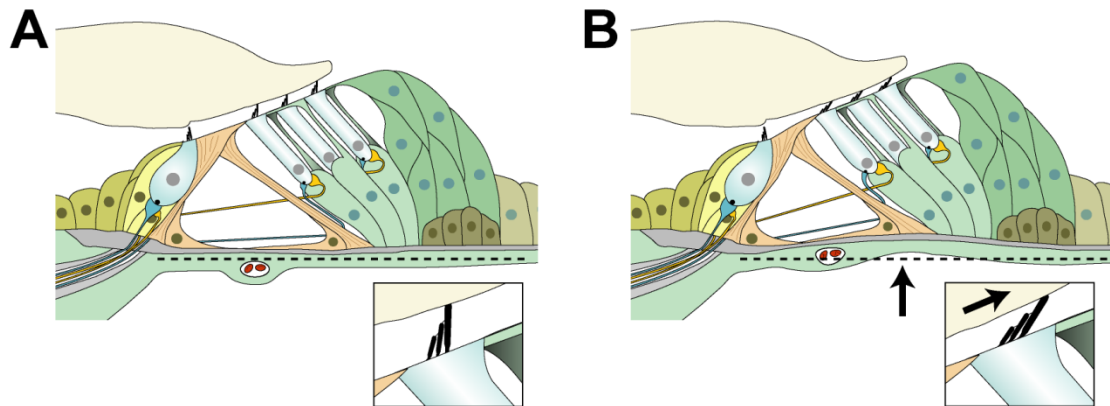
Figure 1.4. Diagram of hair cell stereocilia deflections induced by basilar membrane movements

A, Diagram of the organ of Corti at a resting position (*i.e.* without sound-induced basilar membrane vibrations). *B*, Sound stimulation leads to basilar membrane vibrations toward and away from the scala vestibuli, but only the phase of the upward movement is illustrated. The dashed line is placed as a reference of the basilar membrane position at rest. *Insets* illustrate the OHC bundle deflection that occurs during the basilar membrane movement.

1.4.1 Mechano-electrical transduction

Stereocilia bundles are highly organized actin-filled projections [7, 8]. IHC and OHC stereocilia are usually arranged in three rows, ordered by height in a staircase-like manner

(Figure 1.5B). Within a given bundle, stereocilia are connected by several types of links. In particular, links that connect the top of a stereocilium to the side of a taller stereocilium are known as *tip links* (Figure 1.5B inset). Tip links are formed by the interaction of a dimer (or perhaps a trimer) of cadherin-23 molecules on the top, and a dimer of protocadherin-15 molecules on the bottom (reviewed in [9]).
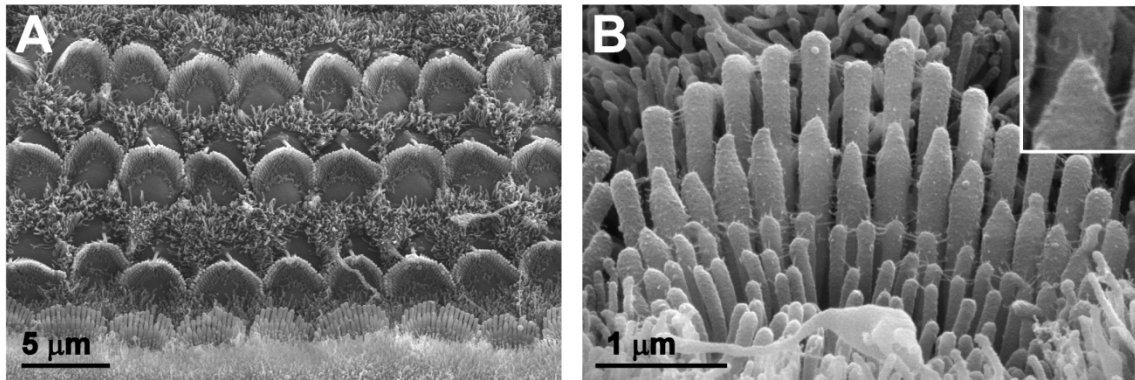
Figure 1.5. View of the apical surface of the organ of Corti
A, Scanning electron micrograph (SEM) showing the apical surface of a wild type organ of Corti dissected at postnatal day 4. The stereocilia bundles of the three rows of OHCs (top) and one row of IHCs (bottom) are visible. *B*, Higher magnification SEM picture of an IHC stereocilia bundle from the explant shown in *A*. Notice the staircase arrangement of the stereocilia rows and the presence of tip links (inset) and side links.

Stereocilia are rigid structures due to a core made up of actin filaments arranged in a paracristaline fashion [10]. Thus, bundle deflections do not bend stereocilia, but instead, cause them to pivot at their base (*taper* region) (Figure 1.6) [11]. This leads to a force build up at the tip link region and mechano-electrical transduction (MET) channel gating. MET channels are located on the top of shorter stereocilia [12], but their molecular identity is still under debate. Tip links are most likely unstretchable structures [13, 14], and it is unknown whether they pull directly on the MET channels or on the membrane nearby to induce their gating. Due to the negative intracellular potential of hair cells (about -50mV) and the large positive extracellular potential in the endolymph, opening of the non-selective cation MET channels produces a large K^+ and Ca^{2+} inward current that

leads to hair cell depolarization (Figure 1.6). Dedicated K^+ channels (KCNQ4 type) on the basolateral membrane mediate the efflux of the large amount of K+ ions that entered through the MET channels [15, 16]. Next, these K+ ions are presumably reabsorbed from the perilymph by neighboring supporting cells (see section 1.6).
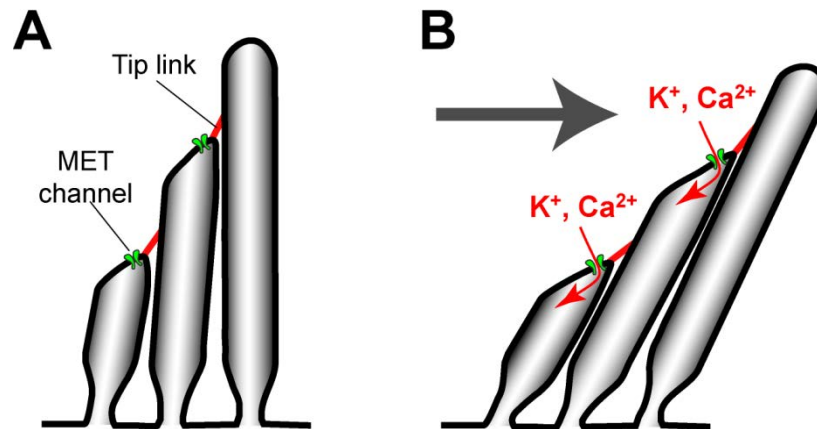
Figure 1.6. Diagram of stereocilia deflection and MET gating
A, Staircase arrangement of hair cell stereocilia at a resting position, where most MET channels are closed. *B*, Stereocilia bundle deflection leads to tension buildup at the tip links and MET gating, allowing the influx of K^+ and Ca^{2+} ions and subsequent hair cell depolarization.

1.4.2 Outer hair cells and cochlear amplification

Changes in the membrane potential of OHCs induce cell shape changes, termed *electromotility*, with depolarizations leading to cell contraction and repolarizations to cell elongation (Figures 1.7A and 1.7B) [17-19]. These changes in cell shape are driven by the protein *prestin*, which is expressed at a high density in the OHC plasma membrane [20, 21]. Prestin molecules exhibit a piezoelectric behavior, since they undergo conformational changes dependent on the membrane potential (reviewed in [22]). Because such piezoelectric action results in the movement of charges in the plasma membrane, changing the membrane potential of OHCs leads to apparent changes in membrane capacitance with a characteristic non-linear relationship (Figure 1.7C). Ultimately, the contractions and elongations of the OHCs, enhance the vibrations of the basilar membrane and thus OHCs act as active amplifiers within the cochlea.

1.4.3 Inner hair cells

IHCs have specialized structures, known as *synaptic ribbons*, where large quantities of neurotransmitter-filled vesicles accumulate (Figure 1.8) (reviewed in [23]). Upon stereocilia bundle deflection, IHCs depolarize and voltage-gated Ca^{2+} channels are activated. The Ca^{2+} influx at the base of the IHCs triggers the release of vesicle contents at the synapses with afferent cochlear nerve endings, with the major neurotransmitter released most likely being glutamate (reviewed in [24]). IHCs are capable of releasing contents from large quantities of vesicles [25] and, in addition, they can sustain vesicle release at high frequencies and for long periods of time [26].
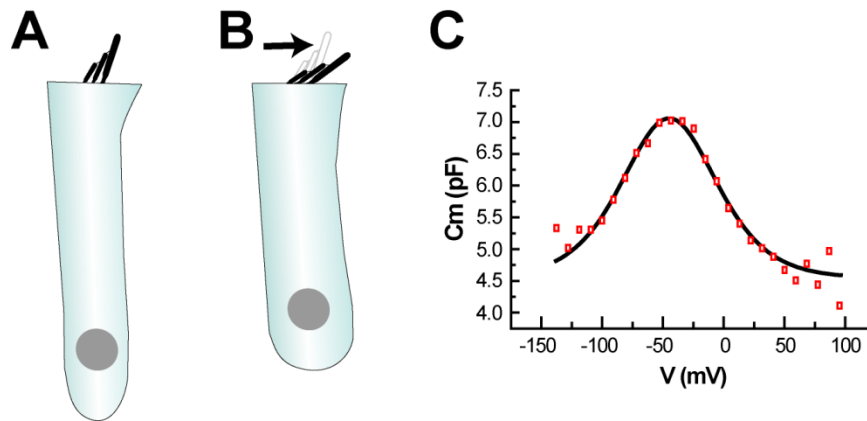
Figure 1.7. Diagram of OHC electromotility

A, Elongated OHC with the stereocilia bundle at a resting position. *B*, OHC contraction after the deflection of its hair bundle. *C*, Typical changes in OHC membrane capacitance (Cm) induced by changes in membrane potential (V). The red squares indicate actual data points obtained from a young postnatal OHC from a wild type mouse, while the black line corresponds to a double Boltzmann fit. The results shown in *C* were obtained by Dr. Ruben Stepanyan, a former member of the Frolenkov laboratory.

1.5 Cochlear innervation

In general, IHCs synapse with afferent neurons while OHCs receive efferent innervation (for a comprehensive review, see [24]). There are two types of *spiral ganglion cells* (SGC), the afferent fibers in the cochlear nerve. The majority of the SGCs

(90 – 95%) are type I large bipolar neurons that innervate IHCs (Figure 1.8A). Each type I SGC receives input from a single IHC, but each IHC synapses with nerve terminals from several type I SGC neurons. The rest of the SGCs (5 – 10%) are the type II pseudounipolar neurons. Each type II SGC neuron branches to innervate several OHCs (Figure 1.8B), sometimes from all three OHC rows [27]. The function of the type II SGC fibers has not been completely elucidated, but they are presumed to be activated in the presence of harmful noise exposure [28].
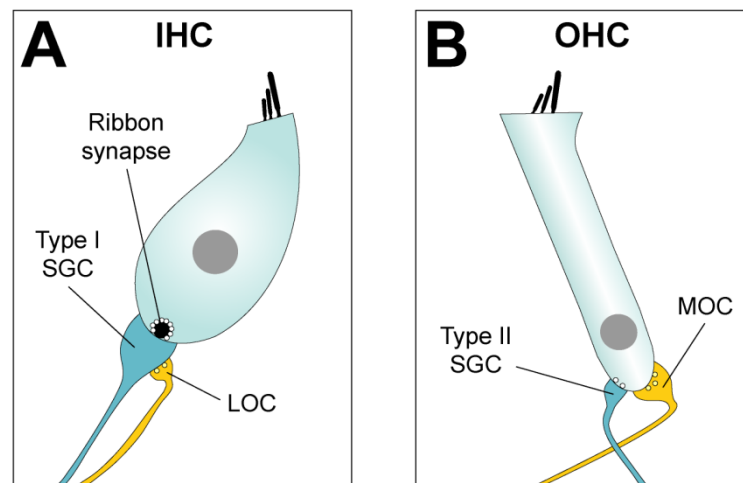
Figure 1.8. IHC and OHC innervation

A, B, Diagrams illustrating the afferent (blue) and efferent (yellow) innervation in IHCs (*A*) and OHCs (*B*). *SGC*, spiral ganglion cell; *LOC*, lateral olivocochlear terminal; *MOC*, medial olivocochlear terminal.

Two types of efferent fibers leave the brain stem and reach the cochlea: the lateral olivocochlear (LOC) and medial olivocochlear (MOC) fibers. LOC fibers innervate the ipsilateral cochlea while the majority of MOC fibers innervate the contralateral cochlea. LOC fibers form synapses with the terminals of the type I SGCs underneath the IHCs (Figure 1.8A) and, since they contain both excitatory (e.g., acetylcholine) and inhibitory (e.g., GABA) neurotransmitters, they presumably fine tune the sensitivity of the SGCs. Each MOC fiber directly innervates several OHCs (Figure 1.8B). The main neurotransmitter in MOC fibers is acetylcholine, which induces OHC hyperpolarization and changes in OHC electromotility. LOC and MOC fibers might provide a feedback

loop controlling hearing sensitivity and amplification to adapt to different sound levels or to protect during noise exposure.

Branches from type II SGCs and efferent fibers can also form synapses with the supporting cells near the OHCs (see sections 1.6.4 and 1.6.5 for more details) [27, 29-31]. The efferent fibers that contact supporting cells are believed to be of MOC origin, but this has yet to be fully determined. Moreover, the functional role of the afferent and efferent innervation of supporting cells remains largely unknown.

1.6 Cochlear supporting cells and fluid-filled compartments

There are several distinct types of supporting cells in the cochlea. They have been named and/or classified based on their morphology and location in relation to the hair cells (Figure 1.3). For more comprehensive reviews see [24, 32].

Supporting cells make up the complex architecture of the organ of Corti and provide physical support for the hair cells. In addition, supporting cells play an important role maintaining the ionic homeostasis of cochlear fluids. All supporting cells are electrochemically connected via gap junctions, with permeability profiles that vary generally between different cell types [33], most likely due to differences in connexin composition of the gap junctions [34]. This gap junctional network allows for the fast spread of small molecules between most supporting cells but limits the propagation of larger molecules. Notably, supporting cells reabsorb the K^+ ions that are released by hair cells into the perilymph after sound stimulation. Presumably, this gap junctional network allows the recycling of the K^+ ions back into the stria vascularis (reviewed in [35, 36]).

Supporting cells also play an important role after hair cell death due to acoustic overstimulation or ototoxic trauma. Supporting cells sense hair cell death via mechanisms that involve the release of ATP to the extracellular space. This generates robust Ca^{2+} waves that can travel throughout the cochlear epithelium [37, 38], but their biological significance still remains under study (see section 1.7 for more details). It is known, however, that some supporting cells can act as macrophages to engulf dying hair cells [39-42]. They can also help reseal the cochlear epithelium to maintain the barrier between different cochlear fluids intact [43-45].

10

1.6.1 Inner sulcus cells and the Kolliker's organ

In the adult mammalian cochlea, the inner sulcus (located medially to the IHCs) is covered by small cuboidal cells. Early in development, however, the inner sulcus is filled with large columnar cells which are collectively known as the *Kolliker's organ* and are in direct contact with the tectorial membrane (Figure 1.9) [46]. The cells of the Kolliker's organ are known to spontaneously release ATP to the extracellular space, which is believed to play an important role in the fine tuning of tonotopicity in cochlear neural pathways (see section 1.7 for more details). The Kolliker's organ gradually decreases in size over the first couple of weeks during postnatal development [46, 47]. While most cells of the Kolliker's organ are presumed to undergo apoptosis, it is still unknown whether some of them can transdifferentiate into the inner sulcus cells of the adult cochlea.
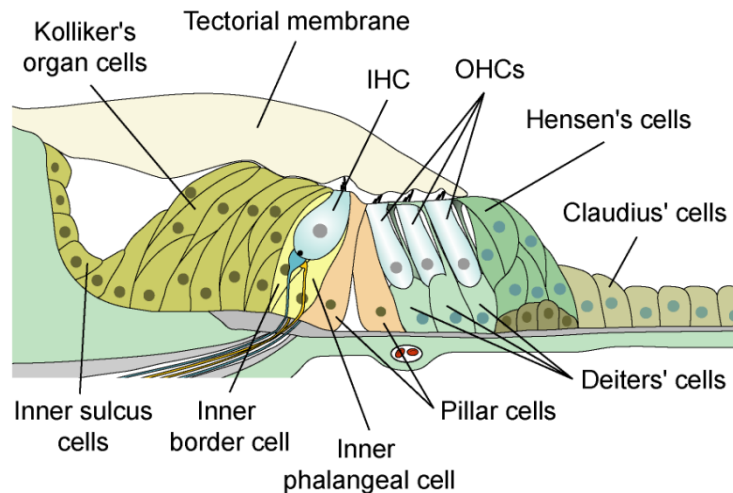
Figure 1.9. Diagram of the cochlear epithelium at an early postnatal age
Cochlear supporting cells are still changing their morphology during early postnatal days. At this developmental stage, the organ of Corti is still collapsed, and no flui-filled spaces are evident yet. In addition, the inner sulcus is filled by the Kolliker's organ.

1.6.2 Inner border and inner phalangeal cells

A thin row of inner border cells is located between the inner sulcus cells (or the cells of the Kolliker's organ) and the IHCs. Inner border cells do not reach all the way to the

reticular lamina and therefore are not in direct contact with the endolymph. A thin row of inner phalangeal cells is present between the IHCs and the inner pillar cells. Inner phalangeal cells provide support for the IHCs and extend small projections to the reticular lamina between adjacent IHCs. Inner border and inner phalangeal cells form an envelope around the base of IHCs, where nerve synapses are formed, and they express high levels of channels and transporters required for the uptake of K^+ ions and glutamate after IHC stimulation [48-51].

1.6.3 Pillar cells

Two rows of pillar cells are located between the rows of IHCs and OHCs. In the adult mammalian cochlea, inner and outer pillar cells separate at the base to create a triangular perilymph-filled space known as the *tunnel of Corti* (compare diagrams of the adult vs. early development cochleae in Figures 1.3 and 1.9, respectively) [52]. Pillar cells have a particular morphology with three distinct regions in each cell (reviewed in [32]). The *feet* of the pillar cells rest directly on the basilar membrane and are filled with actin filaments. The middle regions, also known as pillar *shafts*, are densely packed with arrangements of microtubules and actin filaments [53]. The *head plates* of inner and outer pillar cells are tightly joined together by desmosomes and adherens junctions, with the heads of outer pillar cells partially localized underneath those of inner pillar cells. In addition, each outer pillar head plate surrounds one OHC. Interestingly, the microtubules in these cells have 15 protofilaments (instead of the typical 13 protofilaments found in microtubules from other cell types) [54]. Large amounts of intermediate filaments are found in the feet of outer pillar cells, and lower amounts at the feet of inner pillar cells and head plates of both [55].

1.6.4 Deiters' cells

Three rows of Deiters' cells, also known as outer phalangeal cells, are located underneath of the OHCs and they extend small projections, termed *phalangeal processes*, from their cell body to the reticular lamina. The top region in each Deiters' cell body is shaped like a cup and forms a place where the base of an OHC can rest. The phalangeal process of a given Deiters' cell does not attach to the OHC directly above it, but to a

more apical (1 to 3 cells away) OHC instead. The cytoskeleton within the phalangeal processes of Deiters' cells resembles that of the pillar cell shafts because it contains arrangements of microtubules and actin filaments, but it also contains large amounts of intermediate filaments. These phalangeal processes have been shown to exhibit mechanical changes in isolated Deiters' cells upon stimulation with extracellular ATP [56] or through the uncaging of cytosolic Ca^{2+} [57]. Large amounts of intermediate filaments are also found at the top and bottom regions of the cell body [55].

OHC and Deiters' cell bodies are surrounded by perilymph. In particular, the area between the outer pillar cells and the first row of OHCs and Deiters' cells is known as the *space of Nuel* (Figure 1.3) [52]. Moreover, similarly to inner border and inner phalangeal cells, Deiters' cells express K^{+} channels and transporters needed for the recycling of K^{+} ions upon OHC stimulation [48-50]. Some Deiters' cells have also been reported to form synapses with thin branches from type II SGC fibers [27, 29, 30] and efferent fibers [31]. These synapses have been observed in the Deiters' phallangeal processes as well as in the cell bodies; and they seem to only be present in one half of the cochlear epithelium (apical half in guinea pig and basal half in the cat) [27, 58, 59].

1.6.5 Hensen's and Claudius' cells

Two to three rows of Hensen's cells are located laterally to the OHCs. The perilymph-filled space between the OHCs and the Hensen's cells is known as the *outer tunnel* (Figure 1.3) [52]. Hensen's cells are large columnar cells notorious for the presence of prominent lipid droplets in their cytoplasm [60]. These lipid droplets have been suggested to modify the mechanical properties of the organ of Corti by changing its geometry or increasing the load on the basilar membrane. In addition, Hensen's cells may be able to modulate anti-inflammatory responses by releasing the contents of these lipid droplets into the endolymph [60] in response to certain stimuli (*e.g.*, glucocorticoids) [61]. Similarly to Deiters' cells, some Hensen's cells are in contact with branches from type II SGC fibers. And, there seems to be a direct correlation in Hensen's cells between the presence of lipid droplets and the incidence of innervation by type II SGC fibers [27, 30].

Much less is known about the Claudius' cells, the cuboidal cells that cover the *outer sulcus* of the cochlea (*i.e.* the region from the Hensen's cells to the spiral prominence) in a monolayer fashion.

1.7 Purinergic signaling in cochlear supporting cells

Several types of P1 and P2 receptors are expressed in sensory and supporting cells of the cochlear epithelium and in auditory nerve fibers; moreover, ATP has been shown to be released to the cochlear fluids during the normal development of the cochlea and also after noise exposure or tissue damage (reviewed in [62]). P1 receptors are coupled to G-proteins, and are activated by the binding of adenosine. There are two types of P2 receptors: metabotropic P2Y (G protein-coupled) and ionotropic P2X (ligand-gated ion channels). There are several subtypes of P2Y receptors. They are activated by ATP, UTP, ADP and/or UDP. Moreover, the potencies of each agonist vary between subtypes which allow, to some extent, to identify the expression of P2Y subtypes using pharmacological approaches. There are also several P2X isoforms that can form homomeric or heteromeric channels –with three subunits forming one functional channel. These P2X isoforms are mainly activated by ATP. For a comprehensive review of the pharmacology of P2Y and P2X receptors see references [63, 64].

1.7.1 Spontaneous release of ATP during postnatal development

In rodents, it was shown that the cells of the Kolliker's organ spontaneously release ATP to the extracellular space, which induces Ca^{2+} responses that propagate between supporting cells [65]. These Ca^{2+} responses in the Kolliker's organ were accompanied by changes in their cell shape, specifically, cell crenations that lead to an increase in the extracellular space between adjacent cells [65, 66]. These cell crenations were largely diminished by a Cl^- channel inhibitor, suggesting that the extrusion of water might be the underlying cause of such cell contractions. In addition, the spontaneous release of ATP by the cells of the Kolliker's organ can cause IHCs to depolarize and trigger action potentials in the type I SGC fibers [65, 67]. These spontaneous Ca^{2+} waves peak (in frequency and magnitude) around postnatal days 6 to 8 and they cease soon after the onset of hearing (around postnatal day 12 in mice and rats). Importantly, they were

shown to induce synchronous responses between neighboring IHCs (cell depolarization) and SGCs (excitatory postsynaptic currents and action potentials). And, this correlation between spontaneous Ca^{2+} waves and IHC/SGC responses was limited to areas encoding similar frequencies [65, 67]. Therefore, this spontaneous activation of neighboring IHCs and SGCs before the hearing onset is believed to provide important cues for the tonotopic maturation of auditory neural pathways.

1.7.2 Pathophysiological release of ATP

ATP is also released into the cochlear fluids after noise exposure [68] or hair cell damage [37, 38] and induces robust Ca^{2+} waves able to propagate throughout large areas of the cochlear epithelium [38]. The Ca^{2+} responses in the supporting cells are known to activate several members of the MAP kinase family [37, 69] that seem to favor cell survival. In addition, the release of ATP after noise exposure might be able to trigger action potentials in type II SGC fibers via the activation of P2X receptors [28]. Centrally, these afferent signals could potentially trigger the activation of efferent fibers to modify hearing sensitivity during noise exposure.

Hair cell damage also induces a fast-propagating Ca^{2+} wave along the rows of the sensory hair cells. This wave seems to require the influx of Ca^{2+} from the extracellular space via P2X channels [38], however, its functional role is still under examination.

1.7.3 Mechanism of propagation of ATP-induced Ca^{2+} waves in supporting cells

The expression of P2Y receptors provides supporting cells with high sensitivity to the presence of extracellular ATP, and concentrations in the nanomolar range are able to trigger Ca^{2+} waves that propagate rapidly from cell to cell [37]. When ATP binds P2Y receptors in a supporting cell, it induces an IP_3-dependent increase in intracellular Ca^{2+}. This response propagates to neighboring cells by (*i*) the diffusion of IP_3 through gap junctions, and (*ii*) the further release of ATP through connexin hemichannels (Figure 1.10) [34, 70]. However, it is currently unknown whether the ATP is released through the apical or basolateral membranes. Nonetheless, the self-propagating nature of these ATP-induced Ca^{2+} waves allows them to travel both from supporting cells in the inner to the outer sulcus and vice versa [34].
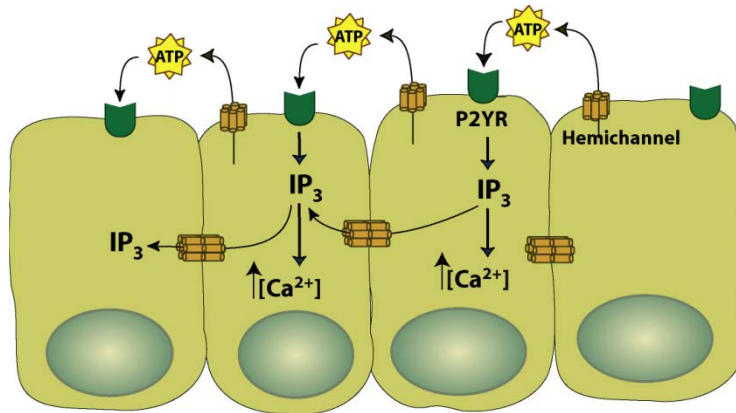
Figure 1.10. Mechanism of propagation of ATP-induced Ca^{2+} waves in supporting cells

ATP that is released to the extracellular fluid after tissue damage, or through connexin hemichannels (*i.e.* one connexon formed by six connexin subunits), binds P2Y metabotropic receptors on the plasma membrane of supporting cells. IP_3 is then generated via the activation of Phospholipase C (PLC) and leads to the release of Ca^{2+} from intracellular stores. IP_3 also diffuses to neighboring cells through gap junctions and somehow induces the release of more ATP, which ultimately leads to the propagation of Ca^{2+} waves from cell to cell [34, 70].

1.8 Impact of noise exposure on hearing thresholds

Acoustic overstimulation typically leads to an increase in hearing thresholds that can be temporary or permanent, depending on the magnitude and duration of the exposure. Clinically, a permanent threshold shift (PTS) is diagnosed when hearing thresholds have not recovered to baseline levels at least 2 weeks after the acoustic overstimulation (Figure 1.11). PTS is associated with extensive damage to the stereocilia bundles and/or sensory/supporting cell death [71-73]. In addition, a decrease in the endocochlear potential, usually recoverable, can occur after the exposure to loud sounds that lead to PTS [72, 74, 75]. In contrast, temporary threshold shifts (TTS) can last from hours to several days, but the hearing thresholds eventually recover to baseline levels (Figure 1.11).
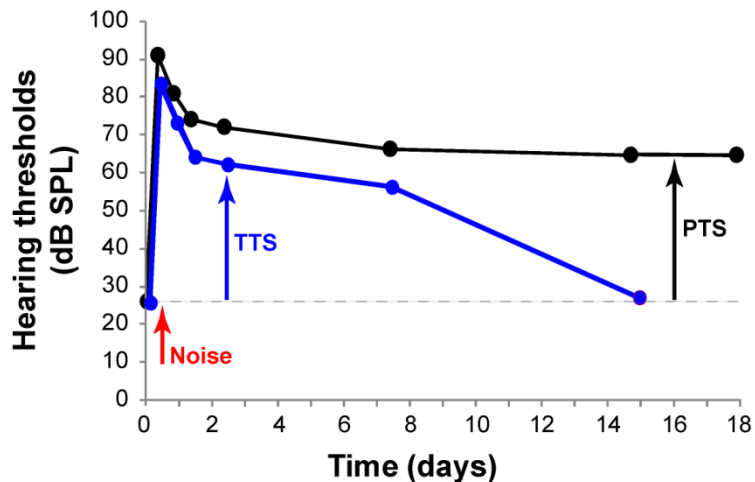
Figure 1.11.Diagram of temporary vs. permanent shifts in hearing thresholds
Acoustic overstimulation leads to an increase in hearing thresholds. This increase is considered to be a temporary threshold shift (TTS) if it recovers around two weeks after the cochlear overstimulation (blue trace). In contrast, if the hearing thresholds continue to be elevated and do not recover, this constitutes a permanent threshold shift (PTS) (black trace). The dashed line indicates the hearing threshold before noise exposure, and the red arrow indicates the time point when noise exposure occurred. *dB SPL*, decibel sound pressure level.

Several histopathological findings that could explain the development of TTS have been identified. For instance, the continuous release of neurotransmitters after IHC overstimulation leads to the swelling of the type I SGC postsynaptic terminals and their retraction away from the IHC basolateral membrane, presumably due to glutamatergic excitotoxicity [76, 77]. In addition, a reduction in the number of presynaptic (IHC) ribbons was also observed soon after the exposure to low noise [77]. Temporary changes in the architecture of the organ of Corti, involving changes in supporting cell shape, have been observed after acoustic overstimulation (see section 1.9). Because changes in the shape of supporting cells can alter the overall tissue geometry (*e.g.*, changing the angle between the tectorial membrane and the OHC stereocilia bundles at the resting position), it is no surprise that these changes can modify hearing sensitivity. Some changes in the cell density and the balance of inhibitory and excitatory circuits in central auditory

17

pathways have also been observed after noise exposure to a TTS-producing noise [78, 79]. These modifications in central auditory pathways represent a secondary level of adaptation to the changes that occur in the periphery; however, they have the potential to alter sound perception after acoustic trauma.

Even though hearing thresholds return to normal levels after a TTS, some of the pathophysiological findings described above do not recover completely [71, 77]. And, in fact, they might constitute a risk factor for the development of PTS after subsequent noise exposures and/or eventually underlie the progression toward age-related hearing loss [80]. However, the occurrence of TTS can also constitute a protective response to minimize tissue damage during longer periods or stronger levels of acoustic ovestimulation. For instance, mice lacking $P2X_2$ channels are more susceptible to develop PTS after exposure to loud noise [81]. Interestingly, when exposed to low noise, these mice do not exhibit changes in hearing thresholds; not even to noise levels that induce TTS in wild type mice. Although the exact role of $P2X_2$ in TTS has not been elucidated yet, it does imply the involvement of extracellular ATP. The TTS protective effects have also been abundantly shown during *sound conditioning* experiments (reviewed in [82]), where animals become resistant to noise that initially induced TTS. The sound conditioning is achieved through long-term exposure to low sound levels, in either a continuous or intermittent manner, and has been shown to prevent PTS after the exposure to a loud and typically damaging noise. Even though the exact mechanisms are largely unknown, there is evidence that these sound conditioning protocols might provide protection by increasing the expression of antioxidants, heat-shock proteins, Ca^{2+} buffers and neurotrophic factors [82].

1.9 Impact of noise exposure on the geometry of the organ of Corti

Several reports have shown a 'contraction' of the organ of Corti (*i.e.* a reduction in the height of the tissue) after noise exposure *in vivo* (awake or anesthetized animals) [71, 73, 74, 83] or *in vitro* (temporal bone preparations) [84-86]. These changes in the tissue architecture often involved (*i*) Hensen's and Deiters' cells getting closer to the basilar membrane and the tunnel of Corti, (*ii*) a reduction in the space of Nuel and (*iii*) the buckling of inner and/or outer pillar cells.

Sound stimulation leads to the vibration of the basilar membrane and the elongation and contraction of OHCs (section 1.4). Therefore, loud and/or prolonged noise exposure can potentially involve damaging tissue vibrations and changes in the architecture of the cochlear epithelium simply as a result of mechanical damage. However, it is plausible that the modified tissue architecture observed after acoustic overstimulation is the result of active changes in the shape of the supporting cells surrounding the sensory hair cells. To date, Deiters' cells are the only type of cochlear supporting cells reported to have Ca^{2+}-dependent contractile machinery (section 1.6.4). The cytoskeleton of pillar cells (in particular of outer pillar cells) resembles that of Deiters' cells and, therefore, they may potentially contract upon an increase of cytosolic Ca^{2+}.

Sound induced depolarizations of the hair cells create currents that are large enough to be measured by an electrode placed near the round window of the cochlea. This technique known as cochlear microphonics can be used to assess cochlear sensitivity (reviewed in [87]). Interestingly, the supporting cell-driven changes in the organ of Corti geometry after acoustic overstimulation seem to be reversible and often correlate with an improvement in cochlear microphonics or with TTS [71, 73, 83, 85].

CHAPTER 2

A comprehensive review of literature on TRPA1 channels

2.1 The TRP channel family

Based on their homology to the *transient receptor potential* (TRP) channels in *Drosophila*, several genes have been grouped into the big TRP family of ion channels [88]. TRP channels have been divided into seven groups according to their amino acid sequence homology: ankyrin (TRPA), canonical (TRPC), melastatin (TRPM), mucolipin (TRPML), NompC-like (TRPN), polycystin (TRPP) and vanilloid (TRPV). The TRPN channel, however, has been found in the genomes of invertebrates (fly and worm [89]) and lower vertebrates (zebrafish [90] and frog [91]) but not in mammalian genomes [90].

TRP proteins have six transmembrane segments (S1 through S6), intracellular amino (N) and carboxy (C) termini [92, 93], and four subunits assemble into homo- or heterotetramers to form functional ion channels (reviewed in [94]). The pore region in TRP channels seems to be comprised of the linker segment between the transmembrane segments S5 and S6. While all TRP channels are permeable to cations, different channels exhibit specific degrees of selectivity between mono- and divalent cations (reviewed in [95]). The intracellular termini of TRP channels vary greatly between subfamilies, but in general they allow the interaction of the channels with intracellular signaling molecules and pathways. For instance, three members of the TRPM subfamily have protein kinase activity in their C-termini [96] and TRP channels usually possess intracellular domains such as ankyrin repeat, pleckstrin homology (PH)-like or EF-hand-like domains (reviewed in [97]) that allow for protein-protein or protein-ligand interactions. TRP channels can be activated by a wide variety of mechanical, thermal and chemical stimuli (reviewed in [98]) and, together with their broad intracellular responses, constitute powerful modulators of cell physiology.

At present, 28 mammalian TRP channels have been identified and their role in human pathophysiology is rapidly growing after the generation of specific TRP knockout mice and the identification of disease-causing TRP mutations in humans (see Table 2.1 for details). A quantitative analysis of mRNA expression of all 28 channels performed in developing cochlear tissue (from embryonic to early postnatal stages) could not detect mRNA of TRPC7 or TRPM8 at all, or TRPV5 in half the samples tested. However, this study did revealed different degrees of expression for the remaining 25 TRP channels [99]. But, given the scope of this dissertation project, the main focus of this review will be on TRPA1 channels.

2.2 TRPA1: from gene to protein

TRPA1 is the only member of the mammalian TRPA subfamily. Given that the animal model used in this dissertation project was the mouse, this review will focus largely on mouse, rat (given its homology) and human (due to its translational relevance) TRPA1 channels.

2.2.1 The mouse Trpa1 gene

The mouse *Trpa1* gene is located in chromosome 1, it contains 27 exons and two TRPA1 splice variants have been identified [100]. While the full TRPA1 mRNA transcript encodes a protein of 1,125 amino acid residues (UCSC ID: uc007ajc.1), the splice variant encodes a protein 30 residues smaller that lacks exon 20 (UCSC ID: uc033fid.1). The missing 30 residues are part of the transmembrane segment S2 and part of the intracellular linker between S2 and S3.

2.2.2 The rat TRPA1 gene

The rat TRPA1 gene is in found in chromosome 5 and, like the mouse TRPA1 gene, it has 27 exons and encodes a 1,125 amino acid protein (UCSC ID: RGD_1303284). No TRPA1 mRNA splice variants have been reported in the rat [100]. Notably, the rat and mouse proteins share over 96% identity (see Appendix B for the protein sequence alignment).

21

Table 2.1. Mammalian TRP channels

Sub-Family	Members*	Mouse knockout phenotypes	Human pathophysiology[†]
TRPA	TRPA1 (ANKTM1)	Defective pain sensitivity to cold, mechanical stimuli, chemical irritants and bradykinin [101, 102]	Debilitating episodes of pain in the upper body [103]
TRPC	TRPC1	Increased body size and impaired salivary gland fluid secretion [104, 105]	
	TRPC2[‡]	Impaired pheromone-induced behaviors [106, 107]	[‡]
	TRPC3	Defective walking behavior [108]	
	TRPC4	Impaired regulation of blood vessel tone and permeability of lung microvessels [109]	
	TRPC5	Reduced anxiety-like behavior [110]	
	TRPC6	Increased blood vessel tone and contractility [111]	Renal dysfunction [112, 113]
	TRPC7	Resistance to pilocarpine-induced seizures [114]	
TRPM	TRPM1	Loss of light-induced inward currents in retinal ON bipolar cells [115-117]	Reduced central vision, nystagmus and eczema [118-121]
	TRPM2	Impaired chemokine production by monocites [122]	Coding SNP associated with bipolar disorder [123]
	TRPM3	Defective pain sensitivity to inflammation and heat [124]	

Table 2.1. Mammalian TRP channels (continued)

TRPM	TRPM4	Augmented degranulation and histame release in mast cells [125], impaired dendritic cell migration [126], and protection against spinal cord injury [127].	Conduction abnormalities in the heart [128-130]
	TRPM5	Abolished sweet, umami and bitter taste reception [131], and defective insulin release [132, 133]	
	TRPM6	Embryonic or early postnatal death with neural tube defects [134]	Hypomagnesemia and hypocalcemia [135, 136]
	TRPM7	Embryonic lethal [137]	Susceptibility for a neurodegenerative disorder [138]
	TRPM8	Defective pain sensitivity to cold [139-141]	
TRPML	TRPML1	Neurodegeneration, elevated plasma gastrin and retinal degeneration [142]	Neurodegeneration with ophthalmologic abnormalities [143, 144]
	TRPML2		
	TRPML3		
TRPP	TRPP1 (PKD2)	Embryonic lethal [145]	Renal cysts leading to renal failure [146]
	TRPP2 (PKD2L1)		
	TRPP3 (PKD2L2)		

Table 2.1. Mammalian TRP channels (continued)

TRPP	TRPP3 (PKD2L2)		
TRPV	TRPV1	Defective pain sensitivity to heat [147], and enhanced insulin sensitivity [148]	
	TRPV2	Impaired innate immunity [149]	
	TRPV3	Impaired behavioral responses to heat [150], and abnormalities in fur and whiskers [151]	Severe skin abnormalities [152]
	TRPV4	Impaired antidiuretic hormone regulation [153, 154], defective pain sensitivity to mechanical stimuli [155], impaired bladder function [156, 157], and hearing loss [158].	Skeletal dysplasia [159-161]; osteoarthritis [162, 163]; muscle paresis, paralysis, atrophy or congenital absence [164-167] and dwarfism [160, 168]. Coding SNP associated with hyponatremia [168]
	TRPV5	Hypercalciuria, polyuria and reduced bone thickness [169, 170]	
	TRPV6	Possible role in intestinal Ca^{2+} absorption [171, 172]	

* Other common names for each member are listed within parenthesis.

[†] Clinical features caused by mutations in human TRP genes. For details about the exact syndromes and inheritance patterns see Appendix A.

[‡] TRPC2 is a pseudogene in humans [173].

2.2.3 The human TRPA1 gene

In humans, the TRPA1 gene is located in chromosome 8, it contains 27 exons, it encodes a protein of 1,119 amino acid residues (UCSC ID: uc003xza.3) and no splice variants have been identified [100]. The human TRPA1 protein shares about 80% identity with both the mouse and rat TRPA1 proteins (see Appendix B for the protein sequence alignment), making mice and rats interest models for the study of TRPA1 function.

2.2.4 Tissue expression of TRPA1

TRPA1 mRNA has been detected in a wide variety of tissues and cell types. In addition, the generation of *Trpa1* knockout (*Trpa1*$^{-/-}$) mice has allowed to confirm TRPA1 expression at the protein level in some of these tissues. Immunolabeling of the TRPA1 protein has also been described in a wide variety of tissues, but only the reports showing strict controls for the antibodies used have been included in this review.

In the mouse, TRPA1 mRNA is highly expressed in dorsal root (DRG), trigeminal and nodose ganglia [174-176] and in the cochlear epithelium [99, 177]. In addition, lower transcription levels have been detected in the tongue [178], stomach, small intestine and colon [179]. The presence of an active *Trpa1* promoter and functional TRPA1 channels in DRG neurons (including C and Aδ fibers) innervating the skin has been confirmed using tissue from wild type and TRPA1-deficient mice [180]. Immunoreactivity against the TRPA1 protein in bronchial epithelium and smooth muscle has also been detected in tissue from wild type but not *Trpa1*$^{-/-}$ mice [181].

In the rat, high expression of TRPA1 mRNA is detected in dorsal root ganglia [174], small intestine and colon [179, 182]. Lower mRNA expression levels are also detected in brain, stomach [179], bladder [183], cerebral arteries [184] and pancreatic beta cells [185].

In human tissues, TRPA1 mRNA has been detected in fibroblasts [181, 186], small intestine, colon, skeletal muscle, heart, pancreas, lymph nodes, spleen [187], skin [188, 189] and stomach [179]. TRPA1 immunolabeling has also been reported in primary lung epithelium, lung smooth muscle cells [181], urethral cells [190] and several cell lines of human origin. However, cautious consideration needs to be given to some of these

immunolabeling reports given the limitations in tests about antigen specificity of the antibodies used.

For more details about TRPA1 tissue expression in the mouse, rat and human, see reference [191].

2.2.5 Channel assembly from TRPA1 subunits

Four TRPA1 subunits assemble to form a functional channel. In mice, the two TRPA1 splice variants can interact (presumably forming heteromeric channels) and lead to increased TRPA1 expression in the plasma membrane and larger agonist-induced currents [100]. There is also evidence that TRPA1 and TRPV1 subunits can form heteromeric channels [192, 193]. Moreover, TRPA1-TRPV1 heteromeric channels seem to have slightly different gating and inactivation kinetics, and sensitivity to both TRPA1 and TRPV1 agonists. Some decreases in agonist sensitivity can be simply explained by the decrease in binding sites (*e.g.*, an agonist specific for TRPV1 could potentially have 4 binding sites in a homomeric TRPV1 channel, but only 2 binding sites in a TRPA1-TRPV1 heteromeric channel with 2 subunits of each type [192]). However, some agonists seem to prefer specific channel configurations and may involve interactions between neighboring subunits.

2.2.6 Ankyrin repeats in the intracellular N-terminus of TRPA1

TRPA1 subunits exhibit six transmembrane domains (see Appendix C for the prediction of transmembrane segments in mouse, rat and human TRPA1 subunits), which are a hallmark in the TRP family. TRPA1 also contains a unique intracellular N-terminus with a large number (~14 to 18) of ankyrin repeats [186] (Figure 2.1). TRPN channels have even larger numbers of ankyrin repeats (~29) but, as mentioned earlier, they are not expressed in mammals.

Ankyrin repeat domains are found in a broad variety of proteins, including transcription factors, scaffold proteins, enzymes, regulatory subunits an even other members of the TRP family (*i.e.* TRPC and TRPV channels, with a rather small number of repeats: 4 to 6). The amino acid sequence of an ankyrin motif varies significantly between proteins but, on average, it consists of 30 to 34 residues arranged into a helix-

turn-helix domain coupled to a β-hairpin loop. The structure of several ankyrin repeats has been resolved and, amusingly, a tandem of five repeats resembles a hand, where the helix-turn-helix domains form the palm and each β-hairpin loop forms a finger.
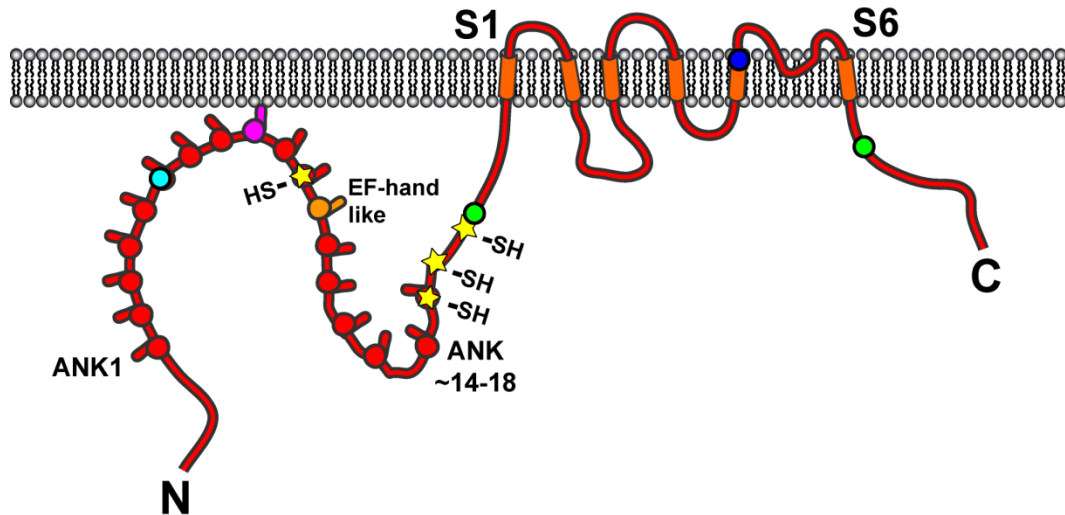
Figure 2.1. Diagram of a TRPA1 channel subunit

The diagram illustrates a TRPA1 subunit with its six transmembrane segments (for clarity, only S1 and S6 are labeled), both intracellular N- and C-termini and several ankyrin repeats (ANK) in the N-terminus. The pore-forming region is located between S5 and S6. The cyan circle indicates a methionine residue required for caffeine activation. A highly hydrophobic ankyrin repeat that might interact with the plasma membrane is shown in magenta (Appendix C). The ankyrin repeat that is known to contain an EF-hand-like domain to bind Ca^{2+} has been colored orange. The yellow starts indicate areas where several cysteine residues are required for channel gating by reactive agonists. The green circles designate cysteine (N) and histidine (C) residues required for activation by Zn^{2+}. The blue circle in S5 shows the position of a glycine residue required for channel gating by cold temperature and inhibition by menthol.

Ankyrin repeats are known to allow protein-protein interactions (that sometimes involve covalent bindings) and, in TRPA1 channels in particular, they are important for agonist-induced gating (see section 2.3 for more details). In fact, one of the ankyrin

repeats in TRPA1 is known bind Ca^{2+} ions [194] but, technically, it does not constitute a classic EF-hand domain [195] (see section 2.3.4 for more details). In addition, it has been proposed that ankyrin repeats might provide elastic properties to proteins that express large numbers of them [196]. For more comprehensive reviews on ankyrin repeats, see [195, 197].

2.2.7 The intracellular C-terminus and pore-forming regions of TRPA1

Based on its homology to the other channels in the TRP family, the pore-forming region in a TRPA1 subunit is thought to be comprised of the loop between the transmembrane segments S5 and S6 (Figure 2.1). TRPA1 channels are permeable to monovalent and divalent cations. The selectivity between K^+, N^+, Cs^+, Mg^{2+} and Ca^{2+} ions has not been extensively characterized for TRPA1 channels, however, results from one study correlate with a non-selective cation channel: $P_{Cs}/P_{Na} = 1.42$, $P_{Mg}/P_{Na} = 1.23$, $P_K/P_{Na} = 1.19$ and $P_{Na}/P_{Ca} = 1.19$ [174]. Consistent with this, TRPA1 permeability to Cl^- is low: $P_{Cl}/P_{Na} = 0.28$ [174]. Single-channel recordings have shown several conductance levels for TRPA1 but, on average, the channel conductance is around 100 pS [175]. Interestingly, single channel conductance is greatly reduced by Ca^{2+} ($\sim$ 54% reduction) [175]. Importantly, these changes in conductance can arise from agonist-induced dilation of the TRPA1 pore [198].

Although most agonists bind to the N-terminus of TRPA1 (see section 2.3), there is evidence suggesting that the intracellular C-terminus is involved in channel gating by a few agonists (*e.g.* Zn^{2+}) [199]. In addition, mutations to several C-terminal amino acid residues show impaired TRPA1 sensitivity to voltage and to the potent agonist, mustard oil [200]. The TRPA1 transmembrane segments S5 and S6 and the pore-forming region are important for the binding and activation by other agonists as well.

2.3 TRPA1 agonists and the mechanisms of TRPA1 channel gating

There is a large inventory of compounds that activate TRPA1 channels; for a comprehensive list see Table 2.2 and reference [191]. Two general mechanisms of ligand-induced TRPA1 gating have been recognized: (*i*) 'classical' binding of structurally-related agonists to –one, perhaps more– binding pockets within the TRPA1

channel, and (*ii*) covalent modifications to the TRPA1 subunits mediated by 'reactive' agonists. These reactive chemical compounds and endogenous agonists typically lead to channel gating by modifying amino-acid residues within the TRPA1 intracellular N-terminus (Figure 2.1) [201, 202]. These covalent modifications can remain in the TRPA1 proteins from minutes to hours, and can sometimes lead to long-lasting TRPA1 channel activation [201-203].

Table 2.2. List of TRPA1 agonists

Agonist	Species *	Mechanism and/or site of action	Other TRP channels[†]	Ref.
Δ^{12}-PGJ$_2$	H	Covalent modifications		[204]
1-butanol	H			[205]
1-heptanol	H			[205]
1-hexanol	H	Interaction with N-terminal Cys and C-terminal His		[205, 206]
1-octanol	H	Interaction with N-terminal Cys and C-terminal His		[205, 206]
1-pentanol	H			[205]
1-propanol	H			[205]
15dPGJ$_2$	H, M	Covalent modifications		[204, 207]
2-APB	H	'Classical' binding	TRPV1, TRPV3	[202, 208]
4-HHE	H, M	Covalent modifications		[207, 209]
4-HNE	H, M, R	N-terminal Cys and Lys covalent modifications		[210, 211]
4-ONE	H, M	Covalent modifications	TRPV1	[207, 209]
8-iso PGA$_2$	H	Covalent modifications		[204]
AA				[212]
Acetaldehyde	H, M			[213]

Table 2.2 List of TRPA1 agonists (continued)

Acrolein	H, M, R	N-terminal Cys covalent modifications		[101, 202, 214]
AITC	H, M, R	N-terminal Cys and Lys covalent modifications		[201, 215]
Allicin	H, M, R			[216]
BITC	H	Covalent modifications		[202]
Butenal	M			[211]
Ca^{2+}	H			[194, 217]
Caffeine	M	Binding to intracellular Met		[178]
Cannabinol	H, R			[215]
Carvacrol	R	'Classical' binding	TRPV3	[218]
CA	H, M	N-terminal Cys covalent modifications		[201, 202, 212]
Cd^{2+}	H, M			[219]
Crotonaldehyde	M, R			[214]
Cu^{2+}	H, M			[219]
DADS	H, R	N-terminal Cys covalent modifications		[202, 216]
Desflurane	M, R			[206, 220]
Diclofenac	H, R	'Classical' binding		[208]
DPDS				[221]
Ethanol	H			[205]
Etomidate	M, R			[206]
Eugenol	M		TRPV1, TRPM8	[212]
FFA	H, R	'Classical' binding		[208]
Flurbiprofen	H, R	'Classical' binding		[208]
Formaldehyde	M		TRPV1	[211]
Gingerol	M		TRPV1	[212]

Table 2.2 List of TRPA1 agonists (continued)

H$^+$	H	Interaction with S5 and S6, and N-terminal cys	TRPV1	[222, 223]
H$_2$O$_2$	M, R	N-terminal Cys and Lys covalent modifications	TRPM2	[207, 224] [225]
Hexenal	M			[211]
Heptenal	M			[211]
Hypochlorite	H, M	N-terminal Cys and Lys covalent modifications		[225]
IA	M	Cys covalent modifications		[201, 211]
IAA	M	Cys covalent modifications		[201]
Icilin	M	'Classical' binding	TRPM8	[201]
Indomethacin	H, R	'Classical' binding		[208]
Isoflurane	M, R			[206, 220]
Ketoprofen	H, R	'Classical' binding		[208]
Lidocaine	H, M, R	Binding to intracellular Cys		[226]
Menthol	H, M	Interaction with S5	TRPM8	[227, 228]
Methanol	H			[205]
Methyl salicylate	M		TRPV1	[212]
MFA	H, R	'Classical' binding		[208]
MOA	M	Cys covalent modifications		[201]
MpBZ	M			[229]
MTSEA	M	N-terminal Cys covalent modifications		[201, 202]
NFA	H, R	'Classical' binding		[208]
Nicotine	H, M	'Classical' binding		[230]
Nifedipine	H	'Classical' binding		[208]
Nitrooleic acid	H, M			[231]
NMM	H	N-terminal Cys covalent modifications		[202]

Table 2.2 List of TRPA1 agonists (continued)

Octenal	M			[211]
Pentenal	H, M			[101, 211]
PGA$_2$	H	Covalent modifications		[204]
Propofol	M, R			[206]
SC	M	Cys covalent modifications		[201]
SCA	M	Cys covalent modifications		[201]
TDI	H, M	Cys covalent modifications		[232]
THC	H, R	'Classical' binding		[202, 215]
Theobromine	M	Binding to intracellular Met		[178]
Theophylline	M	Binding to intracellular Met		[178]
Thymol	H, M	Interaction with S5	TRPM8, TRPV3	[227, 228]
Umbellulone	H, M, R	Covalent modifications		[233]
Zn^{2+}	H, M	Interaction with N-terminal Cys and C-terminal His		[199, 219]

* Species where TRPA1 activation has been reported by the agonist: human (H), mouse (M) or rat (R).

[†] Ligand promiscuity with other mammalian TRP channels.

Abbreviations: *2-APB*, 2-amino-phenyl borane; *4-HHE*, 4-hydroxyhexenal; *4-HNE*, 4-hydroxynonenal ; *4-ONE*, 4-oxononenal; *AA*, arachidonic acid; *AITC*, allyl isothiocyanate (mustard oil); *BITC*, benzyl isothiocyanate; *CA*, cinnamaldehyde; *Cys*, cysteine; *DADS*, diallyl disulfide; *DPDS*, dipropyl disulfide; *FFA*, flufenamic acid; *IA*, iodoacetamide; *IAA*, iodoacetamide alkyne; *MFA*, mefenamic acid; *MOA*, mustard oil alkyne (propargyl isothiocyanate); *MpBZ*, methyl *p*-hydroxybenzoate; *MTSEA*, (2-aminoethyl) methanethiosulphonate; *NFA*, niflumic acid; *NMM*, *N*-methyl maleimide; *Ref.*, References; *SC*, super cinnamaldehyde; *SCA*, super cinnamaldehyde alkyne; *TDI*, toluene diisocyanate; *THC*, Δ^9-tetrahydrocannabinol.

Channel inactivation following covalent modifications could be achieved through several mechanisms. For instance, while some covalent modifications appear to be completely irreversible (*e.g.*, by the reactive agonist *N*-methyl maleimide –NMM) others appear to be temporary [201, 202]. TRPA1 channels are also susceptible to voltage-induced inactivation (after cell depolarizations) [234] and to blockage by intracellular Ca^{2+} [175, 235]. In addition, TRPA1 protein turnover and endocytosis rates would also affect the amount of covalently-modified TRPA1 channels present in the plasma membrane.

2.3.1 Pungent compounds

The pungent perception after the ingestion of certain foods is mediated by the activation of TRPA1 channels in nerve terminals in the mouth. These, sometimes painful, sensations are induced by specific compounds, such as: allyl isothiocyanate –AITC– (also known as 'mustard oil', found in wasabi, mustard and horseradish) [215], cinnamaldehyde –CA– (cinnamon) [212], carvacrol and thymol (oregano and thyme) [218, 227], gingerol (ginger) [212], eugenol (clove) [212], allicin and diallyl disulfide –DADS– (garlic and onion) [216].

Some of these pungent compounds are electrophiles and, as such, can potentially react with neuclophilic amino acid residues like cysteine, lysine and histidine. In fact, the mechanism of TRPA1 gating by some of these reactive agonists (*i.e.* AITC, CA and DADS) has been shown to specifically involve covalent modifications of cysteine and/or lysine residues in the TRPA1 N-terminus (Figure 2.1) [201, 202]. These covalent modifications might even involve to the formation of disulfide bonds between cysteine residues [236]. Several key N-terminal cysteine residues have been reported to be necessary for channel gating by these reactive agonists [201, 202]. Moreover, agonist sensitivity depended on the amount of cysteine residues present (in targeted mutation studies). However, when three of the cysteine residues were mutated in the same construct, TRPA1 sensitivity to non-reactive agonists was also decreased, suggesting a general defect in TRPA1 gating [199]. Similarly, TRPA1 sensitivity to AITC was impaired when several C-terminal lysine, arginine and alanine residues were mutated [200]. The sensitivity of these C-terminal TRPA1 mutants to non-reactive agonists was

not tested and, therefore, it is plausible that these mutations cause structural changes that affect TRPA1 gating.

Because some of these pungent compounds are non-reactive agonists, their mechanism of action seems to involve the 'classical' binding between an agonist and a receptor (*i.e.* TRPA1 channel). In particular, TRPA1 activation by thymol requires amino acid residues located within the transmembrane segment S5 [228].

The noxious effects caused by topical application or subcutaneous injection of these pungent compounds are described in section 2.4.1.

2.3.2 Airborne irritants

Several aldehydes in cigarette smoke, air pollution or tear gas (*e.g.*, acrolein –2-propenal–, crotonaldehyde and acetaldehyde [237]), as well as some volatile environmental (*i.e.* umbellulone) and industrial chemicals (*i.e.* toluene diisocyanate – TDI–, hypochlorite and formaldehyde) are known to gate TRPA1 channels [211, 213, 214, 225, 232, 233]. These reactive agonists seem to activate TRPA1 channels in a manner similar to the reactive pungent agonists described above, which involves covalent modifications to cysteine and lysine residues in the N terminus of TRPA1 subunits (Figure 2.1) [202, 225]. In the airways, they can activate TRPA1 channels present in bronchial epithelial and smooth muscle cells, as well as in neurons innervating the nasal cavity and the bronchi. Inhalation of these volatile TRPA1 agonists causes noxious responses in the meninges and in the respiratory airways, which are described in more detail in section 2.4.1.

2.3.3 Byproducts of reactive oxygen and nitrogen tissue damage

The generation of reactive oxygen and nitrogen species (ROS and RNS, respectively) increases during instances of cellular stress (*e.g.*, inflammation, hypoxia or mechanical trauma). These reactive molecules can cause damage to lipids, proteins and nucleic acids, and can eventually lead to cellular apoptosis.

Some ROS, such as hydrogen peroxide (H_2O_2), act as TRPA1 agonists themselves [207]. Moreover, ROS-induced lipid peroxidation leads to the generation of byproducts such as 4-hydroxynonenal (4-HNE), 4-hydroxyhexenal (4-HHE) and 4-oxononenal (4-

ONE) that can directly bind and trigger TRPA1 channel gating [207, 209-211]. On the other hand, RNS can add highly reactive NO_2 groups to fatty acids. These nitrated phospholipids (*e.g.*, nitrooleic acid –OA-NO$_2$) can bind and activate TRPA1 channels as well [231]. In general, nitrated phospholipids seem to be more potent than peroxidation byproducts in the activation of TRPA1 channels.

Notably, the mechanism of TRPA1 channel activation by 4-HNE seems to involve covalent modifications to the same cysteine and lysine residues required for activation by reactive pungent compounds and airborne chemicals (Figure 2.1) [210].

2.3.4 Divalent cations

As described in section 2.2.6, TRPA1 channels have an ankyrin domain that resembles an EF hand and is able to bind Ca^{2+} (Figure 2.1). Intracellular Ca^{2+} can directly trigger TRPA1 channel gating through its interaction with the EF hand-like domain [194, 217]. Because TRPA1 channels are permeable to Ca^{2+}, channel activation by other agonists can be potentiated after the initial influx of Ca^{2+}.

In a similar manner, TRPA1 channels are permeable to Zn^{2+}, a heavy metal that can directly bind to TRPA1 (on intracellular domains) and trigger channel gating [199]. Some anti-fungal and anti-parasitic drugs that act as Zn^{2+} ionophores can indirectly induce TRPA1 gating by increasing intracellular levels of Zn^{2+} [219]. Specifically, two cysteine and one histidine residues are important for the TRPA1 sensitivity to Zn^{2+} [199]. One of the cysteine residues, located in the N-terminus of TRPA1, is involved in channel gating by reactive agonists as well. The other cysteine residue and the histidine residue are located in the C-terminus of TRPA1 (Figure 2.1).

Other divalent cations that can directly bind and gate TRPA1 channels are Cd^{2+} and Cu^{2+} [219]. Fe^{2+} can modulate TRPA1 activation by other agonists, but Fe^{2+} does not directly gate TRPA1 channels [207, 219].

2.3.5 Noxious cold

Initial reports showed that TRPA1 channels were gated by cold temperatures (< 17°C) [174]. However, even after a decade of studies, researchers do not agree on whether TRPA1 channels can directly sense noxious cold. Several groups have supported the

initial findings and have shown cold sensitivity in TRPA1 channels expressed in heterologous systems [217, 238]. Correlations between the percentages of TRPA1-expressing and cold-sensitive DRG neurons were reported [212, 239]. Meanwhile, other groups failed to find correlations between AITC-sensitive and cold-sensitive DRG neurons [215, 238, 240]. In addition, cold seems to induce a small Ca^{2+} influx in heterologous systems that is independent of TRPA1 channels [217]. This result could indicate that noxious cold indirectly gates TRPA1 channels via a small increase in intracellular Ca^{2+} levels. Another level of complexity was added with the generation of $Trpa1^{-/-}$ mice by two independent groups that showed opposite behavioral results. While one group reported impaired sensitivity to noxious cold in TRPA1-deficient mice [102], the second group found no difference in cold sensation between TRPA1 knockout and wild type mice [101]. Further studies in mice indicated that cold exposure does not directly gate TRPA1 channels but instead potentiates TRPA1 activation when the channel has been primed by a different agonist [241]. Moreover, direct channel gating by cold, if present at all, is a property of mouse and rat but not human TRPA1 channels [242, 243]. A glycine residue in the TRPA1 transmembrane segment S5 is required for cold sensation (Figure 2.1), but other unknown amino acid residues might also be involved. For comprehensive reviews on cold sensitivity by TRPA1 channels see [244, 245].

2.3.6 Pro- and anti-inflammatory agents

Prostaglandins (PGs) are pro-inflammatory agents produced downstream of the hydrolysis of membrane phospholipids via the activity of cyclooxygenases (COXs). Several prostaglandins and their metabolites can trigger TRPA1 gating (*i.e.*, 15dPGJ$_2$, PGA$_2$, 8-iso PGA$_2$ and Δ^{12}-PGJ$_2$) and cause pain [246]. Because only 'reactive' PG metabolites seem to lead to TRPA1 activation [204], the mechanism of channel gating seems to involve covalent modifications, perhaps, of the same amino acid residues targeted by other reactive agonists (Figure 2.1). The inflammatory pain induced by PGs is commonly treated with non-steroidal anti-inflammatory drugs (NSAIDs) that act as COX inhibitors. Interestingly, several of these NSAIDs are TRPA1 agonists as well (e.g., flufenamic acid –FFA–, mefenamic acid, niflumic acid, flurbiprofen, indomethacin, ketoprofen and diclofenac) [208], making them the most puzzling TRPA1 agonists.

While TRPA1 activation has been frequently linked to pain-like behaviors (as described in section 2.4), NSAIDs are extensively known for their analgesic effects. In addition, because these NSAIDs are non-reactive agonist, their mechanism of action probably involves 'clasical' binding or interaction between the agonist and the TRPA1 channel.

2.3.7 Local and general anesthetics

Several anesthetics can activate TRPA1 channels as well. Lidocaine, a membrane-permeable local anesthetic, can activate TRPA1 channels when applied at high concentrations (> 3 mM) [226]. Interestingly, at even higher concentrations (> 100 mM), lidocaine acts as a channel blocker. In addition, the mechanism of TRPA1 activation by lidocaine seems to involve some of the cysteine residues typically targeted by reactive agonists. Some inhalation (*e.g.*, isoflurane and desflurane) and intravenous (*e.g.*, propofol and etomidate) general anesthetics can trigger TRPA1 gating [206]. General anesthetics of the inhalation class seem to activate TRPA1 channels via a mechanism similar to the one used by Zn^{2+} (Figure 2.1). In contrast, intravenous general anesthetics appear to involve a different, yet unknown, mechanism. Because some drugs indirectly activate TRPA1 channels (via an increase in intracellular Zn^{2+}) [219], more studies are required to clarify whether inhalation-type anesthetics can directly bind and gate TRPA1 channels.

2.3.8 Other TRPA1 agonists

Some alcohols, xanthine derivatives and antibacterials are other compounds that can behave as TRPA1 agonists. In addition, menthol and weak acids can induce TRPA1 gating as well.

Primary alcohols (from methanol to 1-octanol) have been shown to activate TRPA1 channels at high concentrations (> 1 mM), with greater potencies exhibited by those with larger carbon chains [205, 206]. However, there is a limit in the length of the alcohol carbon chain that can activate TRPA1 channels since decanol fails to trigger channel gating [206]. In addition, the mechanism of action of these alcohols seems to involve the same cysteine and histidine residues required for TRPA1 gating by Zn^{2+} and inhalation-type anesthetics. Because agonist potency directly correlates with molecule size, the

presence of a binding pocket in TRPA1 subunits has been proposed [206], in manner analogous to other ligand-gated ion channels (e.g., GABA$_A$ and glycine receptors) [247].

Xanthine derivates, such as caffeine, can activate TRPA1 channels as well, and TRPA1 gating by these compounds does not require intracellular Ca^{2+} [178]. This favors the idea of a direct mechanism of channel gating rather than indirect activation via the effect of caffeine on intracellular stores. Moreover, a methionine residue in the intracellular N terminus of mouse TRPA1 is required for caffeine activation (Figure 2.1) [248].

Methyl *p*-hydroxybenzoate (MpBZ), an inert compound with antibacterial properties, can activate TRPA1 channels [229]. The TRPA1 reactive agonists AITC, CA and allicin as well as the non-reactive agonists carvacrol and thymol (described in section 2.3.1) are pungent compounds that exhibit antibacterial properties as well. However, because MpBZ is a non-reactive TRPA1 agonist, the mechanism by which it can trigger channel gating might resemble that of the non-reactive antibacterial/pungent compounds.

TRPA1 channels can directly sense both cytosolic and intracellular weak acidification [222, 223, 249]. Activation after extracellular acidification seems to be a property of human, but not mouse TRPA1 channels. In contrast, channel gating by intracellular protons is a feature conserved between mammals. TRPA1 activation by protons does not require the intracellular N-terminal cysteine residues that are involved in channel gating by reactive agonists. Instead, the transmembrane domains S5 and S6 are involved in TRPA1 sensing of extracellular acidosis. However, it is unknown whether intracellular protons activate TRPA1 channels through the same mechanism or protein region.

Menthol is a non-reactive compound that can activate mammalian TRPA1 channels [227]. Menthol is structurally similar to thymol and carvacrol, which are two non-reactive isomeric pungent compounds known to activate TRPA1 channels (described in section 2.3.1). Similar to thymol, menthol requires residues within the TRPA1 transmembrane segment S5 to induce channel activation [228], which seems to indicate the presence of a binding pocket near the pore region of TRPA1.

2.3.9 Agonists able to inhibit TRPA1 channels

Ca^{2+} has a bimodal effect on the activation of TRPA1 channels by other agonists. While micromolar concentrations of intracellular Ca^{2+} can potentiate TRPA1 activation by reactive and non-reactive agonists (section 2.3.4), higher Ca^{2+} concentrations can lead to channel blockage or inactivation [175, 194, 235].

While a low dosage of menthol acts as a mouse TRPA1 agonist (section 2.3.8), higher concentrations (> 100 µM) are known to inhibit TRPA1 currents [227]. Interestingly, menthol is not able to inhibit human TRPA1 channels, even at high concentrations (3 mM). In addition, the structurally similar compound thymol exhibits mouse TRPA1 inhibition at higher concentrations as well (>250 µM) [227]. This species-dependent inhibition by menthol seems to involve the same TRPA1 region required for its activation (*i.e.* transmembrane segment S5) [228]. Specifically, the same glycine residue that is involved in TRPA1 activation by noxious cold (section 2.3.5) is required for TRPA1 inhibition by menthol [243]. Like menthol, other TRPA1 agonists have shown different responses between species as well. For example, caffeine can trigger mouse and rat TRPA1 gating (section 2.3.8), but it behaves as an inhibitor for human TRPA1 channels [178].

Stimulation with PG metabolites, such as 15d-PGJ2, leads to TRPA1 activation initially (section 2.3.6) but it is subsequently followed by a long-lasting channel inactivation [250].

2.4 TRPA1 in nociceptive neurons

TRPA1 is expressed in about 30 to 50% of the TRPV1-expressing neurons in dorsal root, trigeminal and nodose ganglia [174, 175]. Activation of TRPA1 channels (and TRPV1 channels as well) leads to the depolarization of these neurons and the development of action potentials that typically 'encode' pain-like sensations.

2.4.1 TRPA1 activation in nociceptive neurons

Subcutaneous injections of AITC, CA, MpBZ, H_2O_2, PGs, acetaldehyde, RNS-donors or 4-HNE activate TRPA1 channels in nociceptive neurons innervating the skin. TRPA1 activation in these neurons produces pain, neurogenic inflammation (*e.g.*, through the

release of substance P and calcitonin gene related peptide –CGRP), itch and hyperalgesia to mechanical and thermal stimuli [101, 102, 207, 210, 212, 213, 229, 251].

Inhalation-type general anesthetics induce bronchoconstriction and neurogenic pain [252]. Similarly, the inhalation of TRPA1 volatile agonists like acrolein, formaldehyde or Zn^{2+} induce cough, bronchoconstriction, mucous secretion and a decrease in respiratory rate, among other symptoms [253]. These nociceptive effects presumably occur after the activation of TRPA1 channels in C- and Aδ-fibers innervating the respiratory tract, as well as activation of TRPA1 channels in bronchial epithelial and smooth muscle cells [101]. In mouse models of allergen-induced asthma the airway hyperreactivity was significantly reduced in TRPA1-deficient mice [254]. Inhalation of umbellulone (a reactive compound produced by the 'headache tree') or hypochorite (an oxidative agent in chlorine gas) activates TRPA1 channels in trigeminal neurons innervating the nasal cavity. TRPA1-induced activation of these nociceptive neurons leads to an increase in blood flow in the meninges and the development of migraine headaches [225, 233].

In the gut, stimulation with TRPA1 agonists can increase the proportion of nociceptive neurons that express functional TRPA1 channels [255]. TRPA1 activation in these nociceptive neurons induces the release of pro-inflammatory neuropeptides and leads to mechanical hypersensitivity [255-258]. Impaired regulation of the immune responses in the gut typically underlies the development of inflammatory bowel diseases such as colitis and Crohn's disease [259, 260]. During these chronic inflammatory states, TRPA1 activation has been proposed to modulate, not only the pain responses, but the tissue inflammation as well [261, 262]. However, whether TRPA1 plays a protective or harmful role during inflammatory bowel diseases is still under debate.

Altogether, these findings support the increasing interest in the study of TRPA1 channels and their functional role in neuropathic pain, asthma, chronic obstructive pulmonary disease (COPD) and inflammatory bowel diseases (reviewed in [263-266]).

Notably, PGs, H_2O_2, low pH and byproducts of ROS/RNS damage constitute endogenous TRPA1 agonists that are commonly generated upon tissue stress or injury (Figure 2.2). Because TRPA1 agonists employ several different mechanisms to achieve channel gating or inactivation, the simultaneous exposure to multiple agonists leads to complex responses. While some agonists counter-react the activity of others (perhaps by

competing for the same binding sites), there are agonist combinations that lead to synergistic and potent responses. Moreover, some TRPA1 agonists eventually induce channel inactivation and therefore exert analgesic effects as well. For example, PG metabolites have biphasic responses in nociceptive neurons. Initially they activate TRPA1 channels and produce pain-like behaviors, but later they can provide analgesia against other nociceptive signals through a TRPA1-depenent mechanism [250]. In addition, TRPA1 activation by these endogenous agonists can be potentiated by cold exposure [241].
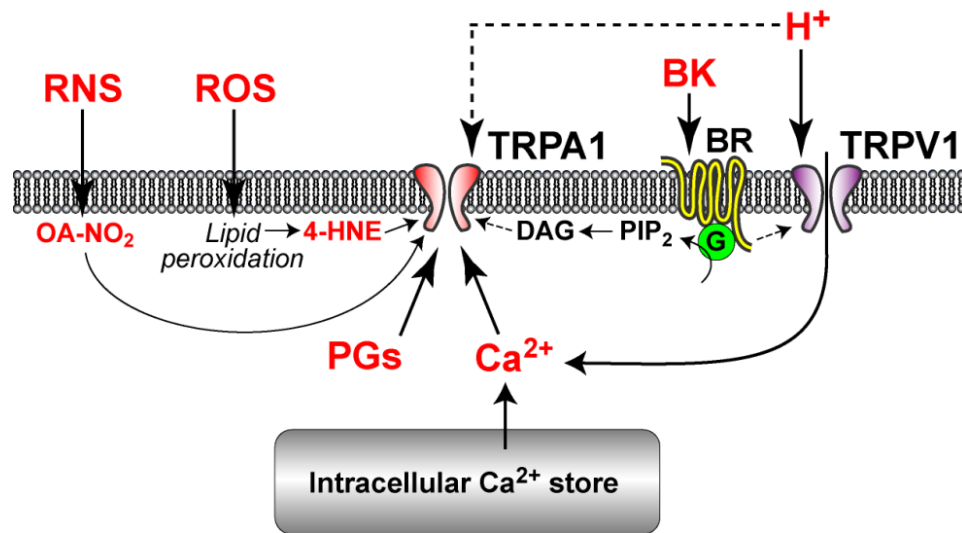
Figure 2.2. Pathways for TRPA1 activation after tissue damage

TRPA1 channels can be directly activated by byproducts of reactive oxygen (ROS) and nitrogen (RNS) species damage (*e.g.,* 4-HNE and OA-NO$_2$), weak acidosis, intracellular Ca^{2+} and prostaglandins (PGs). Additionally, TRPA1 channels can be activated downstream of G-protein coupled receptors (such as the bradykinin –BK– receptor –BR) via the activation of phospholipase C (and perhaps the generation of diacyl-glycerol –DAG). Activation of TRPV1 channels by tissue acidosis can also modulate TRPA1 activity (*e.g.*, secondary to the influx of Ca^{2+}).

2.4.2 Functional interplay between TRPA1 and TRPV1 channels

TRPV1 channels are gated by low pH (Figure 2.2), heat and capsaicin (the main pungent compound of chili peppers) (reviewed in [97]). Several studies have shown that TRPA1 and TRPV1 channels can cross-modulate each others' properties when co-expressed in the same cell (reviewed in [267]). This is of particular importance given the fact that TRPA1 expression in nociceptive neurons seems to be limited to the cells that express TRPV1 channels [174, 175].

TRPA1 and TRPV1 subunits can directly interact by forming heteromeric channels (section 2.2.5). However, it is still possible that the properties of homomeric TRPA1 and TRPV1 channels are regulated through close interaction of the channels in the plasma membrane or via intracellular second messengers. However, most reports showing the functional interplay between TRPA1 and TRPV1 cannot clearly distinguish between these two scenarios (*i.e.* heteromeric channels vs. cross-regulation of homomeric channels). Regardless of the exact mechanism of interaction, TRPA1-specific agonists clearly desensitize (although sometimes increase) responses to TRPV1 agonists when channels are co-expressed [268, 269]. The reverse interaction is also true since capsaicin desensitizes TRPA1-agonist currents. The potency of some TRPA1 agonists can be either lower or higher in cells co-expressing TRPA1 and TRPV1 [270]. Additionally, TRPA1 and TRPV1 single channel properties (conductance, open probability and current-voltage relationships) are modified in cells expressing both proteins [193]. A single point mutation affecting the permeability to Ca^{2+} in TRPV1 subunits is able to modify cell currents in response to TRPA1 agonists [271]. Moreover, TRPA1 channels might get internalized after stimulation with AITC via a mechanism that is inhibited by the expression of TRPV1 [268].

2.5 Regulatory mechanisms of TRPA1 function

TRPA1 channels can be activated and/or regulated by several G-protein coupled receptors (GPCRs) via the generation of second messengers. Some of the GPCRs known to modulate TRPA1 channel gating are the bradykinin receptor [212], m1 muscarinic acetylcholine receptor (m1AChR) [215], protease-activated receptor 2 (PAR2) [272, 273] and P2Y receptors (manuscript in preparation, Vélez-Ortega AC, *et al*., see Appendix D

for details). Notably, bradykinin is a potent pro-inflammatory peptide that induces vasodilation.

Phospholipase C (PLC) signaling downstream of GPCR activation modulates TRPA1 channels (Figure 2.2) as well as other members of the TRP family [212, 274]. Activation of PLC leads to the cleavage of phosphatidylinositol 4,5-biphosphate (PIP_2) from the plasma membrane and generates diacyl glycerol (DAG) and inositol 1,4,5-triphosphate (IP_3). Therefore, PLC stimulation could modulate TRPA1 activity via three mechanisms. First, PIP2 seems to inhibit TRPA1 channels and, therefore, PLC-mediated cleavage of PIP2 would remove such inhibition [273, 275]. Second, because IP_3 leads to the release of Ca^{2+} from intracellular stores, PLC activation could induce TRPA1 gating via the increase in cytosolic Ca^{2+} [212, 215]. Third, DAG application was shown to activate TRPA1 channels as well, but its mechanism of action remains unknown [212]. Interestingly, in the presence of phospholipase-A_2 (PLA_2) activity, DAG can be converted into arachidonic acid (AA), a precursor in the generation of PGs. AA, PGs and their metabolites could activate TRPA1 channels (see section 2.3.6). However, TRPA1 activation downstream of PLC does not seem to require the N-terminal cysteine residues that are involved in channel gating by these reactive agonists [202].

PAR2 and bradykinin receptors can also stimulate protein kinase A (PKA) [272, 273]. Activation of PKA might increase the translocation of TRPA1 channels into the plasma membrane which could explain the increase in TRPA1 currents after stimulation of PKA [276].

The toll-like receptor-7 (TLR7) is involved in innate immune responses. TLR7 recognizes single stranded RNA (*e.g.,* from viruses) and it is typically localized in the endosomes of immune cells (reviewed in [277]). However, TLR7 is also expressed in a subset of DRG neurons [278] and it can be activated by microRNAs (miRNAs). Moreover, miRNA-dependent activation of TLR7 in DRG neurons induces TRPA1 gating and nociceptive behavior in mice [279]. The mechanism of TLR7-mediated TRPA1 activation remains unknown but it does not seem to require the TLR7 intracellular signaling cascade.

Annexin A2 (AnxA2) is involved in the trafficking of proteins to and from the plasma membrane (reviewed in [280]). Recently, AnxA2 was shown to directly interact with

TRPA1 subunits and to be able to control the amount of TRPA1 expression in the plasma membrane (without altering *Trpa1* mRNA levels) [281]. Whether AnxA2-dependent expression of TRPA1 in the plasma membrane is regulated by PKA activity remains to be elucidated.

2.5 TRPA1 as a hair cell MET channel candidate

The inner ear sensory cells (*i.e.* hair cells) have particular cellular specializations (*i.e.* stereocilia bundles) in charge of detecting mechanical stimulation (sound in the cochlea and movement/acceleration in the vestibular system) (section 1.4.1). However, the molecular identity of the mechano-electrical transducer (MET) channel involved in this process is still unknown. Several candidate genes have been proposed in past years. In fact, the TRPA1 channel was proposed as a MET channel candidate in 2004 [177]. TRPA1 expression and channel properties strongly supported this hypothesis.

Trpa1 mRNA was detected in the mouse cochlear epithelium through *in situ* hybridization. Although Trpa1 mRNA was in fact present in the sensory hair cells, mRNA levels appeared to be significantly higher in the surrounding supporting cells (specifically, in Hensen's cells) [177]. Notably, TRPA1 channel properties seemed to perfectly mirror those of the hair cell MET channel: non-selective cation selectivity, average single channel conductance (~98 vs. ~100 pS) and current reduction by Ca^{2+} (53 vs. 54% reduction) [175]. Moreover, the MET channel blockers gentamicin, ruthenium red, Gd^{3+} and amiloride were also able to block TRPA1 channels. However, the half maximal inhibitory concentrations (IC_{50}) differed greatly between TRPA1 and MET channels for Gd^{3+} (0.1 vs. 10 µM) and amiloride (511 vs. 50 µM) [175, 282, 283].

In 2006, knockout mice generated by two independent groups ruled out TRPA1 as the MET channel. [101, 102]. In both groups, the pore-forming region of TRPA1 was deleted, which renders the subunits nonfunctional. The *Trpa1*$^{-/-}$ mice had defects in the nociception of mechanical, chemical and thermal noxious stimuli, yet they exhibited normal hearing and vestibular functions.

2.6 Research hypothesis and scope of the dissertation

Trpa1 mRNA is highly expressed in the inner ear [177], but this tissue is not considered to have prominent nociceptive innervation. Given that $Trpa1^{-/-}$ mice exhibit normal hearing and hair cell mechanotransduction [101, 102], the function of TRPA1 channels in the cochlear epithelium remains elusive.

Acoustic overstimulation leads to an increase in reactive oxygen species (ROS) in the cochlear epithelium (reviewed in [284]). The oxidative stress following a single event of noise exposure can last for several days or even weeks and lead to the accumulation of, among others, the lipid peroxidation byproduct 4-HNE [285]. Because 4-HNE could behave as an endogenous agonist for TRPA1 channels in the cochlea, *we hypothesized that cochlear TRPA1 channels act as sensors for oxidative damage after noise exposure.*

First, we sought to identify the specific cell types within the cochlear epithelium that expressed the TRPA1 gene and that contained functional TRPA1 channels (sections 4.1 and 4.2). Next, we evaluated the responses of the cochlear epithelium to direct application of TRPA1 agonists, such as 4-HNE (sections 4.3 to 4.8). Lastly, we attempted to unveil the physiological significance of the TRPA1-induced responses observed by using *in vitro* and *in vivo* approaches (sections 4.9 to 4.11).

Chapter 3 presents the experimental approaches used and Chapter 4 the results of the experiments and their analyses. In addition, Chapter 5 includes the discussion of the results of this project, taking into account the limitations of the study and possible future directions.

CHAPTER 3
Materials and methods

3.1 Mice

TRPA1-deficient mice ($Trpa1^{-/-}$) and control littermates ($Trpa1^{+/+}$) were a kind gift from Dr. David Corey and Dr. Kelvin Kwan (Harvard University) to the Frolenkov laboratory in 2006. These mice were then backcrossed with C57BL/6 mice. The $Trpa1^{-/-}$ mice, the pore-forming region (exons 22 to 24) was replaced with a vector containing an endoplasmic reticulum (ER) retention signal (KDEL), a stop codon, an internal ribosome entry site (IRES) and the human placental alkaline phosphatase (PLAP) gene as a reporter [102]. Genotyping of these mice was performed as previously published by our laboratory [286].

Given that $Trpa1^{+/-}$ mice have exhibited an intermediate phenotype in several tests [101], all experiments in these study were performed with either $Trpa1^{+/+}$ or $Trpa1^{-/-}$ mice. Therefore, two separate colonies of wild type ($Trpa1^{+/+}$ x $Trpa1^{+/+}$) and TRPA1-deficient ($Trpa1^{-/-}$ x $Trpa1^{-/-}$) breeding pairs were established and maintained. In some cases, to corroborate results obtained with the $Trpa1^{+/+}$ and $Trpa1^{-/-}$ mice from the two separate colonies, $Trpa1^{+/+}$ and $Trpa1^{-/-}$ mice were crossed, breeding pairs between F1 heterozygous ($Trpa1^{+/-}$) siblings were established and F2 $Trpa1^{+/+}$ and $Trpa1^{-/-}$ littermates were used for comparisons within experiments.

All animal procedures were approved by the Institutional Animal Care and Use Committee (IACUC) of the University of Kentucky (protocol 00903M2005).

3.2 Cochlear explants

3.2.1 Tissue dissection

Cochlear explants were isolated during the first postnatal week because cochlear hair cells die rapidly when tissue dissections are performed on or after the second postnatal week. Pups were placed in a cold chamber for 5 to 8 minutes and then decapitated. The skin around the skull and the facial bones were removed. Next, the skull and brain were cut into two hemispheres and placed in a plastic Petri dish with cold (~4-10°C) Leibovitz's L-15 medium (Gibco) were the tissue dissection was continued. The brain and the meninges were removed to expose the inner surface of the skull. The tympanic bullae were dissected out of the temporal bones and placed into a new Petri dish with fresh L-15 medium. The otic capsule was carefully removed and the cochlear epithelium was pulled away from the cochlear modiolus. At this stage, the cochlear epithelium has a tubular conformation thus, in order to flatten out the tissue, the Reissner's membrane was cut. This approach allowed the organ of Corti to remain attached to the outer supporting cells (*i.e.* Claudius' and spiral prominence cells) and the stria vascularis (Figure 3.1A). In contrast, for experiments where the outer supporting cells were not needed, the tissue was held by the spiral limbus while the stria vascularis was pulled away. This maneuver caused the tissue to tear at the level of the Claudius' cells but left the organ of Corti and inner supporting cells intact (Figure 3.1B).

Explants were either allowed to attach to glass-bottom Petri dishes (in experiments with cultured explants) or held by two glass fibers glued onto a coverslip (in experiments on freshly-isolated tissue).

3.2.2 Tissue culture of cochlear explants

For direct attachment of the cochlear explants onto glass-bottom Petri dishes (MatTek Corporation), each explant was placed on a dish with a small amount of culture medium (~ 200 µL), which consisted of Dulbecco's Modified Eagle's Medium (DMEM) (Gibco) supplemented with 7% fetal bovine serum (FBS) (Atlanta Biologicals) and 10 µg/mL ampicillin (Calbiochem). The small amount of medium was dispersed throughout the glass bottom making the liquid surface tension keep the cochlear explant in place. Dishes were temporarily sealed with Parafilm® M (Bemis Company, Inc.) to minimize liquid

evaporation and then placed in an incubator at 37°C and 5% CO_2 for 12-16 h. After this time, the explants had completely attached to the glass (Figure 3.1) so the Parafilm was removed and 2 mL of fresh culture medium were added to each dish. Explants were placed back in the incubator for 1-2 more days before imaging was performed.
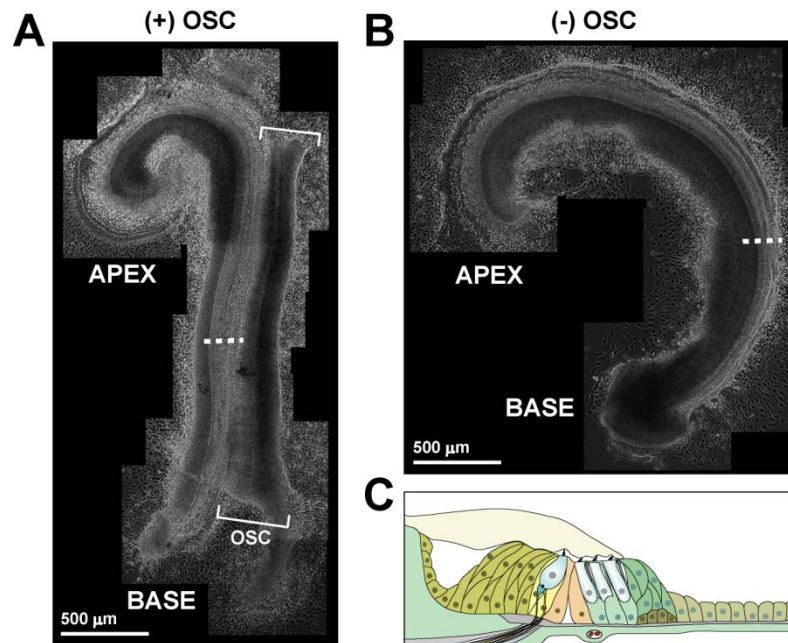
Figure 3.1. Cochlear epithelium attached to a glass-bottom dish

A, B, Several overlapping pictures were taken with a 10X objective to cover the entire length (from base to apex) of a cochlear epithelium with (*A*) or without (*B*) outer supporting cells and stria vascularis (OSC), attached to a glass-bottom Petri dish. *C*, As a reference, a diagram is provided to illustrate the tissue configuration at the cross sections indicated by the two dashed lines.

Often, changes in the morphology of the hair cell stereocilia bundles were observed in cultured cochlear explants that contained outer supporting cells and the stria vascularis (Figure 3.2). In some cases, the rows of OHCs were completely absent (data not shown), an indication that these cells had undergone apoptosis. In fact, a closer examination of the tissue revealed a large quantity of apoptotic cells within the stria vascularis after only 1 day in culture (Figure 3.3). Because cochlear explants that did not contain the outer supporting cells or stria vascularis appeared healthy, we believe the dying cells in the

stria vascularis had a noxious effect on the rest of the tissue. Therefore, as described in the following section, we designed a strategy that would allow us to study cochlear explants immediately after dissection.
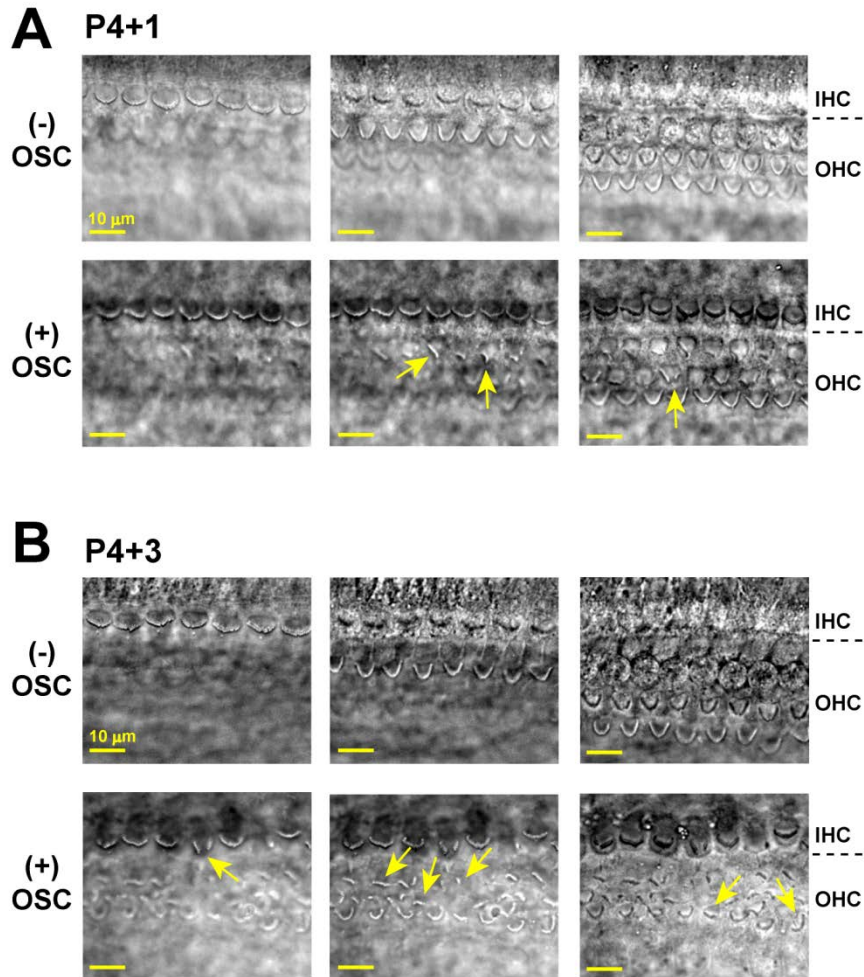
Figure 3.2. Cochlear explants cultured with outer supporting cells and stria vascularis exhibited morphological abnormalities

A, B, Bright field imaging of wild type cochlear explants dissected on postnatal day 4 (P4) and cultured without (*top*) or with (*bottom*) outer supporting cells for 1 (*A*) or 3 days (*B*). Three focal planes of each area are shown to highlight the stereocilia bundles of IHC (*left*) and OHC (*middle* and *right*). Arrow to some of the stereocilia bundles that did not exhibit normal morphology. *IHC*, inner hair cell; *OHC*, outer hair cell; *OSC*, outer supporting cells and stria vascularis.
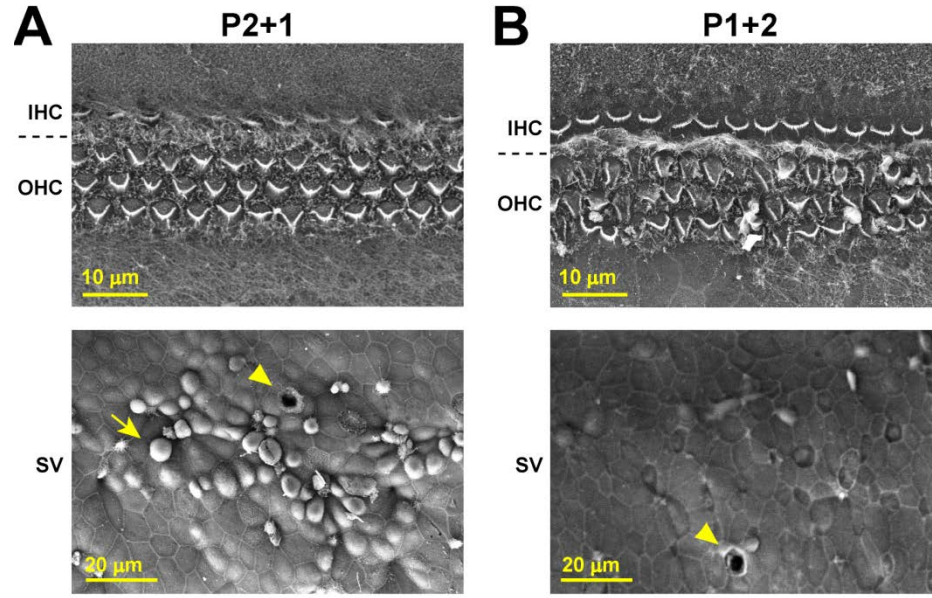
Figure 3.3. Apoptotic cells are observed in the stria vascularis during culture
A, B, Scanning electron micrographs of the organ of Corti (*top*) and stria vascularis (*bottom*) regions from wild type cochlear explants cultured for 1 (*A*) or 2 days (*B*). After 1 day in culture most stereocilia bundles appear normal while several abnormally swollen cells are observed in the stria vascularis (*arrows*). After 2 days in culture, the swelling in the stria was less noticeable but the hair bundle morphology was disorganized. Several 'holes' were observed in the stria (*arrow heads*), and they probably represent areas were apoptotic cells had been recently removed. *IHC*, inner hair cell; *OHC*, outer hair cell; *SV*, stria vascularis.

3.2.3 Freshly-isolated cochlear explants

To perform experiments in freshly isolated cochlear explants, it was necessary to keep the tissue from moving freely. To do so, thin glass fibers were pulled from glass capillaries (World Precission Instruments) using a P-2000 laser puller (Sutter Instrument). The pulled fibers measured ~1-2 cm in length and were fairly flexible. Two fibers were glued onto a glass coverslip (~2 cm in diameter) (Fisherbrand) using the silicone elastomer Sylgard® (World Precission Instruments). The coverslips were placed on a hot plate to quickly cure the elastomer (~3-5 min). Next, the coverslips were mounted on plastic or glass-bottom dishes using a small amount (~1-3 µL) of Sylgard®

and allowed to cure overnight (Figure 3.4A). The cochlear epithelium was placed under the two glass capillaries to keep it in place during imaging and patch clamp recordings (Figure 3.4B).
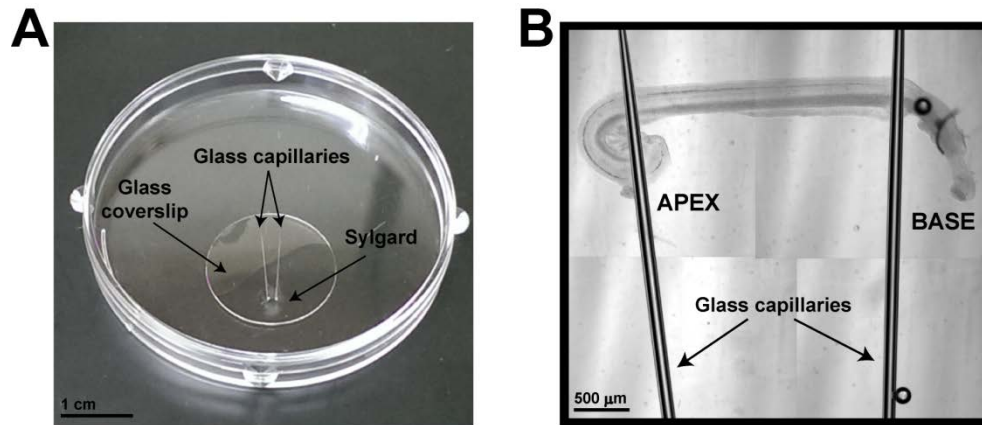
Figure 3.4. Freshly-isolated cochlear tissue held in place by glass capillaries
A, Dish configuration used to hold the cochlear tissue in place for experiments performed in freshly-isolated tissue. *B*, Cochlear tissue placed under the glass capillaries imaged with a 4X objective. Four overlapping images were taken to cover the area shown in the picture.

3.2.4 Identification of cochlear cell types

The highly organized architecture of the cochlear epithelium allows for the identification of its different cell types. Here, the steps to differentiate Hensen's from Claudius' cells will be used as an example.

i) First, the supporting cells types were identified by their location relative to the sensory hair cells in the *x* and *y* axes. The stereocilia bundles of the inner (IHC) and outer (OHC) hair cells are easily identified on the apical surface of cochlear explants (Figures 3.5A and 3.5B) and they provide the first reference about the position of all supporting cells. For instance, the Hensen's and Claudius' cells located toward the lateral side of the OHC (*i.e.,* the bottom of Figures 3.5A and 3.5C).

ii) Because different cell types are observed at different focal planes (Figure 3.5D), at the beginning of every experiment a stack of bright field images spanning the entire thickness of the explant was obtained, with images taken every 1 μm. This image stack

was used as reference during the data analysis. Hensen's cells are columnar cells organized in two (sometimes three) intercalated rows. The first row of Hensen's cells is the closest to the OHCs and is located at a higher *z* plane than the second row of Hensen's cells. In contrast, Claudius' cells are short cuboidal cells arranged in a flat configuration (one-cell thick).
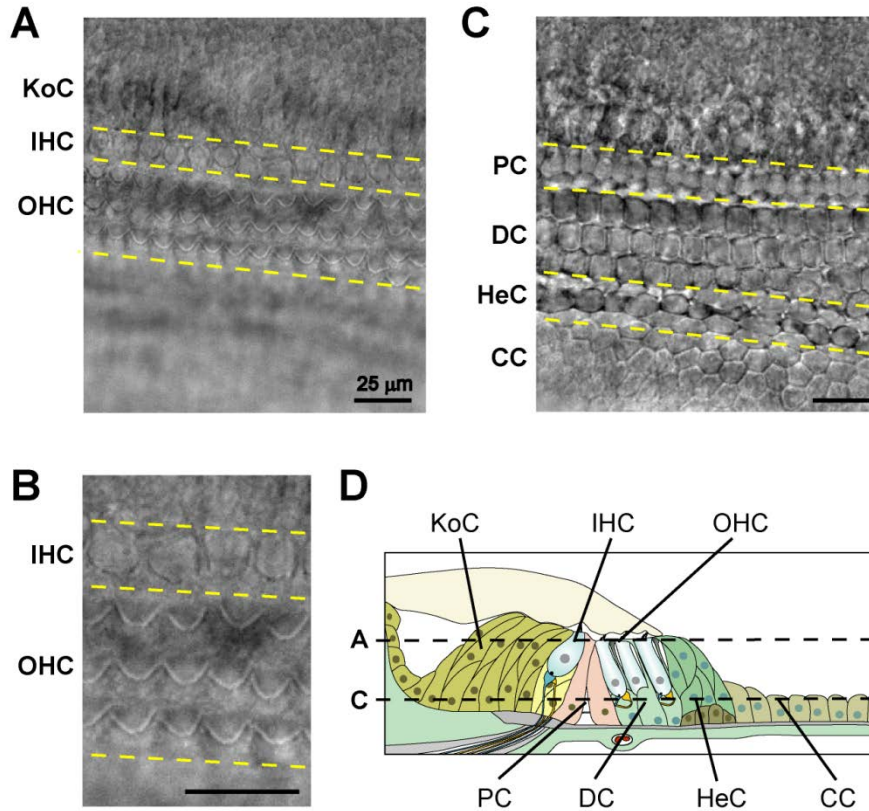
Figure 3.5. Representative bright field images of a cochlear explant taken at two different focal planes

A, Focal plane at the level of the hair cell stereocilia. One row of IHCs, three rows of OHCs and the cells of the Kolliker's organ (KoC) are visible. *B*, Higher magnification of a region from *A* highlighting the IHC and OHC stereocilia bundles. *C*, Focal plane below the hair cell bodies, where pillar (PC), Deiters' (DC), Hensen's (HeC) and Claudius' cells (CC) are visible. *D*, Diagram of a cross-section of the organ of Corti indicating the two focal planes shown in *A* and *C*.

iii) Lastly, the differences in cell morphology also allowed for the identification of boundaries between cell types. While a cross-section of a Hensen's cell exhibits a hexagonal yet almost ovoidal shape, a cross-section of a Claudius' cell looks like a hexagon with sides of similar length (Figure 3.5C).

3.3 Immunohistochemistry

3.3.1 PLAP immunolabeling

Cochlear explants were fixed in a 4% paraformaldehyde (PFA) (Electron Microscopy Sciences) solution in 1X phosphate-buffered saline (PBS) (Gibco) for 1-4 hours. Explants were washed with PBS containing 0.01% Triton-X (Electron Microscopy Sciences). Next, the tissue was placed in a blocking solution that consisted of 10% normal goat serum (NGS) (Invitrogen) in wash buffer for 1h at room temperature (RT). Explants were incubated overnight with a mouse anti-hPLAP clone 8B6 antibody (1:100) (Sigma-Aldrich) in blocking solution at 4°C in a humid chamber. Incubation with a goat anti-mouse Alexa Fluor 488 secondary antibody (1:1000) in blocking solution was performed at room temperature for 2h. Tissue was counterstained in 300 nM 4',6-diamidino-2-phenylindole (DAPI) (Invitrogen) in PBS for 5 min and mounted with ProLong® Gold antifade medium (Invitrogen). The imaging set up used is described in section 3.3.3.

One of the figures in Chapter 4 contains an image obtained by our collaborator K. Kwan (Rutger's University) (manuscript in preparation, Vélez-Ortega, *et al*.). He followed a similar protocol of PLAP immunolabeling. The only differences were in the secondary antibody used (goat anti-mouse Alexa Fluor 568), staining with 500 ng/ml Hoechst 33235 instead of DAPI, and adding phalloidin (1:400) counterstaining as well. His image was obtained with an Olympus FluoView 1000 scanning confocal microscope equipped with at 63X PlanSApo objective (1.42 NA), at 1024x1024 resolution with a pixel dwell time of 2-8 μs.

3.3.2 Immunolabeling of 4-HNE-modified proteins

Tympanic bullae (from noise-exposed and control mice) were perfused with a solution of 4% PFA in 1X PBS and kept for 1 to 4 h at 4°C before further dissection. Perfusion was performed through the oval window after making a hole in the apical end of the otic

capsule. Tissue dissection was performed in distilled water. Samples were washed with PBS and permeabilized for 10 min in a 1% Triton-X solution. Tissue was blocked for 45 min in 10% NGS in PBS and incubated with rabbit polyclonal anti-HNE (1:50) (Abcam) in blocking solution over night at 4°C. Incubation with the secondary mouse anti-rabbit Dylight 488 antibody (1:200) (Jackson Immunoresearch) was performed for 2 h at RT. Samples were counterstained with DAPI (600 nM) for 10 min and mounted in antifade medium. The anti-4-HNE antibody recognizes proteins that have been covalently modified by 4-HNE after oxidative stress. To test the performance of this antibody, we exposed cochlear explants to varying concentrations of hydrogen peroxide (H_2O_2) (Molecular Probes) over night (Figure 3.6).

3.3.3 Imaging set up

An upright Olympus BX51WI spinning disc confocal microscope was used. The microscope was equipped with a 100X LUMPlan FL objective (1.0 numerical aperture – NA) (Olympus), an Olympus U-RFL-T mercury arc lamp, a nanopositioning system for focal plane control (Mad City Labs) and the Evolve 512 EMCCD camera (Photometrics). The camera was used at its full chip resolution (512x512) and digitization (16-bit). The filter cubes used allowed for excitation and emission bandwidths for Alexa Fluor 488, Dylight 488 (488/20 nm and 525/50 nm) and DAPI (350/50 and 460/50 nm) (Olympus). The MetaMorph for Olympus Imaging Series v.7.7 (Molecular Devices) was used for imaging acquisition. All imaging settings (*e.g.,* exposure, gain, readout speed) were kept identical between different samples.

3.4 Drug delivery

3.4.1 Stock and working solutions of the drugs used

ATP and several TRPA1 agonists (4-HNE, CA and AITC) were used for tissue stimulation during different experiments.

4-HNE (Cayman Chemical) was purchased at a 64 mM concentration in ethanol, and 1 μL of this solution was mixed with 320 μL of bath medium to achieve a 200 μM working solution. The 4-HNE stock was stored at -80°C and working solutions were made fresh each time.
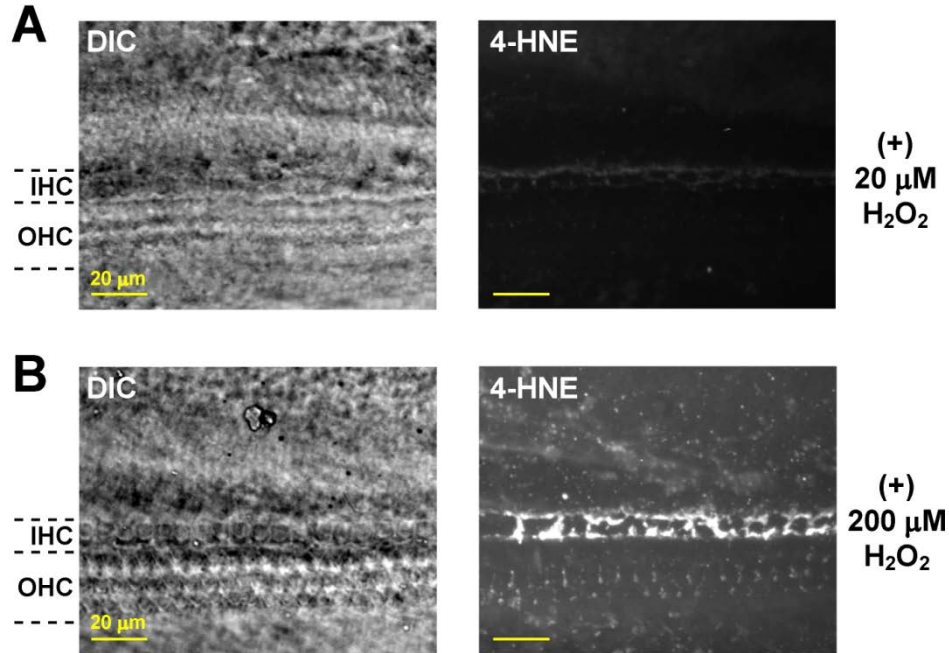
Figure 3.6. Performance test of the 4-HNE antibody

A, *B*, Immunolabeling with the anti- 4-HNE antibody was performed in cochlear explants exposed to 20 (*A*) or 200 µM H_2O_2 (*B*) for ~12 h. Bright field images (*left*) and maximum intensity projections of 4-HNE immunofluorescence (*right*) are shown. Notice that the levels of 4-HNE immunolabeling are higher in the cells exposed to the higher H_2O_2 concentration. In particular, supporting cells surrounding the IHCs show the brightest labeling. *IHC*, inner hair cells; *OHC*, outer hair cells.

CA (Sigma-Aldrich) was dissolved in 60% ethanol to make a 100 mM stock solution (6.3 µL of a 1.05 g/mL CA solution were mixed with 1 mL of 60% ethanol). This stock solution was kept at 4°C and used for up to a week. Working solutions (100 µM) were made by mixing 1 µL of the stock solution with 1 mL of bath medium and made fresh each time.

A 95% AITC solution (Sigma-Aldrich) was dissolved in 60% ethanol to make a 200 mM stock solution (4.9 µL of AITC with 250 µL of 60% ethanol). 1 µL of the stock solution was mixed with 2 mL of bath medium to achieve a working solution at 200 µM. AITC stock solutions were stored at -80°C.

55

ATP-Na$_2$ (Sigma-Aldrich) was diluted in distilled water (Gibco) to a 1 mM concentration (stock solution) and stored at -80°C in small aliquots to avoid thawing-freezing cycles. To achieve their final concentration (2 to 250 µM), ATP aliquots were diluted with bath medium immediately before use.

3.4.2 Glass micro-pipettes

Micro pipettes were pulled from glass capillaries (World Precission Instruments) using a P-2000 laser puller. Capillaries were made of borosilicate glass, 10 cm long, fire polished, contained an internal filament (to facilitate filling with liquid) and outer/inner diameters of 1/0.58 mm. Small diameter (~ 2-3 µm) pipettes were used during the Ca^{2+} imaging experiments while pipettes with larger diameters (~ 6-8 µm) were used during the patch clamping experiments.

3.4.3 Puff stimulation

Glass micro-pipettes were used to stimulate small tissue areas on the cochlear explants with ATP (2 to 250 µM, Sigma-Aldrich) or with the TRPA1 agonists 4-HNE (200 to 400 µM, Cayman Chemical), CA (100 to 200 µM, Sigma-Aldrich) and AITC (100 µM, Sigma-Aldrich). These drugs were always dissolved in the same type of solution present in the bath. The pipette tips were placed ~8 to 10 µm above the tissue surface using a MP-285 micromanipulator (Sutter Instrument).

A pneumatic pico-pump (World Precision Instruments) was used to apply pressure at the back of the pipette and, for fine pressure control, a TraceableTM manometer gauge (Fisher Scientific) was placed in the tubing line between the pico-pump and the pipette. The pico-pump was triggered by a 5 V transistor-transistor logic (TTL) signal delivered by a data acquisition (DAQ) board (National Instruments) controlled by the Clampex or Metamorph software. The delay in the puff stimulation was estimated to be ~ 40 ms (Figure 3.7).
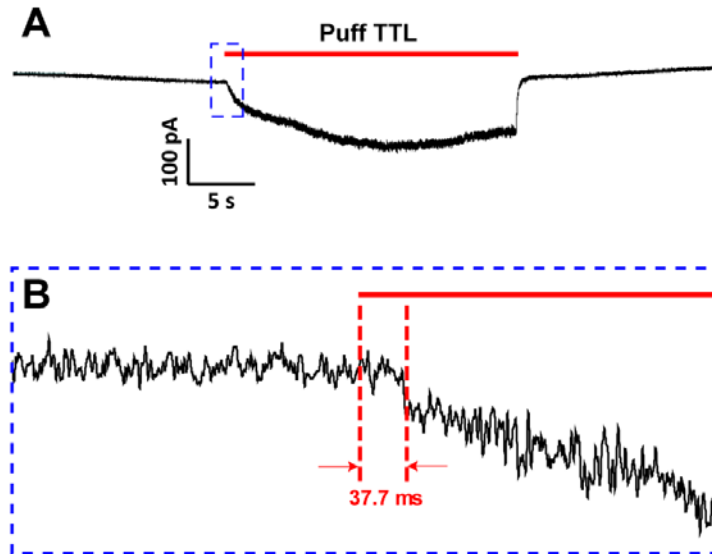
Figure 3.7. System delay during puff stimulation

A,B, The delay between the TTL trigger and the beginning of drug delivery was measured by placing a puff pipette filled with a 2 M KCl solution ~10 μm away from a patch clamping electrode (see section 3.7) connected to a patch amplifier. Changes in the standing current through the electrode were induced after the puff stimulation *(A)* and they typically started ~40 ms after the TTL pulse was delivered *(B)*.

The area to be stimulated was determined by the size of the pipette tip and the pressure applied at the back of the pipette (Figure 3.8). Typically, the pressure applied ranged between 2 to 4 kPa.

3.5 FM1-43 labeling

The use of the small cation dye FM1-43 to assess for the presence of functional TRPA1 channels in cochlear hair cells was previously reported by our laboratory [286]. Briefly, cochlear explants from wild type and *Trpa1$^{-/-}$* mice were pre-treated with 10mM 1,2-Bis[2-aminophenoxy]ethane-N,N,N′,N′-tetraacetic acid (BAPTA) (Sigma-Aldrich) in Ca^{2+}-free Hank's balanced salt solution (HBSS) (Gibco) for 10 min. Next, cochlear explants were incubated with 5 μM FM1-43 for 30 s in Ca^{2+}-free HBSS and immediately washed with standard HBSS.
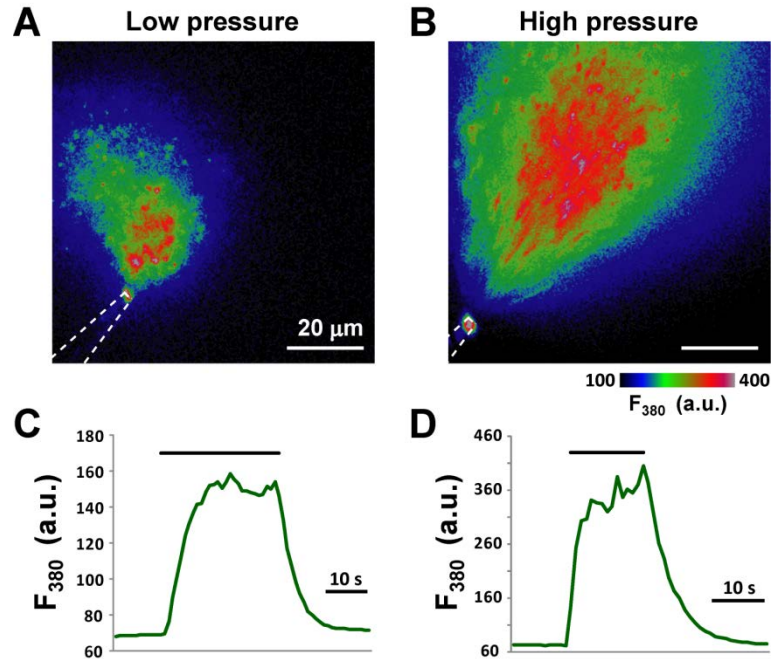
Figure 3.8. Puff stimulation area

A-D, Two pipettes were filled with fluorescent dye (Fura-2) to mimic drug delivery. Notice how the area of puff stimulation changes between low (*A*) and high (*B*) puff pressures. In addition, the increase and decrease in fluorescence during the stimulation with low (C) and high (D) puff pressure is shown. Notice the time correlation between the changes in fluorescence and the TTL pulse (black line) in both conditions. *a.u.*, arbitrary units.

Imaging was performed within 30 min after the incubation with the FM1-43 dye, and it was performed in standard HBSS at RT. The same set up described in section 3.3.3 was used, but the microscope was equipped with a 60X LUMPlan FL N objective (1.0 NA) (Olympus) and with filter cubes for 488/20 nm emission and 525/50 nm excitation (Olympus). Imaging acquisition settings were kept identical between different samples.

3.6 Ratiometric calcium imaging

3.6.1 Loading cells with the Ca^{2+} indicator

Cochlear explants were loaded with the membrane-permeable ratiometric Ca^{2+} indicator: fura-2-acetoxymethyl ester (AM) (Invitrogen). To help solubilize the dye, 50 μg of fura-2-AM were dissolved in 10 μL of a 20% Pluronic acid solution in DMSO

(Invitrogen). This 5 mM stock solution of the dye was stored at < -15°C for up to a month and limited to 3 thawing-freezing cycles. Before each experiment, the stock solution was thawed in a 37°C bath (~20 min) and vigorously mixed (vortexed for ~5 min). The cochlear explants were incubated in L-15 medium containing 2 µL of the stock solution (*i.e.*, 10 µM concentration of the fura-2 dye) for 50 min at RT. Explants were washed and then incubated in fresh L-15 medium for 20 min to allow the complete de-esterification of the dye. Imaging was performed immediately after, in L-15 medium at RT. For some experiments, 50 µM pyridoxalphosphate-6-azophenyl-2',4'-disulfonic acid (PPADS) was added to the bath solution before imaging.

3.6.2 Live cell imaging

Imaging was performed using the set up described in section 3.3.3. However, instead of the mercury arc lamp, the Lambda DG-4 system (Sutter Instrument) was used to control the fast switching between illumination at 340 and 380 nm. Therefore, because the Lambda DG-4 illumination path bypassed the spinning disk unit of the microscope, it was not possible to perform ratiometric Ca^{2+} imaging in a confocal mode. A filter cube in the microscope allowed the emission at 510/80 to be captured by the camera. Three different objectives were used: 40X 0.8 NA (LUMPLFLN40X/W), 60X 1.0 NA (LUMPLFLN60X/W) and 100X 1.0NA (LUMPLFL100XW/IR) (Olympus). In addition, sometimes a secondary custom-made 2X magnification lens was added in the infinity-corrected light path of the microscope. Alternating images between the 340 (F_{340}, Ca^{2+}-bound dye) and 380 nm (F_{380}, Ca^{2+}-free dye) illuminations were obtained to assess changes in intracellular Ca^{2+} levels. At the beginning of each experiment image stacks for the F340 and F380 illuminations were take every 1 µm and covered the entire thickness of the tissue. These stacks were used as references –for cell types and positions– during the data analysis.

3.6.3 Image analysis

Image analysis was performed using the ImageJ software [287] and the Ratio Plus plugin (http://rsb.info.nih.gov/ij/plugins/ratio-plus.html). Each ratio image (R) was obtained by dividing corresponding pixels between the F_{340} and F_{380} images (F_{340}/F_{380}).

Background subtraction for the independent signals was not performed given that the background light was several orders of magnitude smaller than the fura-2 signal. The error that this background light introduced in the ratio measurements was calculated to be around 0.006%. To enhance the changes in intracellular Ca^{2+} with time, ratio images were normalized to the first ratio obtained in the series (R/R_0). A pixel value of 1 would indicate no change in intracellular Ca^{2+} was evident. Instead, a pixel value of 2 would correspond to an increase in intracellular Ca^{2+} but not necessarily a doubling in the amount of Ca^{2+}.

3.6.4 Calculating free Ca^{2+} concentrations from F_{340}/F_{380} ratios

Within each experiment, exposure and gain settings were kept identical for the F_{340} and F_{380} images. However, different objectives and illumination intensities were used between different experiments (Table 3.1), thus a different calibration curve was generated for each situation.

Table 3.1. Imaging conditions used during ratiometric Ca^{2+} imaging

Objective	Extra magnification	F_{340} intensity*	F_{380} intensity*	R^2 value of calibration curve
40X	2X	50%	$< 33\%$ [†]	0.9979
		100%	33%	0.9981
60X	No	100%	33%	0.9989
	2X	100%	33%	0.9872
100X	No	50%	100%	0.9971

* F_{340} and F_{380} intensities are controlled by changing the optical alignment of two galvanometers in the Lambda DG-4 illumination system. Factory preset values are provided to achieve 100%, 50% and 33% of the maximum output for each channel.

† The alignment of the Lambda DG-4 galvanometers was modified. The F_{380} intensity was lower than 33% but the exact value was not determined.

Briefly, a Ca^{2+} calibration buffer kit (Molecular Probes) containing eleven dilutions with free Ca^{2+} ranging from 0 to 39 µM was used to generate calibration curves for all imaging conditions used. Fura-2 pentapotasium salt (Invitrogen) was added to each calibration dilution at a final concentration of 10 µM. To minimize errors, a small volume of the fura-2 dye (6 µL) was added to a large volume of the calibration dilution (2 mL). Next, 300 to 500 µL of each dilution were placed on a Petri dish and F_{340} and F_{380} images were acquired. Special care was taken during imaging acquisition to keep the z position constant between samples.

To determine the dissociation constant (K_d) of the fura-2 indicator, the $Log\left([Ca^{2+}]_{free}\right)$ of the calibration dilutions were plotted (x axis) against $Log\left(\frac{[R - R_{min}]}{[R_{max} - R]} \times \frac{F_{380\,max}}{F_{380\,min}}\right)$ (y axis), where R is the F_{340}/F_{380} ratio for each dilution, R_{min} the F_{340}/F_{380} ratio for the Ca^{2+}-free dilution (0 µM), R_{max} the F_{340}/F_{380} ratio for the saturating Ca^{2+} dilution (39 µM), $F_{380\ max}$ the F_{380} value for 0 µM Ca^{2+} and $F_{380\ min}$ the F_{380} value for 39 µM Ca^{2+}. All graphs resulted in straight lines (R^2 values greater than 0.987) (Figure 3.9 and Table 3.1) where the x intercepts corresponded to $Log\ (K_d)$. Lastly, free intracellular Ca^{2+} concentrations were estimated from experimental F_{340}/F_{380} ratios (R_{Exp}) by using the Grynkiewicz equation [288]:

$$[Ca^{2+}]_{free} = K_d^{EGTA} \times \frac{[R_{Exp} - R_{min}]}{[R_{max} - R_{Exp}]} \times \frac{F^{380}_{max}}{F^{380}_{min}}$$

3.7 Patch clamping recordings

Glass micro-pipettes were pulled from glass capillaries using the P-1000 heating filament puller (Sutter Instrument). Typically, pipettes exhibiting a resistance of 5 to 12 MΩ were used.

In some cases, to gain access to a particular cell within the tissue, it was necessary to remove neighboring cells. For instance, OHCs and Deiters' cells were removed to clear the access to the lateral wall of the pillar cells. The intracellular solution used in the patch pipettes contained (in mM): KCl (12.6), KGlu (131.4), MgCl$_2$ (2), EGTA (0.5), K$_2$HPO$_4$ (8), KH$_2$PO$_4$ (2), Mg$_2$-ATP (2) and Na$_4$-GTP (0.2). The osmolarity and pH of the

intracellular solution was adjusted to match that of the bath solution (typically, 310 mmol/kg and pH 7.4). After achieving a whole-cell configuration, the cell contents were allowed to equilibrate with the patch pipette fluid for 5 min before any recordings were performed. All recordings were performed at room temperature.
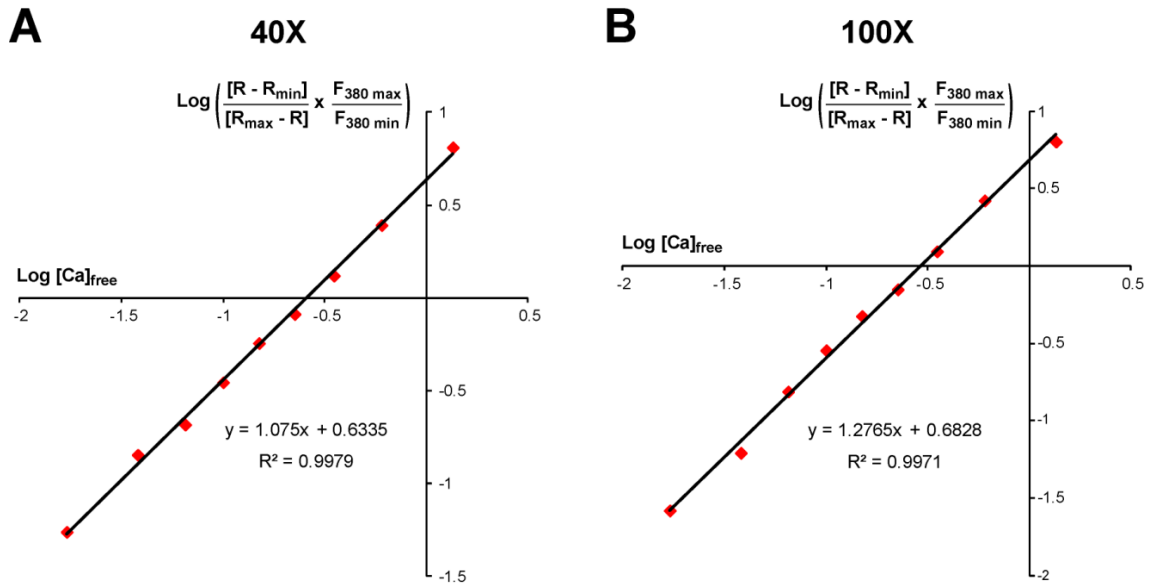
Figure 3.9. Calibration curves for the fura-2 dye

A, B, Calibration curves from 2 (out of 5) settings are shown: 40X objective (with 2X extra magnification) with 50% F_{340} and < 33% F_{380} intensities (*A*), and 100X objective with 50% and 100% intensities (*B*). Values obtained for each dilution were plotted (red diamonds) and data were fitted using a linear regression.

Because all supporting cells are electro-chemically coupled (Figure 3.10), patch clamp recordings had to be performed in the presence of a gap junction blocker. Some of the blockers tested were carbenoxolone disodium salt (CBX) (Sigma-Aldrich) [289], octanol (Sigma-Aldrich) [290] and flufenamic acid (FFA) (Fluka, Sigma-Aldrich) [291]. These gap junction blockers were tested in the bath solution, the intracellular solution, or both. CBX (100 – 500 μM) failed to block the propagation of a fluorescent dye from the patched cell to its neighboring cells (indicating an incomplete block of gap junctions) (Figure 3.11). Octanol seemed to completely block the gap junctions at high

concentrations (1 mM) but impaired cell survival (data not shown), and thus limited the duration of the recordings. However, 100 μM FFA provided a long-lasting blockage of gap junctions without inducing the cell death observed with octanol. Therefore, 100 μM FFA was added to the bath solution (*i.e.* L-15 medium) for all patch clamp experiments. A stock solution of 100 mM FFA in DMSO was kept in small aliquots at -80°C for no more than 4 weeks and freezing/thawing cycles were avoided.
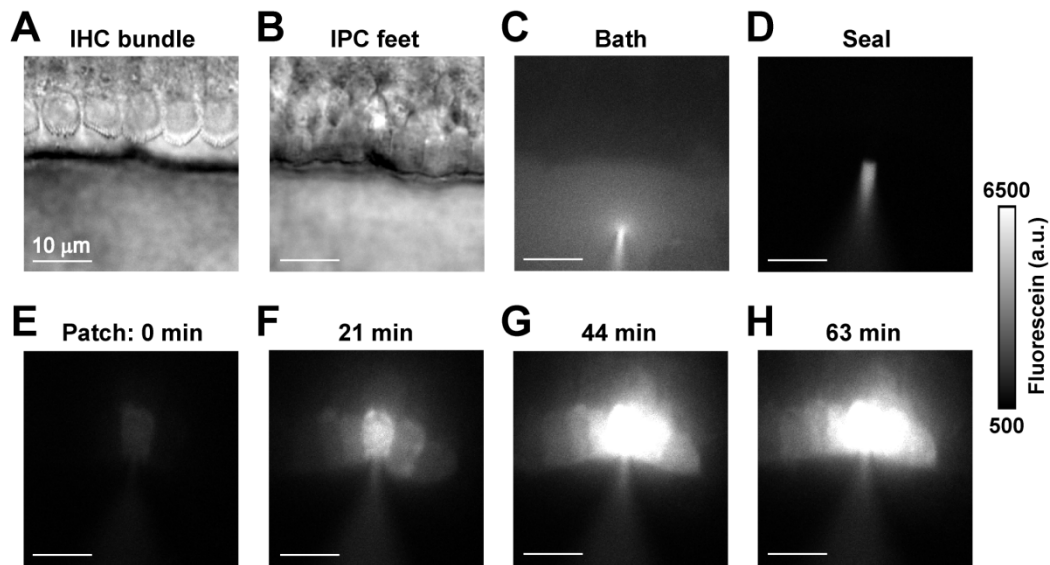
Figure 3.10. Supporting cells are electrochemically coupled via gap junctions
To test the extent of the gap junctional conductance in the cochlear epithelium, 265 μM fluorescein sodium salt (Sigma-Aldrich) was added to the intracellular solution. The results obtained when patching an inner pillar cell (IPC) are shown. *A, B,* Bright field images at the level of inner hair cell (IHC) stereocilia (*A*) and IPC feet (*B*) show the tissue after the removal of the neighboring outer hair cells and Deiter's cells. *C,* The patch pipette in the bath solution shows the leakage of the fluorescent dye. *D,* During the gigaohm seal, no leakage of the fluorescent dye is observed. *E-H,* Whole-cell voltage-clamp configuration of an IPC showing the fluorescent dye within the cell immediately after breaking the membrane (*E*) and its diffusion to neighboring cells 21 (*F*), 44 (*G*) and 63 min (*H*) later.

The microscope described in section 3.3.3 was used, equipped with either a 60X or 100X objective (1.0 NA). A headstage preamplifier was mounted onto MP-285 micromanipulators. During the experiment, the tissue was observed with a Hitachi 1/2" surveillance video camera.

The MultiClamp 700B amplifier together with the pClamp 10 software (Molecular Devices) were used for the patch clamp recordings. The 'membrane test' feature in pClamp was used to monitor (*i*) pipette resistance, (*ii*) patch resistance (*i.e.* gigaohm seal formation) and (*iii*) cell parameters during the whole-cell configuration (*e.g.*, cell resistance, membrane capacitance, and access resistance). These parameters were measured by delivering a 10 mV square pulse at 100 to 500 Hz.
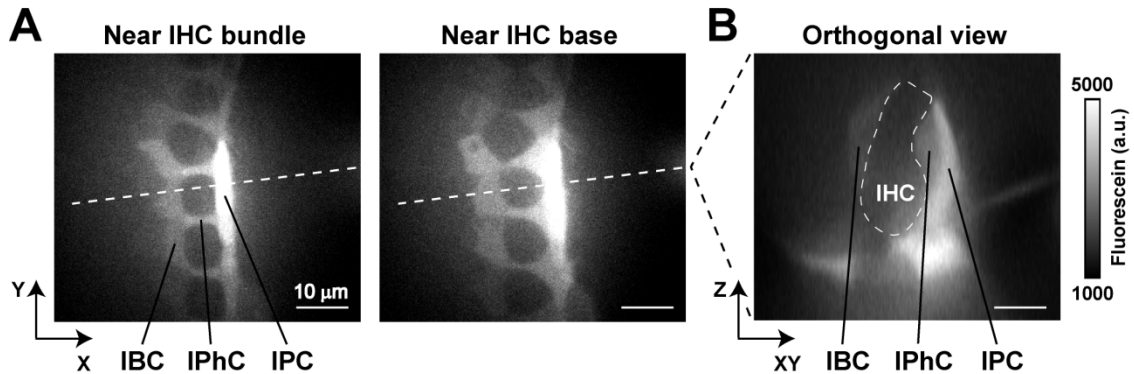
Figure 3.11. CBX fails to block the diffusion of a fluorescent dye between supporting cells

A, An inner pillar cell (IPC) was patch clamped and the fluorescein dye (265 µM) present in the intracellular solution diffused to neighboring cells even in the presence of 500 µM CBX in the intracellular solution. Images at two focal planes are shown: immediately below the inner hair cell (IHC) bundles (*Left*) and near the IHC base (*Right*). *B*, Orthogonal view from the plane indicated with a dashed line in *A*. The patch pipette on the lateral side of the IPC is visible, and also the propagation of the fluorescent dye to cells located on the medial side of the IHC. *IBC*, inner border cell; *IPhC*, inner phalangeal cell; *IPC*, inner pillar cell.

Preliminary experiments were performed to compare several cell parameters between different types of cochlear supporting cells: inner pillar (IPC), outer pillar (OPC), Deiters' (DC), Hensen's (HeC) and Claudius' cells. After achieving a whole-cell configuration, current-voltage (IV) relationships were evaluated using voltage steps from -90 to +90 mV, with steps every 15 mV. These preliminary results indicated differences in membrane capacitance and resting membrane potentials between the different supporting cells (Figure 3.12). These results were used to decide the holding potentials and voltage protocols applied to each cell type. The holding potentials (in mV) were defined as: -40 to -50 (IPC), -20 to -30 (OPC), -10 to -20 (DC) and 0 to +10 (HeC).
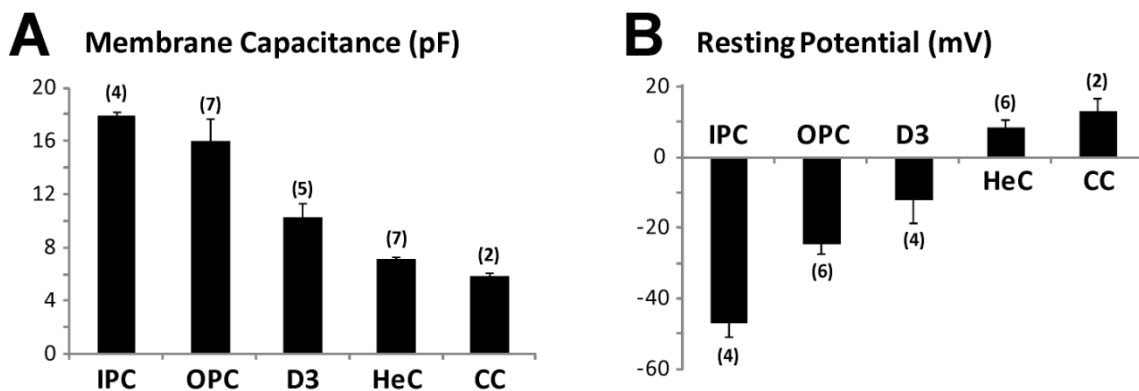
Figure 3.12. Electrophysiological characteristics of cochlear supporting cells
A, B, Average values of membrane capacitance (*A*) and reversal potential (*B*) for the different types of cochlear supporting cells. The numbers of cells averaged are shown within parenthesis above each bar. *IPC*, inner pillar cells; *OPC*, outer pillar cells; *D3*, Deiters' cells from the third row; *HeC*, Hensen's cells; *CC*, Claudius' cells.

Current responses to the puff stimulation with 100 CA were evaluated during a step voltage to -90 mV. In addition, 300 ms ramps from -90 mV to +90 mV were delivered before, during and ~5 min after puff stimulation. Data analysis was performed using the Clampfit 10 software.

3.8 Laser uncaging

3.8.1 Set-up configuration

The microscope described in section 3.3.3 was equipped with a 355 nm diode pumped solid state laser (DPSL-355/30 system, Rapp OptoElectronic) and a 100X LUMPlan FL N (1.0 NA). Using a fiber optic with a diameter of 50 μm, a laser spot size of ~10 μm was achieved (Figure 3.13). Throughout the experiment, cell currents were measured using the Clampex 10 software, and alternating bright field and Ca^{2+} imaging were recorded using the Metamorph software. The Ca^{2+} indicator fluo-4 (Molecular Probes) and a filter cube for 535/45 emission and 475/40 nm excitation were used for intracellular Ca^{2+} imaging.
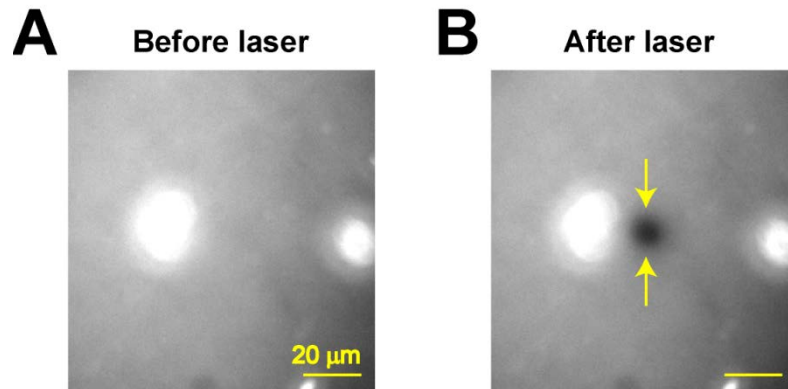
Figure 3.13. Laser spot size

A, Fluorescing grease mounted onto a glass microscope slide (Rapp OptoElectronic) was used to measure the size of the laser spot. *B,* A short laser pulse stimulation left a burned spot on the grease that was used to focus the laser, until a final ~10 μm laser spot was achieved.

3.8.2 Ca^{2+} uncaging in pillar cells

A photolabile Ca^{2+} chelator, nitrophenyl EGTA (NP-EGTA) (Molecular Probes), was delivered to cells via a patch pipette. The intracellular solution contained (in mM): KCl (12.6), KGlu (131.4), $CaCl_2$ (0.7), NP-EGTA (1), K_2HPO_4 (8), KH_2PO_4 (2), Na_4-ATP (2), Na_4-GTP (0.2) and fluo-4 (0.05). L-15 medium supplemented with 100 M μFFA was used as the bath solution. Outer pillar cells were patched at their basolateral membrane

near their feet. Cells were held at their resting potential ~-40 mV throughout the experiment. In control experiments, NP-EGTA was replaced with EGTA.

Baseline recordings were performed for 100 to 300 s before the laser stimulation, and continued for >500 s after that. Laser UV stimulation was performed with 15 to 25 pulses, 1 ms each, delivered at 166 Hz. Intracellular Ca^{2+} and cell diameter were measured by monitoring fluo-4 fluorescence and bright field imaging, respectively, during the experiment. For details about the cell diameter measurements, see section 3.9.3.

3.9 Measurement of tissue displacements and cell contractions

3.9.1 Imaging set-up and software

The microscope described in section 3.3.3 was equipped with a 100X objective (1.0 NA), a halogen bulb lamp (Olympus) and cubes for differential interference contrast (DIC) imaging (Olympus). Time-lapse bright field imaging was performed simultaneously with the ratiometric Ca^{2+} imaging (section 3.6) and during the laser uncaging experiments (section 3.8).

3.9.2 Tissue displacement measurements

TRPA1 activation caused tissue displacements evident during bright field imaging. These tissue movements let to changes in the pattern of light scattering. Therefore, images were analyzed using the ImageJ software [287]. Bright field frames that were taken 10 s apart were subtracted to enhance any movement in the tissue. In the subtracted images (32-bit), pixel values of 0 represented no movement between the two frames, while positive and negative values indicated the presence of tissue displacements. The standard deviation in the pixel values was measured within regions of interest and plotted against time. Due to differences in light intensity, scattering patterns and contrast between samples, results of different experiments were normalized and areas under the curve (A.U.C.) were calculated. Within each experiment, comparisons were made between frames taken before and after the TRPA1 agonist application.

3.9.3 Measuring cell diameters

Bright field images were used to measure cell diameters using a method previously published for OHC electromotility quantification [292]. In summary, pixel intensity profiles were obtained from lines placed across the cells of interest (Figure 3.14A). These measurements were performed for each time frame using the MetaMorph software and its linescan feature (Figure 3.14B).
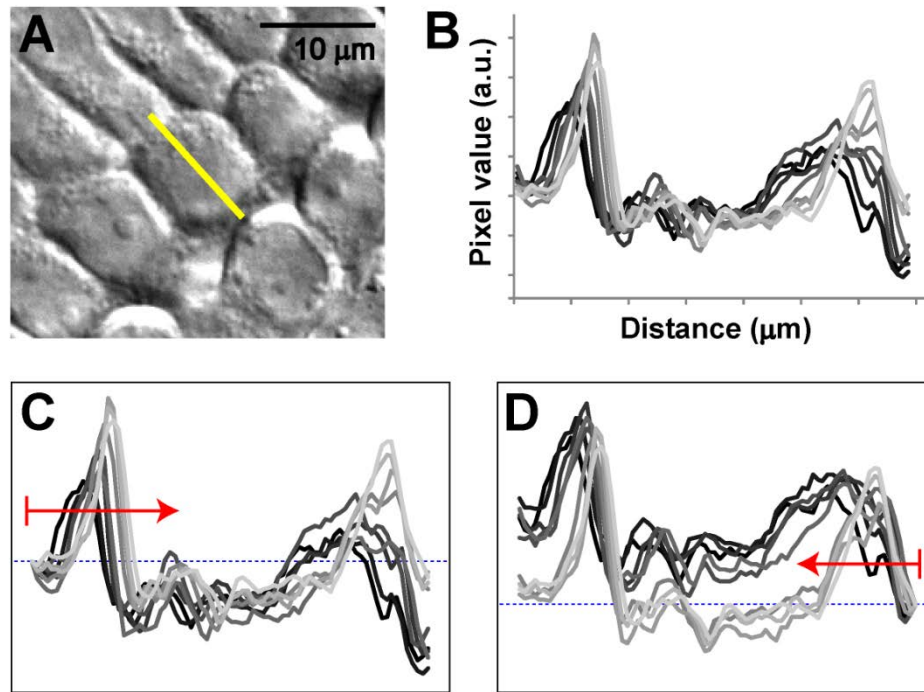
Figure 3.14. Cell diameter measurements

A, Bright field image showing the line used to measure the pixel value profile.
B, Pixel value profiles for the line shown in *A* at different time points (from black to light grey). *C, D*, Cell edge movements were quantified by placing a horizontal line (red line) and finding the first point where each pixel profile was crossed. To do so, line profiles were aligned on the side to be measured (left edge in *C* and right edge in *D*).

Cell edge movements were quantified using algorithms written in the Matlab software. Pixel values along each line were interpolated to increase the number of points by 50 times. Movements at both edges of the cell were quantified after aligning the line profiles

on the side to be measured (Figures 3.14C and 3.14D). The first point crossing a horizontal line (placed by the user) was used to calculate the position of the cell edge. Based on the movement of each edge and the original size of the line, the changes in cell diameter were calculated.

3.10 Auditory brainstem responses (ABR)

3.10.1 Mouse anesthesia

Young adult mice (3 to 4 week old) were anesthetized with intraperitoneal injections of 2,2,2-tribromoethanol (Avertin) (Sigma-Aldrich) at a dosage of 0.4 mg/g of body weight. When required, a 0.1 mg/g boost was injected. Mice were kept on a heated plate during the experiment.

3.10.2 ABR recordings

Subdermal needle electrodes were positioned at the base of each pinna (positive and negative electrodes) and on the top of the head (ground electrode). A speaker (MF-1, Tucker-Davis Technologies) was placed in front of the mouse, 1 inch away from the center of the head.

An Auditory Workstation coupled with the BioSigRP software (Tucker-Davis Technologies) was used to deliver 3 ms tones of a specific frequency (8, 16, 24 and 32 kHz) and sound pressure level decibel (SPL dB). Tones were presented at 200 Hz and with alternating polarity. A threshold was established to reject signals that included outlier signals (*e.g.*, the QRS wave from the heart electrocardiogram). ABR signals were averaged 512 to 1024 times for each frequency and SPL value. A half-interval search algorithm was used to determine the hearing threshold value for each frequency, with a final ~ 3 SPL dB resolution. For conditions where no hearing threshold was detected, the highest SPL value evaluated was assigned (*i.e.* 112 SPL dB). Hearing thresholds were measured before and several time points after noise exposure (Figure 3.15).

A **Baseline**   **B** **Imm. after noise**   **C** **2wk after noise**

50 dB

40 dB

35 dB

30 dB

27 dB

25 dB

1 μV

2 ms

100 dB

95 dB

93 dB

92 dB

91 dB

90 dB

80 dB

70 dB

60 dB

55 dB

52 dB

50 dB

47 dB

45 dB

40 dB
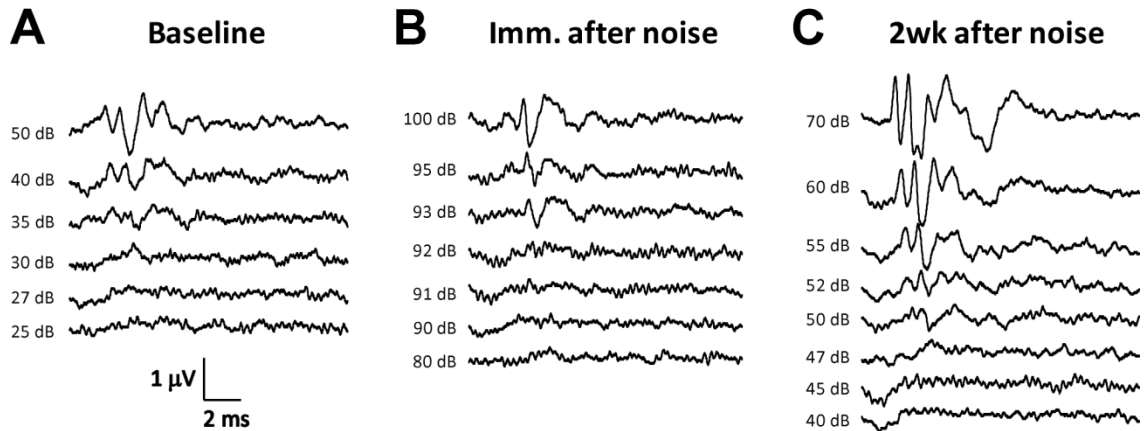
Figure 3.15. Representative ABR traces before and after noise exposure
A-C, Example of ABR traces from the same mouse obtained before (*A*), immediately after (*B*) and 2 weeks after (*C*) noise exposure. Notice that the range of SPL dB values evaluated is different for each panel. For this mouse, the hearing thresholds were assigned as: 30 (*A*), 91 (*B*) and 50 dB (*C*).

For the ABR recordings, two cohorts of mice were used. The first cohort compared wild type and *Trpa1$^{-/-}$* mice from the colonies that were maintained separately. In the second cohort, wild type and *Trpa1$^{-/-}$* littermates were compared. Since no differences were observed between these two cohorts, the data were combined for plotting and analysis purposes.

3.10.3 Noise exposure

Anesthetized mice were exposed to a broadband noise at 100 dB for 30 min. The noise was delivered by a speaker placed in front of the mouse, 1 inch away from the center of the mouse head.

3.11 Distortion product otoacoustic emissions (DPOAE)

These experiments were performed by the technician Stephanie Edelmann, MS, under the supervision of A.C. Vélez-Ortega. Briefly, 3-4 week old mice were anesthetized (as described in section 3.10.1) and a low-noise microphone probe (ER-10B+ model, Etymotic Research Inc.) was placed in the mouse left ear canal. Two tones of f_1 and f_2 frequencies at a ratio of 1.2 (f_1/f_2) were generated by electrostatic speakers and presented

with equal sound pressure levels (SPL). The microphone probe measured the intensity of the $2f_1$-f_2 frequency in the ear canal (*i.e.* DPOAE) together with the noise floor level (*i.e.* intensity of the surrounding frequencies). Several stimuli frequencies (4 to 20 kHz) and SPL values (40 to 70 dB) were evaluated. DPOAE values were measured before noise exposure and at several time points of recovery.

3.12 Statistical analysis

The student's t-test was used to compare the results from wild type and *Trpa1*$^{-/-}$ mice in the following experiments: (*i*) intracellular Ca^{2+} baseline levels and peak responses after TRPA1-agonist puff stimulation, (*ii*) tissue movement after TRPA1 stimulation and (*iii*) changes in intracellular Ca^{2+} and cell diameter after laser stimulation. Changes in intracellular Ca^{2+} levels in cells treated with FFA, were also analyzed using the student's t-test. Differences in peak whole-cell current responses after TRPA1 activation between cells from from wild type and *Trpa1*$^{-/-}$ mice were evaluated using a t-test for samples with unequal variances. Two-way ANOVAs were used to compare ABR and DPOAE results between wild type and *Trpa1*$^{-/-}$ mice. Bonferroni corrections were performed for the multiple comparisons made within the ABR and DPOAE results. The GraphPad Prism software v.5 was used to perform the statistical analyses.

The numbers (*n*) of cells, regions and/or cochlear explants included in each analysis are shown in the corresponding figures. Cells within a given explant were averaged and the statistical analyses were performed using the mean values of each explant. Error bars indicate the standard errors (SEM) around the mean values. Asterisks indicate statistical significant differences with P values < 0.05 (*), < 0.01 (**) and < 0.001 (***).

CHAPTER 4
Results

4.1 TRPA1 is widely expressed in the mammalian cochlea

The presence of *Trpa1* mRNA in the cochlear epithelium has been previously acknowledged [99, 177], however, those studies lacked the spatial resolution needed to clearly identify the specific cell types that express the *Trpa1* gene.

Because all commercially available antibodies against the TRPA1 protein tested so far exhibit various degrees of non-specific binding in cochlear explants from $Trpa1^{-/-}$ mice (personal communication from David Corey, Harvard University and Kelvin Kwan, Rutgers University), the presence of an active *Trpa1* promoter was evaluated using an indirect method. In $Trpa1^{-/-}$ mice the human PLAP gene (*i.e.* the reporter gene used to replace the *Trpa1* pore-forming region in the knockout animals [102]) is driven by the endogenous promoter of the *Trpa1* gene. Therefore, we performed immunolabeling against the human PLAP protein in cochlear explants from wild type and $Trpa1^{-/-}$ mice.

As expected, human PLAP expression was not detected in the cochlear epithelium from wild type mice (Figure 4.1A top). Instead, human PLAP was expressed throughout the entire cochlear epithelium from $Trpa1^{-/-}$ mice, including the sensory inner (IHCs) and outer (OHCs) hair cells and also most types of supporting cells, in particular, Kolliker's organ, pillar, Hensen's and Claudius' cells (Figure 4.1A bottom). The staining against human PLAP was particularly high in the row of pillar cells. Moreover, images at a higher magnification confirmed the bright staining of human PLAP in the pillar cell region and also in the Deiters' cells (Figure 4.1B).
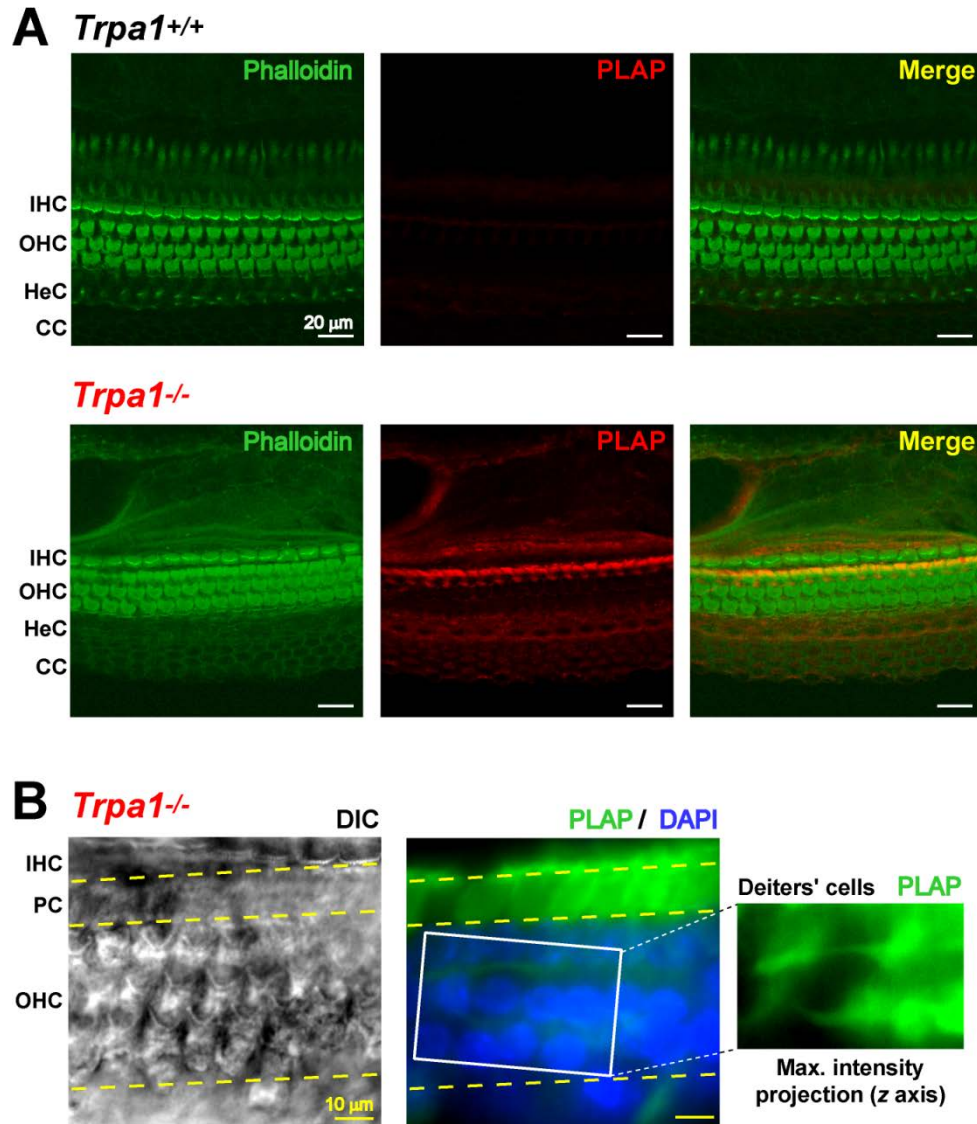
Figure 4.1. TRPA1 is widely expressed in the cochlear epithelium.

A, PLAP immunolabeling (red) and phalloidin counterstaining of actin filaments (green) in cochlear explants from wild type (top) and *Trpa1*$^{-/-}$ mice (bottom). Images courtesy of David Corey and Kelvin Kwan (Harvard University). *B*, PLAP immunolabeling (green) and DAPI counterstaining of a cochlear explant from a *Trpa1*$^{-/-}$ mouse at a higher magnification than in *A*. *Left*, DIC image at a focal plane by the OHC bundles shown as reference. *Middle*, PLAP and DAPI fluorescent signals at a focal plane by the OHC nuclei. *Right*, Z-axis maximum intensity projection of PLAP fluorescent signal within the Deiters' cell region.

This approach allowed us to identify the presence of active TRPA1 promoters in most cell types within the cochlear epithelium; however, it did not provide information about whether these cells express functional TRPA1 channels or details about their subcellular localization.

4.2 Sensory and supporting cells within the cochlear epithelium express functional TRPA1 channels

To assess for the presence of functional TRPA1 channels, we evaluated the uptake of the small fluorescent cation FM1-43 through open TRPA1 channels after stimulation with the agonist cinnamaldehyde (CA) [286]. Explants were pre-treated with a BAPTA-buffered Ca^{2+}-free solution to disrupt the tip links within hair cell stereocilia bundles, thus eliminating the entry of the FM1-43 dye to IHCs and OHCs through the MET channels that are partially open at rest due to the tip link resting tension. A short (30 s) incubation with the FM1-43 dye led to small dye uptake in IHCs and all rows of OHCs in explants from $Trpa1^{-/-}$ (Figure 4.2A) and wild type mice (Figure 4.2B). This small dye uptake might occur via other non-selective cation channels expressed in hair cells (*e.g.* P2X and TRPV1 channels). A similar degree of dye uptake was seen in explants from $Trpa1^{-/-}$ mice when the incubation with FM1-43 was performed in the presence of 200 µM CA (Figure 4.2C). However, in the presence of CA, the dye uptake in wild type explants was considerably increased in IHCs and OHCs, and it was also noticeable in Hensen's cells and the Kolliker's organ (Figure 4.2D). These results indicate the presence of functional TRPA1 channels in wild type IHCs, OHCs, Hensen's and Kolliker's organ cells. Interestingly, no FM1-43 uptake was observed in wild type pillar and Deiters' cells in spite of the presence of PLAP labeling in these cells (Figure 4.2D). Since pillar and Deiter's cells are localized mostly underneath the hair cells and have limited access to the apical surface of the organ of Corti, it is possible that their contact with either the FM1-43 dye or the TRPA1 agonist was limited as well. This could explain the lack of FM1-43 uptake in pillar and Deiters' cells, even if they do express functional TRPA1 channels. Alternatively, due to the complex nature of TRPA1 activation and regulation by several types of agonists and second messengers (*e.g.*, intracellular Ca^{2+} and downstream of phospholipase C –PLC– activation) (reviewed in sections 2.3 and 2.5), it is possible that

pillar and Deiter's cells do express TRPA1 channels but different experimental conditions might be required to trigger channel gating. Similarly, most Claudius' cells expressed PLAP but very few of them showed uptake of the FM1-43 dye (Figure 4.2D). However, as stated earlier, the lack of FM1-43 uptake does not necessarily imply that these cells do not express TRPA1 channels.
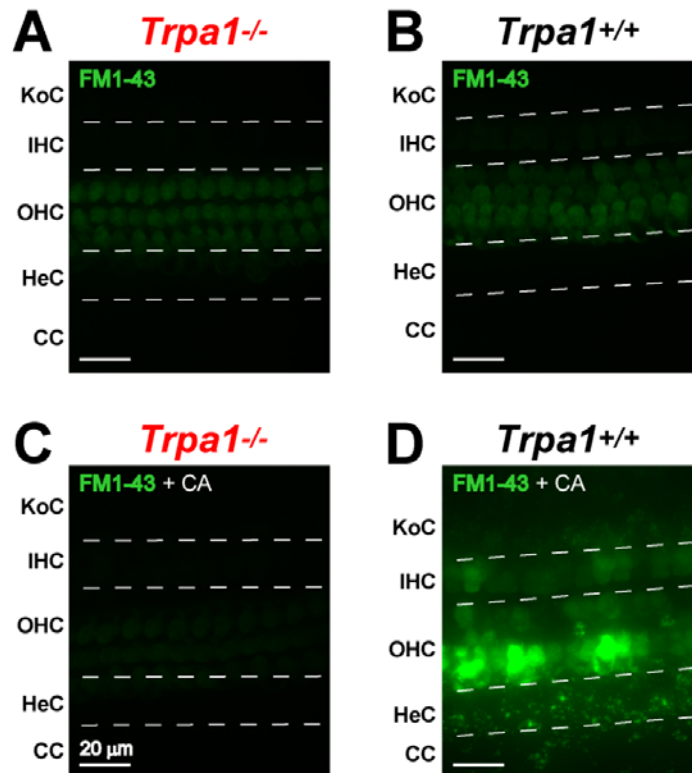
Figure 4.2. IHCs, OHCs, Hensen's and Kolliker's organ cells express functional TRPA1 channels

A-D, FM1-43 uptake (green) in cochlear explants from $Trpa1^{-/-}$ (*A, C*) and wild type mice (*B, D*) after a 30 s incubation with the FM1-43 dye alone (*A, B*) or in the presence of 200 μM the TRPA1 agonist CA (*C, D*). Images shown correspond to maximum intensity projections (z axis) from confocal stacks taken for each field of view. *KoC*, Kolliker's organ; *IHC*, inner hair cell; *OHC*, outer hair cell; *HeC*, Hensen's cells; *CC*, Claudius' cells.

Even though CA-induced FM1-43 uptake does reveal the presence of functional TRPA1 channels, the degree of dye uptake does not necessarily correlate with the amount of channels expressed. Because FM1-43 is a cation, its influx through open TRPA1 channels is greatly affected by the resting potential of a given cell. Moreover, differences between cells types in the kinetics of TRPA1 channel gating and inactivation can also influence the amount of FM1-43 uptake. For example, intracellular Ca^{2+} levels can modify the conductance of TRPA1 at the single-channel level (section 2.2.7) [175].

We concluded that, among the supporting cells, functional TRPA1 channels are present in at least the Hensen's and Kolliker's organ cells.

4.3 TRPA1 activation evokes robust and long-lasting Ca^{2+} responses in Hensen's cells

Next, we used cochlear explants loaded with the ratiometric Ca^{2+} indicator fura-2 to study the responses of sensory and supporting cells to the puff application of TRPA1 agonists. In cochlear explants from wild type mice, puff application with 200 μM 4-hydroxy-nonenal (4-HNE) induced robust Ca^{2+} responses in the Hensen's cells (Figures 4.3A and 4.4A). Typically, we observed a ~ 40 s delay (mean = 38.1 ± 2.0 s, n = 184 cells from 7 explants) between the start of the 4-HNE puff application and the beginning of the robust Ca^{2+} responses (Figure 4.5A). However, a small Ca^{2+} increase was often evident at earlier time points. This somewhat biphasic response would be consistent with the transition from low to high open probability in TRPA1 channels mediated by the initial increase in intracellular Ca^{2+} [175]. The Ca^{2+} responses in Hensen's cells induced by 4-HNE exhibited a very slow decay as well (mean = 0.53 ± 0.05 % s-1, n = 161 cells from 7 explants). This led to long-lasting Ca^{2+} responses even after the end of the 4-HNE puff application (Figures 4.3A and 4.4A).
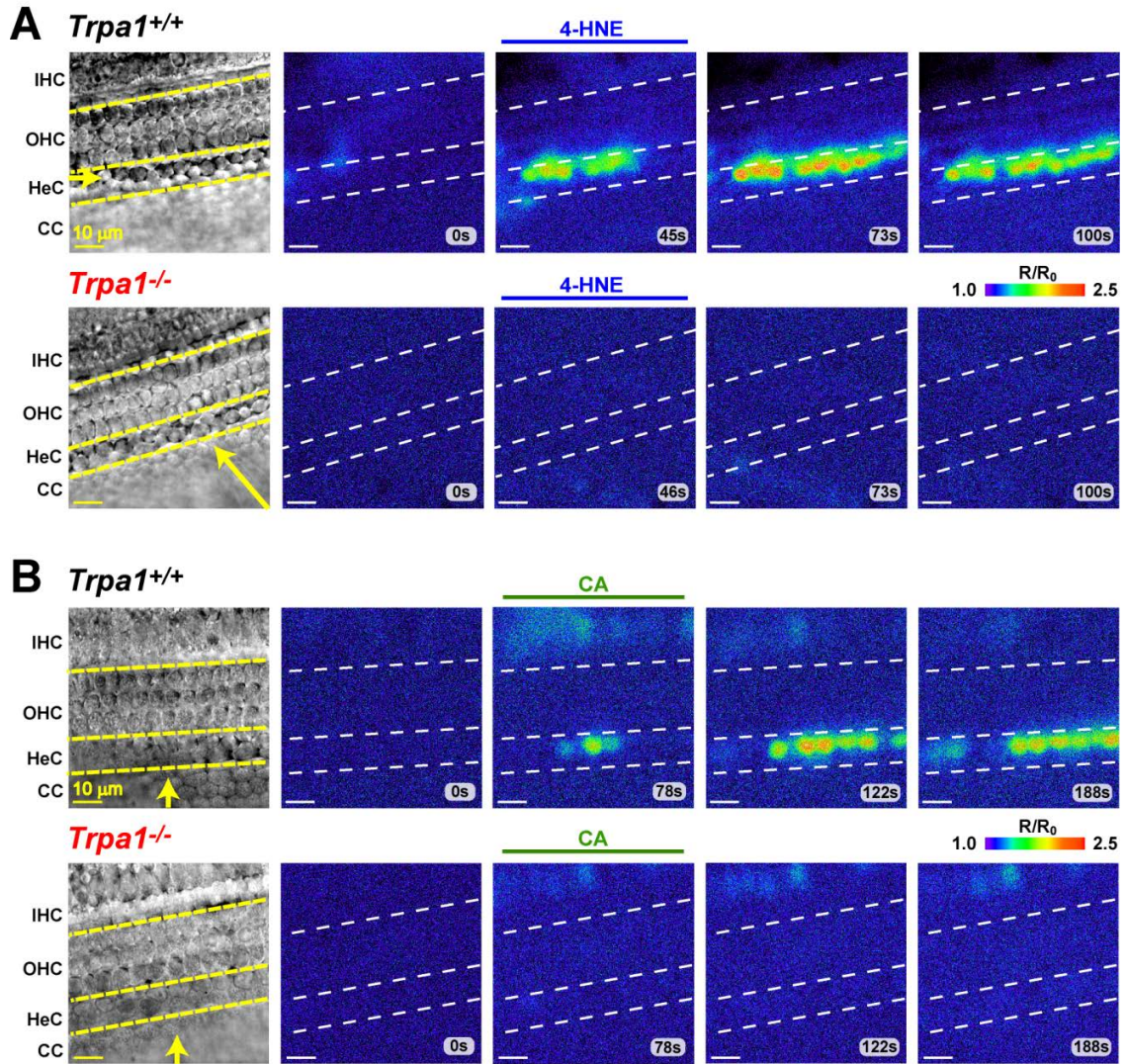
Figure 4.3. TRPA1 agonists induce robust and long-lasting Ca^{2+} responses in wild type Hensen's cells

A, B, Time-lapse ratiometric Ca^{2+} imaging ($R = F_{340}/F_{380}$) normalized to baseline (R_0) of cochlear explants from wild type (*top*) and $Trpa1^{-/-}$ mice (*bottom*) stimulated by puff application of 200 µM 4-HNE (*A*) or 100 µM CA (*B*). To the left of each series of Ca^{2+} images, a bright field image is shown as reference to indicate the types of sensory and supporting cells within the field of view. Dashed lines indicate boundaries between different cell types. Arrows indicate the position and direction of puff application. *IHC*, inner hair cells; *OHC*, outer hair cells; *HeC*, Hensen's cells; *CC*, Claudius' cells.
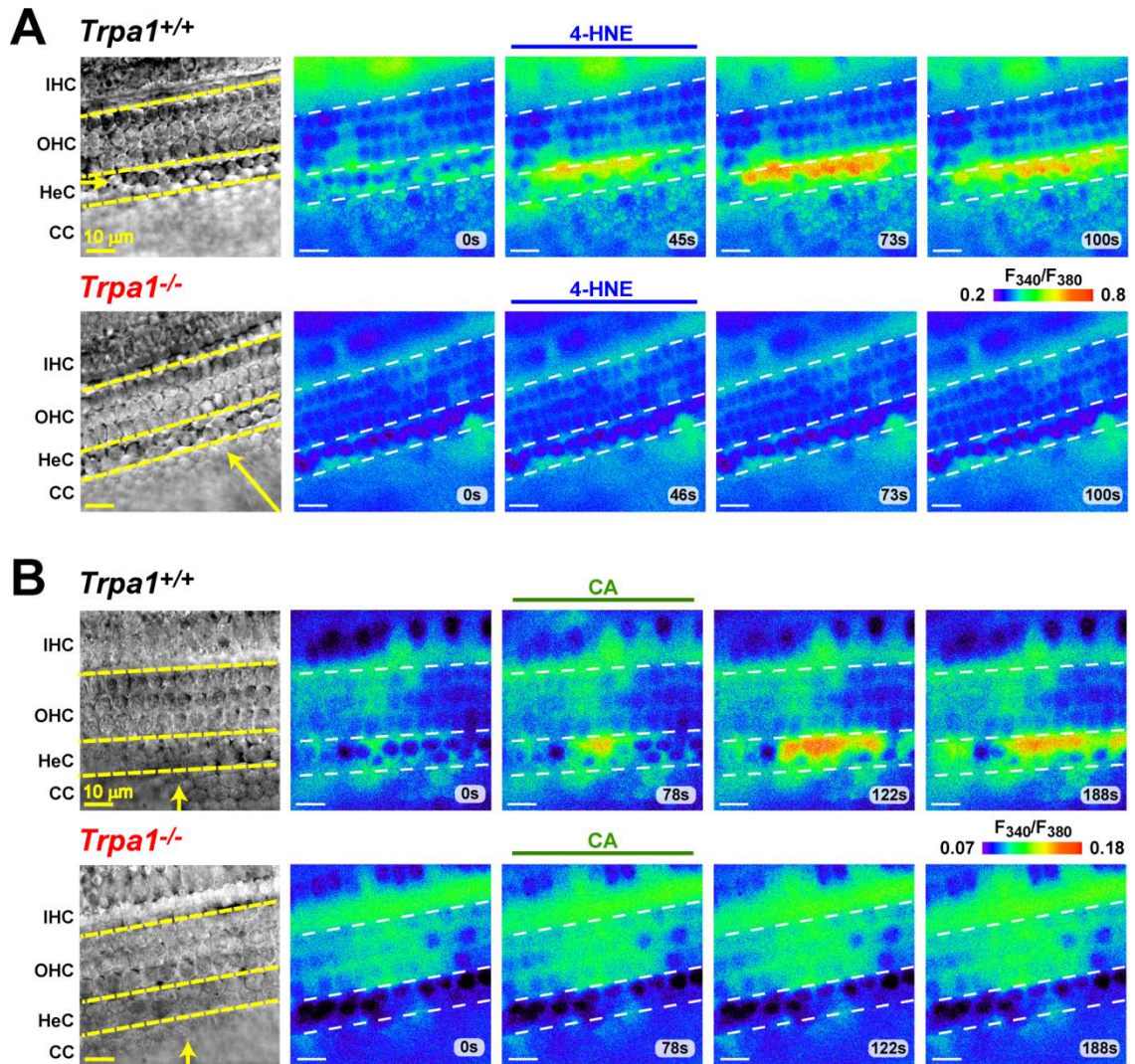
Figure 4.4. Intracellular Ca²⁺ levels from Figure 4.3 without normalization to the baseline

A, B, Time-lapse ratiometric Ca^{2+} imaging (F_{340}/F_{380}) of cochlear explants from wild type (*top*) and *Trpa1⁻/⁻* mice (*bottom*) stimulated by puff application of 200 μM 4-HNE (*A*) or 100 μM CA (*B*). To the left of each series of Ca^{2+} images, a bright field image is shown as reference to indicate the types of sensory and supporting cells within the field of view. Dashed lines indicate boundaries between different cell types. Arrows indicate the position and direction of puff application. *IHC*, inner hair cells; *OHC*, outer hair cells; *HeC*, Hensen's cells; *CC*, Claudius' cells.
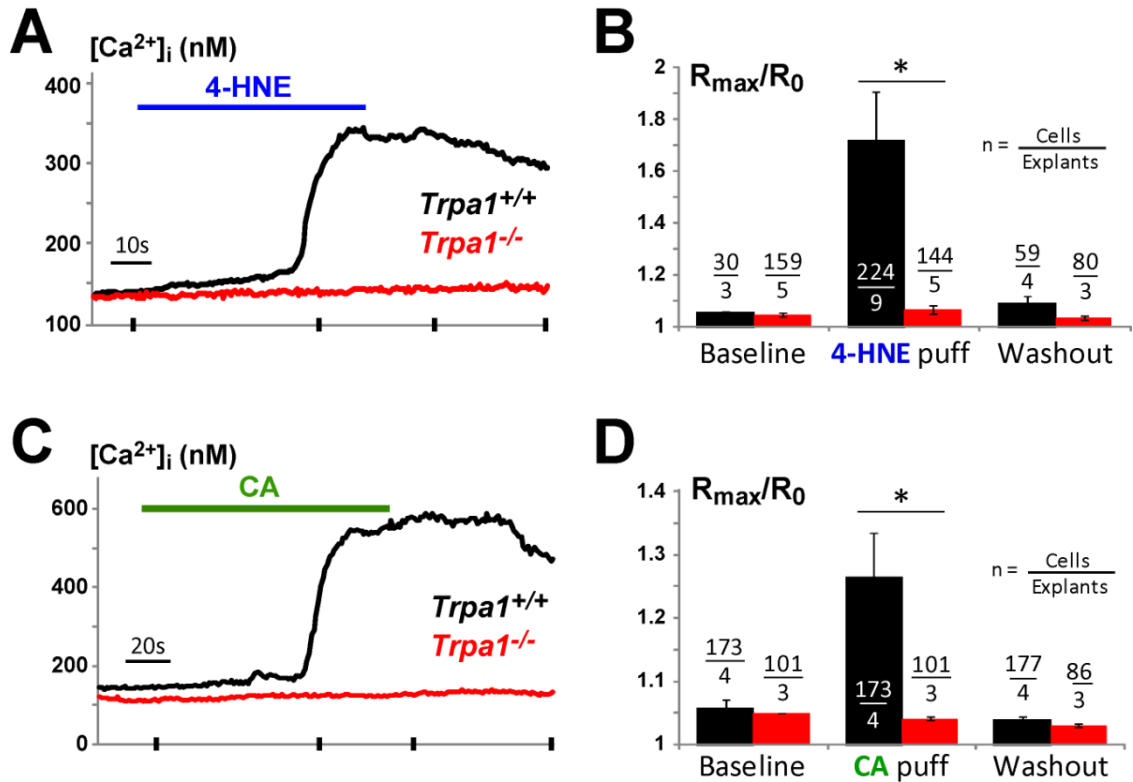
Figure 4.5. TRPA1 agonists induce robust Ca2+ responses in Hensen's cells from wild type but not Trpa1$^{-/-}$ mice

A, C, Changes in intracellular Ca^{2+} levels (in nM) in Hensen's cells from wild type (*black*) or *Trpa1*$^{-/-}$ mice (*red*) in response to puff application of 4-HNE (*A*) or CA (*C*). The traces were obtained from the same experiments shown in Figures 4.3 and 4.4, and the lines in the *x*-axis indicate the time points for each of the panels shown in those figures. *B, D*, Peak Ca^{2+} responses (R$_{max}$) relative to baseline levels (R$_0$) were evaluated in time windows (95 s) before (*baseline*), during and immediately after (*puff*) and about 5 min after (*washout*) agonist stimulation. Bars show mean ± SEM values. The number of cells/explants included is shown above each bar. (*) indicates a P value < 0.05 determined by a Student's t-test.

Similar robust Ca^{2+} responses (*i.e.* delayed and long-lasting) were elicited by other TRPA1 agonists such as CA (100 µM) (Figures 4.3B, 4.4B and 4.5C) and mustard oil (allyl isothiocyanate –AITC–, 100 µM) (Figure 4.6) in wild type Hensen's cells. As expected, the same puff application with 4-HNE and CA failed to induce Ca^{2+} responses in cochlear explants from $Trpa1^{-/-}$ mice (Figures 4.3, 4.4 and 4.5).

All three TRPA1 agonists tested also failed to induce Ca^{2+} responses in the supporting Claudius's cells (Figures 4.3, 4.4 and 4.6). These results are consistent with the lack of FM1-43 uptake in Claudius's cells after stimulation with CA (Figure 4.2).
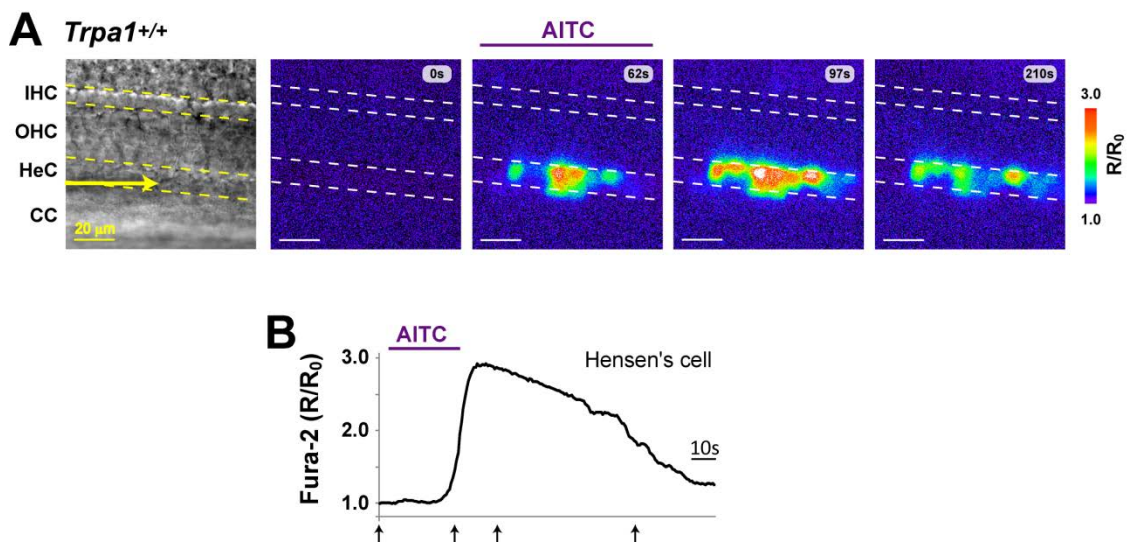
Figure 4.6. Mustard oil induces Ca^{2+} responses in Hensen's cells with similar kinetics to 4-HNE and CA

A, Time-lapse Ca^{2+} imaging (R/R_0) of a wild type cochlear epithelium showing the response to 100 µM mustard oil (AITC) puff application. A bright field image (*left*) is shown as reference and the yellow arrow indicates the position and direction of puff application. Dashed lines indicate boundaries between different cell types. *IHC*, inner hair cells; *OHC*, outer hair cells; *HeC*, Hensen's cells; *CC*, Claudius' cells. *B*, Changes in intracellular Ca^{2+} (R/R_0) in one of the Hensen's cells shown in *A*. Arrows below the *x*-axis indicate the time points when the panels shown in *A* were taken.

To our surprise, puff application with either 4-HNE, CA or AITC did not induce prominent Ca^{2+} responses in the sensory IHCs and OHCs (Figures 4.3, 4.4 and 4.6). These results did not correlate with our findings of FM1-43 uptake in IHCs and OHCs after stimulation with CA (Figure 4.2). We wondered whether this discrepancy could arise from the different CA concentrations and delivery methods used. The FM1-43 experiments were performed with a CA concentration (200 µM) that was double of that used for the Ca^{2+} imaging (100 µM). However, puff application with a higher concentration of 4-HNE (400 µM, double of what was used previously) also failed to induce Ca^{2+} responses in IHCs and OHCs (Figure 4.7).
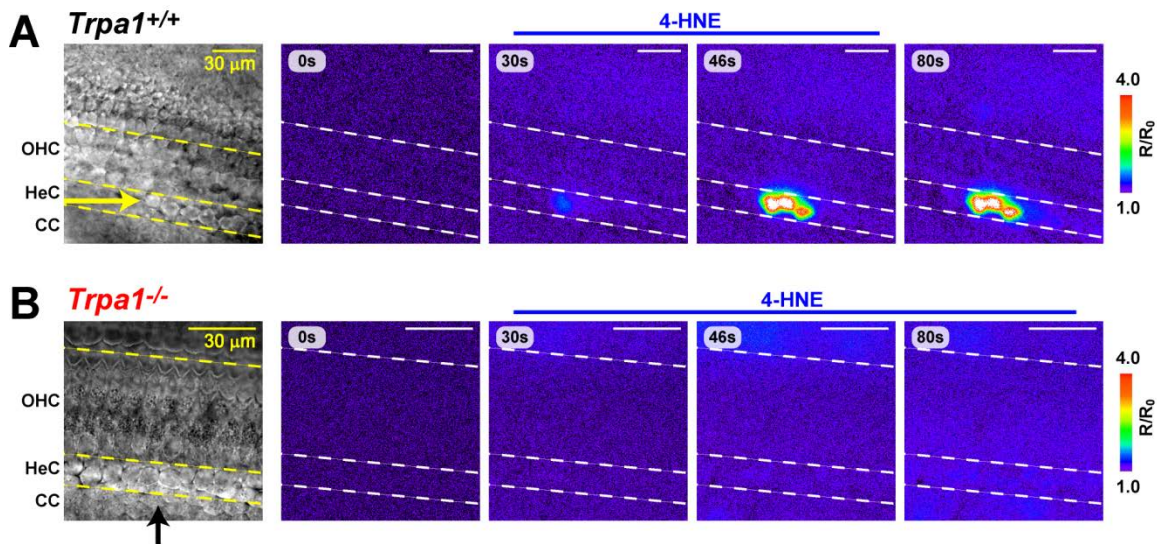
Figure 4.7. Sensory hair cells fail to show Ca^{2+} responses even after stimulation with a high concentration of a TRPA1 agonist

A, *B*, Time-lapse Ca^{2+} imaging (R/R$_0$) of cochlear epitheliums from wild type (A) and *Trpa1$^{-/-}$* mice (B) showing the response to 400 µM 4-HNE puff application. A bright field image (*left*) is shown as reference and the arrows indicate the position and direction of the puff application. Notice that the puff was applied for a longer time on the *Trpa1$^{-/-}$* explant. Dashed lines indicate boundaries between different cell types. *OHC*, outer hair cells; *HeC*, Hensen's cells; *CC*, Claudius' cells.

For the FM1-43 experiments, cells were stimulated by CA present in the bath solution while, during the Ca^{2+} imaging experiments, CA stimulation was performed using a puff pipette. CA present in the bath solution certainly stimulates a larger number of cells because it covers the entire tissue. However, the exposure to the CA-containing bath was limited to 30 s, which is a much shorter stimulation duration than the one used with the puff application (~ 60 s). We previously confirmed the presence of functional TRPA1 channels in sensory IHC and OHCs, and suggested that channel expression was limited to the basolateral membrane in these cells [286]. Here, we believe the discrepancy between the FM1-43 and Ca^{2+} imaging experiments mainly arises from the exposure to BAPTA in the former. The exposure to a BAPTA-buffered Ca^{2+}-free solution is likely to compromise the tight junction barrier of the reticular lamina (*i.e.* the barrier formed by the connection between all cells of the cochlear epithelium at their apical side) [293, 294]. A compromised tight junction barrier might allow CA to activate TRPA1 channels in the basolateral membrane of IHCs and OHCs during the FM1-43 experiments. In contrast, the tight junction barrier is intact during our Ca^{2+} imaging experiments, thus limiting the access of CA to the basolateral membranes.

Because particularly long-lasting Ca^{2+} responses to TRPA1 activation were observed in Hensen's cells but not anywhere else within the cochlear epithelium, we believe Hensen's cells could be the major sensors for oxidative damage (*i.e.* 4-HNE) in the cochlea. Therefore, we also wondered whether the absence of TRPA1 channels would alter the resting intracellular Ca^{2+} levels in *Trpa1*$^{-/-}$ Hensen's cells. However, we found no differences in the baseline intracellular Ca^{2+} between Hensen's cells from wild type and *Trpa1*$^{-/-}$ mice (Figure 4.8).
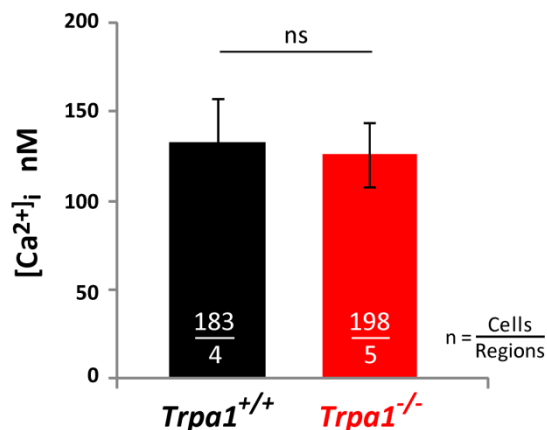
Figure 4.8. Hensen's cells from wild type and TRPA1-deficient mice exhibit similar resting intracellular Ca^{2+} levels

Intracellular Ca^{2+} levels (in nM) of Hensen's cells from wild type (black) and *Trpa1$^{-/-}$* mice (red) were estimated from ratiometric Ca^{2+} imaging with the fura-2 dye. Bars show mean ± SEM values. The number of cells/regions included in the analysis is shown for each bar. A P value > 0.86 was determined using a Student's t-test.

4.4 Responses to TRPA1 agonists in the Hensen's cells are modulated by the levels of intracellular Ca^{2+} levels

The robust long-lasting responses to TRPA1 agonists in Hensen's cells did not lead to cell death. In fact, the intracellular Ca^{2+} levels in Hensen's cells slowly decreased to baseline-like levels (Figure 4.9A). Moreover, upon subsequent stimulations with the same TRPA1 agonist, Hensen's cells were able to once again exhibit similar long-lasting Ca^{2+} responses. However, the peak responses were considerably different between consecutive puff stimulations. We also noticed that, after TRPA1 agonist stimulation, the intracellular Ca^{2+} in the Hensen's cells recovered to a level that was slightly higher than the pre-stimulation level.
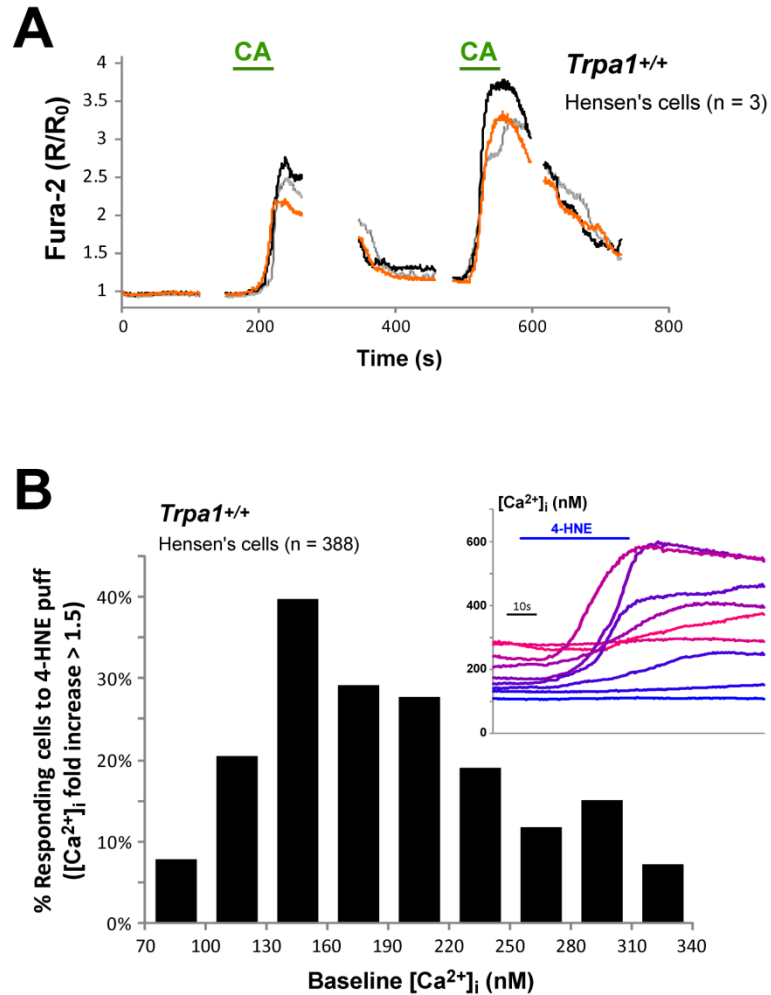
Figure 4.9. Intracellular Ca^{2+} modulates responses to TRPA1 agonists
A, Representative traces of the intracellular Ca^{2+} levels (R/R$_0$) of three Hensen's cells subjected to two consecutive puff stimulations with 100 µM CA. The breaks in the Ca^{2+} traces correspond to time points where imaging was paused to minimize cytotoxicity due to UV overexposure. *B*, Histogram showing the percentages of cells that responded to 400 M 4-HNE based on their intracellular Ca^{2+} level (in nM) at the time of puff stimulation (baseline). A responding cell was defined to have more than a 1.5 fold increase in intracellular Ca^{2+} after 4-HNE stimulation. *Inset*, Representative traces of changes in intracellular Ca^{2+} levels from some of the cells included in the histogram. All traces shown in the *inset* are from cells analyzed within the same field of view but over several puff applications.

We hypothesized that the differences in magnitude of the responses to TRPA1 agonist stimulation dependent on the levels of intracellular Ca^{2+} at the time of the puff application. To test this, the number of Hensen's cells that responded to the stimulation with 400 μM 4-HNE was compared to their intracellular Ca^{2+} level at the moment of the puff application. To determine the 'responding' cells, we chose an arbitrary threshold level assuming that a cell was responding if we observed at least a 1.5 fold increase in intracellular Ca^{2+} upon stimulation with 4-HNE. Our results showed that the majority of responding cells exhibited intermediate levels of intracellular Ca^{2+} (~130 to 220 nM). However, cells with low (~100 nM) or high (> 250 nM) intracellular Ca^{2+} levels often failed to mount robust Ca^{2+} responses to the application of the TRPA1 agonist (Figure 4.9B). It is noteworthy to highlight that the lack of responses in cells that had high intracellular Ca^{2+} baseline levels was not due to dye saturation (Figure 4.9B inset). These results further support the notion that TRPA1 channel activity is modified by intracellular Ca^{2+} [175, 194, 235]. While an increase in intracellular Ca^{2+} can initially potentiate the responses of TRPA1 to other agonists, higher Ca^{2+} levels seem to inactivate the channel.

4.5 Cells of the Kolliker's organ exhibit oscillating Ca^{2+} responses after TRPA1 agonist stimulation

In contrast to the delayed and long-lasting responses to TRPA1 agonists exhibited by Hensen's cells, 4-HNE puff stimulation led to fast and short-lived Ca^{2+} waves in the Kolliker's organ (Figure 4.10). These differences in the kinetics of TRPA1-induced Ca^{2+} responses might arise from the differences in Ca^{2+} handling properties between cell types.
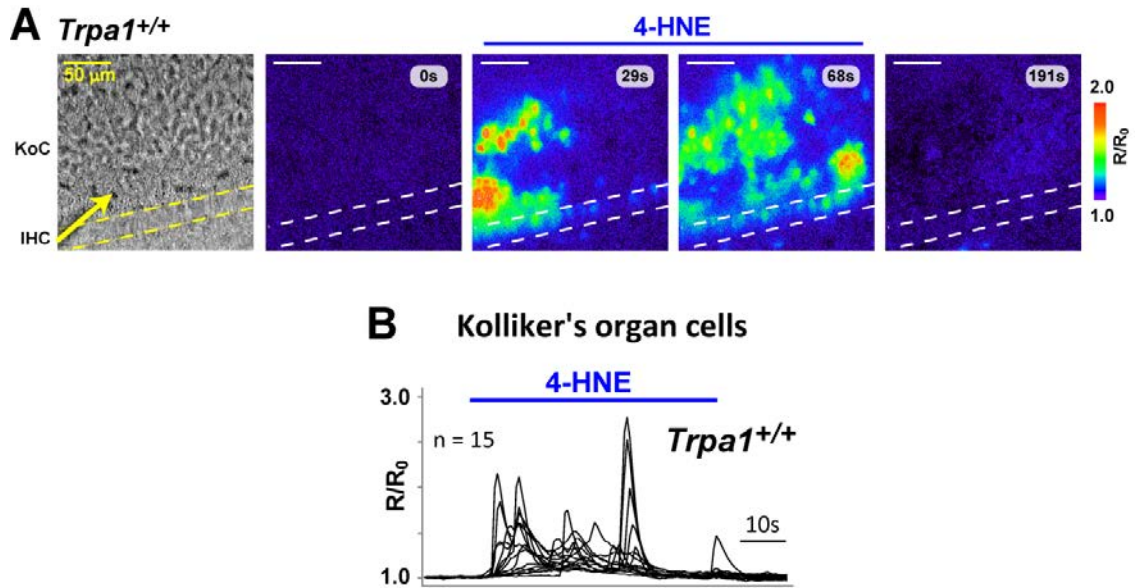
Figure 4.10. 4-HNE induces fast and short-lived Ca^{2+} responses in the cells of the Kolliker's organ

A, Time-lapse Ca^{2+} imaging (R/R_0) of the Kolliker's organ from a wild type mouse during puff stimulation with 200 µM 4-HNE. A bright field image (*left*) is shown as reference and the yellow arrow indicates the position and direction of puff application. Dashed lines indicate boundaries between different cell types. *KoC,* Kolliker's organ cells; *IHC*, inner hair cells. *B*, Traces showing the changes in intracellular Ca^{2+} in response to 4-HNE in 15 Kolliker's organ cells from the region shown in *A*.

We also observed striking differences between the Ca^{2+} responses in supporting cells evoked by activation of TRPA1 channels and ATP receptors. In contrast to TRPA1 channels, puff application of low doses of ATP (*e.g.* 2 µM) induced oscillating and relatively short-lived Ca^{2+} responses in Kolliker's organ, Hensen's and Claudius' cells (Figure 4.11A). The oscillating nature of these Ca^{2+} waves is presumed to involve the (*i*) activation/inactivation cycles of the G protein-coupled P2Y receptors, (*ii*) IP_3-induced release of Ca^{2+} from intracellular stores and (*iii*) feedback inhibition of Ca^{2+} on IP_3 receptors (Figure 4.11C) [295].
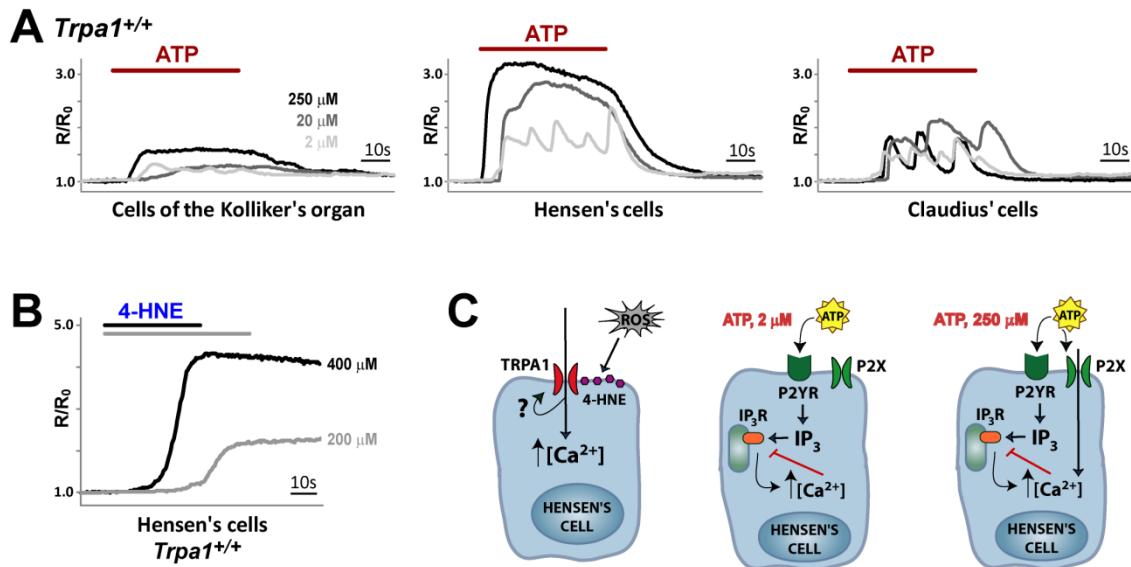
Figure 4.11. Oscillating and sustained Ca^{2+} responses in cochlear supporting cells might reflect different Ca^{2+} handling properties

A, Representative Ca^{2+} traces showing the changes in intracellular Ca^{2+} (R/R0) in Kolliker's organ (*left*), Hensen's (*middle*) and Claudius' cells (*right*) after stimulation with increasing concentrations of ATP (2, 20 and 250 µM). *B*, Intracellular Ca^{2+} traces (R/R0) of Hensen's cells after stimulation with increasing concentrations of 4-HNE (200 and 400 µM). *C*, Diagrams showing the signaling pathways involved after activation of TRPA1, P2Y or P2X receptors/channels.

On the other hand, stimulation with high doses of ATP (*e.g.* 250 µM) activates P2X ionotropic channels as well (Figure 4.11C). The large influx of Ca^{2+} through P2X channels might overwhelm Ca^{2+} buffers in the cell and lead to a sustained increase in intracellular Ca^{2+} instead of the oscillating behavior. While puff stimulation with 250 µM ATP led to sustained Ca^{2+} responses in Kolliker's organ and Hensen's cells, Claudius' cells continued to exhibit oscillating Ca^{2+} responses (Figure 4.11A). Because all of these cochlear supporting cells seem to express functional P2X channels (reviewed in [62]), the different Ca^{2+} responses to the same concentration of ATP are likely to arise from unique Ca^{2+} handling properties within each cell type. However, we cannot rule out the

possibility that differences in the expression levels and subunits of P2X and P2Y receptors underlie these results.

Interestingly, puff stimulation with a high concentration of ATP did not lead to long-lasting Ca^{2+} responses in the Hensen's cells like the ones observed after stimulation with TRPA1 agonists (compare the middle panel in Figure 4.11A with 4.11B). This result indicates that Hensen's cells are able to clear a large increase in intracellular Ca^{2+} quickly. Therefore, the long-lasting Ca^{2+} responses elicited by the TRPA1 agonists might indicate that the channel itself gets temporarily locked into an open configuration (Figure 4.11C). In fact, the three TRPA1 agonists tested (4-HNE, CA and AITC) are reactive agonists that can covalently bind to TRPA1 subunits to trigger channel gating [201, 202, 210]. Differences in the redox state between Hensen's and Kolliker's organ cells (*e.g.*, expression and availability of antioxidants) could also explain the different Ca^{2+} responses observed upon stimulation with TRPA1 agonists.

4.6 TRPA1-dependent Ca^{2+} responses in the Hensen's cell can propagate to the Kolliker's organ

When applying multiple puff stimulations with TRPA1 agonists within a specific Hensen's cell region, we often observed the development of Ca^{2+} waves in the cells of the Kolliker's organ (Figure 4.12A). The Kolliker's organ can spontaneously trigger Ca^{2+} waves during the early postnatal development (section 1.7.1), however, the Ca^{2+} waves that we noticed in the Kolliker's organ seemed to coincide with the time of puff application in the Hensen's cell region (Figure 4.12B).
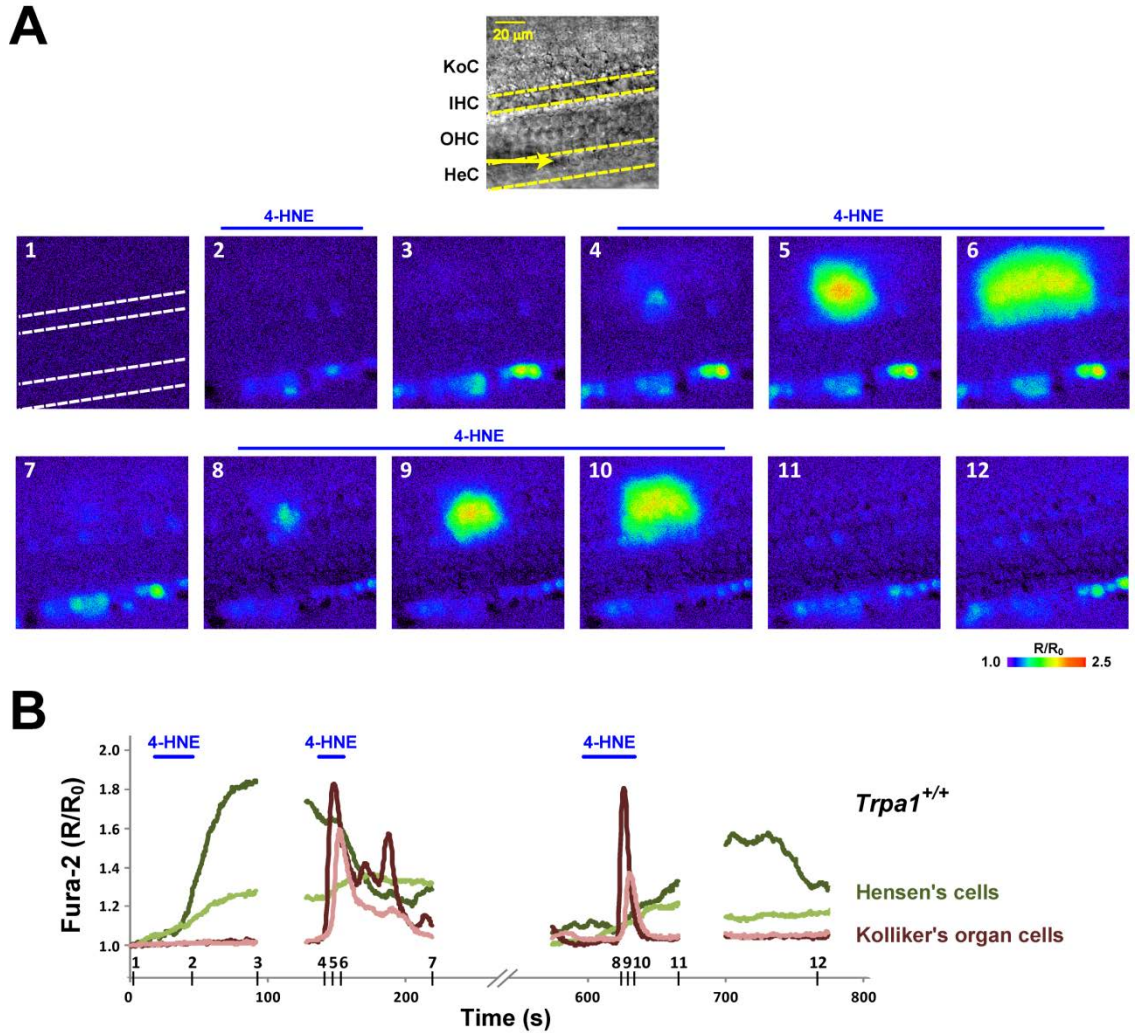
Figure 4.12. Puff stimulation with TRPA1 agonists at the Hensen's cell region also triggers Ca^{2+} waves in the Kolliker's organ

A, Time lapse ratiometric Ca^{2+} imaging (R/R_0) of a cochlear epithelium after puff stimulation with 400 µM at the Hensen's cell region. A bright field image (*top*) is shown as reference and the yellow arrow indicates the position and direction of puff application. Dashed lines indicate boundaries between different cell types. *KoC*, Kolliker's organ cells; *IHC*, inner hair cells; *OHC*, outer hair cells; *HeC*, Hensen's cells. *B*, Representative Ca^{2+} traces from two Hensen's (shades of green) and Kolliker's organ cells (shades of red) from the experiment shown in *A*. Breaks in the traces represent time point where imaging was paused to minimize cytotoxicity due to UV overexposure. The numbers in the *x* axis indicate the time points where the frames in panel *A* where taken.

To test whether these 'secondary' Ca^{2+} waves were the result of TRPA1 agonist diffusion, we performed a similar experiment in cochlear explants dissected on very early postnatal days (P1-P2). At this developmental age, the cells of the Kolliker's organ did not respond to direct puff stimulation with TRPA1 agonists (Figure 4.13A bottom and data not shown). However, puff stimulation with 4-HNE at the Hensen's cell region of the same explant (and field of view) was indeed able to trigger Ca^{2+} waves in the Kolliker's organ (Figure 4.13A top).
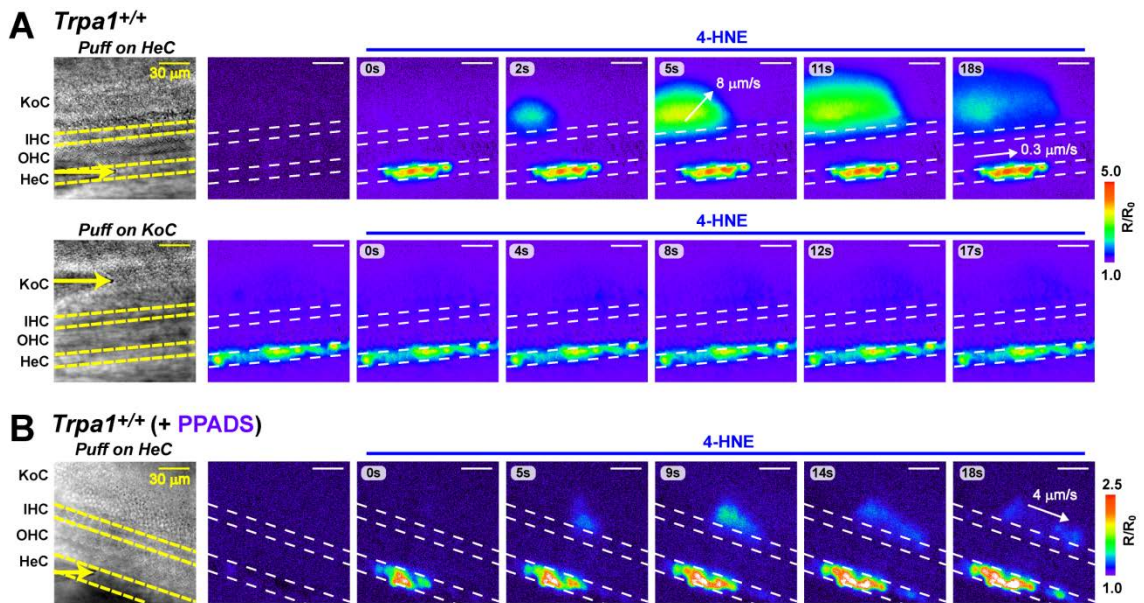
Figure 4.13. TRPA1-dependent activation of Hensen's cells propagates to the Kolliker's organ and triggers Ca^{2+} waves that require extracellular ATP

A, B, Time-lapse ratiometric Ca^{2+} imaging of cochlear explants dissected on postnatal days 1 or 2. The imaging was performed in the absence (*A*) or presence (*B*) of the P2X and P2Y antagonist PPADS (50 µM). Stimulation with 400 µM 4-HNE was delivered via puff pipettes (yellow arrows) at the Hensen's cell region (*A top* and *B*) or at the Kolliker's organ (*A bottom*). Dashed lines indicate boundaries between different cell types. *KoC*, Kolliker's organ cells; *IHC*, inner hair cells; *OHC*, outer hair cells; *HeC*, Hensen's cells.

The Ca^{2+} responses that propagated to the Kolliker's organ –after puff stimulation with TRPA1 agonists at the Hensen's cell region– were able to travel from cell to cell at a much faster speed (*e.g.*, 0.3 µm/s in the Hensen's cells vs. 8 µm/s in the Kolliker's organ). In addition, the Ca^{2+} waves in the Kolliker's organ exhibited rising speeds and clearance rates that were higher than for the Ca^{2+} responses in the Hensen's cells (as an example, compare the traces in Figure 4.12B). The kinetics of the 'secondary' Ca^{2+} waves observed in the Kolliker's organ resembled those of the spontaneous Ca^{2+} waves that these cells exhibit during early postnatal days (section 1.7.1). The mechanism of propagation of the spontaneous Ca^{2+} waves has been previously elucidated and, among other signaling molecules, it involves the release of ATP to the extracellular space and the activation of P2Y receptors on neighboring cells (Figure 1.10) [34, 70]. Therefore, we wondered whether extracellular ATP was also involved in these 'secondary' Ca^{2+} waves. In the presence of 50 µM PPADS –a P2X and P2Y antagonist– the puff stimulation with 4-HNE in the Hensen's cell region generated Ca^{2+} responses that were still able to propagate toward the medial cochlear side. However, in the presence of the purinergic receptor blocker, the Ca^{2+} waves were limited to the rows of supporting cells immediately adjacent to the IHCs, presumably the inner border cells (Figure 4.13B). These results suggest that activation of TRPA1 channels in the Hensen's cells is able to trigger the already known ATP-dependent and self-propagating Ca^{2+} waves.

Interestingly, the TRPA1-induced Ca^{2+} responses in the Hensen's cells never propagated toward the lateral side of the cochlea (*i.e.*, toward the Claudius' cells and the spiral prominence). Moreover, the propagation of these Ca^{2+} responses toward the medial side of the cochlea did not involve the sensory hair cells given that we never observed changes in the intracellular Ca^{2+} of IHCs or OHCs. As previously described [65], we did observe that, after these ATP-dependent Ca^{2+} waves were generated in the Kolliker's organ, some of them were able to induce an increase in intracellular Ca^{2+} in the IHCs (*e.g.*, compare panels 5 and 6 in Figure 4.12A). Because all supporting cells are electrochemically coupled via gap junctions, it is possible that the TRPA1-induced Ca^{2+} responses in the Hensen's cells propagate to the Kolliker's organ via Deiters' and pillar cells. Sadly, we were not able to test this hypothesis using Ca^{2+} imaging because the fura-2 dye failed to load such cells (Figure 4.14).
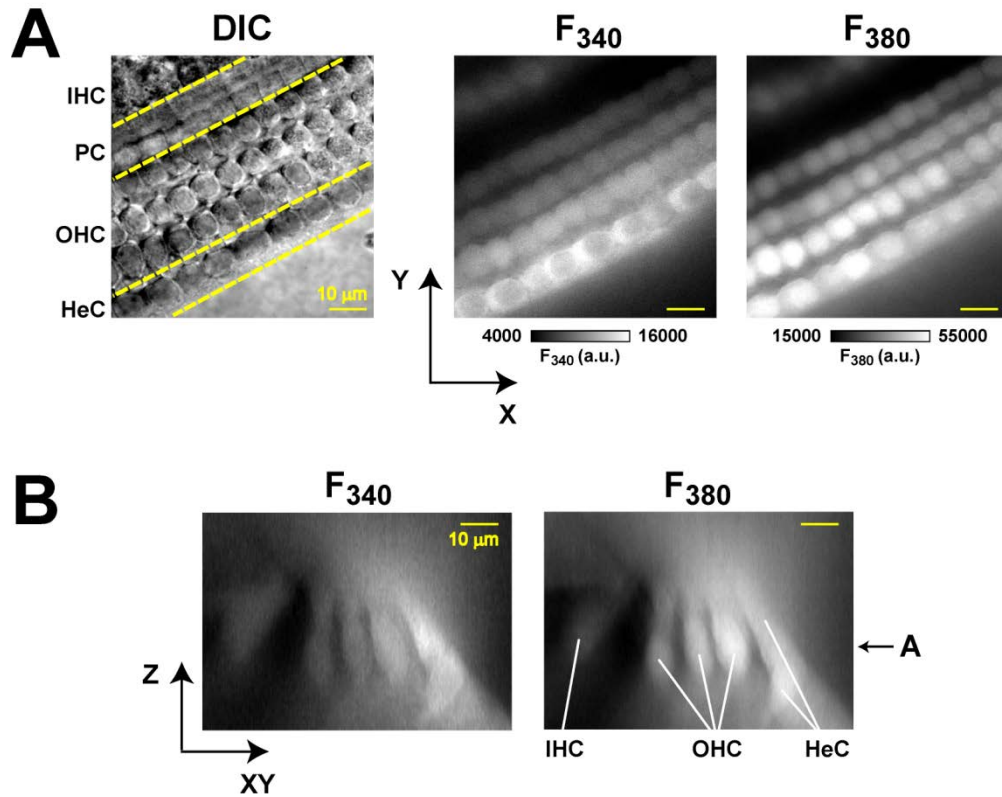
Figure 4.14. The ratiometric fura-2 Ca^{2+} indicator fails to load pillar and Deiters' cells

A, Representative images of the fura-2 fluoresce with 340 (F$_{340}$) and 380 nm (F$_{380}$) illuminations showing one row of IHCs, three rows of OHCs and one row of Hensen's cells. The corresponding bright field image at the same focal plane is shown as reference (*left*). Dashed lines indicate the boundaries between cell types. *B*, Orthogonal view of the same tissue shown in A from stacks of images taken every 1 μm. Notice that the fluorescent images were not taken in a confocal mode and, therefore, there is plenty of out-of-focus light above and below the hair cells. *IHC*, inner hair cells; *PC*, pillar cells; *OHC*, outer hair cells; *HeC*, Hensen's cells.

4.7 In the presence of a gap junction blocker Claudius' cells exhibit TRPA1-mediated Ca^{2+} responses

Because TRPA1-dependent Ca^{2+} responses in the Hensen's cells might be able to propagate across the cochlear epithelium via the gap juntional conductance between supporting cells, we decided to evaluate the responses to TRPA1 agonists in the presence of a known gap junction blocker, FFA.

FFA behaves as an agonist of rat and human TRPA1 (see section 2.3.6) but it is unknown whether it can activate mouse TRPA1 channels as well. First, we tested whether the presence of FFA in the bath solution could alter the levels of intracellular Ca^{2+} in the Hensen's cells, but found no differences between FFA-treated and control cells (Figure 4.15).
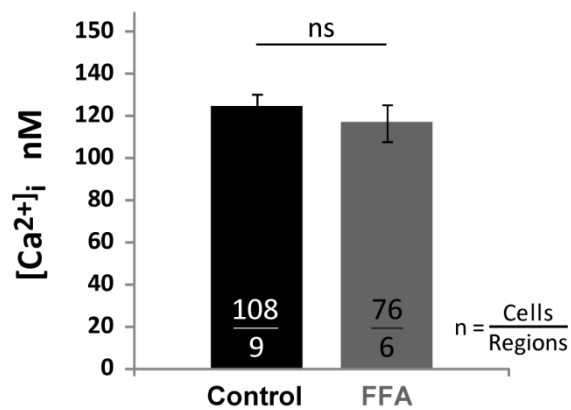
Figure 4.15. Presence of FFA in the bath solution does not change the resting Ca^{2+} level in Hensen's cells

Resting intracellular Ca^{2+} levels (in nM) of Hensen's in the presence (*grey*) or absence (*black*) of the gap junction blocker FFA (100 μM) in the bath solution. Intracellular Ca^{2+} levels were determined from ratiometric Ca^{2+} images of cells loaded with the fura-2 dye. Ca^{2+} levels from cells that were monitored for up to 50 min after adding FFA are included in the graph. Mean ± SEM values are shown. The number of cells/regions included in the analysis is shown for each bar. A P value > 0.4 was determined using a Student's t-test.

93

Next, we evaluated the Ca^{2+} responses to the application of 200 μM 4-HNE before and after the addition of the gap junction blocker FFA to the bath solution. As shown previously, in the absence of FFA the stimulation with 4-HNE led to delayed, robust and long-lasting Ca^{2+} responses in the Hensen's cells but no responses were observed in the Claudius' cells (Figures 4.16A and 4.16B). To our surprise, in the presence of FFA Claudius' cells were now able to respond to the puff stimulation with the TRPA1 agonist (Figures 4.16C to 4.16F). The 4-HNE-induced Ca^{2+} responses in Claudius' cells were more robust after a 30 min exposure to FFA than they were after only 10 min with the blocker (compare Figures 4.16C and 4.16E). Moreover, in the presence of FFA, the delay in the Ca^{2+} responses –relative to the beginning of the puff application– decreased with time for both Hensen's and Claudius' cells (Figures 4.16B, 4.16D and 4.16F).

Two alternative scenarios could explain the TRPA1-mediated responses in Claudius' cells that are only seen after the incubation with FFA. First, FFA might be acting as an agonist for mouse TRPA1. In this case, a concentration of 100 μM FFA may have been too low to elicit changes in intracellular Ca^{2+} (Figure 4.15) but, FFA together with 200 μM 4-HNE could have exerted a synergistic effect on the TRPA1 channels present in Claudius's cells. FFA and 4-HNE activate TRPA1 channels through different mechanisms. While 4-HNE is a reactive agonist that binds intracellular cysteine residues in TRPA1, FFA is a non-reactive agonist that might activate TRPA1 after interacting with, perhaps, a pocket-like domain. Interestingly, FFA is known to have a synergistic action when applied together with CA –another reactive agonist that activates TRPA1 in a manner similar to 4-HNE [201]. Of note, high concentrations (400 μM) of 4-HNE alone failed to induce Ca^{2+} responses in Claudius' cells (Figure 4.13 and data not shown). Therefore, a synergistic effect between FFA and 4-HNE seems a more likely explanation than a simple additive effect of both agonists.

If FFA does not behave as an agonist for mouse TRPA1, an alternative explanation would involve FFA-induced changes in the intracellular environment that could favor TRPA1 gating. It is plausible that blocking the electrochemical connection between different types of supporting cells might lead to changes in resting potentials and/or intracellular redox states which can potentiallyalter TRPA1 channel activation kinetics.

Because the presence of the gap junction blocker changed the responses of the cells to TRPA1 activation, we were not able to test whether the gap junctional conductance is require for the propagation of TRPA1-induced Ca^{2+} waves from the Hensen's cells to the Kolliker's organ.
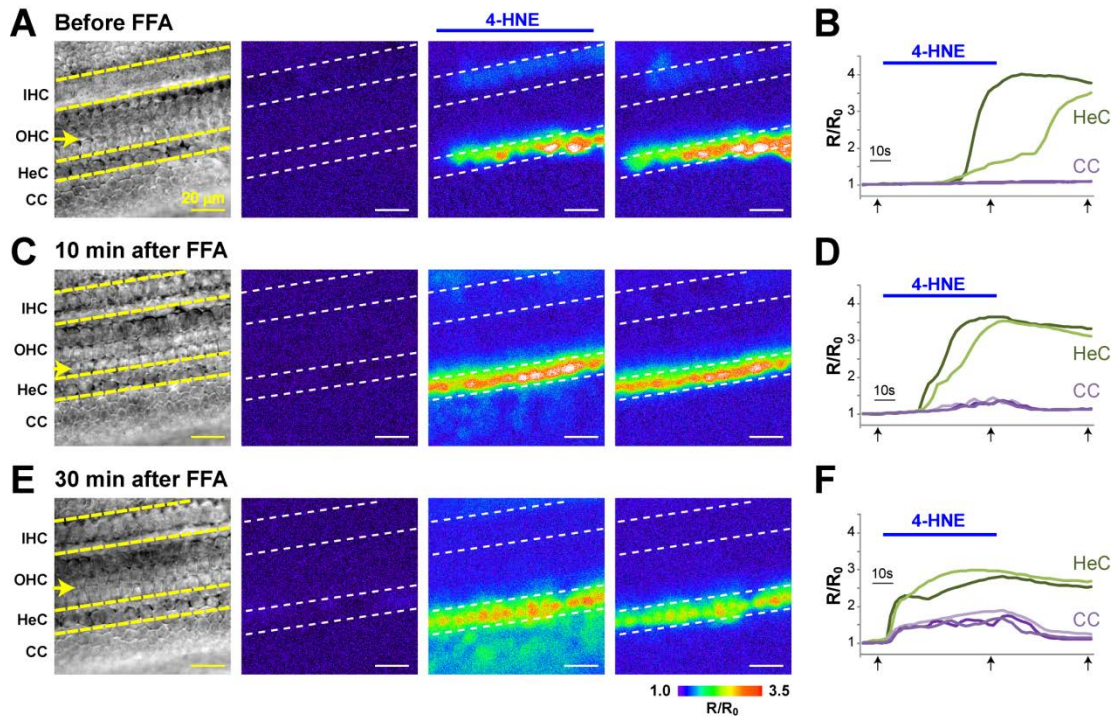
Figure 4.16. In the presence of FFA, 4-HNE induces Ca^{2+} responses in Claudius' cells

A, C, E, Time-lapse ratiometric Ca^{2+} imaging (R/R$_0$) showing the responses to 4-HNE (200 µM) in cochlear explants before (*A*) and 10 min (*B*) and 30 min (*C*) after adding the gap junction blocker FFA (100 µM) to the bath solution. A bright field image (*left*) is shown as reference and the yellow arrow indicates the position and direction of puff application. Dashed lines indicate boundaries between different cell types. *IHC*, inner hair cells; *OHC*, outer hair cells; *HeC*, Hensen's cells; *CC*, Claudius' cells. *B, D, E*, Traces indicating the changes in intracellular Ca^{2+}(R/R$_0$) in two Hensen's cells (shades of green) and two Claudius' cells (shades of purple) from the data shown in panels *A, C* and *E*.

4.8 Deiters' cells express functional TRPA1 channels

Given that the membrane-permeable fura-2 dye failed to load pillar and Deiter's cells (Figure 4.14), we decided to perform patch clamp recordings to test whether these cells express functional TRPA1 channels or not. Changes in whole-cell currents after the puff application of 100 µM CA were monitored. However, in order to measure the currents in individual cells, the gap junction blocker FFA was added to the bath solution. As shown previously, the presence of FFA did not seem to change resting intracellular Ca^{2+} levels or inhibit the responses to TRPA1 agonists in Hensen's cells (Figures 4.15 and 4.16). Therefore we were confident that, even if FFA behaves as an agonist for mouse TRPA1 channels, we should still be able to see TRPA1 currents after the stimulation with CA. In fact, FFA and CA have a synergistic effect in rat TRPA1 channels [208].

As expected, puff stimulation with CA induced large inward currents in Hensen's cells from wild type but not from *Trpa1*$^{-/-}$ mice (Figures 4.17A and 4.17D). The current-voltage (I-V) relationship of the CA-induced responses in Hensen's cells exhibited prominent rectification at negative potentials and, presumably, channel inactivation at positive potentials. This I-V relationship differs from the typical behavior of TRPA1 channels in heterologous expression systems (see Appendix D for a typical I-V relationship obtained in HEK-293 cells transfected with a mouse TRPA1 construct).

Although the behavior of TRPA1 can differ between transfected and native channels [245, 267, 268, 296], we wondered whether FFA could be modifying the I-V relationship of TRPA1 currents in Hensen's cells. To test this, we evaluated the CA-mediated currents in the presence of a different gap junction blocker. We performed whole-cell patch clamp recordings of Hensen's cells in the presence of 1 mM octanol in the bath solution. Octanol was chosen because this gap junction blocker does not seem to be an agonist for mouse TRPA1 channels [205]. However, the I-V relationships obtained in the presence of octanol were indistinguishable from the ones obtained in the presence of FFA (compare Figures 4.17A and 4.18).
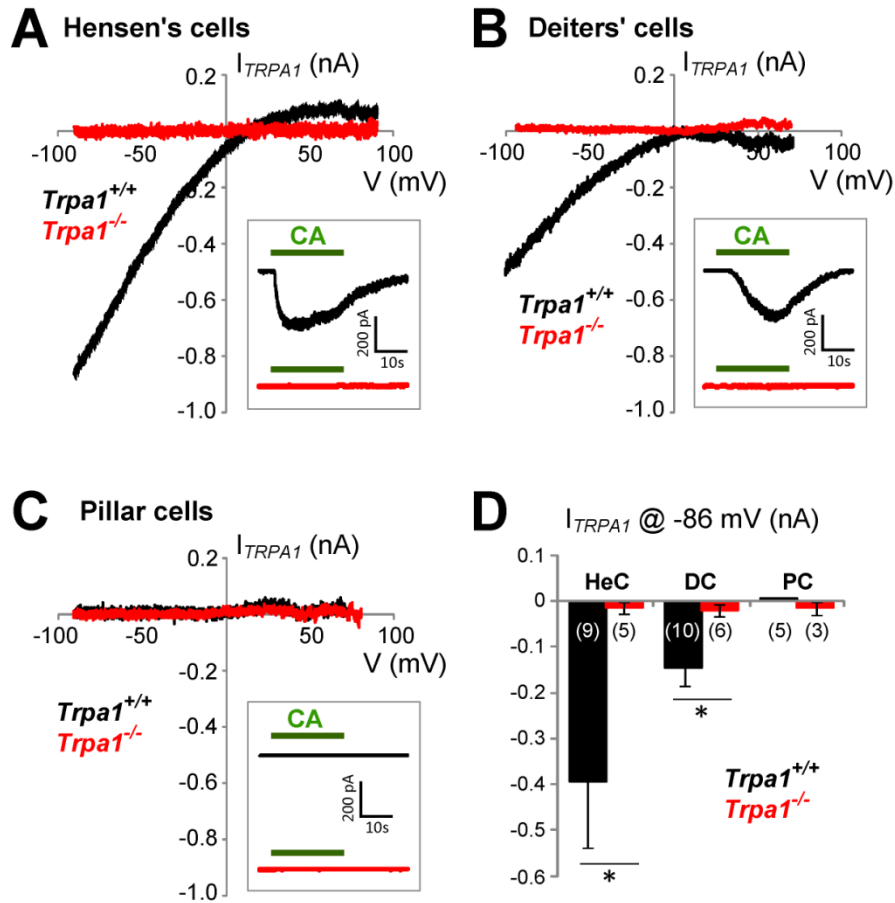
Figure 4.17. TRPA1-mediated inward currents in Hensen's and Deiters's cells
A-C, Representative current-voltage (I-V) relationships for CA-induced currents
($I_{Puff} - I_{Baseline}$) in Hensen's (*A*), Deiters' (*B*) and pillar cells (*C*) from wild type
(black) and *Trpa1*$^{-/-}$ mice (red). *Insets*, Representative inward currents elicited
by the puff application of 100 µM CA. D, Average peak inward currents
triggered by the puff application of CA and measured at a holding potential of -
86 mV. Bars show mean ± SEM values. The number of cell included in the
analysis is shown for each bar. (*) indicates a P value < 0.05 determined by a t-
test for samples with unequal variance.
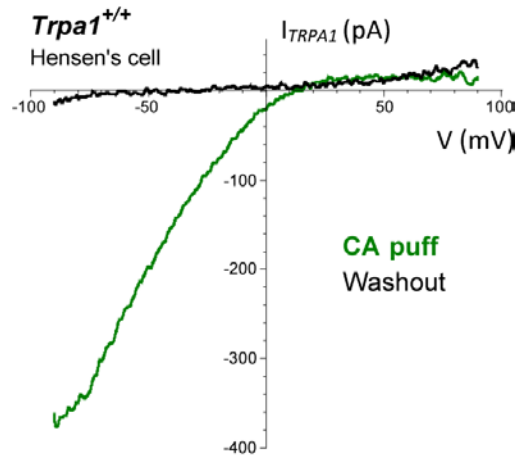
Figure 4.18. Current-voltage relationship of TRPA1 activation in the presence of a different gap junction blocker

Current-voltage relationship of a wild type Hensen's cell during the puff stimulation with CA ($I_{Puff} - I_{Baseline}$) (green) and 5 min after washout ($I_{Washout} - I_{Baseline}$) (black). Recordings were performed in the presence of 1 mM octanol.

We also observed CA-mediated current responses in wild type Deiters' cells and they had I-V relationships similar to the ones seen in Hensen's cells (Figure 4.17B). These results indicate that Deiter's cells express functional TRPA1 channels as well. However, the magnitude of the TRPA1 responses (*i.e.* peak currents) appeared to be smaller in Deiters' than in Hensen's cells (Figure 4.17D).

When similar recordings were performed in pillar cells, we were not able to observe changes in whole-cell currents elicited by the puff application of CA (Figures 4.17C and 4.17D). These results were unexpected given the bright PLAP staining exhibited by pillar cells (Figure 4.1). However, as it was the case for Claudius' cells, it is possible that the experimental conditions used here (*e.g.*, Ca^{2+} levels in the intracellular solution, type and concentration of the agonist used, whole-cell instead of perforated patch) were not ideal to allow TRPA1 channel gating.

4.9 TRPA1 stimulation induces tissue movement that seems to originate at pillar and Deiter's cells

Bright field imaging performed during puff stimulation with 200 µM 4-HNE indicated the presence of slow, yet prominent, tissue movements within the cochlear epithelium (Figure 4.19A). These 4-HNE-induced tissue displacements were often delayed relative to the beginning of the puff stimulation (Figure 4.19B), a feature similar to the delay in the TRPA1-induced Ca^{2+} responses seen in Hensen's cells. Interestingly, puff stimulation with 4-HNE induced prominent tissue movement in cochlear explants from wild type but not from $Trpa1^{-/-}$ mice (Figures 4.19C and 4.19D).

The TRPA1-induced tissue displacements were large and caused changes in the field of view and/or focal plane during imaging. However, when bright field imaging was performed near the pillar cell feet, prominent cell contractions were observed specifically in outer pillar cells (Figure 4.20B) and, sometimes, in Deiters' cells as well (Figure 4.20C).
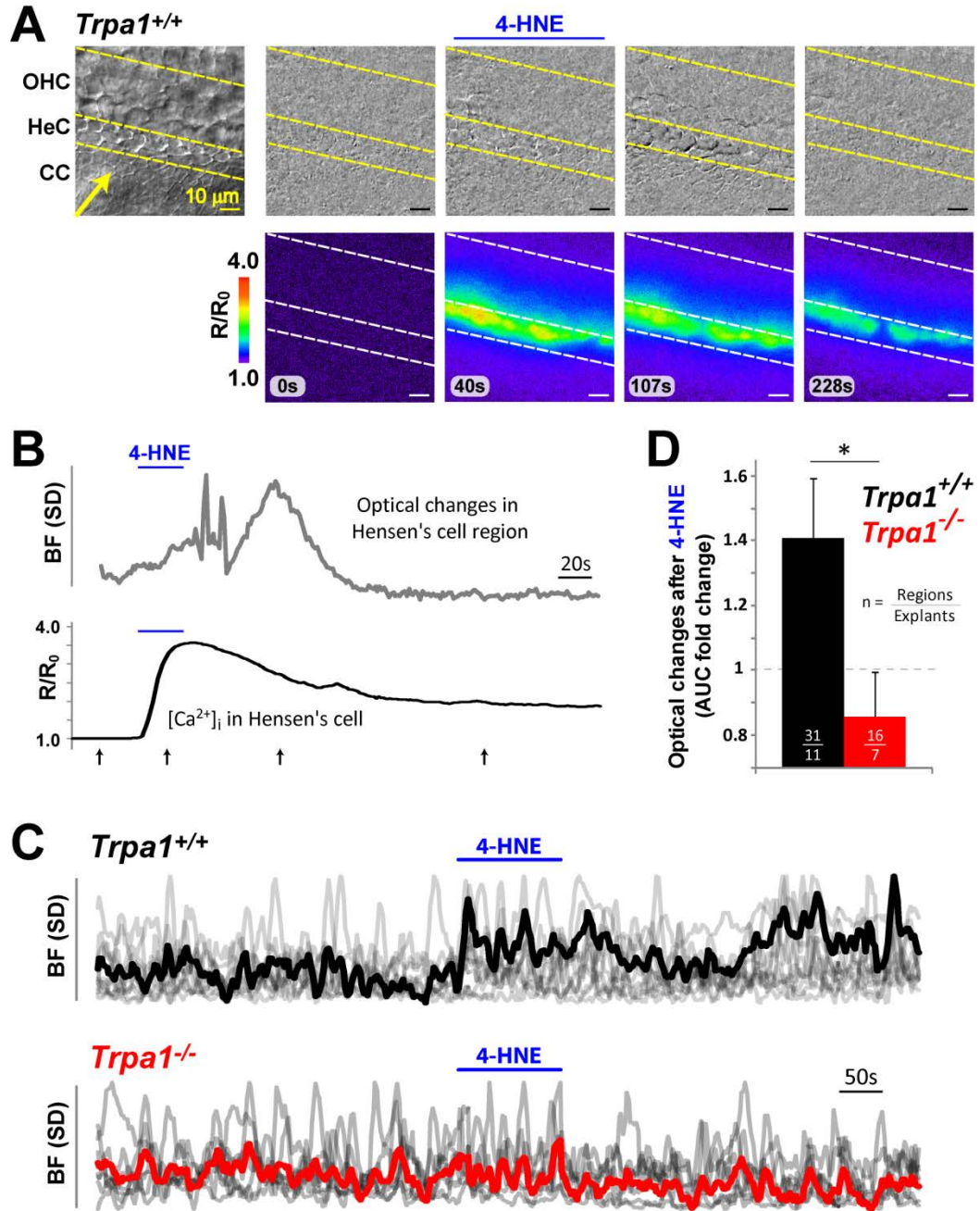
Figure 4.19. TRPA1 activation induces prominent tissue movement

A, Changes in time-lapse bright field (*top*) and Ca^{2+} imaging (R/R_0) (*bottom*) of a wild type cochlear explant during puff stimulation with 200 µM 4-HNE. The top panel shows subtracted frames from images taken 10 s apart to enhance the areas were tissue movement was observed. A non-subtracted bright field image (*left*) is shown as reference. The yellow arrow indicates the position and direction of puff application. Dashed lines indicate the boundaries between

different cell types. *OHC*, outer hair cells; *HeC*, Hensen's cells; *CC*, Claudius' cells. *B, top*, Trace showing the changes in the standard deviation (SD) of pixel values from the subtracted bright field (BF) images shown in *A*. *B*, *bottom*, Trace showing the intracellular Ca^{2+} levels (R/R_0) of one of the Hensen's cells from panel *A*. Arrows indicate the time points where the panels in *A* were taken. *C*, SD changes in subtracted BF images from wild type (*top*) and *Trpa1$^{-/-}$* explants (*bottom*) stimulated with 200 µM 4-HNE. Individual traces (grey) were normalized to the same height. For drawing purposes, the average traces for explants from wild type (black) and *Trpa1$^{-/-}$* mice (red) were normalized to comparable baseline levels (*i.e.* the region of each trace before the puff application). *D*, Bar graph showing the fold changes in area-under-the-curve (AUC) values obtained from the traces shown in C and comparing time points before and during/after the puff stimulation with 4-HNE ($AUC_{Puff}/AUC_{Baseline}$). A value of 1 (dashed line) indicates that the TRPA1 stimulation did not induce tissue movement. Bars show mean ± SEM values. The number of regions/explants included in the analysis is shown for each bar. (*) indicates a P value < 0.05 determined by a Student's t-test.
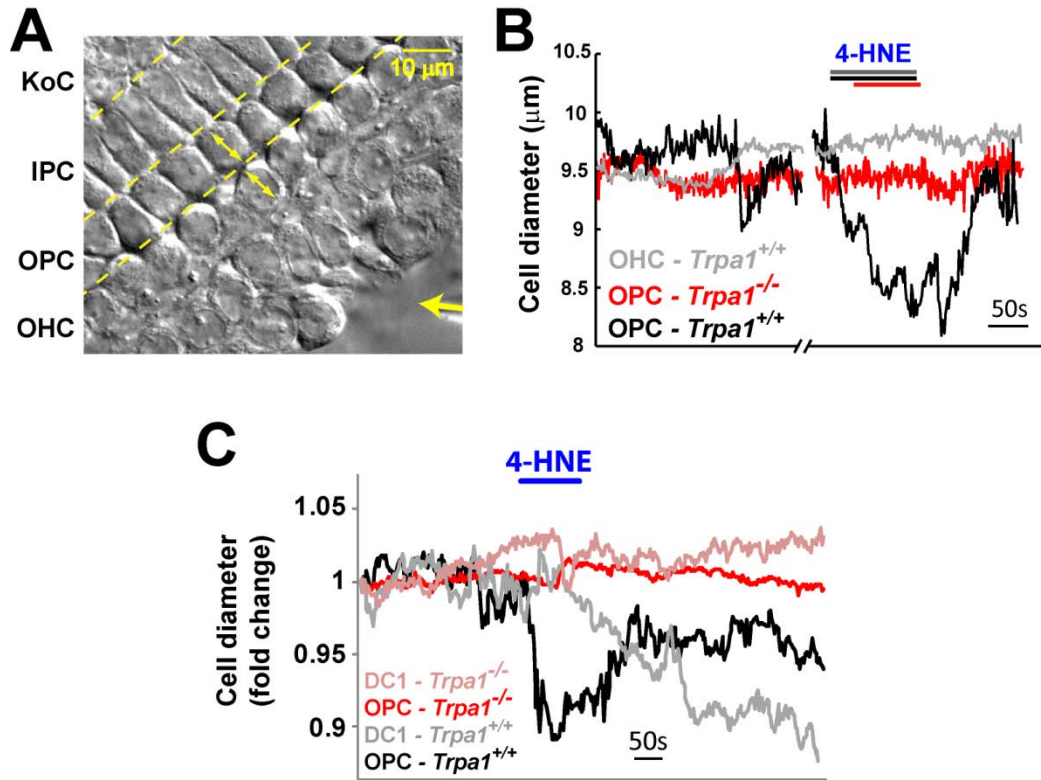
Figure 4.20. Tissue displacements seem to originate by the contractions of pillar and Deiters' cells

A, Bright field image showing the axis (yellow double-headed arrows) used to measure cell diameter changes in OHCs and OPCs. Hensen's cells were removed so the puff application could reach areas underneath the tight junction barrier. Dashed lines show the boundaries between cell types. The yellow single-headed arrow indicates the position and direction of puff application. *B*, Changes in cell diameter after puff stimulation with 200 μM 4-HNE in an OPC (black) and an OHC (grey) from the wild type explant shown in A. For comparison, the diameter measurements of an OPC from a *Trpa1*^{−/−} explant (red) are shown as well. *C*, Changes in cell diameter after puff stimulation with 200 μM 4-HNE in OPCs (black and red) and DCs (grey and pink) from wild type (black and grey) and *Trpa1*^{−/−} (red and pink) mice. Cell diameters were measured using the same axis shown in *A*. *KoC*, Kolliker's organ cells; *IPC*, inner pillar cells; O*PC*, outer pillar cells; *OHC*, outer hair cells.

In section 4.6, we showed that TRPA1 activation in Hensen's cells is able to trigger Ca^{2+} waves that depend on the release of ATP to the extracellular space. Since ATP itself can lead to changes in the shape of the Kolliker's organ cells [65, 66], we wondered whether ATP could trigger shape changes in pillar cells as well. In fact, puff stimulation with 2 μM ATP induced changes in the cell diameter of pillar cells that were similar to the ones observed after TRPA1 stimulation (Figure 4.21). Interestingly, ATP puff stimulation was sometimes able to induce changes in the shape of OHCs (Figure 4.21). These ATP-induced changes in OHCs were observed in cochlear explants at about postnatal day 6, a developmental age when the functional expression of prestin –the OHC motor– could be starting. Therefore, we believe that ATP stimulation is depolarizing OHCs via the activation of P2X channels and triggering prestin-indued cell shape changes. Therefore, the tissue movements observed after ATP puff stimulation were far more complex that the TRPA1-induced tissue displacements.
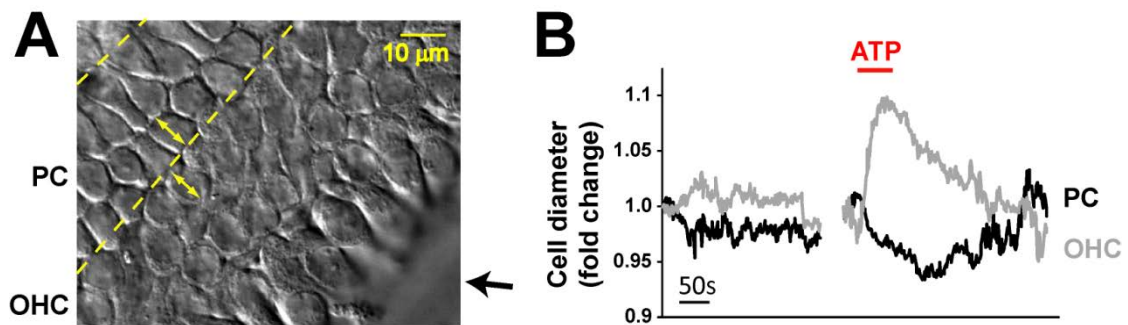
Figure 4.21. ATP puff stimulation induces pillar cell contraction

A, Bright field image showing the OHC and PC (yellow arrows) used to measure cell diameter changes. Hensen's cells were removed so the puff application could reach areas underneath the tight junction barrier. Dashed lines show the boundaries between cell types. The puff pipette was located at the edge of the field of view as indicated by the black arrow. *PC*, pillar cell; *OHC*, outer hair cell. *B*, Changes in cell diameter after puff stimulation with 2 μM ATP in an outer PC (black) and OHC (grey) from the wild type explant shown in A. *KoC*, Kolliker's organ cells; *PC*, pillar cells; *OHC*, outer hair cells.

4.10 Cochlear pillar cells posses Ca^{2+}-dependent contractile machinery

The phalangeal processes of Deiter's cells are known to exhibit mechanical responses after the stimulation with ATP or after Ca^{2+} uncaging [56, 57]. However, it is unknown whether pillar cells can exhibit similar Ca^{2+}-dependent active mechanical responses. Activation of ATP receptors or TRPA1 channels can both lead to an increase in intracellular Ca^{2+}. Therefore, we decided to test whether an increase of the cytosolic Ca^{2+} concentration was sufficient to trigger changes in the shape of pillar cells. We used the photo-labile Ca^{2+} chelator o-nitrophenyl ethylene glycol tetraacetic acid (NP-EGTA) to deliver 'caged Ca^{2+}' to outer pillar cells using a whole-cell patch clamp configuration (Figure 4.22A). Stimulation with a UV laser produced an immediate increase of intracellular Ca^{2+} (Figure 4.22B) that was followed by a slow cell contraction (Figure 4.22C). These changes in intracellular Ca^{2+} and cell diameter were not observed in control outer pillar cells were the photo-labile Ca^{2+} chelator had been replaced with regular EGTA (Figures 4.22D and 4.22E).

Cell currents were also monitored during the experiment and only cells that did not exhibit changes in the holding current were considered for the quantification of cell diameters. Changes in the holding currents after the UV stimulation were similar (P > 0.56) between cells containing caged Ca^{2+} (ΔIm = -4.29 ± 2.8 pA) and control cells (ΔIm = -3.23 ± 0.9 pA). Therefore, the Ca^{2+}-induced shape changes in pillar cells are unlikely to be driven by the potential osmotic responses associated with Ca^{2+}-dependent ion conductances.

In addition to the mechanical responses driven by Deiters' cells, here we show that active changes in the shape of pillar cells could also underlie the tissue movements observed in the cochlear epithelium after TRPA1 stimulation. We believe this is the first report showing that cochlear pillar cells possess Ca^{2+}-dependent contractile machinery.
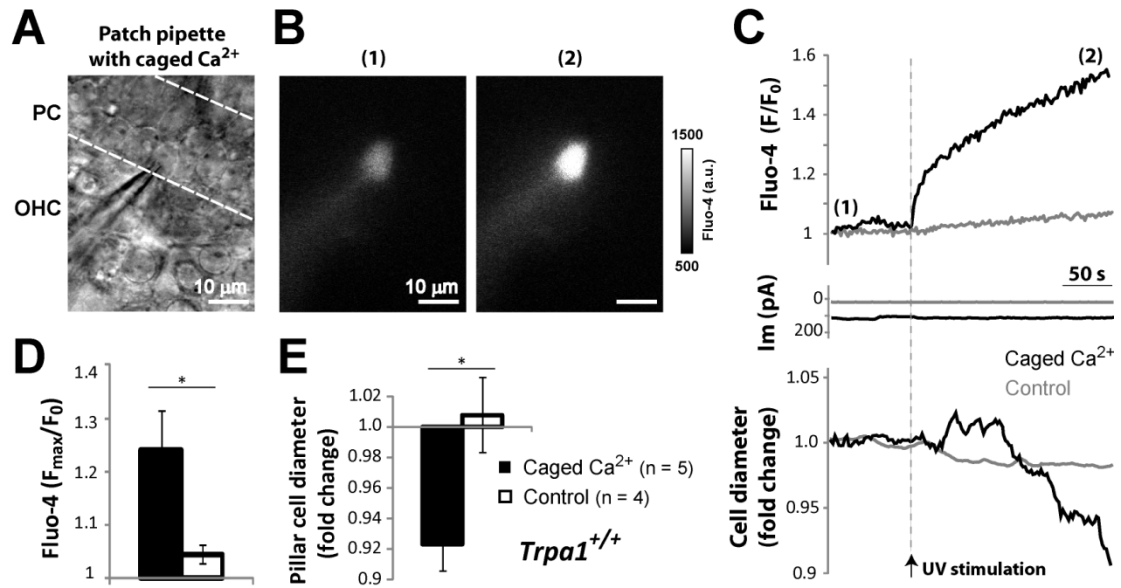
Figure 4.22. Outer pillar cells exhibit cell contractions after an increase in intracellular Ca^{2+}

A, Bright field image illustrating the experimental approach used to deliver the caged Ca^{2+} to individual outer pillar cells via whole-cell patch clamping. The caged compound (1 mM, NP-EGTA) was present in the intracellular solution (which contained 0.7 mM CaCl$_2$). *PC*, pillar cells; *OHC*, outer hair cells. *B*, Representative change in intracellular Ca^{2+} evaluated through the fluorescent dye fluo-4 present in the intracellular solution (50 µM). Images were obtained before (*1*) and after (*2*) stimulation with the UV laser. *a.u.*, arbitrary units. *C*, Representative traces showing the changes in intracellular Ca^{2+} (*top*), whole-cell currents (*middle*) and cell diameter (*bottom*) of a cell loaded with the caged compound (black) or with regular EGTA (grey). The dashed line represents the time where UV stimulation occurred. *D, E,* Average peak increase in intracellular Ca^{2+} (F$_{max}$/F$_0$) (*D*) and decrease in cell diameter (*E*) of cells loaded with caged Ca^{2+} (filled bars) or control EGTA (open bars). Bars show mean ± SEM values. The number of cells included for both analyses are shown in panel *E*. (*) indicates a P value < 0.05 determined by a Student's t-test.

105

4.11 TRPA1 contributes to a long-lasting inhibition of cochlear amplification after noise exposure

We hypothesized that the activation of cochlear TRPA1 channels *in vivo* may occur after the oxidative damage following acoustic trauma. This activation would induce changes in the pillar cell shape and modify the geometry of the cochlear epithelium and alter hearing sensitivity. Therefore, we decided to test hearing thresholds and cochlear amplification after exposing young adult (3-4 weeks old) wild type and $Trpa1^{-/-}$ mice to noise.

First, we confirmed that, in agreement with published literature [101, 102], $Trpa1^{-/-}$ mice and their wild type littermates exhibit identical hearing thresholds before noise exposure (Figure 4.23).
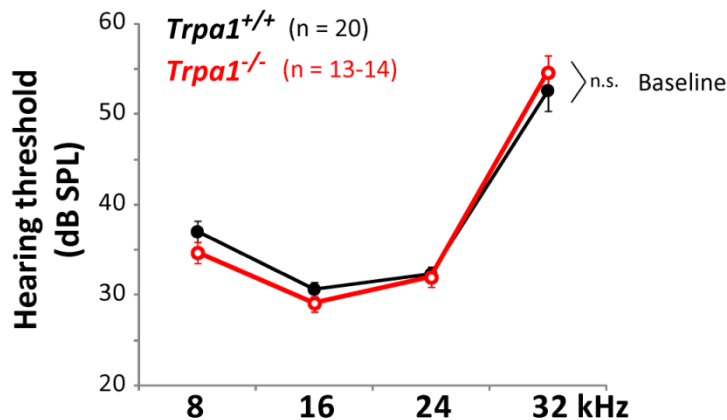
Figure 4.23. Trpa1$^{-/-}$ mice exhibit normal hearing thresholds
Hearing thresholds were determined in wild type (black) and $Trpa1^{-/-}$ mice (red) by evaluating the auditory brainstem responses (ABR) to tone stimulations at 8, 16, 24 and 32 kHz. Mean ± SEM values are plotted. A P value > 0.6 was determined using a two-way ANOVA.

Next, we exposed the mice to a broadband noise at 100 dB for 30 min. Immediately after the noise exposure, hearing thresholds were significantly higher in $Trpa1^{-/-}$ mice (Figure 4.24A). However, five days after the noise exposure, wild type mice were the ones exhibiting significantly higher hearing thresholds (Figure 4.24A).
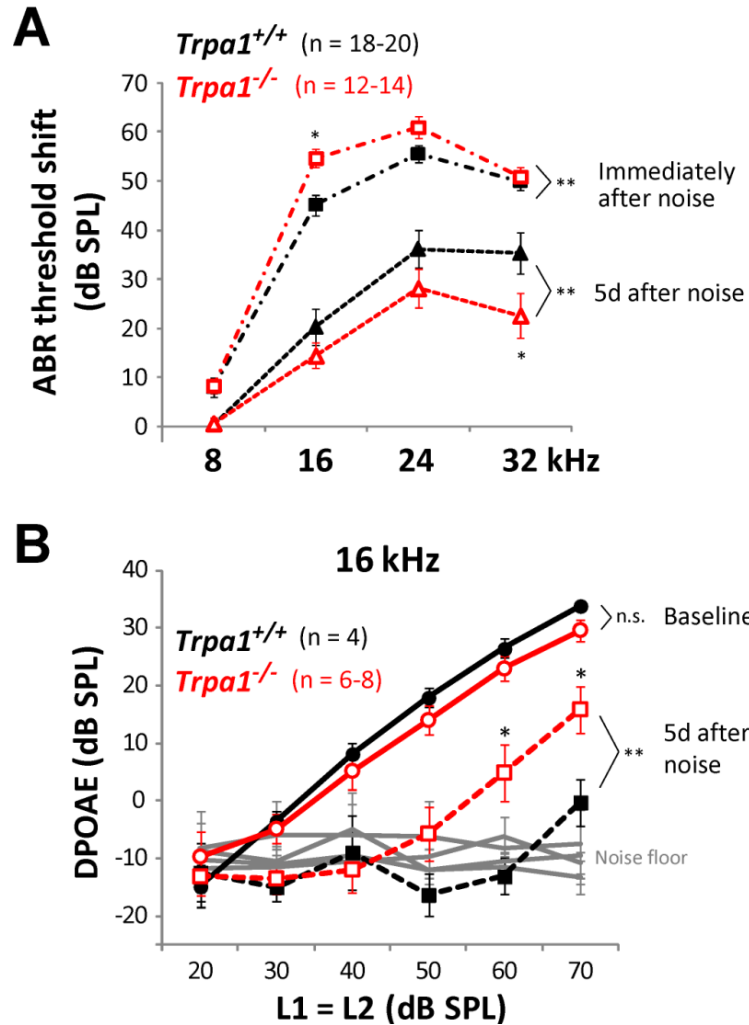
Figure 4.24. TRPA1 channels mediate a long-lasting inhibition of hearing thresholds after noise exposure

A, Hearing threshold shifts (*i.e.* relative to thresholds before noise exposure) measured via auditory brainstem responses (ABR). *B*, OHC function essesntial for cochlear amplification was measured with distortion product otoacoustic emissions (DPOAE) at 16 kHz. Wild type (black) and *Trpa1$^{-/-}$* mice (red) were evaluated immediately after (dash-dot lines) and/or 5 days after (dashed lines) noise exposure. Mean ± SEM values are plotted. (**) indicates a P value < 0.01 determined using a two-way ANOVA, and (*) P < 0.05 determined after Bonferroni corrections.

The changes in the hearing thresholds after noise exposure indicated that, in spite of initially exhibiting a greater hearing loss, *Trpa1*⁻ᐟ⁻ mice are able to recover hearing thresholds a faster rate than wild type mice (Figure 4.25). The hearing thresholds in mammals crucially depend on the cochlear amplification provided by the OHC electromotility. Thus, we wondered whether the differences in the recovery of hearing thresholds between wild type and *Trpa1*⁻ᐟ⁻ mice resulted from the modulation of the electromechanical feedback of OHCs that can be assessed by measuring distortion product otoacoustic emissions (DPOAE). We found that 5 days after noise exposure the DPOAE was significantly lower in wild type mice (Figure 4.24B). These results suggest that, after noise exposure, TRPA1 channels maintain hearing thresholds elevated by delaying the recovery of the cochlear amplifier.
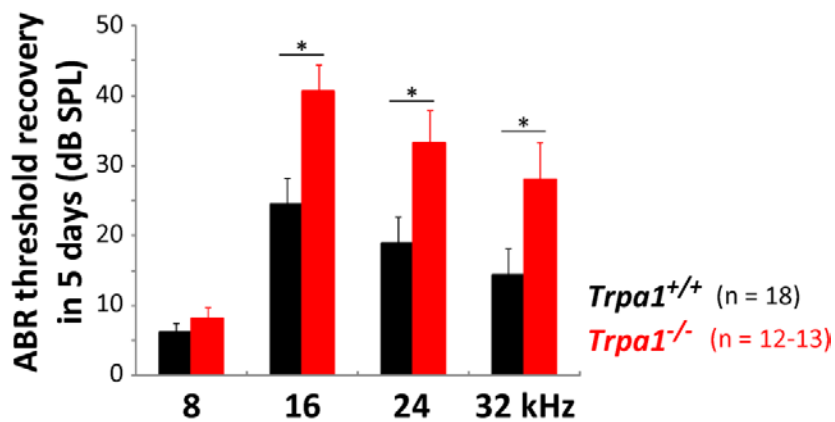
Figure 4.25 Faster recovery of ABR hearing thresholds in Trpa1⁻ᐟ⁻ mice
Degree of recovery of auditory brainstem responses (ABR) in 5 days for wild type (black) and *Trpa1*⁻ᐟ⁻ mice (red). Data were calculated as the difference between hearing thresholds immediately after noise exposure minus the hearing thresholds 5 days later. The same data shown in Figure 4.24A were used for this analysis. Bars show mean ± SEM values. (*) indicates a P value < 0.05 determined by Student's t-tests.

Because the delayed recovery of hearing thresholds in wild type mice might represent the effect of a TRPA1-mediated 'protective' mechanism, we exposed mice to a second round of noise on day 5 of recovery. Two weeks after the second noise exposure, the

hearing thresholds at 8 and 16 kHz had recovered to normal levels but were still elevated for 24 and 32 kHz (Figure 4.26). Therefore, this protocol of noise exposure led to a mixture of temporary (TTS) and permanent (PTS) threshold shifts in both wild type and *Trpa1*$^{-/-}$ mice. We did not observe significant differences between the hearing thresholds of wild type and *Trpa1*$^{-/-}$ mice after the two weeks of recovery (P > 0.6). Because we observed PTS even in wild type animals, it is very plausible that the noise protocol used was too damaging to reveal the potential protective effect of TRPA1 activation.
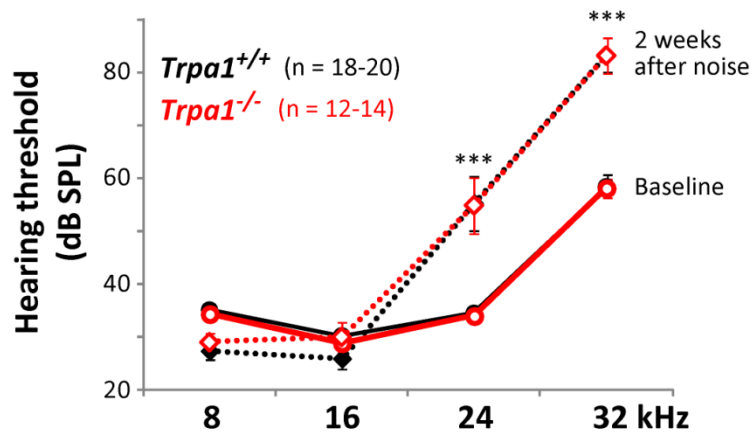
Figure 4.26. The noise exposure used leads to permanent threshold shifts in the high frequency range

Hearing thresholds were determined in wild type (black) and *Trpa1*$^{-/-}$ mice (red) before (Baseline, solid lines) and 2 weeks after a second noise exposure (dotted lines) by evaluating the auditory brainstem responses (ABR) to tone stimulations at 8, 16, 24 and 32 kHz. Mean ± SEM values are plotted. (***) indicates a P value < 0.001 (after Bonferroni corrections) between hearing thresholds at baseline and after 2 weeks of recovery for each mouse group.

Noise exposure leads to the generation of reactive oxygen and nitrogen species in the cochlea. Moreover, these reactive species continue to be generated for days after the initial acoustic trauma [285]. Therefore, we wondered whether our protocol of noise exposure was able to lead to an increase in oxidative damage that could last for at least 5 days. We performed immunolabeling of 4-HNE-modified proteins in cochleae from wild

type mice. In agreement with our hypothesis, we found increased amounts of 4-HNE-modified proteins 5 days after noise exposure (Figure 4.27). These results indicate that, even 5 days after the noise exposure, TRPA1 channels could get activated due to prominent presence of oxidative tissue damage. Moreover, the TRPA1-mediated changes of the shape of pillar cells could maintain the geometry of the cochlear epithelium in a modified shape that decreases the cochlear amplification.
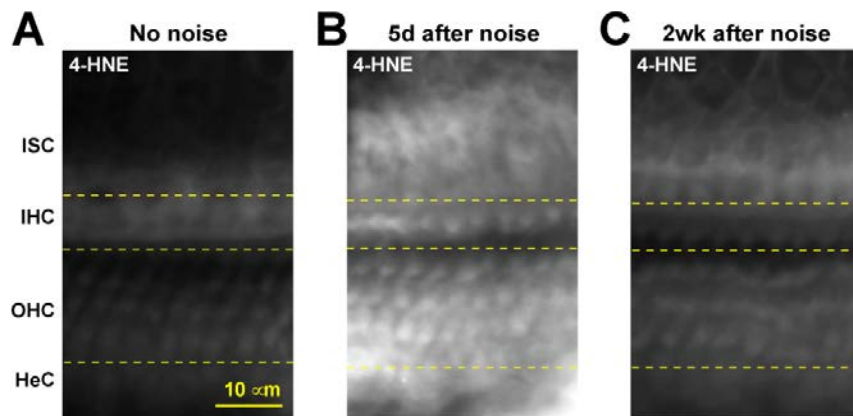
Figure 4.27. 4-HNE-modified proteins are increased in the cochlear epithelium 5 days after noise exposure

A-C, Immunolabeling against 4-HNE-modified proteins in cochleae from wild type mice not exposed to noise (*A*) or at 5 days (*B*) or 2 weeks (*C*) after noise exposure. *ISC*, inner sulcus cells; *IHC*, inner hair cells; *OHC*, outer hair cells; *HeC*, Hensen's cells.

CHAPTER 5

Discussion of results, study limitations and future directions

TRPA1 channels have gained the reputation of broad damage sensors in numerous tissues and pathological conditions. They are highly expressed in a subset of nociceptive neurons where they are involved in the detection of 'harmful' stimuli and the modulation of mechanical –and perhaps thermal– hyperalgesia. TRPA1 channels are also expressed in non-neuronal tissues where they might alter inflammatory and immune responses, through poorly understood mechanisms. TRPA1 mRNA expression has also been reported in the mammalian inner ear [177]. However, *Trpa1$^{-/-}$* mice have normal hearing and balance (*i.e.* cochlear and vestibular functions, respectively), as well as normal mechano-electrical transduction in the inner ear sensory cells (hair cells) [101, 102]. We *hypothesized* that, similar to its function in other tissues, TRPA1 channels in the inner ear act as tissue damage sensors; for instance, during the oxidative damage induced by acoustic trauma.

Our results show that, indeed, TRPA1 channels in the cochlear epithelium can be activated by byproducts of oxidative tissue damage. However, in the inner ear, TRPA1 channels seem to be doing more than merely "sensing" the damage. Our results uncovered a novel TRPA1-initated pathway of communication between different types of non-sensory (supporting) cochlear cells. The Hensen's cells seem to act as major 'sensors' for tissue damage, while other supporting cells (*i.e.* pillar and Deiters' cells) types are the main 'effectors' by changing the geometry of the organ of Corti thus altering hearing sensitivity. This pathway represents a hitherto unknown mechanism of cochlear regulation.

5.1 Propagation of TRPA1-mediated signals across the cochlear epithelium

Our results indicate the presence of an active TRPA1 promoter throughout the entire cochlear epithelium. We also demonstrated TRPA1 channel activity in most supporting cell types either with FM1-43 uptake, Ca^{2+} imaging or whole-cell patch clamp recordings. In some supporting cells, these different techniques produced different results. We did find that the kinetics of the responses to TRPA1 activation were somewhat unique for each type of supporting cell. For instance, Hensen's cells exhibited robust and long-lasting Ca^{2+} responses to all TRPA1 agonists tested, while Claudius' cells only responded to TRPA1 agonists when the gap junction blocker FFA was present in the bath solution.

The particularly long-lasting behavior of the TRPA1-mediated responses in Hensen's cells seems to indicate that in these cells the channel is locked in an open configuration. This might arise from (*i*) the reactive nature of the TRPA1 agonists tested and/or (*ii*) a positive feedback provided by the intracellular Ca^{2+} levels. To test whether the long-lasting responses to TRPA1 stimulation are the result of long-lasting covalent modifications in its intracellular N-terminus, additional experiments should be performed using non-reactive agonists, such as icilin, since they seem to activate TRPA1 via a 'classical' lock-and-key mechanism.

Interestingly, the TRPA1-mediated Ca^{2+} responses in Hensen's cells never propagated to their immediate neighbors, the Claudius' cells. Instead, TRPA1-mediated Ca^{2+} responses in the Hensen's cells always propagated toward the medial side of the cochlea, and elicited Ca^{2+} waves in the Kolliker's organ. These 'secondary' Ca^{2+} waves in the Kolliker's organ required the release of ATP to the extracellular space for their cell-to-cell propagation. Therefore, we believe the Ca^{2+} responses that we observed in the Kolliker's organ are secondary to the activation of TRPA1 channels in Hensen's cells and correspond to the Ca^{2+} waves that have been previously described by others (Figure 1.10) [37, 70].

Extracellular ATP is thought to be an important signaling molecule during tissue damage in the cochlea. Damage of a single sensory hair cell is able to trigger robust ATP-dependent self-propagating Ca^{2+} waves in the cochlear epithelium; mice lacking $P2X_2$ receptors are more susceptible to noise-induced permanent hearing loss [81]; and low

levels of ATP have been detected in the cochlear fluids after acoustic overstimulation [68]. It has been demonstrated that ATP-initiated Ca^{2+} waves in the cochlear epithelium are sustained by and critically depend on the Ca^{2+}-evoked release of ATP into the extracellular fluid [295]. However, the exact mechanism initiating the very first release of ATP into cochlear fluids remains unknown. Our results revealed a previously unknown and never considered mechanism: the activation of TRPA1 channels in the Hensen's cells might initiate Ca^{2+} waves that trigger the release of ATP to the extracellular space. Once the ATP is released outside the cell, it can maintain secondary Ca^{2+} waves through previously described mechanisms (Figure 1.10) [37, 70] and/or activate TRPA1 channels in other supporting cells downstream of metabotropic P2Y receptors (manuscript in preparation, Vélez-Ortega AC, *et al.*, see Appendix D for details). Therefore, the activation of TRPA1 channels may represent a long-sought event that initiates protective ATP signaling in the cochlea during noise exposure. Obviously, our results do not refute other potential mechanisms of ATP release, such as the one hypothesized for cells within the stria vascularis [68, 297]. However, ATP release associated with Ca^{2+} waves propagating after TRPA1 activation in Hensen's cells would result in the most effective local rise of extracellular ATP right in the organ of Corti region.

The activation of TRPA1 channels downstream of P2Y receptors has been studied in transfected HEK-293 cells but not in cochlear supporting cells (manuscript in preparation, Vélez-Ortega AC, *et al.*, see Appendix D for details). Therefore, patch clamp recordings could be performed in cochlear supporting cells from wild type and *Trpa1*$^{-/-}$ mice to evaluate for the presence of TRPA1-induced inward currents after puff stimulation with a very low concentration of ATP –that may activate P2Y but not P2X receptors–.

TRPA1 activation in the Hensen's cells is unlikely to stimulate direct ATP release from these cells to the extracellular fluid; otherwise, the Claudius' cells –which express P2Y receptors– would have exhibited Ca^{2+} responses secondary to the TRPA1 stimulation of Hensen's cells. If Hensen's cells do release ATP to the extracellular space after TRPA1 activation, one plausible explanation for the absence of responses in the Claudius' cells would require the (*i*) release of ATP through the basolateral membrane of Hensen's cells and (*ii*) the expression of P2Y receptors in the apical surface of Claudius'

cells. However, the exact subcellular localization of P2Y receptors in Claudius' cells is unknown.

The exact mechanism of propagation of TRPA1-dependent Ca^{2+} responses from the Hensen's cells toward the Kolliker's organ has not been completely resolved. We did not observe the involvement of inner (IHC) and outer (OHC) hair cells in this propagation but, because the ratiometric Ca^{2+} dye used failed to load pillar and Deiters' cells, we were unable to see whether the Ca^{2+} responses propagated through these two types of supporting cells. Several unsuccessful attempts to load pillar and Deiters' cells with the Ca^{2+} dye were performed as follows:

i) Nearby supporting and/or hair cells were removed to disrupt the tight junctional barrier at the reticular lamina of the cochlear epithelium and thus allow uptake of the Ca^{2+} dye through the basolateral membranes. Unfortunately, supporting cells can quickly re-seal the reticular lamina. Therefore, we had to remove a substantial number of cells to guarantee that the reticular lamina would not be resealed during the incubation with the Ca^{2+} dye. This caused extensive damage to the tissue and considerable alterations of its geometry and cell shapes.

ii) The approach described above resulted in the uptake of the Ca^{2+} dye only by pillar and Deiters' cells that were in close proximity to the site of tissue damage. Therefore, to increase the amount of Ca^{2+} dye present underneath the reticular lamina, puff pipettes were used to establish a perfusion system between the rows of pillar cells (*i.e.* the space that constitutes the tunnel of Corti in the adult cochlea). This perfusion strategy often led to pressure build up underneath the tissue when the "exit" pathway was resealed (*i.e.* secondary area where cells had been removed to allow for the perfusion to occur). This increase in fluid pressure underneath the reticular lamina disrupted connections between the basolateral membranes of supporting cells, as evidenced during bright field imaging.

iii) To minimize the excretion of the intracellular Ca^{2+} dye, we also loaded the cochlear explants in the presence of 250 μM of the organic anion-transport inhibitor sulfinpyrazone (Invitrogen) [298, 299]. This strategy slightly improved the loading of other cell types, but not of pillar and Deiters' cells.

iv) Normally, the cochlear explants were incubated in the presence of the Ca^{2+} dye for 50 min at room temperature. In order to decrease incubation times in some of the

approaches described above, the dye concentration was increased and/or the incubation was performed at 37°C. Once again, this approach failed to improve the loading of pillar and Deiters' cells with the Ca^{2+} dye.

v) The loading of the ratiometric Ca^{2+} dye was also evaluated in rat cochlear explants because they have slightly larger cells and, therefore, a greater surface area of pillar and Deiters' cells that would be exposed to the Ca^{2+} dye. However, rat pillar and Deiters' cells also failed to uptake the Ca^{2+} dye.

vi) The goal of the five strategies described above was to improve the loading of pillar and Deiters' cells in freshly-dissected cochlear explants. The loading with the Ca^{2+} dye greatly improved in Deiters' cells from explants that had been cultured for 2-3 days. However, after this time in culture, the Deiters' cells were no longer located underneath the OHCs; instead, the OHCs had slid between the rows of Deiters' cells. In addition to the alterations in tissue organization after 2-3 days in culture, the OHCs were more susceptible to undergo apoptosis after the stimulation with the TRPA1 agonists. Therefore, we were not able to use cultured cochlear explants to evaluate the propagation of TRPA1-induced Ca^{2+} waves from the Hensen's cells toward the Kolliker's organ.

To overcome the difficulties in loading pillar and Deiters' cells with the membrane-permeable ratiometric Ca^{2+} dye (fura-2, AM), other types of Ca^{2+} indicators could be employed such as the genetically encoded G-CaMP3 [300] or D3cpv [301] Ca^{2+} reporters. Vectors encoding these Ca^{2+} indicators are commercially available (Addgene plasmids #22692 and #36323, respectively) and could be used to transfect cells from cochlear explants via electroporation [302, 303] or gene gun [304]. Alternatively, transgenic mice with conditional expression of G-CaMP3 limited to cells expressing the Cre recombinase are also commercially available (Jackson laboratories, stock number 014538). They could be bred with mice that express Cre under a ubiquitous promoter or under promoters specific for cochlear supporting cells (*e.g.*, Cre expression under the Prox1 promoter would be limited to outer pillar and Deiters' cells [305]).

It is possible that TRPA1-initiated Ca^{2+} responses at the Hensen's cells propagate through the gap junctional conductance to the Kolliker's organ via Deiters' and pillar cells. Interestingly, the permeability of gap junctions connecting Hensen's to pillar cells is very different from the permeability between Hensen's and Claudius' cells [33, 34].

Our whole-cell recordings showed that Deiters' cells express functional TRPA1 channels too but we were unable to detect TRPA1-mediated currents in pillar cells. However, if pillar cells do express TRPA1 channels, it is possible that they were simply not gated due to the conditions of our experimental approach. In fact, Claudius' cells failed to exhibit TRPA1-mediated Ca^{2+} responses during our initial experimental conditions, but we eventually revealed the presence of functional TRPA1 channels in these cells as well.

Regardless of the exact mechanism of cell-to-cell propagation, the TRPA1-induced Ca^{2+} responses in the Hensen's cells consistently traveled in a unidirectional way. This behavior differed from other types of Ca^{2+} waves elicited after hair cell damage. ATP-dependent self-propagating Ca^{2+} waves triggered after the death of a single hair cell can propagate in all directions around the damaged site, even to Claudius' cells [37, 38]. TRPA1-initiated Ca^{2+} responses in Hensen's cells are likely to require the propagation of a second messenger that may be specific for some unique gap junctions between these cell types [33, 34], which would account for the inability of the signal to propagate toward the Claudius' cells. The physiological significance of this special mechanism of propagation of TRPA1-initiated Ca^{2+} responses from the Hensen's cells toward the Kolliker's organ may be to simply ensure the activation of supporting cells that have poor access to the apical surface of the cochlear epithelium (*e.g.* pillar and Deiters' cells). This could be the case when, for instance, byproducts of oxidative stress are mainly present in the endolymph.

Altogether, our results indicate that (*i*) Hensen's cells mount robust Ca^{2+} responses in the presence of oxidative damage via the activation of TRPA1 channels; and (*ii*) this responses are able to propagate to the Kolliker's organ and trigger Ca^{2+} waves that release ATP to the extracellular space (Figure 5.1).

The ATP-induced Ca^{2+} waves after hair cell death are known to activate intracellular signaling cascades that may promote cell survival [37, 69]. Because TRPA1 activation can trigger ATP-dependent Ca^{2+} waves, it is possible that similar –if not the same– signaling pathways are activated. Of note, Hensen's cells might exert anti-inflammatory actions by releasing into the extracellular space the contents of their lipid droplets, which are rich in the anti-inflammatory protein annexin A1 [61]. Perhaps, the long-lasting

increase in intracellular Ca^{2+} induced after TRPA1 activation of Hensen's cells can activate the signaling pathways involved in the release of the lipid contents.
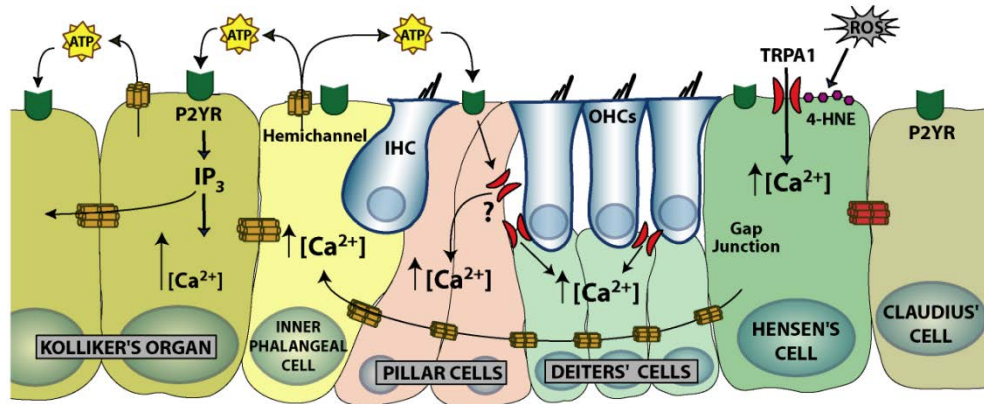
Figure 5.1. Diagram of Ca^{2+} responses and their propagation after TRPA1 stimulation in the cochlear epithelium

Hensen's cells seem to be the major sensors of oxidative damage in the cochlea. The TRPA1-mediated Ca^{2+} responses in Hensen's cells can propagate toward the Kolliker's organ (presumably involving the gap junctional conductance through Deiters' and pillar cells) but do not propagate toward the Claudius's cells. After making their way to the Kolliker's organ, ATP-dependent self-propagating Ca^{2+} responses are elicited. Because extracellular ATP can activate TRPA1 channels downstream of P2Y receptor signaling, the release of ATP in the Kolliker's organ could initiate secondary activation of TRPA1 channels. Deiters' cells express TRPA1 channels and can respond to direct agonist stimulation. Pillar cells may also express TRPA1 channels despite our inability to evoke TRPA1 responses in these cells during whole-cell patch clamp experiments.

The activation of TRPA1 channels in the cochlear epithelium after the stimulation with 4-HNE, a byproduct of oxidative tissue damage, indicates that TRPA1 channels behave as tissue damage sensors in the cochlea, similarly to their role in nociceptive neurons. TRPA1 channel activation in nociceptive neurons leads to membrane depolarization and triggers action potentials that result in the sensation of pain. 'Ear pain'

is generated by the activation of nociceptive neurons innervating the outer and middle ear since the inner ear is not considered to have nociceptive innervation. Cochlear supporting cells do not trigger action potentials; instead, TRPA1 activation leads to an increase in cytosolic Ca^{2+} that might activate several signaling cascades. The signaling cascades activated after TRPA1 gating in cochlear supporting cells might be similar to those observed in TRPA1-expressing non-neuronal cells (*e.g.*, epithelial and smooth muscle cells in the lung). In particular, the A549 cell line derived from human lung epithelial cells shows a robust increase in the phosphorylation of ERK1/2 and Akt2 after TRPA1 stimulation with mustard oil [306]. Similar, results were obtained in HEK-293 cells transfected with human or mouse TRPA1 [306]. Therefore, activation of TRPA1 channels in the inner ear might trigger pro cell-survival signaling cascades similar to those activated by extracellular ATP (*i.e.* involving ERK1/2 phosphorylation).

In this study, however, we did not pursue the changes in cell signaling cascades after TRPA1 activation. Instead, we decided to study the effect of TRPA1 activation in the mechanical properties of the cochlear epithelium. This approach was considered after noticing that TRPA1 activation induced prominent tissue displacements observed during bright field imaging.

5.2 TRPA1 activation induces changes in the geometry of the cochlear epithelium

The TRPA1-mediated Ca^{2+} responses described above led to a slow but prominent movement within the cochlear epithelium. Because the tissue displacements involved changes in a three-dimensional (3D) fashion, they were hard to study through imaging obtained from a 2D plane. Luckily, when the direction of the tissue movement was aligned with the focal plane that was being imaged, we noticed prominent cell contractions in the pillar cells and Deiters' cells.

Flash photolysis of caged Ca^{2+} led to long-lasting contractions in outer pillar cells, indicating that these cells possess Ca^{2+}-dependent contractile machinery. The phalangeal processes of Deiters' cells have been reported to exhibit mechanical responses after an increase in intracellular Ca^{2+} [56, 57]. Therefore, outer pillar cells together with Deiters' cells might contribute to the TRPA1-dependent tissue movements observed. However, we believe we are the first to show that pillar cells in the organ of Corti possess Ca^{2+}-

dependent contractile machinery. Notably the phalangeal processes of Deiter's cells and the stalks of pillar cells possess a cytoskeleton rich in microtubules and actin filaments (reviewed in [32]). To understand the machinery driving the Ca^{2+}-dependent changes in cell shape, future studies could evaluate TRPA1-dependent tissue displacements in the presence of pharmacological treatments that modify the cytoskeleton dynamics. In particular, several drugs that enhance or inhibit the polymerization of actin filaments o microtubules have been shown to modify the stiffness of cochlear pillar cells [307]. Moreover, an inhibitor of myosin II was able to both increase and decrease –depending on the developmental age– the stiffness of pillar cells [307].

In an attempt to 'quantify' the magnitude of the TRPA1-induced tissue displacements, we tried to perform an optical flow analysis of the bright field time-lapse image sequences. This type of analysis measures the relative motion of specific pixels within a sequence of images, and it is often used to track the movement of edges and objects. The analysis was performed with the collaboration of Dr. Brandon K. Fornwalt and Dr. Jonathan Suever from the Department of Physiology at the University of Kentucky. Unfortunately, we were unable to track the changes in cell shape with this technique. The major problem arises from the assumption that the pixels to be tracked will not exhibit significant changes in grayscale values over time. However, changes in the shape of cells alter the light scattering pattern in the image, which results in prominent changes in pixel value intensity (Figure 5.2). To overcome the problem of pixel value changes for optical flow analysis, we would need to perform significant modifications to existing algorithms.
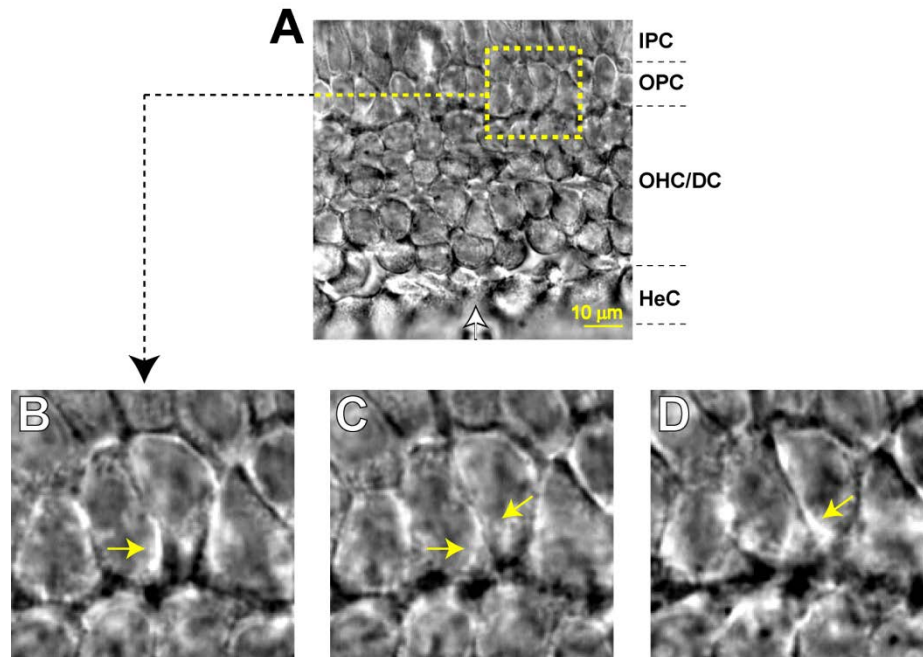
Figure 5.2. Tissue movement during bright field imaging leads to changes in pixel intensity values

A, Bright field image showing an example of a region within the cochlear epithelium where tissue displacements were evaluated after puff stimulation with TRPA1 agonists. The white arrow indicates the position and direction of puff application. *B-C*, Sub-region from the image in A (indicated by the dashed window) is shown at a higher magnification and from three different time points (B-C) during the time lapse imaging. Yellow arrows indicate areas where cell contractions led to changes in pixel intensity values between frames (compare arrows in panel *C*, with the corresponding pair in either *B* or *D*).

A simpler approach we used to detect the presence of tissue movements by subtracting frames taken 10 s apart. This analysis is sensitive to both pixel movement as well as changes in pixel value. It revealed two distinct peaks in the average trace for 4-HNE-induced movement from the wild type explants (Figure 4.19C, top). Due to the type of analysis used, a second peak could simply represent the time point when the tissue is recovering toward its original shape. However, the study of the individual bright field recordings showed that, in some explants, the 4-HNE-induced movements occurred

several minutes after the puff stimulation (*i.e.* near the end of the recording) (data not shown). Therefore, the second peak observed in Figure 4.19C (top) indicates the average time point where the movement occurred in the explants that exhibited a delay.

To fully understand which cell types are involved and what type of changes (*e.g.*, elongation vs. contraction) orchestrate the tissue displacements triggered after TRPA1 stimulation, we believe that the imaging technique used needs to provide information in 4D (*x, y, z* and *time*). Using a cell-membrane dye (CellMask^{TM}, Molecular Probes) we successfully labeled the plasma membrane of hair cells and supporting cells within the cochlear epithelium (Figure 5.3).
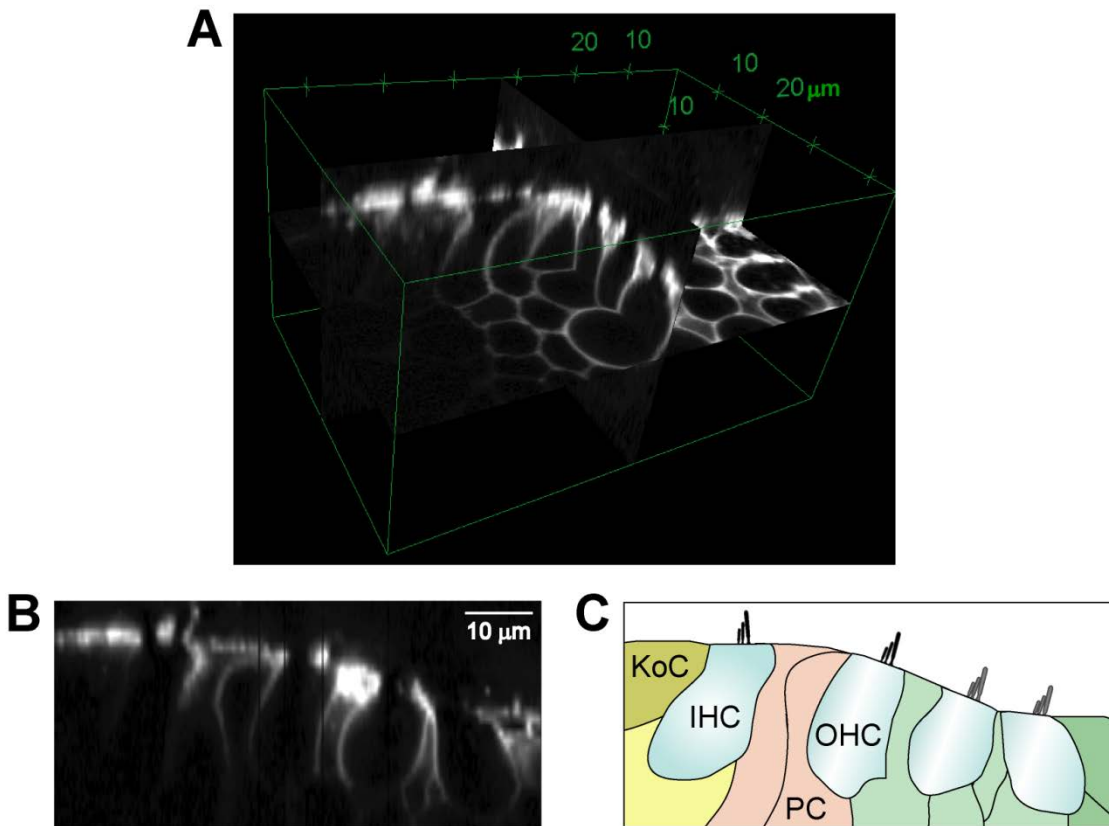
Figure 5.3. Labeling of cell membranes in the cochlear epithelium for 3D imaging reconstruction

A, Representative 3D view of a cochlear explant labeled with the plasma membrane dye CellMask^{TM}. *B*, An orthogonal view from the tissue shown in *A*. *C*, Diagram illustrating the cell types observed in the image from *B*.

121

Using a spinning disc confocal microscope (section 3.3.3) for the time-lapse imaging, we were able to obtain 3D stacks every ~ 3-5 s. The stacks consisted of 5 to 10 confocal images acquired every 3 μm. Because the TRPA1-induced tissue displacements are slow, we believe this imaging speed is sufficient for the study of this type of movements. However, this type of labeling seemed to compromise the integrity of the plasma membrane and caused cell death in some sensory and supporting cells during the puff application of 4-HNE. As an alternative, 4D imaging could be performed using tissue from the mT/mG mouse, a reporter mouse that exhibits ubiquitous expression of a membrane-targeted fluorescent marker. In fact, this mouse was recently used to study the architecture of live cochlear epithelium via 3D image stacks [308]. In a future study, we consider collaborating with Dr. Anthony Ricci (Stanford School of Medicine) to cross the mT/mG transgenic mice with our TRPA1-deficient mice, in order to study the TRPA1-mediated shape changes in the organ of Corti of older mice.

In the adult cochlear epithelium, the heads of inner and outer pillar cells are in close contact while their feet are separated at the basilar membrane. This 'triangular' orientation of the pillar cells forms the tunnel of Corti, a fluid-filled space between the rows of inner and outer hair cells. Regardless of the type of movement induced by TRPA1 stimulation, it is clear that any changes in the shape of pillar cells can potentially modify the entire geometry of the organ of Corti (Figure 5.4).

As a consequence, the resting angle between the OHC stereocilia and the tectorial membrane (Figure 1.4) might change, and this would have an impact on hearing sensitivity.
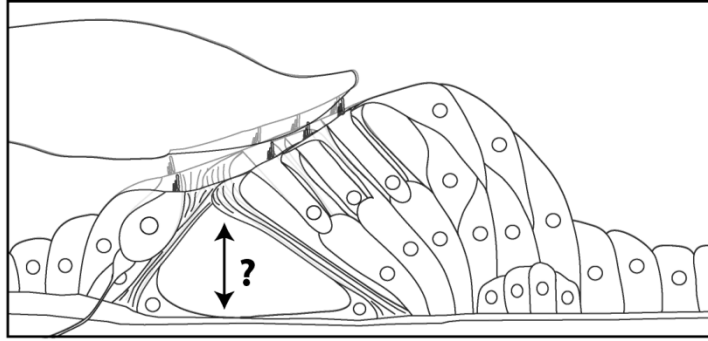
Figure 5.4. Changes in pillar cell shape can alter the geometry of the organ of Corti

Diagram illustrating how the changes in the shape of pillar cells can alter the angle between the reticular lamina and the tectorial membrane. This change in the tissue geometry would modify the angles between the OHC stereocilia and the tectorial membrane during sound stimulation. Consequently, changes in pillar cell shape would alter the hearing sensitivity.

5.3 TRPA1-mediated inhibition of cochlear amplification

After acoustic trauma, ATP is released into the cochlear fluids [68] and reactive oxygen and nitrogen species are generated in the cochlear epithelium [284, 285]. Therefore, noise exposure could lead to the activation of cochlear TRPA1 channels either through endogenous agonists or downstream of P2Y receptor activation (manuscript in preparation, Vélez-Ortega AC, *et al*., see Appendix D for details).

We showed the contraction of pillar cells in response to puff application of TRPA1 agonists or ATP. The release of ATP into cochlear fluids may mediate changes in pillar and Deiters' cell shape during and immediately after the noise exposure. In contrast, the byproducts of oxidative stress could continue to activate TRPA1 channels and lead to the changes in pillar cell shape for several days after the acoustic trauma.

As reviewed in section 1.9, noise exposure is known to cause changes in the architecture of the organ of Corti. However, whether these changes were simply the result of mechanical damage or were driven by active changes in the shape of some cells was unknown. Here we propose that acoustic overstimulation leads to TRPA1-mediated Ca^{2+}-dependent changes in the shape of pillar and Deiters' cells that can potentially alter the

entire geometry of the cochlear epithelium. Interestingly, a reduction in cochlear microphonics (*i.e.* an alternative method to test the cochlear sensitivity) has been shown to correlate with changes in the shape of cochlear supporting cells after acoustic overstimulation [85]. We found that wild type mice have a delayed recovery of hearing sensitivity after noise exposure when compared to *Trpa1*$^{-/-}$ mice. And we believe this reduction in hearing sensitivity results from the TRPA1-initiated changes in the geometry of the organ of Corti. Therefore, TRPA1 activation in cochlear supporting cells could be one of the mechanisms driving the development of TTS via the changes in the geometry of the organ of Corti.

We propose a model where noise exposure leads to the activation of the cochlear TRPA1 channels through two different pathways (Figure 5.5). During noise exposure, the ATP that is acutely released into the cochlear fluids could activate TRPA1 channels downstream of the P2Y receptors. TRPA1 activation may result in changes in the geometry of the organ of Corti that would decrease hearing sensitivity and provide some degree of protection to the cochlear sensory epithelium. For instance, a reduction in glutamatergic excitotoxicity would result in a lesser degree of postsynaptic afferent terminal retraction from the IHC. The loss of this TRPA1-mediated protection could explain why immediately after noise exposure *Trpa1*$^{-/-}$ mice exhibited higher hearing thresholds than wild type mice.

OHC electromotility via the piezoelectric behavior of prestin in the plasma membrane constitutes the cochlear amplifier. Given that TRPA1 channels are expressed in OHC [286], TRPA1 activation during noise exposure could also modulate hearing sensitivity by exerting a direct effect on prestin function. However, we did not observe Ca^{2+} responses in OHCs after puff application with any of the TRPA1 agonists tested. Nevertheless, it is necessary to study the impact of TRPA1 activation on OHC electromotility to fully understand its contribution in the differences that we observed between wild type and *Trpa1*$^{-/-}$ mice during and immediately after noise exposure.

While the release of ATP into cochlear fluids might be an acute phenomenon after noise exposure, the generation of reactive oxygen species after acoustic overstimulation can last for several days or weeks [285]. During this period of time, TRPA1 channels would continue to be activated, for example, by lipid peroxidation byproducts like 4-

HNE. This long-lasting activation of TRPA1 channels might maintain a modified geometry of the organ of Corti and explain the longer-lasting TTS that we observed in wild type mice.
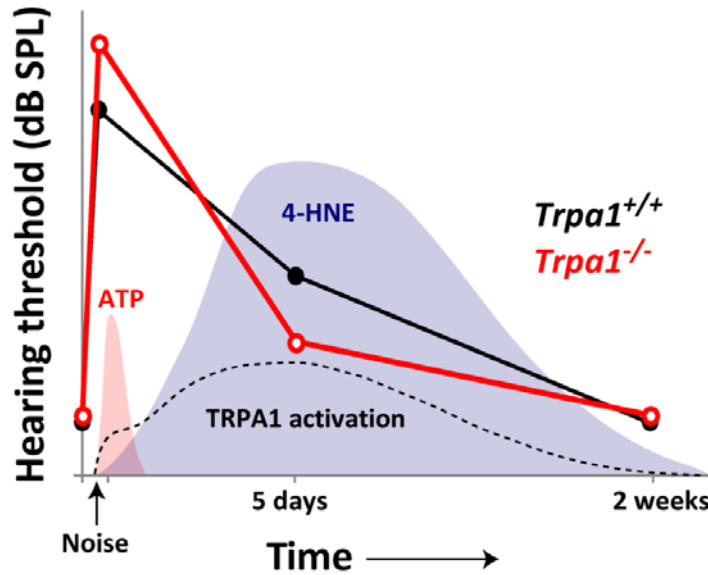
Figure 5.5. TRPA1 activation after ATP release or 4-HNE production in the cochlea modulates hearing thresholds

Diagram illustrating representative changes in hearing thresholds for wild type (black) and *Trpa1⁻/⁻* mice, and the two pathways that could activate TRPA1 channels after noise exposure. The acute release of ATP into the cochlear fluids could initiate the changes in tissue geometry during the noise exposure and limit the damage-induced increase in hearing threshold. Later, the chronic exposure to byproducts of oxidative tissue damage, like 4-HNE, might maintain the tissue with the modified geometry for days after the acoustic trauma. This long-lasting inhibition of cochlear amplification might protect from damaging loud sounds while the organ of Corti structures are repaired.

Further studies could be designed, using multiple noise exposure protocols, to test whether TRPA1-mediated changes in hearing sensitivity in fact protect against noise-induced hearing loss. We tried a couple of protocols with noise exposure at 2 or 3 different time points. However, 2 weeks after the last episode of noise exposure, all mice

exhibited high levels of PTS across most frequencies tested. We believe that, for multiple noise exposures, it will be necessary to decrease the magnitude of the noise used. Moreover, we evaluated hearing thresholds 2 weeks after the noise exposure to assess for the development of permanent threshold shifts (PTS) after noise exposure. We now believe that it would appropriate to continue measuring the recovery of hearing thresholds for longer time points (*e.g.*, 4 to 6 weeks after noise exposure) to better estimate the development of PTS. Additionally, it would be interesting to test whether exposure to low noise makes *Trpa1*$^{-/-}$ mice more susceptible to develop age-related hearing loss. Similarly, it has not been reported whether patients suffering from the familial episodic pain syndrome due to a gain-of-function mutation in TRPA1 channels exhibit elevated hearing thresholds or perhaps age-related hearing loss [103]. To this date, there is only one human pedigree reported to carry mutations in the TRPA1 gene. Interestingly, these individuals are from a small region near my hometown in Colombia and I am quite familiar with one of the groups involved in the original report of the mutation: the Molecular Genetics group from the University of Antioquia (Colombia) led by Dr. Grabiel Bedoya. I performed the research for my Master's degree in the same institution –and the exact same building– where this group is located which might facilitate future collaborations. Initially we could perform hearing tests in all members of this pedigree and establish whether carriers of the mutation exhibit higher hearing thresholds than age-matched non-carriers within the same family.

5.4 Closing remarks

In summary, in this study I have demonstrated that:

i) TRPA1 agonists, including the endogenous byproducts of oxidative stress, evoke robust and long-lasting Ca^{2+} responses in Hensens' cells;

ii) these responses are able to propagate to the Kolliker's organ and trigger Ca^{2+} waves that release ATP to the extracellular space;

iii) the propagation of Ca^{2+} waves is accompanied by prominent tissue displacements originated at pillar and perhaps Deiters' cells;

iv) pillar cells possess active Ca^{2+}-dependent contractile machinery that could change the geometry of the organ of Corti and regulate hearing sensitivity during and long after noise exposure; and

v) the hearing thresholds of TRPA1-deficient mice are indeed more susceptible to acoustic trauma during noise exposure and show a decrease in the long-lasting temporal shift of hearing thresholds due to, we believe, the loss of the protective component in this threshold shift.

To the best of our knowledge, all of these results are novel and represent a hitherto unknown mechanism of cochlear regulation after noise exposure.

APPENDIX A

List of syndromes associated to mutations in human TRP genes with their respective entry numbers in the *Online Mendelian Inheritance in Man* (OMIM) catalog (*i.e.* MIM numbers). The OMIM catalog can be accessed at http://www.omim.org.

AD   Autosomal dominant

AR   Autosomal recesive

Ref.   References

TRP gene	Syndrome	Inheritance	MIM number	Ref.
TRPA1	Familial episodic pain syndrome	AD	615040	[103]
TRPC6	Focal segmental glomerulosclerosis 2	AD	603965	[112, 113]
TRPM1	Congenital stationary night blindness type 1C	AR	613216	[118-121]
TRPM2	Coding SNP associated with bipolar disorder		609633	[123]
TRPM4	Progressive familial heart block type 1B	AD	604559	[128-130]
TRPM6	Hypomagnesemia with secondary hypocalcemia	AR	602014	[135, 136]
TRPM7	Susceptibility to amyotrophic lateral sclerosis- Parkinsonism/ dementia complex		105500	[138]
TRPML1	Mucolipidosis IV	AR	252650	[143, 144]
TRPP1	Polycystic kidney disease	AD	613095	Reviewed in [146]
TRPV3	Olmsted syndrome	AD	614594	[152]
TRPV4	Brachyolmia type 3	AD	113500	[159]
	Digital arthropathy-brachydactyly	AD	606835	[162, 163]
	Metatropic dysplasia	AD	156530	[161, 309, 310]
	Charcot-Marie-Tooth neurophathy type 2C	AD	606071	[164-167]
	Congenital nonprogressive distal spinal muscular atrophy	AD	600175	[164]
	Scapuloperoneal spinal muscular atrophy	AD	181405	[164, 165]

TRPV4	Parastremmatic dwarfism	AD	168400	[160]
	Maroteaux spondyloepiphyseal dysplasia	AD	184095	[160]
	Kozlowski spondylometaphyseal dysplasia	AD	184252	[161]
	Coding SNP associated with hyponatremia		613508	[168]

Protein BLAST: Sequence alignment between the human (top, UCSC ID: uc003xza.3) mouse (bottom, UCSC ID: uc007ajc.1) and rat (UCSC ID: RGD_1303284) TRPA1 proteins. There percentage of identity between ortholog pairs and the percentage of coverage for each alignment are shown below:

% identity (including gaps)

	Human	Mouse	Rat
Human	---	80.2	80.1
Mouse		---	96.7
Rat			---

% coverage (of both)

	Human	Mouse	Rat
Human	---	99.5	99.5
Mouse		---	99.9
Rat			---

| Identical amino acid residues

\+   Similarly charged amino acid residues

–   Gap inserted in the amino acid sequence

Human → 0001 MKRSLRKMWRPGEKKEPQGVVYEDVPDDTEDFKESLKVVFEGSAYGLQNFNK-QKKLKRC 0059
              ||| ||++ | |+|| ||||| | +| + ||| || || |++| | ++|| +
Mouse → 0001 MKRGLRRILLPEERKEVQGVVYRGVGEDMDCSKESFKVDIEGDMCRLEDFIKNRRKLSKY 0060

       0060 DDMDTFFLHYAAAEGQIELMEKITRDSSLEVLHEMDDYGNTPLHCAVEKNQIESVKFLLS 0119
            +| + ||+|||||||+|||| | || |||+ || ||||||||| ||||+|||||||
       0061 EDENLCPLHHAAAEGQVELMELIINGSSCEVLNIMDGYGNTPLHCAAEKNQVESVKFLLS 0120

       0120 RGANPNLRNFNMMAPLHIAVQGMNNEVMKVLLEHRTIDVNLEGENGNTAVIIACTTNNSE 0179
            +||||||| |||+||||| || |||+||| ||+ ++||||||||||++ | +|||
       0121 QGANPNLRNRNMMSPLHIAVHGMYNEVIKVLTEHKATNINLEGENGNTALMSTCAKDNSE 0180

       0180 ALQILLKKGAKPCKSNKWGCFPIHQAAFSGSKECMEIILRFGEEHGYSRQLHINFMNNGK 0239
            ||||||+|||| ||||||| +|+||||||+|+|||+|| +||++|||| ||||+|+ |
       0181 ALQILLEKGAKLCKSNKWGDYPVHQAAFSGAKKCMELILAYGEKNGYSRETHINFVNHKK 0240

       0240 ATPLHLAVQNGDLEMIKMCLDNGAQIDPVEKGRCTAIHFAATQGATEIVKLMISSYSGSV 0299
            |+|||||||+|||+|||||||||| || +| +| |+|||||||||+||||||||||+||
       0241 ASPLHLAVQSGDLDMIKMCLDNGAHIDMMENAKCMALHFAATQGATDIVKLMISSYTGSS 0300

       0300 DIVNTTDGCHETMLHRASLFDHHELADYLISVGADINKIDSEGRSPLILATASASWNIVN 0359
            |||| || ||+|||||||+||+||+|||||||||+|||||||||||||||||||||||
       0301 DIVNAVDGNQETLLHRASLFDHHDLAEYLISVGADINSTDSEGRSPLILATASASWNIVN 0360

       0360 LLLSKGAQVDIKDNFGRNFLHLTVQQPYGLKNLRPEFMQMQQIKELVMDEDNDGCTPLHY 0419
            ||| |||+|||||+ |||||||||||||||+||||||||||||+||||||||||||||||
       0361 LLLCKGAKVDIKDHLGRNFLHLTVQQPYGLRNLRPEFMQMQHIKELVMDEDNDGCTPLHY 0420

       0420 ACRQGGPGSVNNLLGFNVSIHSKSKDKKSPLHFAASYGRINTCQRLLQDISDTRLLNEGD 0479
            ||||| | ||||||||||||||||||||||||||||||||||||||||||||||||||||
       0421 ACRQGVPVSVNNLLGFNVSIHSKSKDKKSPLHFAASYGRINTCQRLLQDISDTRLLNEGD 0480

       0480 LHGMTPLHLAAKNGHDKVVQLLLKKGALFLSDHNGWTALHHASMGGYTQTMKVILDTNLK 0539
            ||||||||||||||||||||||||||||||||||||||||||||||||||||||||||||
       0481 LHGMTPLHLAAKNGHDKVVQLLLKKGALFLSDHNGWTALHHASMGGYTQTMKVILDTNLK 0540

       0540 CTDRLDEDGNTALHFAAREGHAKAVALLLSHNADIVLNKQQASFLHLALHNKRKEVVLTI 0599
            |||||||+||||||||||||||||||+|||+||||+|||+|||||||||||||||||||+
       0541 CTDRLDEEGNTALHFAAREGHAKAVAMLLSYNADILLNKKQASFLHIALHNKRKEVVLTT 0600

       0600 IRSKRWDECLKIFSHNSPGNKCPITEMIEYLPECMKVLLDFCMLHSTEDKSCRDYYIEYN 0659
            ||+||||||| ++|+|||| |+|| ||+|||||||||||||+ ||||||||+||+||||
       0601 IRNKRWDECLQVFTHNSPSNRCPIMEMVEYLPECMKVLLDFCMIPSTEDKSCQDYHIEYN 0660

       0660 FKYLQCPLEFTKK-TPTQDVIYEPLTALNAMVQNNRIELLNHPVCKEYLLMKWLAYGFRA 0718
            |||||||| ||| |||||+|||| || |||+||||||||||||+||||||||| |||||
       0661 FKYLQCPLSMTKKVAPTQDVVYEPLTILNVMVQHNRIELLNHPVCREYLLMKWCAYGFRA 0720

       0719 HMMNLGSYCLGLIPMTILVVNIKPGMAFNSTGIINETSD-HSEILDTTNSYLIKTCMILV 0777
            |||||||||||||||||||+||| |+|||||||| || || | +|| ||+ || |||||
       0721 HMMNLGSYCLGLIPMTLLVVKIQPGMAFNSTGIINGTSSTHEERIDTLNSFPIKICMILV 0780

       0778 FLSSIFGYCKEAGQIFQQKRNYFMDISNVLEWIIYTTGIIFVLPLFVEIPAHLQWQCGAI 0837
            ||||||||||| |||||||||||+| |||+||||| |||||||||||| |||++||||||
       0781 FLSSIFGYCKEVIQIFQQKRNYFLDYNNALEWVIYTTSIIFVLPLFLNIPAYMQWQCGAI 0840

       0838 AVYFYWMNFLLYLQRFENCGIFIVMLEVILKTLLRSTVVFIFLLLAFGLSFYILLNLQDP 0897
            |++||||||||||||||||||||||||||||| |||||| |||||||||||||||+||| ||
       0841 AIFFYWMNFLLYLQRFENCGIFIVMLEVIFKTLLRSTGVFIFLLLAFGLSFYVLLNFQDA 0900

       0898 FSSPLLSIIQTFSMMLGDINYRESFLEPYLRNELAHPVLSFAQLVSFTIFVPIVLMNLLI 0957
            ||+||||+|||||||||||||+++||| |||||+++||| |||||+| ||++||+||||||||
       0901 FSTPLLSLIQTFSMMLGDINYRDAFLEPLFRNELAYPVLTFGQLIAFTMFVPIVLMNLLI 0960

       0958 GLAVGDIAEVQKHASLKRIAMQVELHTSLEKKLPLWFLRKVDQKSTIVYPNKPRSGGML- 1016
            |||||||||||||||||||||||||||+|||||||+|||||+|||||||+|||||||+|| | ||
       0961 GLAVGDIAEVQKHASLKRIAMQVELHTNLEKKLPLWYLRKVDQRSTIVYPNRPRHGRMLR 1020

       1017 -FHIFCFLFCTGEIRQEIPNADKSLEMEILKQYRLKDLTFLLEKQHELIKLIIQKMEII 1075
             || | + | |||+|| | |||||||||||||||| ||||||||||||||||||||
       1021 FFHYFLNM---QETRQEVPNIDTCLEMEILKQYRLKDLTSLLEKQHELIKLIIQKMEII 1077

       1076 SETEDDDSHCSFQDRFKKEQMEQRNSRWNTVLRAVKAKTH 1115
            |||||+|+|||||||||||++|| +|+|| || ||| |||
       1078 SETEDEDNHCSFQDRFKKERLEQMHSKWNFVLNAVKTKTH 1117

132

Human → 0001 MKRSLRKMWRPGEKKEPQGVVYEDVPDDTEDFKESLKVVFEGSAYGLQNFNK-QKKLKRC 0059
              |||||||++ || |+|| |||||| | | + ||| || || |+ | | ++|| +
Rat →   0001 MKRSLRRVLRPEERKEVQGVVYRGVGKDMDCSKESFKVDIEGDMCRLEAFIKNRRKLSKY 0060

         0060 DDMDTFFLHYAAAEGQIELMEKITRDSSLEVLHEMDDYGNTPLHCAVEKNQIESVKFLLS 0119
              +| + ||+|||||+|||+ | || || |+ |||||||| | ||||+||||||||
         0061 EDENLCLLHHAAAEGQVELMQLIINGSSCEALNVMDDYGNTPLHWAAEKNQVESVKFLLS 0120

         0120 RGANPNLRNFNMMAPLHIAVQGMNNEVMKVLLEHRTIDVNLEGENGNTAVIIACTTNNSE 0179
              +|||||||| |||||||||||||| |||+||| ||+ ++|||||||||++ | +|||
         0121 QGANPNLRNRNMMAPLHIAVQGMYNEVIKVLTEHKATNINLEGENGNTALMSTCAKDNSE 0180

         0180 ALQILLKKGAKPCKSNKWGCFPIHQAAFSGSKECMEIILRFGEEHGYSRQLHINFMNNGK 0239
              ||||||+|||| ||||||| +|+||||||+| |||+|| +||+ ||||+ ||||+|+ |
         0181 ALQILLEKGAKLCKSNKWGDYPVHQAAFSGAKRCMELILAYGEKTGYSREAHINFVNHKK 0240

         0240 ATPLHLAVQNGDLEMIKMCLDNGAQIDPVEKGRCTAIHFAATQGATEIVKLMISSYSGSV 0299
              |+|||||||+|||+|||||||+|| || +| +| |+|||||||||+||||||||+||
         0241 ASPLHLAVQSGDLDMIKMCLDSGAHIDMMENAKCMALHFAATQGATDIVKLMISSYTGSS 0300

         0300 DIVNTTDGCHETMLHRASLFDHHELADYLISVGADINKIDSEGRSPLILATASASWNIVN 0359
              |||| || ||+|||||||||||+||||||||||+| ||||||||||||||||||||
         0301 DIVNAVDGNQETLLHRASLFDHHDLADYLISVGADINSTDSEGRSPLILATASASWNIVN 0360

         0360 LLLSKGAQVDIKDNFGRNFLHLTVQQPYGLKNLRPEFMQMQQIKELVMDEDNDGCTPLHY 0419
              ||||||+|||||+ |||||||||||||||+|||||||+ || ||||||||||||||||||
         0361 LLLSKGAKVDIKDHLGRNFLHLTVQQPYGLRNLRPEFLQMQHIKELVMDEDNDGCTPLHY 0420

         0420 ACRQGGPGSVNNLLGFNVSIHSKSKDKKSPLHFAASYGRINTCQRLLQDISDTRLLNEGD 0479
              ||||| | |||||| ||||+|||||||||||||||||||||||||||||||||||||||
         0421 ACRQGAPVSVNNLLRFNVSVHSKSKDKKSPLHFAASYGRINTCQRLLQDISDTRLLNEGD 0480

         0480 LHGMTPLHLAAKNGHDKVVQLLLKKGALFLSDHNGWTALHHASMGGYTQTMKVILDTNLK 0539
              ||||||||||||||||||||||||||||||||||||||||||||||||||||||||||||
         0481 LHGMTPLHLAAKNGHDKVVQLLLKKGALFLSDHNGWTALHHASMGGYTQTMKVILDTNLK 0540

         0540 CTDRLDEDGNTALHFAAREGHAKAVALLLSHNADIVLNKQQASFLHLALHNKRKEVVLTI 0599
              |||||||+||||||||||||||||||+|||+||||+|||+|||||||||||||||||||
         0541 CTDRLDEEGNTALHFAAREGHAKAVAMLLSYNADILLNKKQASFLHIALHNKRKEVVLTT 0600

         0600 IRSKRWDECLKIFSHNSPGNKCPITEMIEYLPECMKVLLDFCMLHSTEDKSCRDYYIEYN 0659
              |||||||||++|+|+|| |+|| || ||+|||||||||||||+ |||||||+||+||||
         0601 IRSKRWDECLQVFTHDSPSNRCPIMEMVEYLPECMKVLLDFCMIPSTEDKSCQDYHIEYN 0660

         0660 FKYLQCPLEFTKK-TPTQDVIYEPLTALNAMVQNNRIELLNHPVCKEYLLMKWLAYGFRA 0718
              |||||||| ||| ||||||||||||||| || |||+||||||||+|||||||+||||||
         0661 FKYLQCPLSMTKKVTPTQDVIYEPLTILNVMVQHNRIELLNHPVCREYLLMKWCAYGFRA 0720

         0719 HMMNLGSYCLGLIPMTILVVNIKPGMAFNSTGIINET-SDHSEILDTTNSYLIKTCMILV 0777
              ||||||||||||||||+||| |+||| |+||||||||| | ++| ||+ +| |||||
         0721 HMMNLGSYCLGLIPMTLLVVKIQPGMAFNSTGIINETISTHEERINTLNSFPLKICMILV 0780

         0778 FLSSIFGYCKEAGQIFQQKRNYFMDISNVLEWIIYTTGIIFVLPLFVEIPAHLQWQCGAI 0837
              |||||||||| |||||||||+| +| |||+|+| +|||||++|++ ++|||||||||
         0781 FLSSIFGYCKEVVQIFQQKRNYFLDYNNALEWVIYTTSMIFVLPLFLDIPAYMQWQCGAI 0840

         0838 AVYFYWMNFLLYLQRFENCGIFIVMLEVILKTLLRSTVVFIFLLLAFGLSFYILLNLQDP 0897
              |++||||||||||||||||||||||||||+||||||+|||||||||||||||+||| ||
         0841 AIFFYWMNFLLYLQRFENCGIFIVMLEVIFKTLLRSTGVFIFLLLAFGLSFYVLLNFQDA 0900

         0898 FSSPLLSIIQTFSMMLGDINYRESFLEPYLRNELAHPVLSFAQLVSFTIFVPIVLMNLLI 0957
              ||+||||+|||||||||||||| |||+|||| |||+|||| ||++| ||++|||||||||
         0901 FSTPLLSLIQTFSMMLGDINYRDAFLEPLFRNELAYPVLTFGQLIAFTMFVPIVLMNLLI 0960

         0958 GLAVGDIAEVQKHASLKRIAMQVELHTSLEKKLPLWFLRKVDQKSTIVYPNKPRSGGMLF 1017
              ||||||||||||||||||||||||||+||||| |+|||||+|||||+|||| | | ||
         0961 GLAVGDIAEVQKHASLKRIAMQVELHTNLEKKLPFWYLRKVDQRSTIVYPNRPRHGRML- 1019

         1018 HIFCFLFCTGEIRQEIPNADKSLEMEILKQKYRLKDLTFLLEKQHELIKLIIQKMEIISE 1077
              | + | ||| || | |||||||||||||||||| |||||||||||||||||||
         1020 RFFHYFLSMQETRQEAPNIDTCLEMEILKQKYRLKDLTSLLEKQHELIKLIIQKMEIISE 1079

         1078 TEDDDSHCSFQDRFKKEQMEQRNSRWNTVLRAVKAKTH 1115
              |||+|+||||||||||||||++|| +|+|| || ||| ||
         1080 TEDEDNHCSFQDRFKKERLEQMHSKWNFVLNAVKTKTH 1117

133

```
Mouse → 0001 MKRGLRRILLPEERKEVQGVVYRGVGEDMDCSKESFKVDIEGDMCRLEDFIKNRRKLSKY 0060
              ||| |||+| |||||||||||||||+|||||||||||||||||| |||||||||||||||
Rat   → 0001 MKRSLRRVLRPEERKEVQGVVYRGVGKDMDCSKESFKVDIEGDMCRLEAFIKNRRKLSKY 0060

         0061 EDENLCPLHHAAAEGQVELMELIINGSSCEVLNIMDGYGNTPLHCAAEKNQVESVKFLLS 0120
              |||||| ||||||||||||||+|||||||| ||+|| ||||||| |||||||||||||||
         0061 EDENLCLLHHAAAEGQVELMQLIINGSSCEALNVMDDYGNTPLHWAAEKNQVESVKFLLS 0120

         0121 QGANPNLRNRNMMSPLHIAVHGMYNEVIKVLTEHKATNINLEGENGNTALMSTCAKDNSE 0180
              |||||||||||||+|||||| |||||||||||||||||||||||||||||||||||||||
         0121 QGANPNLRNRNMMAPLHIAVQGMYNEVIKVLTEHKATNINLEGENGNTALMSTCAKDNSE 0180

         0181 ALQILLEKGAKLCKSNKWGDYPVHQAAFSGAKKCMELILAYGEKNGYSRETHINFVNHKK 0240
              |||||||||||||||||||||||||||||||||+|||||||||||| ||||||||||||
         0181 ALQILLEKGAKLCKSNKWGDYPVHQAAFSGAKRCMELILAYGEKTGYSREAHINFVNHKK 0240

         0241 ASPLHLAVQSGDLDMIKMCLDNGAHIDMMENAKCMALHFAATQGATDIVKLMISSYTGSS 0300
              ||||||||||||||||||||||+||||||||||||||||||||||||||||||||||||
         0241 ASPLHLAVQSGDLDMIKMCLDSGAHIDMMENAKCMALHFAATQGATDIVKLMISSYTGSS 0300

         0301 DIVNAVDGNQETLLHRASLFDHHDLAEYLISVGADINSTDSEGRSPLILATASASWNIVN 0360
              |||||||||||||||||||||||||+|||||||||||||||||||||||||||||||||
         0301 DIVNAVDGNQETLLHRASLFDHHDLADYLISVGADINSTDSEGRSPLILATASASWNIVN 0360

         0361 LLLCKGAKVDIKDHLGRNFLHLTVQQPYGLRNLRPEFMQMQHIKELVMDEDNDGCTPLHY 0420
              ||| ||||||||||||||||||||||||||||||||+|||||||||||||||||||||||
         0361 LLLSKGAKVDIKDHLGRNFLHLTVQQPYGLRNLRPEFLQMQHIKELVMDEDNDGCTPLHY 0420

         0421 ACRQGVPVSVNNLLGFNVSIHSKSKDKKSPLHFAASYGRINTCQRLLQDISDTRLLNEGD 0480
              ||||| |||||||+|||| ||+||||||||||||||||||||||||||||||||||||||
         0421 ACRQGAPVSVNNLLRFNVSVHSKSKDKKSPLHFAASYGRINTCQRLLQDISDTRLLNEGD 0480

         0481 LHGMTPLHLAAKNGHDKVVQLLLKKGALFLSDHNGWTALHHASMGGYTQTMKVILDTNLK 0540
              |||||||||||||||||||||||||||||||||||||||||||||||||||||||||||
         0481 LHGMTPLHLAAKNGHDKVVQLLLKKGALFLSDHNGWTALHHASMGGYTQTMKVILDTNLK 0540

         0541 CTDRLDEEGNTALHFAAREGHAKAVAMLLSYNADILLNKKQASFLHIALHNKRKEVVLTT 0600
              |||||||||||||||||||||||||||||||||||||||||||||||||||||||||||
         0541 CTDRLDEEGNTALHFAAREGHAKAVAMLLSYNADILLNKKQASFLHIALHNKRKEVVLTT 0600

         0601 IRNKRWDECLQVFTHNSPSNRCPIMEMVEYLPECMKVLLDFCMIPSTEDKSCQDYHIEYN 0660
              ||+|||||||||||+|||||||||||||||||||||||||||||||||||||||||||||
         0601 IRSKRWDECLQVFTHDSPSNRCPIMEMVEYLPECMKVLLDFCMIPSTEDKSCQDYHIEYN 0660

         0661 FKYLQCPLSMTKKVAPTQDVVYEPLTILNVMVQHNRIELLNHPVCREYLLMKWCAYGFRA 0720
              ||||||||||||||| |||||+||||||||||||||||||||||||||||||||||||||
         0661 FKYLQCPLSMTKKVTPTQDVIYEPLTILNVMVQHNRIELLNHPVCREYLLMKWCAYGFRA 0720

         0721 HMMNLGSYCLGLIPMTLLVVKIQPGMAFNSTGIINGTSSTHEERIDTLNSFPIKICMILV 0780
              |||||||||||||||||||||||||||||||||| |||||||+|||||+||||||||||
         0721 HMMNLGSYCLGLIPMTLLVVKIQPGMAFNSTGIINETISTHEERINTLNSFPLKICMILV 0780

         0781 FLSSIFGYCKEVIQIFQQKRNYFLDYNNALEWVIYTTSIIFVLPLFLNIPAYMQWQCGAI 0840
              ||||||||||||+|||||||||||||||||||||||||+|||||||||+|||||||||||
         0781 FLSSIFGYCKEVVQIFQQKRNYFLDYNNALEWVIYTTSMIFVLPLFLDIPAYMQWQCGAI 0840

         0841 AIFFYWMNFLLYLQRFENCGIFIVMLEVIFKTLLRSTGVFIFLLLAFGLSFYVLLNFQDA 0900
              |||||||||||||||||||||||||||||||||||||||||||||||||||||||||||
         0841 AIFFYWMNFLLYLQRFENCGIFIVMLEVIFKTLLRSTGVFIFLLLAFGLSFYVLLNFQDA 0900

         0901 FSTPLLSLIQTFSMMLGDINYRDAFLEPLFRNELAYPVLTFGQLIAFTMFVPIVLMNLLI 0960
              |||||||||||||||||||||||||||||||||||||||||||||||||||||||||||
         0901 FSTPLLSLIQTFSMMLGDINYRDAFLEPLFRNELAYPVLTFGQLIAFTMFVPIVLMNLLI 0960

         0961 GLAVGDIAEVQKHASLKRIAMQVELHTNLEKKLPLWYLRKVDQRSTIVYPNRPRHGRMLR 1020
              ||||||||||||||||||||||||||||||||||| |||||||||||||||||||||||
         0961 GLAVGDIAEVQKHASLKRIAMQVELHTNLEKKLPFWYLRKVDQRSTIVYPNRPRHGRMLR 1020

         1021 FFHYFLNMQETRQEVPNIDTCLEMEILKQKYRLKDLTSLLEKQHELIKLIIQKMEIISET 1080
              ||||||+||||||| ||||||||||||||||||||||||||||||||||||||||||||
         1021 FFHYFLSMQETRQEAPNIDTCLEMEILKQKYRLKDLTSLLEKQHELIKLIIQKMEIISET 1080

         1081 EDEDNHCSFQDRFKKERLEQMHSKWNFVLNAVKTKTHCSISHPD 1124
              ||||||||||||||||||||||||||||||||||||||||||||
         1081 EDEDNHCSFQDRFKKERLEQMHSKWNFVLNAVKTKTHCSISHPD 1124
```

134

APPENDIX C

Prediction of transmembrane domains in human (UCSC ID: uc003xza.3), mouse (UCSC ID: uc007ajc.1), and rat (UCSC ID: RGD_1303284) TRAP1 protens using the TMpred software (http://www.ch.embnet.org/software/TMPRED_form.html) [311] release 25 (which is based on the SwissProt database release 25). Windows of 14 to 33 amino acid residues were used for the predictions. TMpred scores higher than 500 are considered significant (red dashed lines).

TMpred compares an amino-acid sequence of interest to a database of naturally occurring transmembrane proteins. Sequence, hydrophobicity score, flanking regions, domain orientation, among others, are used for the comparisons and score calculations.

Notice that, in addition to the six channel forming transmembrane segments (S1 to S6), a highly hydrophobic domain was predicted in the N-terminal region of human, mouse and rat TRPA1 proteins (roughly from amino acid residues 350 to 360). In addition, a hydrophobic domain was predicted in the C-terminal region of the human TRPA1 protein (around the amino acid residue 1020). These intracellular hydrophobic regions might constitute domains that closely interact with the plasma membrane.

    i-o   Inside (cytoplasmic) to outside (luminal) orientation

    o-i   Outside to inside orientation
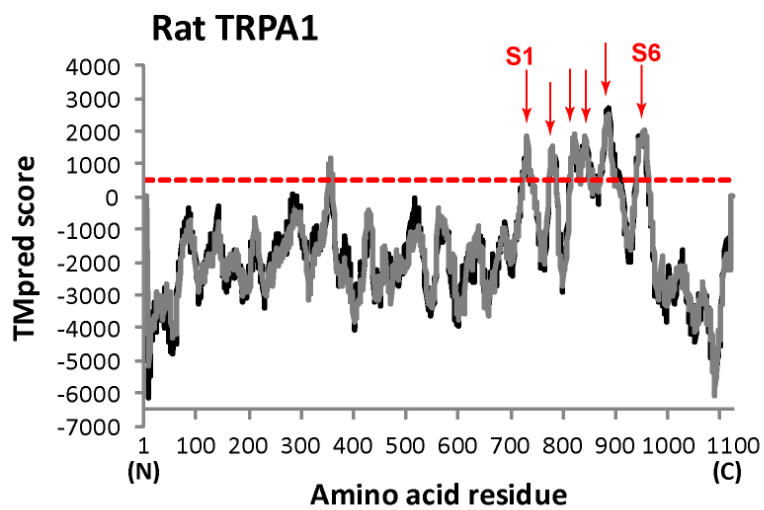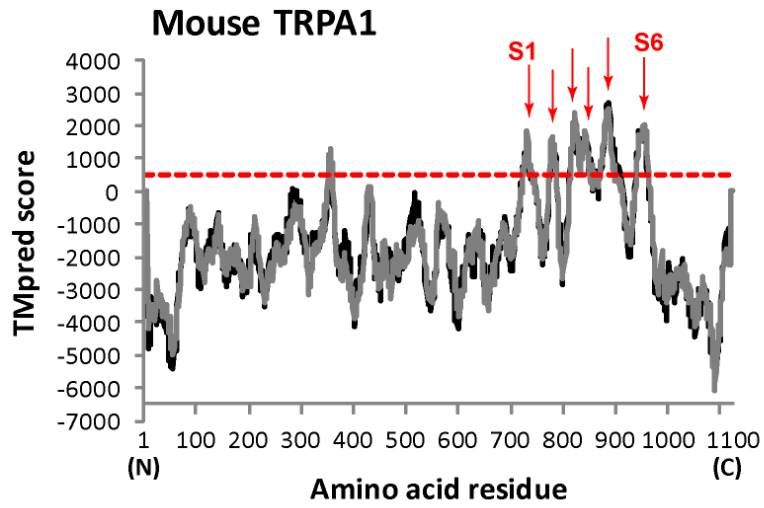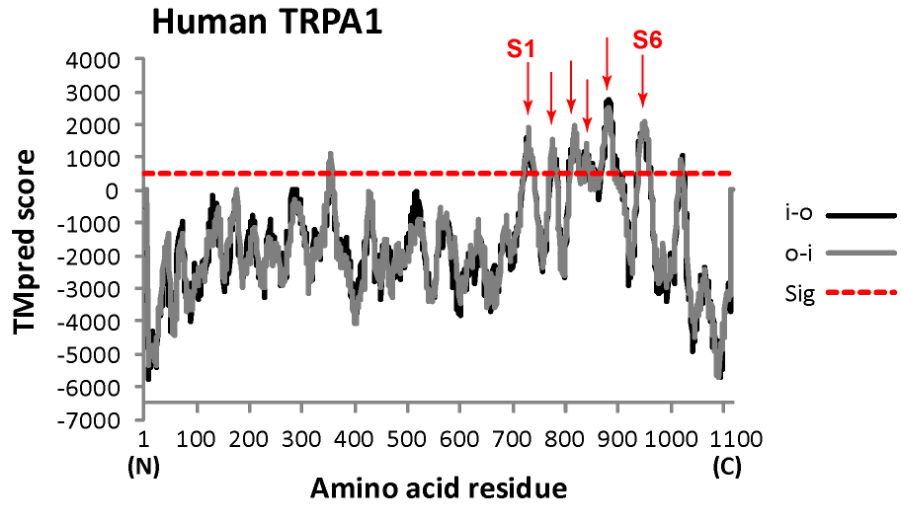
APPENDIX D

TRPA1 channels are activated downstream of ATP metabotropic P2Y receptors. These set of experiments were performed by Ruben Stepanyan, PhD, during his postdoctoral training in the Frolenkov laboratory.

Current-voltage responses to 20 μM AITC (A) and 10 μM ATP (B) puff stimulation of HEK-293 cells transfected with a Trpa1-IRES-GFP construct (blue squares), a GFP-only construct ("mock", black circles) or not transfected (black triangles). Insets show representative current traces to the puff stimulation with AITC or ATP.

A

AITC (20 µM)

TRPA1

No transfection

Mock transfection

0.25 nA

2 min

I (nA)

1.5

1.0

0.5

-0.5

-150   -100   -50   50   100 (mV)

■ TRPA1 (n=6)
▲ No transfection (n=4)
● Mock (n=5)

B

ATP (10 µM)

TRPA1

No transfection

Mock transfection

0.1 nA

1 min

I (nA)

0.6

0.4

0.2

-0.2

-0.4

-150   -100   -50   50   100 (mV)

■ TRPA1 (n=8)
▲ No transfection (n=4)
● Mock (n=6)
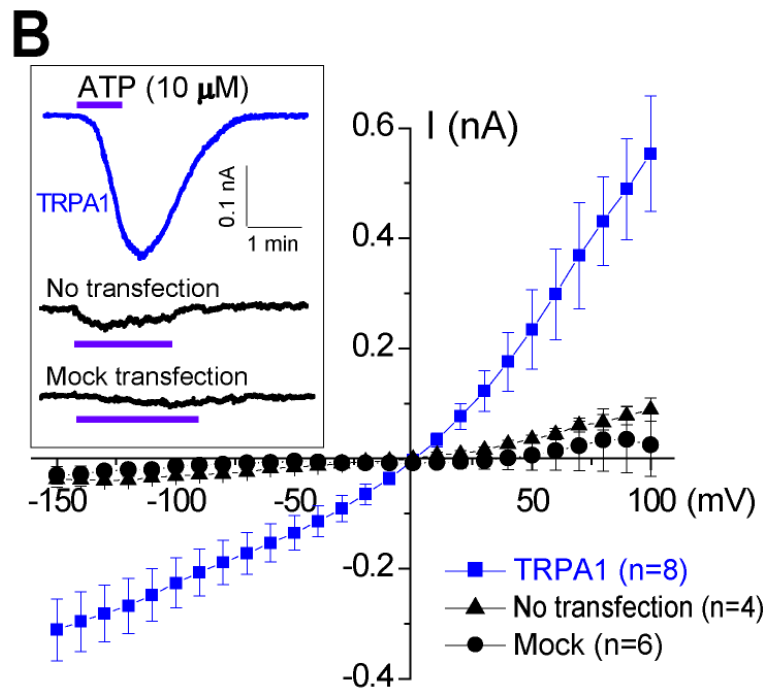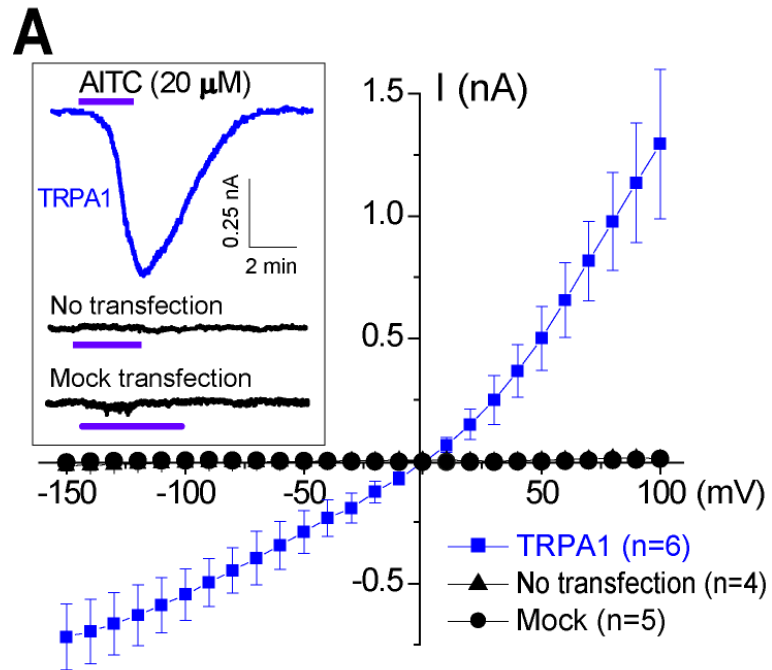
REFERENCES

1.   Von Békésy, G., *Experiments in hearing*. McGraw-Hill series in psychology1960, New York,: McGraw-Hill. 745 p.

2.   Olson, E.S. and Mountain, D.C., *In vivo measurement of basilar membrane stiffness*. J Acoust Soc Am, 1991. **89**(3): p. 1262-75.

3.   Frolenkov, G.I., Belyantseva, I.A., Friedman, T.B., and Griffith, A.J., *Genetic insights into the morphogenesis of inner ear hair cells*. Nat Rev Genet, 2004. **5**(7): p. 489-98.

4.   Davis, H., *Biophysics and physiology of the inner ear*. Physiol Rev, 1957. **37**(1): p. 1-49.

5.   Allen, J.B., *Cochlear micromechanics--a physical model of transduction*. J Acoust Soc Am, 1980. **68**(6): p. 1660-70.

6.   Gavara, N., Manoussaki, D., and Chadwick, R.S., *Auditory mechanics of the tectorial membrane and the cochlear spiral*. Curr Opin Otolaryngol Head Neck Surg, 2011. **19**(5): p. 382-7.

7.   Flock, A. and Cheung, H.C., *Actin filaments in sensory hairs of inner ear receptor cells*. J Cell Biol, 1977. **75**(2 Pt 1): p. 339-43.

8.   Tilney, L.G., Derosier, D.J., and Mulroy, M.J., *The organization of actin filaments in the stereocilia of cochlear hair cells*. J Cell Biol, 1980. **86**(1): p. 244-59.

9.   Sakaguchi, H., Tokita, J., Muller, U., and Kachar, B., *Tip links in hair cells: molecular composition and role in hearing loss*. Curr Opin Otolaryngol Head Neck Surg, 2009. **17**(5): p. 388-93.

10.   DeRosier, D.J., Tilney, L.G., and Egelman, E., *Actin in the inner ear: the remarkable structure of the stereocilium*. Nature, 1980. **287**(5780): p. 291-6.

11.   Karavitaki, K.D. and Corey, D.P., *Sliding adhesion confers coherent motion to hair cell stereocilia and parallel gating to transduction channels*. J Neurosci, 2010. **30**(27): p. 9051-63.

12.   Beurg, M., Fettiplace, R., Nam, J.H., and Ricci, A.J., *Localization of inner hair cell mechanotransducer channels using high-speed calcium imaging*. Nat Neurosci, 2009. **12**(5): p. 553-8.

13.   Sotomayor, M., Weihofen, W.A., Gaudet, R., and Corey, D.P., *Structure of a force-conveying cadherin bond essential for inner-ear mechanotransduction*. Nature, 2012. **492**(7427): p. 128-32.

14.   Kachar, B., Parakkal, M., Kurc, M., Zhao, Y., and Gillespie, P.G., *High-resolution structure of hair-cell tip links*. Proc Natl Acad Sci U S A, 2000. **97**(24): p. 13336-41.

15. Kubisch, C., Schroeder, B.C., Friedrich, T., Lutjohann, B., El-Amraoui, A., Marlin, S., et al., *KCNQ4, a novel potassium channel expressed in sensory outer hair cells, is mutated in dominant deafness.* Cell, 1999. **96**(3): p. 437-46.

16. Marcotti, W. and Kros, C.J., *Developmental expression of the potassium current IK,n contributes to maturation of mouse outer hair cells.* J Physiol, 1999. **520 Pt 3**: p. 653-60.

17. Brownell, W.E., Bader, C.R., Bertrand, D., and de Ribaupierre, Y., *Evoked mechanical responses of isolated cochlear outer hair cells.* Science, 1985. **227**(4683): p. 194-6.

18. Kachar, B., Brownell, W.E., Altschuler, R., and Fex, J., *Electrokinetic shape changes of cochlear outer hair cells.* Nature, 1986. **322**(6077): p. 365-8.

19. Ashmore, J.F., *A fast motile response in guinea-pig outer hair cells: the cellular basis of the cochlear amplifier.* J Physiol, 1987. **388**: p. 323-47.

20. Zheng, J., Shen, W., He, D.Z., Long, K.B., Madison, L.D., and Dallos, P., *Prestin is the motor protein of cochlear outer hair cells.* Nature, 2000. **405**(6783): p. 149-55.

21. Belyantseva, I.A., Adler, H.J., Curi, R., Frolenkov, G.I., and Kachar, B., *Expression and localization of prestin and the sugar transporter GLUT-5 during development of electromotility in cochlear outer hair cells.* J Neurosci, 2000. **20**(24): p. RC116.

22. Dallos, P., Zheng, J., and Cheatham, M.A., *Prestin and the cochlear amplifier.* J Physiol, 2006. **576**(Pt 1): p. 37-42.

23. Nouvian, R., Beutner, D., Parsons, T.D., and Moser, T., *Structure and function of the hair cell ribbon synapse.* J Membr Biol, 2006. **209**(2-3): p. 153-65.

24. Raphael, Y. and Altschuler, R.A., *Structure and innervation of the cochlea.* Brain Res Bull, 2003. **60**(5-6): p. 397-422.

25. Glowatzki, E. and Fuchs, P.A., *Transmitter release at the hair cell ribbon synapse.* Nat Neurosci, 2002. **5**(2): p. 147-54.

26. Beutner, D., Voets, T., Neher, E., and Moser, T., *Calcium dependence of exocytosis and endocytosis at the cochlear inner hair cell afferent synapse.* Neuron, 2001. **29**(3): p. 681-90.

27. Fechner, F.P., Nadol, J.J., Burgess, B.J., and Brown, M.C., *Innervation of supporting cells in the apical turns of the guinea pig cochlea is from type II afferent fibers.* J Comp Neurol, 2001. **429**(2): p. 289-98.

28. Weisz, C., Glowatzki, E., and Fuchs, P., *The postsynaptic function of type II cochlear afferents.* Nature, 2009. **461**(7267): p. 1126-9.

29. Burgess, B.J., Adams, J.C., and Nadol, J.B., Jr., *Morphologic evidence for innervation of Deiters' and Hensen's cells in the guinea pig.* Hear Res, 1997. **108**(1-2): p. 74-82.

30. Fechner, F.P., Burgess, B.J., Adams, J.C., Liberman, M.C., and Nadol, J.B., Jr., *Dense innervation of Deiters' and Hensen's cells persists after chronic deefferentation of guinea pig cochleas.* J Comp Neurol, 1998. **400**(3): p. 299-309.

31. Wright, C.G. and Preston, R.E., *Efferent nerve fibers associated with the outermost supporting cells of the organ of Corti in the guinea pig.* Acta Otolaryngol, 1976. **82**(1-2): p. 41-7.

32. Slepecky, N., *Structure of the Mammalian Cochlea*, in *The Cochlea*, P. Dallos, A. Popper, and R. Fay, Editors. 1996, Springer New York. p. 44-129.

33. Jagger, D.J. and Forge, A., *Compartmentalized and signal-selective gap junctional coupling in the hearing cochlea.* J Neurosci, 2006. **26**(4): p. 1260-8.

34. Majumder, P., Crispino, G., Rodriguez, L., Ciubotaru, C.D., Anselmi, F., Piazza, V., et al., *ATP-mediated cell-cell signaling in the organ of Corti: the role of connexin channels.* Purinergic Signal, 2010. **6**(2): p. 167-87.

35. Mistrik, P. and Ashmore, J., *The role of potassium recirculation in cochlear amplification.* Curr Opin Otolaryngol Head Neck Surg, 2009. **17**(5): p. 394-9.

36. Wangemann, P., *K(+) cycling and its regulation in the cochlea and the vestibular labyrinth.* Audiol Neurootol, 2002. **7**(4): p. 199-205.

37. Gale, J.E., Piazza, V., Ciubotaru, C.D., and Mammano, F., *A mechanism for sensing noise damage in the inner ear.* Curr Biol, 2004. **14**(6): p. 526-9.

38. Lahne, M. and Gale, J.E., *Damage-induced cell-cell communication in different cochlear cell types via two distinct ATP-dependent Ca waves.* Purinergic Signal, 2010. **6**(2): p. 189-200.

39. Anttonen, T., Belevich, I., Kirjavainen, A., Laos, M., Brakebusch, C., Jokitalo, E., et al., *How to Bury the Dead: Elimination of Apoptotic Hair Cells from the Hearing Organ of the Mouse.* J Assoc Res Otolaryngol, 2014.

40. Abrashkin, K.A., Izumikawa, M., Miyazawa, T., Wang, C.H., Crumling, M.A., Swiderski, D.L., et al., *The fate of outer hair cells after acoustic or ototoxic insults.* Hear Res, 2006. **218**(1-2): p. 20-9.

41. Forge, A., *Outer hair cell loss and supporting cell expansion following chronic gentamicin treatment.* Hear Res, 1985. **19**(2): p. 171-82.

42. Taylor, R.R., Nevill, G., and Forge, A., *Rapid hair cell loss: a mouse model for cochlear lesions.* J Assoc Res Otolaryngol, 2008. **9**(1): p. 44-64.

43. Forge, A., Jagger, D.J., Kelly, J.J., and Taylor, R.R., *Connexin30-mediated intercellular communication plays an essential role in epithelial repair in the cochlea.* J Cell Sci, 2013. **126**(Pt 7): p. 1703-12.

44. McDowell, B., Davies, S., and Forge, A., *The effect of gentamicin-induced hair cell loss on the tight junctions of the reticular lamina.* Hear Res, 1989. **40**(3): p. 221-32.

45. Raphael, Y. and Altschuler, R.A., *Scar formation after drug-induced cochlear insult.* Hear Res, 1991. **51**(2): p. 173-83.

46. Hinojosa, R., *A note on development of Corti's organ.* Acta Otolaryngol, 1977. **84**(3-4): p. 238-51.

47. Knipper, M., Gestwa, L., Ten Cate, W.J., Lautermann, J., Brugger, H., Maier, H., et al., *Distinct thyroid hormone-dependent expression of TrKB and p75NGFR in nonneuronal cells during the critical TH-dependent period of the cochlea.* J Neurobiol, 1999. **38**(3): p. 338-56.

48. Hibino, H., Horio, Y., Inanobe, A., Doi, K., Ito, M., Yamada, M., et al., *An ATP-dependent inwardly rectifying potassium channel, KAB-2 (Kir4. 1), in cochlear stria vascularis of inner ear: its specific subcellular localization and correlation with the formation of endocochlear potential.* J Neurosci, 1997. **17**(12): p. 4711-21.

49. Boettger, T., Hubner, C.A., Maier, H., Rust, M.B., Beck, F.X., and Jentsch, T.J., *Deafness and renal tubular acidosis in mice lacking the K-Cl co-transporter Kcc4.* Nature, 2002. **416**(6883): p. 874-8.

50. Taylor, R.R., Jagger, D.J., and Forge, A., *Defining the cellular environment in the organ of Corti following extensive hair cell loss: a basis for future sensory cell replacement in the Cochlea.* PLoS One, 2012. **7**(1): p. e30577.

51. Jin, Z.H., Kikuchi, T., Tanaka, K., and Kobayashi, T., *Expression of glutamate transporter GLAST in the developing mouse cochlea.* Tohoku J Exp Med, 2003. **200**(3): p. 137-44.

52. Ulfendahl, M., Scarfone, E., Flock, A., Le Calvez, S., and Conradi, P., *Perilymphatic fluid compartments and intercellular spaces of the inner ear and the organ of Corti.* Neuroimage, 2000. **12**(3): p. 307-13.

53. Zetes, D.E., Tolomeo, J.A., and Holley, M.C., *Structure and mechanics of supporting cells in the guinea pig organ of Corti.* PLoS One, 2012. **7**(11): p. e49338.

54. Saito, K. and Hama, K., *Structural diversity of microtubules in the supporting cells of the sensory epithelium of guinea pig organ of Corti.* J Electron Microsc (Tokyo), 1982. **31**(3): p. 278-81.

55. Mogensen, M.M., Henderson, C.G., Mackie, J.B., Lane, E.B., Garrod, D.R., and Tucker, J.B., *Keratin filament deployment and cytoskeletal networking in a sensory epithelium that vibrates during hearing.* Cell Motil Cytoskeleton, 1998. **41**(2): p. 138-53.

56. Bobbin, R.P., *ATP-induced movement of the stalks of isolated cochlear Deiters' cells.* Neuroreport, 2001. **12**(13): p. 2923-6.

57. Dulon, D., Blanchet, C., and Laffon, E., *Photo-released intracellular Ca2+ evokes reversible mechanical responses in supporting cells of the guinea-pig organ of Corti.* Biochem Biophys Res Commun, 1994. **201**(3): p. 1263-9.

58. Simmons, D.D. and Liberman, M.C., *Afferent innervation of outer hair cells in adult cats: I. Light microscopic analysis of fibers labeled with horseradish peroxidase.* J Comp Neurol, 1988. **270**(1): p. 132-44.

59. Simmons, D.D. and Liberman, M.C., *Afferent innervation of outer hair cells in adult cats: II. Electron microscopic analysis of fibers labeled with horseradish peroxidase.* J Comp Neurol, 1988. **270**(1): p. 145-54.

60. Merchan, M.A., Merchan, J.A., and Ludena, M.D., *Morphology of Hensen's cells.* J Anat, 1980. **131**(Pt 3): p. 519-23.

61. Kalinec, F., Webster, P., Maricle, A., Guerrero, D., Chakravarti, D.N., Chakravarti, B., et al., *Glucocorticoid-stimulated, transcription-independent release of annexin A1 by cochlear Hensen cells.* Br J Pharmacol, 2009. **158**(7): p. 1820-34.

62. Housley, G.D., Bringmann, A., and Reichenbach, A., *Purinergic signaling in special senses.* Trends Neurosci, 2009. **32**(3): p. 128-41.

63. von Kügelgen, I., *Pharmacology of mammalian P2X- and P2Y-receptors.* BIOTREND Reviews, 2008. **03**.

64. Jacobson, K.A., *P2X and P2Y receptors.* Tocris Bioscience Scientific Review Series.

65. Tritsch, N.X., Yi, E., Gale, J.E., Glowatzki, E., and Bergles, D.E., *The origin of spontaneous activity in the developing auditory system.* Nature, 2007. **450**(7166): p. 50-5.

66. Tritsch, N.X., Zhang, Y.X., Ellis-Davies, G., and Bergles, D.E., *ATP-induced morphological changes in supporting cells of the developing cochlea.* Purinergic Signal, 2010. **6**(2): p. 155-66.

67. Tritsch, N.X. and Bergles, D.E., *Developmental regulation of spontaneous activity in the Mammalian cochlea.* J Neurosci, 2010. **30**(4): p. 1539-50.

68. Munoz, D.J., Kendrick, I.S., Rassam, M., and Thorne, P.R., *Vesicular storage of adenosine triphosphate in the guinea-pig cochlear lateral wall and concentrations of ATP in the endolymph during sound exposure and hypoxia.* Acta Otolaryngol, 2001. **121**(1): p. 10-5.

69. Lahne, M. and Gale, J.E., *Damage-induced activation of ERK1/2 in cochlear supporting cells is a hair cell death-promoting signal that depends on extracellular ATP and calcium.* J Neurosci, 2008. **28**(19): p. 4918-28.

70. Anselmi, F., Hernandez, V.H., Crispino, G., Seydel, A., Ortolano, S., Roper, S.D., et al., *ATP release through connexin hemichannels and gap junction transfer of second messengers propagate Ca2+ signals across the inner ear.* Proc Natl Acad Sci U S A, 2008. **105**(48): p. 18770-5.

71. Nordmann, A.S., Bohne, B.A., and Harding, G.W., *Histopathological differences between temporary and permanent threshold shift.* Hear Res, 2000. **139**(1-2): p. 13-30.

72. Hirose, K. and Liberman, M.C., *Lateral wall histopathology and endocochlear potential in the noise-damaged mouse cochlea.* J Assoc Res Otolaryngol, 2003. **4**(3): p. 339-52.

73. Wang, Y., Hirose, K., and Liberman, M.C., *Dynamics of noise-induced cellular injury and repair in the mouse cochlea.* J Assoc Res Otolaryngol, 2002. **3**(3): p. 248-68.

74. Ohlemiller, K.K., Rosen, A.D., Rellinger, E.A., Montgomery, S.C., and Gagnon, P.M., *Different cellular and genetic basis of noise-related endocochlear potential reduction in CBA/J and BALB/cJ mice.* J Assoc Res Otolaryngol, 2011. **12**(1): p. 45-58.

75. Ohlemiller, K.K. and Gagnon, P.M., *Genetic dependence of cochlear cells and structures injured by noise.* Hear Res, 2007. **224**(1-2): p. 34-50.

76. Puel, J.L., Ruel, J., Gervais d'Aldin, C., and Pujol, R., *Excitotoxicity and repair of cochlear synapses after noise-trauma induced hearing loss.* Neuroreport, 1998. **9**(9): p. 2109-14.

77. Kujawa, S.G. and Liberman, M.C., *Adding insult to injury: cochlear nerve degeneration after "temporary" noise-induced hearing loss.* J Neurosci, 2009. **29**(45): p. 14077-85.

78. Heeringa, A.N. and van Dijk, P., *The dissimilar time course of temporary threshold shifts and reduction of inhibition in the inferior colliculus following intense sound exposure.* Hear Res, 2014. **312**: p. 38-47.

79. Scholl, B. and Wehr, M., *Disruption of balanced cortical excitation and inhibition by acoustic trauma.* J Neurophysiol, 2008. **100**(2): p. 646-56.

80. Kujawa, S.G. and Liberman, M.C., *Acceleration of age-related hearing loss by early noise exposure: evidence of a misspent youth.* J Neurosci, 2006. **26**(7): p. 2115-23.

81. Housley, G.D., Morton-Jones, R., Vlajkovic, S.M., Telang, R.S., Paramananthasivam, V., Tadros, S.F., et al., *ATP-gated ion channels mediate adaptation to elevated sound levels.* Proc Natl Acad Sci U S A, 2013. **110**(18): p. 7494-9.

82. Niu, X. and Canlon, B., *Protective mechanisms of sound conditioning.* Adv Otorhinolaryngol, 2002. **59**: p. 96-105.

83. Harding, G.W., Baggot, P.J., and Bohne, B.A., *Height changes in the organ of Corti after noise exposure.* Hear Res, 1992. **63**(1-2): p. 26-36.

84. Fridberger, A., Flock, A., Ulfendahl, M., and Flock, B., *Acoustic overstimulation increases outer hair cell Ca2+ concentrations and causes dynamic contractions of the hearing organ.* Proc Natl Acad Sci U S A, 1998. **95**(12): p. 7127-32.

85. Flock, A., Flock, B., Fridberger, A., Scarfone, E., and Ulfendahl, M., *Supporting cells contribute to control of hearing sensitivity.* J Neurosci, 1999. **19**(11): p. 4498-507.

86. Fridberger, A., Widengren, J., and Boutet de Monvel, J., *Measuring hearing organ vibration patterns with confocal microscopy and optical flow.* Biophys J, 2004. **86**(1 Pt 1): p. 535-43.

87. Guinan, J.J., Jr., Salt, A., and Cheatham, M.A., *Progress in cochlear physiology after Bekesy.* Hear Res, 2012. **293**(1-2): p. 12-20.

88. Clapham, D.E., *TRP channels as cellular sensors.* Nature, 2003. **426**(6966): p. 517-24.

89. Walker, R.G., Willingham, A.T., and Zuker, C.S., *A Drosophila mechanosensory transduction channel.* Science, 2000. **287**(5461): p. 2229-34.

90. Sidi, S., Friedrich, R.W., and Nicolson, T., *NompC TRP channel required for vertebrate sensory hair cell mechanotransduction.* Science, 2003. **301**(5629): p. 96-9.

91. Shin, J.B., Adams, D., Paukert, M., Siba, M., Sidi, S., Levin, M., et al., *Xenopus TRPN1 (NOMPC) localizes to microtubule-based cilia in epithelial cells, including inner-ear hair cells.* Proc Natl Acad Sci U S A, 2005. **102**(35): p. 12572-7.

92. Vannier, B., Zhu, X., Brown, D., and Birnbaumer, L., *The membrane topology of human transient receptor potential 3 as inferred from glycosylation-scanning mutagenesis and epitope immunocytochemistry.* J Biol Chem, 1998. **273**(15): p. 8675-9.

93. Dohke, Y., Oh, Y.S., Ambudkar, I.S., and Turner, R.J., *Biogenesis and topology of the transient receptor potential Ca2+ channel TRPC1.* J Biol Chem, 2004. **279**(13): p. 12242-8.

94. Schaefer, M., *Homo- and heteromeric assembly of TRP channel subunits.* Pflugers Arch, 2005. **451**(1): p. 35-42.

95. Owsianik, G., Talavera, K., Voets, T., and Nilius, B., *Permeation and selectivity of TRP channels.* Annu Rev Physiol, 2006. **68**: p. 685-717.

96. Runnels, L.W., Yue, L., and Clapham, D.E., *TRP-PLIK, a bifunctional protein with kinase and ion channel activities.* Science, 2001. **291**(5506): p. 1043-7.

97. Nilius, B. and Owsianik, G., *The transient receptor potential family of ion channels.* Genome Biol, 2011. **12**(3): p. 218.

98. Bandell, M., Macpherson, L.J., and Patapoutian, A., *From chills to chilis: mechanisms for thermosensation and chemesthesis via thermoTRPs.* Curr Opin Neurobiol, 2007. **17**(4): p. 490-7.

99. Asai, Y., Holt, J.R., and Geleoc, G.S., *A quantitative analysis of the spatiotemporal pattern of transient receptor potential gene expression in the developing mouse cochlea.* J Assoc Res Otolaryngol, 2010. **11**(1): p. 27-37.

100. Zhou, Y., Suzuki, Y., Uchida, K., and Tominaga, M., *Identification of a splice variant of mouse TRPA1 that regulates TRPA1 activity.* Nat Commun, 2013. **4**: p. 2399.

101. Bautista, D.M., Jordt, S.E., Nikai, T., Tsuruda, P.R., Read, A.J., Poblete, J., et al., *TRPA1 mediates the inflammatory actions of environmental irritants and proalgesic agents.* Cell, 2006. **124**(6): p. 1269-82.

102. Kwan, K.Y., Allchorne, A.J., Vollrath, M.A., Christensen, A.P., Zhang, D.S., Woolf, C.J., et al., *TRPA1 contributes to cold, mechanical, and chemical nociception but is not essential for hair-cell transduction.* Neuron, 2006. **50**(2): p. 277-89.

103. Kremeyer, B., Lopera, F., Cox, J.J., Momin, A., Rugiero, F., Marsh, S., et al., *A gain-of-function mutation in TRPA1 causes familial episodic pain syndrome.* Neuron, 2010. **66**(5): p. 671-80.

104. Dietrich, A., Kalwa, H., Storch, U., Mederos y Schnitzler, M., Salanova, B., Pinkenburg, O., et al., *Pressure-induced and store-operated cation influx in vascular smooth muscle cells is independent of TRPC1.* Pflugers Arch, 2007. **455**(3): p. 465-77.

105. Liu, X., Cheng, K.T., Bandyopadhyay, B.C., Pani, B., Dietrich, A., Paria, B.C., et al., *Attenuation of store-operated Ca2+ current impairs salivary gland fluid secretion in TRPC1(-/-) mice.* Proc Natl Acad Sci U S A, 2007. **104**(44): p. 17542-7.

106. Stowers, L., Holy, T.E., Meister, M., Dulac, C., and Koentges, G., *Loss of sex discrimination and male-male aggression in mice deficient for TRP2.* Science, 2002. **295**(5559): p. 1493-500.

107. Leypold, B.G., Yu, C.R., Leinders-Zufall, T., Kim, M.M., Zufall, F., and Axel, R., *Altered sexual and social behaviors in trp2 mutant mice.* Proc Natl Acad Sci U S A, 2002. **99**(9): p. 6376-81.

108. Hartmann, J., Dragicevic, E., Adelsberger, H., Henning, H.A., Sumser, M., Abramowitz, J., et al., *TRPC3 channels are required for synaptic transmission and motor coordination.* Neuron, 2008. **59**(3): p. 392-8.

109. Tiruppathi, C., Freichel, M., Vogel, S.M., Paria, B.C., Mehta, D., Flockerzi, V., et al., *Impairment of store-operated Ca2+ entry in TRPC4(-/-) mice interferes with increase in lung microvascular permeability.* Circ Res, 2002. **91**(1): p. 70-6.

110. Riccio, A., Li, Y., Moon, J., Kim, K.S., Smith, K.S., Rudolph, U., et al., *Essential role for TRPC5 in amygdala function and fear-related behavior.* Cell, 2009. **137**(4): p. 761-72.

111.   Dietrich, A., Mederos, Y.S.M., Gollasch, M., Gross, V., Storch, U., Dubrovska, G., et al., *Increased vascular smooth muscle contractility in TRPC6-/- mice.* Mol Cell Biol, 2005. **25**(16): p. 6980-9.

112.   Winn, M.P., Conlon, P.J., Lynn, K.L., Farrington, M.K., Creazzo, T., Hawkins, A.F., et al., *A mutation in the TRPC6 cation channel causes familial focal segmental glomerulosclerosis.* Science, 2005. **308**(5729): p. 1801-4.

113.   Reiser, J., Polu, K.R., Moller, C.C., Kenlan, P., Altintas, M.M., Wei, C., et al., *TRPC6 is a glomerular slit diaphragm-associated channel required for normal renal function.* Nat Genet, 2005. **37**(7): p. 739-44.

114.   Phelan, K.D., Shwe, U.T., Abramowitz, J., Birnbaumer, L., and Zheng, F., *Critical role of canonical transient receptor potential channel 7 in initiation of seizures.* Proc Natl Acad Sci U S A, 2014. **111**(31): p. 11533-8.

115.   Morgans, C.W., Zhang, J., Jeffrey, B.G., Nelson, S.M., Burke, N.S., Duvoisin, R.M., et al., *TRPM1 is required for the depolarizing light response in retinal ON-bipolar cells.* Proc Natl Acad Sci U S A, 2009. **106**(45): p. 19174-8.

116.   Shen, Y., Heimel, J.A., Kamermans, M., Peachey, N.S., Gregg, R.G., and Nawy, S., *A transient receptor potential-like channel mediates synaptic transmission in rod bipolar cells.* J Neurosci, 2009. **29**(19): p. 6088-93.

117.   Koike, C., Obara, T., Uriu, Y., Numata, T., Sanuki, R., Miyata, K., et al., *TRPM1 is a component of the retinal ON bipolar cell transduction channel in the mGluR6 cascade.* Proc Natl Acad Sci U S A, 2010. **107**(1): p. 332-7.

118.   Li, Z., Sergouniotis, P.I., Michaelides, M., Mackay, D.S., Wright, G.A., Devery, S., et al., *Recessive mutations of the gene TRPM1 abrogate ON bipolar cell function and cause complete congenital stationary night blindness in humans.* Am J Hum Genet, 2009. **85**(5): p. 711-9.

119.   Audo, I., Kohl, S., Leroy, B.P., Munier, F.L., Guillonneau, X., Mohand-Said, S., et al., *TRPM1 is mutated in patients with autosomal-recessive complete congenital stationary night blindness.* Am J Hum Genet, 2009. **85**(5): p. 720-9.

120.   van Genderen, M.M., Bijveld, M.M., Claassen, Y.B., Florijn, R.J., Pearring, J.N., Meire, F.M., et al., *Mutations in TRPM1 are a common cause of complete congenital stationary night blindness.* Am J Hum Genet, 2009. **85**(5): p. 730-6.

121.   Nakamura, M., Sanuki, R., Yasuma, T.R., Onishi, A., Nishiguchi, K.M., Koike, C., et al., *TRPM1 mutations are associated with the complete form of congenital stationary night blindness.* Mol Vis, 2010. **16**: p. 425-37.

122.   Yamamoto, S., Shimizu, S., Kiyonaka, S., Takahashi, N., Wajima, T., Hara, Y., et al., *TRPM2-mediated Ca2+influx induces chemokine production in monocytes that aggravates inflammatory neutrophil infiltration.* Nat Med, 2008. **14**(7): p. 738-47.

123.   McQuillin, A., Bass, N.J., Kalsi, G., Lawrence, J., Puri, V., Choudhury, K., et al., *Fine mapping of a susceptibility locus for bipolar and genetically related unipolar affective disorders, to a region containing the C21ORF29 and TRPM2 genes on chromosome 21q22.3.* Mol Psychiatry, 2006. **11**(2): p. 134-42.

124.   Vriens, J., Owsianik, G., Hofmann, T., Philipp, S.E., Stab, J., Chen, X., et al., *TRPM3 is a nociceptor channel involved in the detection of noxious heat.* Neuron, 2011. **70**(3): p. 482-94.

125. Vennekens, R., Olausson, J., Meissner, M., Bloch, W., Mathar, I., Philipp, S.E., et al., *Increased IgE-dependent mast cell activation and anaphylactic responses in mice lacking the calcium-activated nonselective cation channel TRPM4.* Nat Immunol, 2007. **8**(3): p. 312-20.

126. Barbet, G., Demion, M., Moura, I.C., Serafini, N., Leger, T., Vrtovsnik, F., et al., *The calcium-activated nonselective cation channel TRPM4 is essential for the migration but not the maturation of dendritic cells.* Nat Immunol, 2008. **9**(10): p. 1148-56.

127. Gerzanich, V., Woo, S.K., Vennekens, R., Tsymbalyuk, O., Ivanova, S., Ivanov, A., et al., *De novo expression of Trpm4 initiates secondary hemorrhage in spinal cord injury.* Nat Med, 2009. **15**(2): p. 185-91.

128. Kruse, M., Schulze-Bahr, E., Corfield, V., Beckmann, A., Stallmeyer, B., Kurtbay, G., et al., *Impaired endocytosis of the ion channel TRPM4 is associated with human progressive familial heart block type I.* J Clin Invest, 2009. **119**(9): p. 2737-44.

129. Liu, H., El Zein, L., Kruse, M., Guinamard, R., Beckmann, A., Bozio, A., et al., *Gain-of-function mutations in TRPM4 cause autosomal dominant isolated cardiac conduction disease.* Circ Cardiovasc Genet, 2010. **3**(4): p. 374-85.

130. Stallmeyer, B., Zumhagen, S., Denjoy, I., Duthoit, G., Hebert, J.L., Ferrer, X., et al., *Mutational spectrum in the Ca(2+)--activated cation channel gene TRPM4 in patients with cardiac conductance disturbances.* Hum Mutat, 2012. **33**(1): p. 109-17.

131. Zhang, Y., Hoon, M.A., Chandrashekar, J., Mueller, K.L., Cook, B., Wu, D., et al., *Coding of sweet, bitter, and umami tastes: different receptor cells sharing similar signaling pathways.* Cell, 2003. **112**(3): p. 293-301.

132. Brixel, L.R., Monteilh-Zoller, M.K., Ingenbrandt, C.S., Fleig, A., Penner, R., Enklaar, T., et al., *TRPM5 regulates glucose-stimulated insulin secretion.* Pflugers Arch, 2010. **460**(1): p. 69-76.

133. Colsoul, B., Schraenen, A., Lemaire, K., Quintens, R., Van Lommel, L., Segal, A., et al., *Loss of high-frequency glucose-induced Ca2+ oscillations in pancreatic islets correlates with impaired glucose tolerance in Trpm5-/- mice.* Proc Natl Acad Sci U S A, 2010. **107**(11): p. 5208-13.

134. Walder, R.Y., Yang, B., Stokes, J.B., Kirby, P.A., Cao, X., Shi, P., et al., *Mice defective in Trpm6 show embryonic mortality and neural tube defects.* Hum Mol Genet, 2009. **18**(22): p. 4367-75.

135. Schlingmann, K.P., Weber, S., Peters, M., Niemann Nejsum, L., Vitzthum, H., Klingel, K., et al., *Hypomagnesemia with secondary hypocalcemia is caused by mutations in TRPM6, a new member of the TRPM gene family.* Nat Genet, 2002. **31**(2): p. 166-70.

136. Walder, R.Y., Landau, D., Meyer, P., Shalev, H., Tsolia, M., Borochowitz, Z., et al., *Mutation of TRPM6 causes familial hypomagnesemia with secondary hypocalcemia.* Nat Genet, 2002. **31**(2): p. 171-4.

137. Jin, J., Desai, B.N., Navarro, B., Donovan, A., Andrews, N.C., and Clapham, D.E., *Deletion of Trpm7 disrupts embryonic development and thymopoiesis without altering Mg2+ homeostasis.* Science, 2008. **322**(5902): p. 756-60.

138. Hermosura, M.C., Nayakanti, H., Dorovkov, M.V., Calderon, F.R., Ryazanov, A.G., Haymer, D.S., et al., *A TRPM7 variant shows altered sensitivity to magnesium that may contribute to the pathogenesis of two Guamanian neurodegenerative disorders.* Proc Natl Acad Sci U S A, 2005. **102**(32): p. 11510-5.

139. Bautista, D.M., Siemens, J., Glazer, J.M., Tsuruda, P.R., Basbaum, A.I., Stucky, C.L., et al., *The menthol receptor TRPM8 is the principal detector of environmental cold.* Nature, 2007. **448**(7150): p. 204-8.

140. Colburn, R.W., Lubin, M.L., Stone, D.J., Jr., Wang, Y., Lawrence, D., D'Andrea, M.R., et al., *Attenuated cold sensitivity in TRPM8 null mice.* Neuron, 2007. **54**(3): p. 379-86.

141. Dhaka, A., Murray, A.N., Mathur, J., Earley, T.J., Petrus, M.J., and Patapoutian, A., *TRPM8 is required for cold sensation in mice.* Neuron, 2007. **54**(3): p. 371-8.

142. Venugopal, B., Browning, M.F., Curcio-Morelli, C., Varro, A., Michaud, N., Nanthakumar, N., et al., *Neurologic, gastric, and opthalmologic pathologies in a murine model of mucolipidosis type IV.* Am J Hum Genet, 2007. **81**(5): p. 1070-83.

143. Bargal, R., Avidan, N., Ben-Asher, E., Olender, Z., Zeigler, M., Frumkin, A., et al., *Identification of the gene causing mucolipidosis type IV.* Nat Genet, 2000. **26**(1): p. 118-23.

144. Bach, G., Webb, M.B., Bargal, R., Zeigler, M., and Ekstein, J., *The frequency of mucolipidosis type IV in the Ashkenazi Jewish population and the identification of 3 novel MCOLN1 mutations.* Hum Mutat, 2005. **26**(6): p. 591.

145. Pennekamp, P., Karcher, C., Fischer, A., Schweickert, A., Skryabin, B., Horst, J., et al., *The ion channel polycystin-2 is required for left-right axis determination in mice.* Curr Biol, 2002. **12**(11): p. 938-43.

146. Gall, E.C., Audrezet, M.P., Meur, Y.L., Chen, J.M., and Ferec, C., *Genetics and Pathogenesis of Autosomal Dominant Polycystic Kidney Disease: Twenty Years On.* Hum Mutat, 2014.

147. Caterina, M.J., Leffler, A., Malmberg, A.B., Martin, W.J., Trafton, J., Petersen-Zeitz, K.R., et al., *Impaired nociception and pain sensation in mice lacking the capsaicin receptor.* Science, 2000. **288**(5464): p. 306-13.

148. Razavi, R., Chan, Y., Afifiyan, F.N., Liu, X.J., Wan, X., Yantha, J., et al., *TRPV1+ sensory neurons control beta cell stress and islet inflammation in autoimmune diabetes.* Cell, 2006. **127**(6): p. 1123-35.

149. Link, T.M., Park, U., Vonakis, B.M., Raben, D.M., Soloski, M.J., and Caterina, M.J., *TRPV2 has a pivotal role in macrophage particle binding and phagocytosis.* Nat Immunol, 2010. **11**(3): p. 232-9.

150. Moqrich, A., Hwang, S.W., Earley, T.J., Petrus, M.J., Murray, A.N., Spencer, K.S., et al., *Impaired thermosensation in mice lacking TRPV3, a heat and camphor sensor in the skin.* Science, 2005. **307**(5714): p. 1468-72.

151. Cheng, X., Jin, J., Hu, L., Shen, D., Dong, X.P., Samie, M.A., et al., *TRP channel regulates EGFR signaling in hair morphogenesis and skin barrier formation.* Cell, 2010. **141**(2): p. 331-43.

152. Lin, Z., Chen, Q., Lee, M., Cao, X., Zhang, J., Ma, D., et al., *Exome sequencing reveals mutations in TRPV3 as a cause of Olmsted syndrome.* Am J Hum Genet, 2012. **90**(3): p. 558-64.

153. Liedtke, W. and Friedman, J.M., *Abnormal osmotic regulation in trpv4-/- mice.* Proc Natl Acad Sci U S A, 2003. **100**(23): p. 13698-703.

154. Mizuno, A., Matsumoto, N., Imai, M., and Suzuki, M., *Impaired osmotic sensation in mice lacking TRPV4.* Am J Physiol Cell Physiol, 2003. **285**(1): p. C96-101.

155. Suzuki, M., Mizuno, A., Kodaira, K., and Imai, M., *Impaired pressure sensation in mice lacking TRPV4.* J Biol Chem, 2003. **278**(25): p. 22664-8.

156. Birder, L., Kullmann, F.A., Lee, H., Barrick, S., de Groat, W., Kanai, A., et al., *Activation of urothelial transient receptor potential vanilloid 4 by 4alpha-phorbol 12,13-didecanoate contributes to altered bladder reflexes in the rat.* J Pharmacol Exp Ther, 2007. **323**(1): p. 227-35.

157. Gevaert, T., Vriens, J., Segal, A., Everaerts, W., Roskams, T., Talavera, K., et al., *Deletion of the transient receptor potential cation channel TRPV4 impairs murine bladder voiding.* J Clin Invest, 2007. **117**(11): p. 3453-62.

158. Tabuchi, K., Suzuki, M., Mizuno, A., and Hara, A., *Hearing impairment in TRPV4 knockout mice.* Neurosci Lett, 2005. **382**(3): p. 304-8.

159. Rock, M.J., Prenen, J., Funari, V.A., Funari, T.L., Merriman, B., Nelson, S.F., et al., *Gain-of-function mutations in TRPV4 cause autosomal dominant brachyolmia.* Nat Genet, 2008. **40**(8): p. 999-1003.

160. Nishimura, G., Dai, J., Lausch, E., Unger, S., Megarbane, A., Kitoh, H., et al., *Spondylo-epiphyseal dysplasia, Maroteaux type (pseudo-Morquio syndrome type 2), and parastremmatic dysplasia are caused by TRPV4 mutations.* Am J Med Genet A, 2010. **152A**(6): p. 1443-9.

161. Krakow, D., Vriens, J., Camacho, N., Luong, P., Deixler, H., Funari, T.L., et al., *Mutations in the gene encoding the calcium-permeable ion channel TRPV4 produce spondylometaphyseal dysplasia, Kozlowski type and metatropic dysplasia.* Am J Hum Genet, 2009. **84**(3): p. 307-15.

162. Amor, D.J., Tudball, C., Gardner, R.J., Lamande, S.R., Bateman, J.F., and Savarirayan, R., *Familial digital arthropathy-brachydactyly.* Am J Med Genet, 2002. **108**(3): p. 235-40.

163. Lamande, S.R., Yuan, Y., Gresshoff, I.L., Rowley, L., Belluoccio, D., Kaluarachchi, K., et al., *Mutations in TRPV4 cause an inherited arthropathy of hands and feet.* Nat Genet, 2011. **43**(11): p. 1142-6.

164. Auer-Grumbach, M., Olschewski, A., Papic, L., Kremer, H., McEntagart, M.E., Uhrig, S., et al., *Alterations in the ankyrin domain of TRPV4 cause congenital distal SMA, scapuloperoneal SMA and HMSN2C.* Nat Genet, 2010. **42**(2): p. 160-4.

165. Deng, H.X., Klein, C.J., Yan, J., Shi, Y., Wu, Y., Fecto, F., et al., *Scapuloperoneal spinal muscular atrophy and CMT2C are allelic disorders caused by alterations in TRPV4.* Nat Genet, 2010. **42**(2): p. 165-9.

166. Landoure, G., Zdebik, A.A., Martinez, T.L., Burnett, B.G., Stanescu, H.C., Inada, H., et al., *Mutations in TRPV4 cause Charcot-Marie-Tooth disease type 2C.* Nat Genet, 2010. **42**(2): p. 170-4.

167. Klein, C.J., Shi, Y., Fecto, F., Donaghy, M., Nicholson, G., McEntagart, M.E., et al., *TRPV4 mutations and cytotoxic hypercalcemia in axonal Charcot-Marie-Tooth neuropathies.* Neurology, 2011. **76**(10): p. 887-94.

168. Tian, W., Fu, Y., Garcia-Elias, A., Fernandez-Fernandez, J.M., Vicente, R., Kramer, P.L., et al., *A loss-of-function nonsynonymous polymorphism in the osmoregulatory TRPV4 gene is associated with human hyponatremia.* Proc Natl Acad Sci U S A, 2009. **106**(33): p. 14034-9.

169. Hoenderop, J.G., van Leeuwen, J.P., van der Eerden, B.C., Kersten, F.F., van der Kemp, A.W., Merillat, A.M., et al., *Renal Ca2+ wasting, hyperabsorption, and reduced bone thickness in mice lacking TRPV5.* J Clin Invest, 2003. **112**(12): p. 1906-14.

170. van der Eerden, B.C., Hoenderop, J.G., de Vries, T.J., Schoenmaker, T., Buurman, C.J., Uitterlinden, A.G., et al., *The epithelial Ca2+ channel TRPV5 is essential for proper osteoclastic bone resorption.* Proc Natl Acad Sci U S A, 2005. **102**(48): p. 17507-12.

171. Bianco, S.D., Peng, J.B., Takanaga, H., Suzuki, Y., Crescenzi, A., Kos, C.H., et al., *Marked disturbance of calcium homeostasis in mice with targeted disruption of the Trpv6 calcium channel gene.* J Bone Miner Res, 2007. **22**(2): p. 274-85.

172. Benn, B.S., Ajibade, D., Porta, A., Dhawan, P., Hediger, M., Peng, J.B., et al., *Active intestinal calcium transport in the absence of transient receptor potential vanilloid type 6 and calbindin-D9k.* Endocrinology, 2008. **149**(6): p. 3196-205.

173. Wes, P.D., Chevesich, J., Jeromin, A., Rosenberg, C., Stetten, G., and Montell, C., *TRPC1, a human homolog of a Drosophila store-operated channel.* Proc Natl Acad Sci U S A, 1995. **92**(21): p. 9652-6.

174. Story, G.M., Peier, A.M., Reeve, A.J., Eid, S.R., Mosbacher, J., Hricik, T.R., et al., *ANKTM1, a TRP-like channel expressed in nociceptive neurons, is activated by cold temperatures.* Cell, 2003. **112**(6): p. 819-29.

175. Nagata, K., Duggan, A., Kumar, G., and Garcia-Anoveros, J., *Nociceptor and hair cell transducer properties of TRPA1, a channel for pain and hearing.* J Neurosci, 2005. **25**(16): p. 4052-61.

176. Nassenstein, C., Kwong, K., Taylor-Clark, T., Kollarik, M., Macglashan, D.M., Braun, A., et al., *Expression and function of the ion channel TRPA1 in vagal afferent nerves innervating mouse lungs.* J Physiol, 2008. **586**(6): p. 1595-604.

177. Corey, D.P., Garcia-Anoveros, J., Holt, J.R., Kwan, K.Y., Lin, S.Y., Vollrath, M.A., et al., *TRPA1 is a candidate for the mechanosensitive transduction channel of vertebrate hair cells.* Nature, 2004. **432**(7018): p. 723-30.

178. Nagatomo, K. and Kubo, Y., *Caffeine activates mouse TRPA1 channels but suppresses human TRPA1 channels.* Proc Natl Acad Sci U S A, 2008. **105**(45): p. 17373-8.

179. Nozawa, K., Kawabata-Shoda, E., Doihara, H., Kojima, R., Okada, H., Mochizuki, S., et al., *TRPA1 regulates gastrointestinal motility through serotonin release from enterochromaffin cells.* Proc Natl Acad Sci U S A, 2009. **106**(9): p. 3408-13.

180. Kwan, K.Y., Glazer, J.M., Corey, D.P., Rice, F.L., and Stucky, C.L., *TRPA1 modulates mechanotransduction in cutaneous sensory neurons.* J Neurosci, 2009. **29**(15): p. 4808-19.

181. Nassini, R., Pedretti, P., Moretto, N., Fusi, C., Carnini, C., Facchinetti, F., et al., *Transient receptor potential ankyrin 1 channel localized to non-neuronal airway cells promotes non-neurogenic inflammation.* PLoS One, 2012. **7**(8): p. e42454.

182. Kono, T., Kaneko, A., Omiya, Y., Ohbuchi, K., Ohno, N., and Yamamoto, M., *Epithelial transient receptor potential ankyrin 1 (TRPA1)-dependent adrenomedullin upregulates blood flow in rat small intestine.* Am J Physiol Gastrointest Liver Physiol, 2013. **304**(4): p. G428-36.

183. Streng, T., Axelsson, H.E., Hedlund, P., Andersson, D.A., Jordt, S.E., Bevan, S., et al., *Distribution and function of the hydrogen sulfide-sensitive TRPA1 ion channel in rat urinary bladder.* Eur Urol, 2008. **53**(2): p. 391-9.

184. Earley, S., Gonzales, A.L., and Crnich, R., *Endothelium-dependent cerebral artery dilation mediated by TRPA1 and Ca2+-Activated K+ channels.* Circ Res, 2009. **104**(8): p. 987-94.

185. Cao, D.S., Zhong, L., Hsieh, T.H., Abooj, M., Bishnoi, M., Hughes, L., et al., *Expression of transient receptor potential ankyrin 1 (TRPA1) and its role in insulin release from rat pancreatic beta cells.* PLoS One, 2012. **7**(5): p. e38005.

186. Jaquemar, D., Schenker, T., and Trueb, B., *An ankyrin-like protein with transmembrane domains is specifically lost after oncogenic transformation of human fibroblasts.* J Biol Chem, 1999. **274**(11): p. 7325-33.

187. Stokes, A., Wakano, C., Koblan-Huberson, M., Adra, C.N., Fleig, A., and Turner, H., *TRPA1 is a substrate for de-ubiquitination by the tumor suppressor CYLD.* Cell Signal, 2006. **18**(10): p. 1584-94.

188. Bellono, N.W., Kammel, L.G., Zimmerman, A.L., and Oancea, E., *UV light phototransduction activates transient receptor potential A1 ion channels in human melanocytes.* Proc Natl Acad Sci U S A, 2013. **110**(6): p. 2383-8.

189. Atoyan, R., Shander, D., and Botchkareva, N.V., *Non-neuronal expression of transient receptor potential type A1 (TRPA1) in human skin.* J Invest Dermatol, 2009. **129**(9): p. 2312-5.

190. Gratzke, C., Streng, T., Waldkirch, E., Sigl, K., Stief, C., Andersson, K.E., et al., *Transient receptor potential A1 (TRPA1) activity in the human urethra--evidence for a functional role for TRPA1 in the outflow region.* Eur Urol, 2009. **55**(3): p. 696-704.

191. Liu, B.F., L.; Nilius, B.; Owsianik, G.; Jordt, S. E.; Clapham, D. E., *Transient Receptor Potential channels: TRPA1.* IUPHAR/BPS Guide to PHARMACOLOGY, 2014. **http://www.guidetopharmacology.org/GRAC/ObjectDisplayForward?objectId=485**.

192. Fischer, M.J., Balasuriya, D., Jeggle, P., Goetze, T.A., McNaughton, P.A., Reeh, P.W., et al., *Direct evidence for functional TRPV1/TRPA1 heteromers.* Pflugers Arch, 2014.

193. Staruschenko, A., Jeske, N.A., and Akopian, A.N., *Contribution of TRPV1-TRPA1 interaction to the single channel properties of the TRPA1 channel.* J Biol Chem, 2010. **285**(20): p. 15167-77.

194. Doerner, J.F., Gisselmann, G., Hatt, H., and Wetzel, C.H., *Transient receptor potential channel A1 is directly gated by calcium ions.* J Biol Chem, 2007. **282**(18): p. 13180-9.

195. Gaudet, R., *A primer on ankyrin repeat function in TRP channels and beyond.* Mol Biosyst, 2008. **4**(5): p. 372-9.

196. Howard, J. and Bechstedt, S., *Hypothesis: a helix of ankyrin repeats of the NOMPC-TRP ion channel is the gating spring of mechanoreceptors.* Curr Biol, 2004. **14**(6): p. R224-6.

197. Mosavi, L.K., Cammett, T.J., Desrosiers, D.C., and Peng, Z.Y., *The ankyrin repeat as molecular architecture for protein recognition.* Protein Sci, 2004. **13**(6): p. 1435-48.

198. Chen, J., Kim, D., Bianchi, B.R., Cavanaugh, E.J., Faltynek, C.R., Kym, P.R., et al., *Pore dilation occurs in TRPA1 but not in TRPM8 channels.* Mol Pain, 2009. **5**: p. 3.

199. Hu, H., Bandell, M., Petrus, M.J., Zhu, M.X., and Patapoutian, A., *Zinc activates damage-sensing TRPA1 ion channels.* Nat Chem Biol, 2009. **5**(3): p. 183-90.

200. Samad, A., Sura, L., Benedikt, J., Ettrich, R., Minofar, B., Teisinger, J., et al., *The C-terminal basic residues contribute to the chemical- and voltage-dependent activation of TRPA1.* Biochem J, 2011. **433**(1): p. 197-204.

201. Macpherson, L.J., Dubin, A.E., Evans, M.J., Marr, F., Schultz, P.G., Cravatt, B.F., et al., *Noxious compounds activate TRPA1 ion channels through covalent modification of cysteines.* Nature, 2007. **445**(7127): p. 541-5.

202. Hinman, A., Chuang, H.H., Bautista, D.M., and Julius, D., *TRP channel activation by reversible covalent modification.* Proc Natl Acad Sci U S A, 2006. **103**(51): p. 19564-8.

203. Koivisto, A., *Sustained TRPA1 activation in vivo.* Acta Physiol (Oxf), 2012. **204**(2): p. 248-54.

204. Taylor-Clark, T.E., Undem, B.J., Macglashan, D.W., Jr., Ghatta, S., Carr, M.J., and McAlexander, M.A., *Prostaglandin-induced activation of nociceptive neurons via direct interaction with transient receptor potential A1 (TRPA1).* Mol Pharmacol, 2008. **73**(2): p. 274-81.

205. Komatsu, T., Uchida, K., Fujita, F., Zhou, Y., and Tominaga, M., *Primary alcohols activate human TRPA1 channel in a carbon chain length-dependent manner.* Pflugers Arch, 2012. **463**(4): p. 549-59.

206. Matta, J.A., Cornett, P.M., Miyares, R.L., Abe, K., Sahibzada, N., and Ahern, G.P., *General anesthetics activate a nociceptive ion channel to enhance pain and inflammation.* Proc Natl Acad Sci U S A, 2008. **105**(25): p. 8784-9.

207. Andersson, D.A., Gentry, C., Moss, S., and Bevan, S., *Transient receptor potential A1 is a sensory receptor for multiple products of oxidative stress.* J Neurosci, 2008. **28**(10): p. 2485-94.

208. Hu, H., Tian, J., Zhu, Y., Wang, C., Xiao, R., Herz, J.M., et al., *Activation of TRPA1 channels by fenamate nonsteroidal anti-inflammatory drugs.* Pflugers Arch, 2010. **459**(4): p. 579-92.

209. Taylor-Clark, T.E., McAlexander, M.A., Nassenstein, C., Sheardown, S.A., Wilson, S., Thornton, J., et al., *Relative contributions of TRPA1 and TRPV1 channels in the activation of vagal bronchopulmonary C-fibres by the endogenous autacoid 4-oxononenal.* J Physiol, 2008. **586**(14): p. 3447-59.

210. Trevisani, M., Siemens, J., Materazzi, S., Bautista, D.M., Nassini, R., Campi, B., et al., *4-Hydroxynonenal, an endogenous aldehyde, causes pain and neurogenic*

inflammation through activation of the irritant receptor TRPA1. Proc Natl Acad Sci U S A, 2007. **104**(33): p. 13519-24.

211. Macpherson, L.J., Xiao, B., Kwan, K.Y., Petrus, M.J., Dubin, A.E., Hwang, S., et al., *An ion channel essential for sensing chemical damage.* J Neurosci, 2007. **27**(42): p. 11412-5.

212. Bandell, M., Story, G.M., Hwang, S.W., Viswanath, V., Eid, S.R., Petrus, M.J., et al., *Noxious cold ion channel TRPA1 is activated by pungent compounds and bradykinin.* Neuron, 2004. **41**(6): p. 849-57.

213. Bang, S., Kim, K.Y., Yoo, S., Kim, Y.G., and Hwang, S.W., *Transient receptor potential A1 mediates acetaldehyde-evoked pain sensation.* Eur J Neurosci, 2007. **26**(9): p. 2516-23.

214. Andre, E., Campi, B., Materazzi, S., Trevisani, M., Amadesi, S., Massi, D., et al., *Cigarette smoke-induced neurogenic inflammation is mediated by alpha,beta-unsaturated aldehydes and the TRPA1 receptor in rodents.* J Clin Invest, 2008. **118**(7): p. 2574-82.

215. Jordt, S.E., Bautista, D.M., Chuang, H.H., McKemy, D.D., Zygmunt, P.M., Hogestatt, E.D., et al., *Mustard oils and cannabinoids excite sensory nerve fibres through the TRP channel ANKTM1.* Nature, 2004. **427**(6971): p. 260-5.

216. Bautista, D.M., Movahed, P., Hinman, A., Axelsson, H.E., Sterner, O., Hogestatt, E.D., et al., *Pungent products from garlic activate the sensory ion channel TRPA1.* Proc Natl Acad Sci U S A, 2005. **102**(34): p. 12248-52.

217. Zurborg, S., Yurgionas, B., Jira, J.A., Caspani, O., and Heppenstall, P.A., *Direct activation of the ion channel TRPA1 by Ca2+.* Nat Neurosci, 2007. **10**(3): p. 277-9.

218. Xu, H., Delling, M., Jun, J.C., and Clapham, D.E., *Oregano, thyme and clove-derived flavors and skin sensitizers activate specific TRP channels.* Nat Neurosci, 2006. **9**(5): p. 628-35.

219. Andersson, D.A., Gentry, C., Moss, S., and Bevan, S., *Clioquinol and pyrithione activate TRPA1 by increasing intracellular Zn2+.* Proc Natl Acad Sci U S A, 2009. **106**(20): p. 8374-9.

220. Eilers, H., Cattaruzza, F., Nassini, R., Materazzi, S., Andre, E., Chu, C., et al., *Pungent general anesthetics activate transient receptor potential-A1 to produce hyperalgesia and neurogenic bronchoconstriction.* Anesthesiology, 2010. **112**(6): p. 1452-63.

221. Takahashi, N., Kuwaki, T., Kiyonaka, S., Numata, T., Kozai, D., Mizuno, Y., et al., *TRPA1 underlies a sensing mechanism for O2.* Nat Chem Biol, 2011. **7**(10): p. 701-11.

222. de la Roche, J., Eberhardt, M.J., Klinger, A.B., Stanslowsky, N., Wegner, F., Koppert, W., et al., *The molecular basis for species-specific activation of human TRPA1 protein by protons involves poorly conserved residues within transmembrane domains 5 and 6.* J Biol Chem, 2013. **288**(28): p. 20280-92.

223. Takahashi, N., Mizuno, Y., Kozai, D., Yamamoto, S., Kiyonaka, S., Shibata, T., et al., *Molecular characterization of TRPA1 channel activation by cysteine-reactive inflammatory mediators.* Channels (Austin), 2008. **2**(4): p. 287-98.

224. Wehage, E., Eisfeld, J., Heiner, I., Jungling, E., Zitt, C., and Luckhoff, A., *Activation of the cation channel long transient receptor potential channel 2*

(LTRPC2) by hydrogen peroxide. A splice variant reveals a mode of activation independent of ADP-ribose. J Biol Chem, 2002. **277**(26): p. 23150-6.

225. Bessac, B.F., Sivula, M., von Hehn, C.A., Escalera, J., Cohn, L., and Jordt, S.E., *TRPA1 is a major oxidant sensor in murine airway sensory neurons.* J Clin Invest, 2008. **118**(5): p. 1899-910.

226. Leffler, A., Lattrell, A., Kronewald, S., Niedermirtl, F., and Nau, C., *Activation of TRPA1 by membrane permeable local anesthetics.* Mol Pain, 2011. **7**: p. 62.

227. Karashima, Y., Damann, N., Prenen, J., Talavera, K., Segal, A., Voets, T., et al., *Bimodal action of menthol on the transient receptor potential channel TRPA1.* J Neurosci, 2007. **27**(37): p. 9874-84.

228. Xiao, B., Dubin, A.E., Bursulaya, B., Viswanath, V., Jegla, T.J., and Patapoutian, A., *Identification of transmembrane domain 5 as a critical molecular determinant of menthol sensitivity in mammalian TRPA1 channels.* J Neurosci, 2008. **28**(39): p. 9640-51.

229. Fujita, F., Moriyama, T., Higashi, T., Shima, A., and Tominaga, M., *Methyl p-hydroxybenzoate causes pain sensation through activation of TRPA1 channels.* Br J Pharmacol, 2007. **151**(1): p. 153-60.

230. Talavera, K., Gees, M., Karashima, Y., Meseguer, V.M., Vanoirbeek, J.A., Damann, N., et al., *Nicotine activates the chemosensory cation channel TRPA1.* Nat Neurosci, 2009. **12**(10): p. 1293-9.

231. Taylor-Clark, T.E., Ghatta, S., Bettner, W., and Undem, B.J., *Nitrooleic acid, an endogenous product of nitrative stress, activates nociceptive sensory nerves via the direct activation of TRPA1.* Mol Pharmacol, 2009. **75**(4): p. 820-9.

232. Taylor-Clark, T.E., Kiros, F., Carr, M.J., and McAlexander, M.A., *Transient receptor potential ankyrin 1 mediates toluene diisocyanate-evoked respiratory irritation.* Am J Respir Cell Mol Biol, 2009. **40**(6): p. 756-62.

233. Nassini, R., Materazzi, S., Vriens, J., Prenen, J., Benemei, S., De Siena, G., et al., *The 'headache tree' via umbellulone and TRPA1 activates the trigeminovascular system.* Brain, 2012. **135**(Pt 2): p. 376-90.

234. Wan, X., Lu, Y., Chen, X., Xiong, J., Zhou, Y., Li, P., et al., *Bimodal voltage dependence of TRPA1: mutations of a key pore helix residue reveal strong intrinsic voltage-dependent inactivation.* Pflugers Arch, 2014. **466**(7): p. 1273-87.

235. Wang, Y.Y., Chang, R.B., Waters, H.N., McKemy, D.D., and Liman, E.R., *The nociceptor ion channel TRPA1 is potentiated and inactivated by permeating calcium ions.* J Biol Chem, 2008. **283**(47): p. 32691-703.

236. Wang, L., Cvetkov, T.L., Chance, M.R., and Moiseenkova-Bell, V.Y., *Identification of in vivo disulfide conformation of TRPA1 ion channel.* J Biol Chem, 2012. **287**(9): p. 6169-76.

237. Facchinetti, F., Amadei, F., Geppetti, P., Tarantini, F., Di Serio, C., Dragotto, A., et al., *Alpha,beta-unsaturated aldehydes in cigarette smoke release inflammatory mediators from human macrophages.* Am J Respir Cell Mol Biol, 2007. **37**(5): p. 617-23.

238. Reid, G., *ThermoTRP channels and cold sensing: what are they really up to?* Pflugers Arch, 2005. **451**(1): p. 250-63.

239. Sawada, Y., Hosokawa, H., Hori, A., Matsumura, K., and Kobayashi, S., *Cold sensitivity of recombinant TRPA1 channels.* Brain Res, 2007. **1160**: p. 39-46.

240. Munns, C., AlQatari, M., and Koltzenburg, M., *Many cold sensitive peripheral neurons of the mouse do not express TRPM8 or TRPA1.* Cell Calcium, 2007. **41**(4): p. 331-42.

241. del Camino, D., Murphy, S., Heiry, M., Barrett, L.B., Earley, T.J., Cook, C.A., et al., *TRPA1 contributes to cold hypersensitivity.* J Neurosci, 2010. **30**(45): p. 15165-74.

242. Namer, B., Seifert, F., Handwerker, H.O., and Maihofner, C., *TRPA1 and TRPM8 activation in humans: effects of cinnamaldehyde and menthol.* Neuroreport, 2005. **16**(9): p. 955-9.

243. Chen, J., Kang, D., Xu, J., Lake, M., Hogan, J.O., Sun, C., et al., *Species differences and molecular determinant of TRPA1 cold sensitivity.* Nat Commun, 2013. **4**: p. 2501.

244. Kwan, K.Y. and Corey, D.P., *Burning cold: involvement of TRPA1 in noxious cold sensation.* J Gen Physiol, 2009. **133**(3): p. 251-6.

245. Caspani, O. and Heppenstall, P.A., *TRPA1 and cold transduction: an unresolved issue?* J Gen Physiol, 2009. **133**(3): p. 245-9.

246. Dall'Acqua, M.C., Bonet, I.J., Zampronio, A.R., Tambeli, C.H., Parada, C.A., and Fischer, L., *The contribution of transient receptor potential ankyrin 1 (TRPA1) to the in vivo nociceptive effects of prostaglandin E(2).* Life Sci, 2014. **105**(1-2): p. 7-13.

247. Mascia, M.P., Trudell, J.R., and Harris, R.A., *Specific binding sites for alcohols and anesthetics on ligand-gated ion channels.* Proc Natl Acad Sci U S A, 2000. **97**(16): p. 9305-10.

248. Nagatomo, K., Ishii, H., Yamamoto, T., Nakajo, K., and Kubo, Y., *The Met268Pro mutation of mouse TRPA1 changes the effect of caffeine from activation to suppression.* Biophys J, 2010. **99**(11): p. 3609-18.

249. Wang, Y.Y., Chang, R.B., Allgood, S.D., Silver, W.L., and Liman, E.R., *A TRPA1-dependent mechanism for the pungent sensation of weak acids.* J Gen Physiol, 2011. **137**(6): p. 493-505.

250. Weng, Y., Batista-Schepman, P.A., Barabas, M.E., Harris, E.Q., Dinsmore, T.B., Kossyreva, E.A., et al., *Prostaglandin metabolite induces inhibition of TRPA1 and channel-dependent nociception.* Mol Pain, 2012. **8**: p. 75.

251. Miyamoto, T., Dubin, A.E., Petrus, M.J., and Patapoutian, A., *TRPV1 and TRPA1 mediate peripheral nitric oxide-induced nociception in mice.* PLoS One, 2009. **4**(10): p. e7596.

252. Satoh, J. and Yamakage, M., *Desflurane induces airway contraction mainly by activating transient receptor potential A1 of sensory C-fibers.* J Anesth, 2009. **23**(4): p. 620-3.

253. Ghilarducci, D.P. and Tjeerdema, R.S., *Fate and effects of acrolein.* Rev Environ Contam Toxicol, 1995. **144**: p. 95-146.

254. Caceres, A.I., Brackmann, M., Elia, M.D., Bessac, B.F., del Camino, D., D'Amours, M., et al., *A sensory neuronal ion channel essential for airway inflammation and hyperreactivity in asthma.* Proc Natl Acad Sci U S A, 2009. **106**(22): p. 9099-104.

255. Christianson, J.A., Bielefeldt, K., Malin, S.A., and Davis, B.M., *Neonatal colon insult alters growth factor expression and TRPA1 responses in adult mice.* Pain, 2010. **151**(2): p. 540-9.

256. Brierley, S.M., Hughes, P.A., Page, A.J., Kwan, K.Y., Martin, C.M., O'Donnell, T.A., et al., *The ion channel TRPA1 is required for normal mechanosensation and is modulated by algesic stimuli.* Gastroenterology, 2009. **137**(6): p. 2084-2095 e3.

257. Cattaruzza, F., Spreadbury, I., Miranda-Morales, M., Grady, E.F., Vanner, S., and Bunnett, N.W., *Transient receptor potential ankyrin-1 has a major role in mediating visceral pain in mice.* Am J Physiol Gastrointest Liver Physiol, 2010. **298**(1): p. G81-91.

258. Yang, J., Li, Y., Zuo, X., Zhen, Y., Yu, Y., and Gao, L., *Transient receptor potential ankyrin-1 participates in visceral hyperalgesia following experimental colitis.* Neurosci Lett, 2008. **440**(3): p. 237-41.

259. Moossavi, S., Zhang, H., Sun, J., and Rezaei, N., *Host-microbiota interaction and intestinal stem cells in chronic inflammation and colorectal cancer.* Expert Rev Clin Immunol, 2013. **9**(5): p. 409-22.

260. Kennedy, P.J., Cryan, J.F., Dinan, T.G., and Clarke, G., *Irritable bowel syndrome: A microbiome-gut-brain axis disorder?* World J Gastroenterol, 2014. **20**(39): p. 14105-14125.

261. Engel, M.A., Leffler, A., Niedermirtl, F., Babes, A., Zimmermann, K., Filipovic, M.R., et al., *TRPA1 and substance P mediate colitis in mice.* Gastroenterology, 2011. **141**(4): p. 1346-58.

262. Kun, J., Szitter, I., Kemeny, A., Perkecz, A., Kereskai, L., Pohoczky, K., et al., *Upregulation of the transient receptor potential ankyrin 1 ion channel in the inflamed human and mouse colon and its protective roles.* PLoS One, 2014. **9**(9): p. e108164.

263. Bessac, B.F. and Jordt, S.E., *Breathtaking TRP channels: TRPA1 and TRPV1 in airway chemosensation and reflex control.* Physiology (Bethesda), 2008. **23**: p. 360-70.

264. Geppetti, P., Patacchini, R., Nassini, R., and Materazzi, S., *Cough: The Emerging Role of the TRPA1 Channel.* Lung, 2010. **188 Suppl 1**: p. S63-8.

265. Bautista, D.M., Pellegrino, M., and Tsunozaki, M., *TRPA1: A gatekeeper for inflammation.* Annu Rev Physiol, 2013. **75**: p. 181-200.

266. Nassini, R., Materazzi, S., Benemei, S., and Geppetti, P., *The TRPA1 Channel in Inflammatory and Neuropathic Pain and Migraine.* Rev Physiol Biochem Pharmacol, 2014.

267. Akopian, A.N., *Regulation of nociceptive transmission at the periphery via TRPA1-TRPV1 interactions.* Curr Pharm Biotechnol, 2011. **12**(1): p. 89-94.

268. Akopian, A.N., Ruparel, N.B., Jeske, N.A., and Hargreaves, K.M., *Transient receptor potential TRPA1 channel desensitization in sensory neurons is agonist dependent and regulated by TRPV1-directed internalization.* J Physiol, 2007. **583**(Pt 1): p. 175-93.

269. Spahn, V., Stein, C., and Zollner, C., *Modulation of transient receptor vanilloid 1 activity by transient receptor potential ankyrin 1.* Mol Pharmacol, 2014. **85**(2): p. 335-44.

270. Akopian, A.N., Ruparel, N.B., Patwardhan, A., and Hargreaves, K.M., *Cannabinoids desensitize capsaicin and mustard oil responses in sensory neurons via TRPA1 activation.* J Neurosci, 2008. **28**(5): p. 1064-75.

271. Patil, M.J., Jeske, N.A., and Akopian, A.N., *Transient receptor potential V1 regulates activation and modulation of transient receptor potential A1 by Ca2+.* Neuroscience, 2010. **171**(4): p. 1109-19.

272. Chen, Y., Yang, C., and Wang, Z.J., *Proteinase-activated receptor 2 sensitizes transient receptor potential vanilloid 1, transient receptor potential vanilloid 4, and transient receptor potential ankyrin 1 in paclitaxel-induced neuropathic pain.* Neuroscience, 2011. **193**: p. 440-51.

273. Dai, Y., Wang, S., Tominaga, M., Yamamoto, S., Fukuoka, T., Higashi, T., et al., *Sensitization of TRPA1 by PAR2 contributes to the sensation of inflammatory pain.* J Clin Invest, 2007. **117**(7): p. 1979-87.

274. Minke, B., *The TRP channel and phospholipase C-mediated signaling.* Cell Mol Neurobiol, 2001. **21**(6): p. 629-43.

275. Wang, S., Dai, Y., Fukuoka, T., Yamanaka, H., Kobayashi, K., Obata, K., et al., *Phospholipase C and protein kinase A mediate bradykinin sensitization of TRPA1: a molecular mechanism of inflammatory pain.* Brain, 2008. **131**(Pt 5): p. 1241-51.

276. Schmidt, M., Dubin, A.E., Petrus, M.J., Earley, T.J., and Patapoutian, A., *Nociceptive signals induce trafficking of TRPA1 to the plasma membrane.* Neuron, 2009. **64**(4): p. 498-509.

277. Uematsu, S. and Akira, S., *Toll-Like receptors (TLRs) and their ligands.* Handb Exp Pharmacol, 2008(183): p. 1-20.

278. Liu, T., Xu, Z.Z., Park, C.K., Berta, T., and Ji, R.R., *Toll-like receptor 7 mediates pruritus.* Nat Neurosci, 2010. **13**(12): p. 1460-2.

279. Park, C.K., Xu, Z.Z., Berta, T., Han, Q., Chen, G., Liu, X.J., et al., *Extracellular microRNAs activate nociceptor neurons to elicit pain via TLR7 and TRPA1.* Neuron, 2014. **82**(1): p. 47-54.

280. Monastyrskaya, K., Babiychuk, E.B., and Draeger, A., *The annexins: spatial and temporal coordination of signaling events during cellular stress.* Cell Mol Life Sci, 2009. **66**(16): p. 2623-42.

281. Avenali, L., Narayanan, P., Rouwette, T., Cervellini, I., Sereda, M., Gomez-Varela, D., et al., *Annexin A2 Regulates TRPA1-Dependent Nociception.* J Neurosci, 2014. **34**(44): p. 14506-16.

282. Kimitsuki, T., Nakagawa, T., Hisashi, K., Komune, S., and Komiyama, S., *Gadolinium blocks mechano-electric transducer current in chick cochlear hair cells.* Hear Res, 1996. **101**(1-2): p. 75-80.

283. Rusch, A., Kros, C.J., and Richardson, G.P., *Block by amiloride and its derivatives of mechano-electrical transduction in outer hair cells of mouse cochlear cultures.* J Physiol, 1994. **474**(1): p. 75-86.

284. Henderson, D., Bielefeld, E.C., Harris, K.C., and Hu, B.H., *The role of oxidative stress in noise-induced hearing loss.* Ear Hear, 2006. **27**(1): p. 1-19.

285. Yamashita, D., Jiang, H.Y., Schacht, J., and Miller, J.M., *Delayed production of free radicals following noise exposure.* Brain Res, 2004. **1019**(1-2): p. 201-9.

286. Stepanyan, R.S., Indzhykulian, A.A., Velez-Ortega, A.C., Boger, E.T., Steyger, P.S., Friedman, T.B., et al., *TRPA1-mediated accumulation of aminoglycosides in mouse cochlear outer hair cells.* J Assoc Res Otolaryngol, 2011. **12**(6): p. 729-40.

287. Rasband, W.S., *ImageJ, U.S. National Institutes of Health, Bethesda, Maryland, USA.* http://imagej.nih.gov/ij/, 1997-2014.

288. Grynkiewicz, G., Poenie, M., and Tsien, R.Y., *A new generation of Ca2+ indicators with greatly improved fluorescence properties.* J Biol Chem, 1985. **260**(6): p. 3440-50.

289. Davidson, J.S. and Baumgarten, I.M., *Glycyrrhetinic acid derivatives: a novel class of inhibitors of gap-junctional intercellular communication. Structure-activity relationships.* J Pharmacol Exp Ther, 1988. **246**(3): p. 1104-7.

290. Eskandari, S., Zampighi, G.A., Leung, D.W., Wright, E.M., and Loo, D.D., *Inhibition of gap junction hemichannels by chloride channel blockers.* J Membr Biol, 2002. **185**(2): p. 93-102.

291. Harks, E.G., de Roos, A.D., Peters, P.H., de Haan, L.H., Brouwer, A., Ypey, D.L., et al., *Fenamates: a novel class of reversible gap junction blockers.* J Pharmacol Exp Ther, 2001. **298**(3): p. 1033-41.

292. Frolenkov, G.I., Kalinec, F., Tavartkiladze, G.A., and Kachar, B., *Cochlear outer hair cell bending in an external electric field.* Biophys J, 1997. **73**(3): p. 1665-72.

293. Farshori, P. and Kachar, B., *Redistribution and phosphorylation of occludin during opening and resealing of tight junctions in cultured epithelial cells.* J Membr Biol, 1999. **170**(2): p. 147-56.

294. Gorodeski, G.I., Jin, W., and Hopfer, U., *Extracellular Ca2+ directly regulates tight junctional permeability in the human cervical cell line CaSki.* Am J Physiol, 1997. **272**(2 Pt 1): p. C511-24.

295. Piazza, V., Ciubotaru, C.D., Gale, J.E., and Mammano, F., *Purinergic signalling and intercellular Ca2+ wave propagation in the organ of Corti.* Cell Calcium, 2007. **41**(1): p. 77-86.

296. Salas, M.M., Hargreaves, K.M., and Akopian, A.N., *TRPA1-mediated responses in trigeminal sensory neurons: interaction between TRPA1 and TRPV1.* Eur J Neurosci, 2009. **29**(8): p. 1568-78.

297. White, P.N., Thorne, P.R., Housley, G.D., Mockett, B., Billett, T.E., and Burnstock, G., *Quinacrine staining of marginal cells in the stria vascularis of the guinea-pig cochlea: a possible source of extracellular ATP?* Hear Res, 1995. **90**(1-2): p. 97-105.

298. Di Virgilio, F., Fasolato, C., and Steinberg, T.H., *Inhibitors of membrane transport system for organic anions block fura-2 excretion from PC12 and N2A cells.* Biochem J, 1988. **256**(3): p. 959-63.

299. Di Virgilio, F., Steinberg, T.H., and Silverstein, S.C., *Organic-anion transport inhibitors to facilitate measurement of cytosolic free Ca2+ with fura-2.* Methods Cell Biol, 1989. **31**: p. 453-62.

300. Tian, L., Hires, S.A., Mao, T., Huber, D., Chiappe, M.E., Chalasani, S.H., et al., *Imaging neural activity in worms, flies and mice with improved GCaMP calcium indicators.* Nat Methods, 2009. **6**(12): p. 875-81.

301. Palmer, A.E., Giacomello, M., Kortemme, T., Hires, S.A., Lev-Ram, V., Baker, D., et al., *Ca2+ indicators based on computationally redesigned calmodulin-peptide pairs.* Chem Biol, 2006. **13**(5): p. 521-30.

302. Woods, C., Montcouquiol, M., and Kelley, M.W., *Math1 regulates development of the sensory epithelium in the mammalian cochlea.* Nat Neurosci, 2004. **7**(12): p. 1310-8.

303. Jones, J.M., Montcouquiol, M., Dabdoub, A., Woods, C., and Kelley, M.W., *Inhibitors of differentiation and DNA binding (Ids) regulate Math1 and hair cell formation during the development of the organ of Corti.* J Neurosci, 2006. **26**(2): p. 550-8.

304. Belyantseva, I.A., *Helios Gene Gun-mediated transfection of the inner ear sensory epithelium.* Methods Mol Biol, 2009. **493**: p. 103-23.

305. Mellado Lagarde, M.M., Cox, B.C., Fang, J., Taylor, R., Forge, A., and Zuo, J., *Selective ablation of pillar and deiters' cells severely affects cochlear postnatal development and hearing in mice.* J Neurosci, 2013. **33**(4): p. 1564-76.

306. Buch, T.R., Schafer, E.A., Demmel, M.T., Boekhoff, I., Thiermann, H., Gudermann, T., et al., *Functional expression of the transient receptor potential channel TRPA1, a sensor for toxic lung inhalants, in pulmonary epithelial cells.* Chem Biol Interact, 2013. **206**(3): p. 462-71.

307. Szarama, K.B., Gavara, N., Petralia, R.S., Kelley, M.W., and Chadwick, R.S., *Cytoskeletal changes in actin and microtubules underlie the developing surface mechanical properties of sensory and supporting cells in the mouse cochlea.* Development, 2012. **139**(12): p. 2187-97.

308. Soons, J.A., Ricci, A.J., Steele, C.R., and Puria, S., *Cytoarchitecture of the Mouse Organ of Corti from Base to Apex, Determined Using In Situ Two-Photon Imaging.* J Assoc Res Otolaryngol, 2014.

309. Dai, J., Kim, O.H., Cho, T.J., Schmidt-Rimpler, M., Tonoki, H., Takikawa, K., et al., *Novel and recurrent TRPV4 mutations and their association with distinct phenotypes within the TRPV4 dysplasia family.* J Med Genet, 2010. **47**(10): p. 704-9.

310. Camacho, N., Krakow, D., Johnykutty, S., Katzman, P.J., Pepkowitz, S., Vriens, J., et al., *Dominant TRPV4 mutations in nonlethal and lethal metatropic dysplasia.* Am J Med Genet A, 2010. **152A**(5): p. 1169-77.

311. Hofmann, K.S., W., *TMbase - A database of membrane spanning proteins segments.* Biol Chem Hoppe-Seyler, 1993. **374**(1-6).

VITA

A. Catalina Vélez-Ortega

Education

Dec/2003	*Biomedical Engineer* Antioquia School of Engineering & Health Sciences Institute, Colombia Dissertation: "Design and construction of an insulin pum prototype"
Dec/2009	*Master of Science in Biology* University of Antioquia, Colombia Dissertation: "Evaluation of the T-dependent costimulation in B cells from patients with common variable immunodeficiency"
Dec/2014	*Doctor of Phylosophy in Physiology* (Dissertation defense date: Dec/3/2014) University of Kentucky, Lexington, KY Dissertation: "TRPA1 channels in cochlear supporting cells regulate hearing sensitivity after noise exposure"

Professional Experience

Jan/2003 to Jul/2003	*Visitor Scholar* Department of Chemical & Biomolecular Engineering The Ohio State University, Columbus, OH Advisor: Shang-Tian Yang, Ph.D.
Jul/2003 to Dec/2003	*Assistant Engineer* Department of Engineering and Maintenance CES Clinic, Colombia
Oct/2004 to Jun/2008	*Graduate Research Assistant* Group of Primary Immunodeficiencies University of Antioquia, Colombia Advisor: José Luis Franco, M.D., Ph.D.

Jan/2005 to   *Adjunct Profesor of English as a Second Language (ESL)*
Jun/2008   Language Center
               EAFIT University, Colombia

Jul/2008 to   *Visitor Scholar*
Jul/2009   Department of Microbiology, Immunology & Molecular Genetics
               University of Kentucky, Lexington, KY
               Advisor: Francesc Martí, Ph.D.

Aug/2009 to   *Graduate Research Assistant*
May/2010   Integrated Biomedical Sciences Rotations
               Department of Physiology & Department of Microbiology, Immunology
               & Molecular Genetics, University of Kentucky, Lexington, KY
               Advisors: Gregory I. Frolenkov, Ph.D., Karyn Esser, Ph.D. and Francesc
               Martí, Ph.D.

May/2010 to   *Graduate Research Assistant*
Dec/2014   Department of Physiology, University of Kentucky, Lexington, KY
               Advisor: Gregory I. Frolenkov, Ph.D.

May/2010 to   *Referee*
Present   Revista Ingeniería Biomédica (ISSN 1909-9762)

Awards

2007   - Jeffrey Modell Foundation Award ($500) to Poster presented at the XII Latin
         American Group for Primary Immunodeficiencies (LAGID) Meeting. Sao Paulo,
         Brazil.
         - Clinical Immunology Society (CIS) Grant (travel + housing + meal expenses
         covered) to participate in the 6th Summer School in Primary Immunodeficiency
         Diseases. Miami, FL.

2008   - Travel Award ($500) by the Clinical Immunology Society (CIS).
         - Travel Award ($200) by the Biology Department of the University of Antioquia.

2011   - Marine Biological Laboratory (MBL) Grant (tuition + housing + meal + partial
         travel expenses covered) to participate in the 3rd Summer Course in Biology of the
         Inner Ear: Experimental and Analytical Approaches. Woods Hole, MA.

2012   - Travel Award ($400) by The Graduate School of the University of Kentucky

2013   - Travel Award ($400) by The Graduate School of the University of Kentucky
         - One of the three winners at the University of Kentucky 3-Minute Thesis (3MT)

2014　- Travel Award ($300) by the Education Committee of the Biophysical Society.
　　　- Travel Award ($500) by the Association for Research in Otolaryngology (ARO).
　　　- Judge for the University of Kentucky 3MT competition for Master's students.
　　　- Travel Award ($625) by the Gordon Research Seminar in Auditory System.
　　　- Travel Award ($400) by The Graduate School of the University of Kentucky.

Professional Society Affiliations

2007-2009　　Clinical Immunology Society (CIS)

2010-Present　The Association for Research in Otolaryngology (ARO)

2011-2014　　American Association for the Advancement of Science (AAAS)

2012-Present　Biophysical Society

2013-2014　　Kentucky Physiological Society (KY-PHYS), American Physiological Society (APS) chapter

Invited Seminars

Nov/4/2007　*"CD19 deficiency in humans: A Model for the Characterization of BCR-mediated Signal Transduction in Human B cells"*. Research Seminar. 6th Summer School in Primary Immunodeficiency Diseases. Miami, FL.

Dec/14/2007　"X-*linked susceptibility to mycobacteria is caused by mutations in the NEMO impairing CD40-dependent IL-12 production"*. Short Research Seminar. 1st Update in Primary Immunodeficiencies, Minisymposium. Group of Primary Immunodeficiencies, University of Antioquia. Medellín, Colombia.

May/8/2008　*"About biomedical engineers and research"*. Invited speaker, Ignacio Escobar Mejía Symposium. Biomedical Engineering Program, Antioquia School of Engineering (EIA), Colombia.

Dec/12/2008　*"Novel mutations in a Japanese patient with CD19 deficiency"*. Short Research Seminar. 2nd Update in Primary Immunodeficiencies, Minisymposium. Group of Primary Immunodeficiencies, University of Antioquia. Medellín, Colombia.

Dec/14/2011　*"Do TRPA1-mediated responses in supporting cells protect the cochlea from noise damage?"* Research Seminar. Physiology Department Seminar Series, University of Kentucky, Lexington, KY.

Oct/4/2012 *"Studying the cellular and molecular mechanisms of hearing"*. Research Seminar. Invited speaker, Biomedical Engineering Program, Antioquia School of Engineering (EIA), Colombia.

Feb/25/2014 *"TRPA1 channels regulate cochlear amplification"*. Podium Presentation. ARO 37th Midwinter Meeting, San Diego, CA.

Jul/12/2014 *"TRPA1 channels in supporting cells regulate cochlear amplification"*. Podium Presentation. Gordon Research Seminar, Bates College, Lewiston, ME.

Published Abstracts (Poster Presentations)

1. Moncada MA, **Vélez-Ortega AC**, Hershfield M, Orrego JC, Candotti F, Olivares M, Coll Y, Patiño PJ, Franco JL. Preferential expansion of T cells in a patient with severe combined immunodeficiency (SCID) due to adenosine deaminase (ADA). 2007. XII Latin American Group for Primary Immunodeficiencies (LAGID) Meeting. Sao Paulo, Brazil. *Clinics, 62, Suppl: 2, S48.*

2. **Vélez-Ortega AC**, Rios NA, Patiño PJ, Orrego JC, Franco JL. Common variable immunodeficiecy (CVID): An update from the group of primary immunodeficiencies in Colombia. 2007. XII Latin American Group for Primary Immunodeficiencies (LAGID) Meeting. Sao Paulo, Brazil. *Clinics, 62, Suppl: 2, S48.*

3. **Vélez-Ortega AC**, Moncada MA, Muñoz S, Patiño PJ and Franco JL. Differences in T-cell dependent B cell stimulation in common variable immunodeficiency (CVID) patients and healthy controls after allogenic stimulation. 2007. XII Latin American Group for Primary Immunodeficiencies (LAGID) Meeting. Sao Paulo, Brazil. *Clinics, 62, Suppl: 2, S48.*

4. **Vélez-Ortega AC,** Moncada MA, Patiño PJ, Franco JL. Coestimulación T-dependiente en la diferenciación del linfocito B en inmunodeficiencia común variable (IDCV). 2007. VI Congreso de Alergia, Asma e Inmunología. Medellín, Colombia. *Revista de Inmunoalergia, May 2007, 100.*

5. **Vélez-Ortega A**, Cardona L, Moncada M, Franco J. Differences after heterologous T-cell dependent costimulation in B cells from common variable immunodeficiency (CVID) patients and healthy controls. 2008. Federation of Clinical Immunology Societies (FOCIS) Meeting. Boston, MA. Abst. #F.85. *Clinical Immunology, 127 (S1), S71.*

6. Franco J, Moncada M, **Vélez-Ortega A**, Orrego J. Abnormalities in peripheral blood B cells in patients with hyperimmunoglobulinemia E syndrome (HIES). 2008. Federation of Clinical Immunology Societies (FOCIS) Meeting. Boston, MA. Abst. #F.86. *Clinical Immunology, 127 (S1), S71.*

7. **Vélez-Ortega AC**, Moncada MA, Cardona LF, Muñoz S, Franco JL. Defective T-dependent costimulation of B cells in common variable immunodeficiency. 2008. XIIIth European Society for Immunodeficiencies (ESID) Meeting. 's-Hertogenbosch, The Netherlands. *Clinical and Experimental Immunology, 154 (S1), 214.*

8. Franco JL, Moncada MA, **Vélez-Ortega AC**, Gómez-Rodriguez J, Dutra AC, Muñoz S, Orrego JC, Montoya J. CD4 deficiency in a child with a congenital syndrome and recurrent infections. 2008. XIIIth European Society for Immunodeficiencies (ESID) Meeting. 's-Hertogenbosch, The Netherlands. *Clinical and Experimental Immunology, 154 (S1), 216.*

9. Ellis GI, Reneer MC, **Vélez-Ortega AC**, Norris A, Martí F. Control of human induced regulatory T cell differentiation by peroxisome proliferator activated receptor-γ through the endogenous synthesis of retinoic acid. 2010. 18th United European Gastroenterology Week (UEGW). Barcelona, Spain. *Gut, 59, Suppl: III, A23.*

10. **Vélez-Ortega AC**, Indzhykulian AA, Sinha GP, Frolenkov GI. Imaging stereocilia links in live auditory hair cells. 2012. 56th Annual Meeting of the Biophysical Society. San Diego, CA. Abst. #3326-Pos. *Biophysical Journal, 102 (3), Suppl:1, 655a.*

11. **Vélez-Ortega AC**, Belov O, Novak P, Rawashdeh SA, Sinha GP, Korchev YE, Frolenkov GI. High-Speed Hopping Probe Scanning Ion Conductance Microscopy. 58th Annual Meeting of the Biophysical Society. Abst. #4024-Pos. *Biophysical Journal, 106 (2), Suppl:1, 797a-8a.*

Other Abstracts (Poster Presentations)

1. Kermicle MC, **Vélez-Ortega AC**, Martí F. Molecular mechanisms of pheripheral Treg development. 2008. 37th Autumn Immunology Conference (AIC). Chicago, IL.

2. **Vélez-Ortega AC**, Kermicle MC, Daniel J. Estes, Michael Mayer, Martí F. Characterization of early TCR-signaling events in induced regulatory T cells. 2008. 37th Autumn Immunology Conference (AIC). Chicago, IL.

3. Kermicle MC, **Vélez-Ortega AC**, Temprano J, Martí F. Role of PPARγ in the generation of peripherally-induced human suppressor T cells. 2009. Center for Clinical and Translational Science (CCTS) Spring Conference. Lexington, KY.

4. **Vélez-Ortega AC**, Kermicle MC, Norris A, Kiefer A, Estes DJ, Mayer M, Martí F. Rewiring the cell signaling network: A molecular strategy to control the functional plasticity of T cells. 2009. Center for Clinical and Translational Science (CCTS) Spring Conference. Lexington, KY.

5. Kermicle MC, **Vélez-Ortega AC**, Norris A, Gardner T, Temprano J, Martí F. Effects of hormonal intake on regulatory T cell development. 2009. 38th Autumn Immunology Conference (AIC), Chicago, IL.

6. **Vélez-Ortega AC**, Stepanyan R, Indzhykulian A, Frolenkov GI. TRPA1-mediated damage sensing in the inner ear. 2011. Association for Research in Otolaryngology (ARO) 34th Midwinter Meeting. Baltimore, MD. Abst. #943.

7. Sinha G, **Vélez-Ortega AC**, Frolenkov G. Scanning ion conductance imaging of highly convoluted nanoscale structures at the surface of living cells: adaptive approach curve analysis. 2011. 55th Annual Meeting of Biophysical Society. Baltimore, MD. Abst. #4416.

8. Moncada-Vélez M, **Vélez AC**, Rojas J, Prando C, Marín N, Montoya JH, Gómez-Rodríguez J, Dutra A, Orrego JC, García LF, Boisson-Dupuis S, Casanova JL, Franco JL. Immunodeficiency associated to a germline mutation in the human CD4 gene. 2011. 2nd The Latin American Society for Immunodeficiencies (LASID) Meeting. Mexico City, Mexico.

9. **Vélez-Ortega AC**, Stepanyan R, Sinha GP, Frolenkov GI. Does oxidative stress generate distinct types of calcium waves in the supporting cells of the organ of Corti? 2012. Association for Research in Otolaryngology (ARO) 35th Midwinter Meeting. San Diego, CA. Abst. #141.

10. **Vélez-Ortega AC**, Indzhykulian AA, Sinha GP, Frolenkov GI. Time-lapse nanoscale imaging of stereocilia in live auditory hair cells using hopping probe scanning ion conductance microscopy. 2012. Biophysical Society Kentucky Regional Networking Meeting, Bluegrass Molecular Biophysics Networking Symposium. Lexington, KY.

11. **Vélez-Ortega AC**, Indzhykulian A, Frolenkov GI. Stereocilia tenting is present in live hair cells and involves remodeling of the actin core. 2013. Association for Research in Otolaryngology (ARO) 36th Midwinter Meeting. Baltimore, MD. Abst. #466.

12. **Vélez-Ortega AC,** Maimaiti S, Stepanyan R, Frolenkov GI. TRPA1-mediated damage sensing by the cochlear supporting cells. 2013. Kentucky Physiological Society (KY-PHYS) Inaugural Meeting, a Chapter of the American Physiological Society (APS). Lexington, KY. Abst. #30.

13. Syam D, Alexander AJ, **Velez-Ortega C,** Sinha GP, Frolenkov GI. Does Myosin-XVa deficiency result in constitutively open mechanotransduction channels? 2013. Kentucky Physiological Society (KY-PHYS) Inaugural Meeting, a Chapter of the American Physiological Society (APS). Lexington, KY. Abst. #37.

14. Syam D, Alexander AJ, **Velez-Ortega C**, Sinha GP, Frolenkov GI. Degeneration of cochlear outer hair cells in the mouse model of non-syndromic deafness DFNB3. 2013. 8th Annual Center for Clinical and Translational Science (CCTS) Spring Conference. Lexington, KY.

15. Syam D, Alexander AJ, **Velez-Ortega C**, Sinha GP, Frolenkov GI. Does sustained activation of mechanotransduction channels result in stereocilia degeneration in the mouse model of non-syndromic deafness, DFNB3? 2013. Kentucky EPSCoR Annual Conference. Louisville, KY.

16. **Vélez-Ortega AC**, Edelmann SE, Park C, Stepanyan R, Kwan KY, Sinha GP, Corey DP, Frolenkov GI. TRPA1 channels regulate cochlear amplification. Gordon Research Conference in Auditory System. 2014 in Bates College, Lewiston, ME.

Podium Presentations

1. **Vélez-Ortega AC**, Edelmann SE, Park C, Stepanyan R, Kwan KY, Sinha GP, Corey DP, Frolenkov GI. Supporting cells sense noise-induced damage via TRPA1 channels and protect the cochlea by actively changing the geometry of the organ of Corti. ARO 37th Midwinter Meeting. 2014 in San Diego, CA.

2. **Vélez-Ortega AC**, Edelmann SE, Park C, Stepanyan R, Kwan KY, Sinha GP, Corey DP, Frolenkov GI. TRPA1 channels regulate cochlear amplification. Gordon Research Seminar in Auditory System. 2014 in Bates College, Lewiston, ME.

Published Manuscripts

1. Mocada-Vélez M, **Vélez-Ortega A**, Orrego J, Santisteban I, Jagadeesh J, Olivares M, Olaya N, Hershfield M, Candotti F, Franco J. Somatic mosaicism due to monoallelic reversion of a homozygous mutation in T cells of a patient with Severe Combined Immunodeficiency due to Adenosine Deaminase Deficiency. *Scand J Immunol. 2011; 74 (5): 471-81.*

2. Reener MC, Estes DJ, **Vélez-Ortega AC**, Norris A, Mayer M, Marti F. Peripherally induced human regulatory T cells uncouple Kv1.3 activation from TCR-associated signaling. *Eur J Immunol. 2011; 41 (11): 3170-5.*

3. Stepanyan R, Indzhykulian AA, **Vélez-Ortega AC**, Boger ET, Steyger PS, Friedman TB, Frolenkov GI. TRPA1-mediated accumulation of aminoglycosides in mouse cochlear outer hair cells. *J Assoc Res Otolaryngol. 2011; 12 (60): 729-40.*

4. Ellis GI, Reneer MC, **Vélez-Ortega AC**, Norris A, Martí F. Generation of induced regulatory T cells from primary human naïve and memory T cells. *J Vis Exp. 2012; (62): e3738.*

5. **Vélez-Ortega AC***, Temprano J*, Reener MC, Norris A, Marti F. Enhanced capacity to generate suppressor T cells associated with improved asthma symptoms in patients taking oral contraceptive treatment. *J Asthma. 2013; 50(3): 223-30.*

6. **Vélez AC***, Castaño DM*, Patiño PJ, Gómez RD, Orrego JC, Moncada MA, Cardona LF, Franco JL. Common variable immunodeficiency: clinical and immunological characterization of patients and homogeneous subgroup definition by means of B lymphocyte subpopulation typing [Article in Spanish]. *Biomédica. 2015; 35(1): (in press).*

Pending Manuscripts

1. **Vélez-Ortega AC**, Stepanyan R, Edelmann SE, Park C, Kwan KY, Sinha GP, Corey DP, Frolenkov GI. TRPA1 channels in supporting cells of the inner ear regulate cochlear amplification. *(To be submitted)*

2. **Vélez-Ortega AC**, Indzhykulian AA, Frolenkov GI. Stereocilia tip remodeling in mammalian auditory hair cells. *(In preparation)*

3. **Vélez-Ortega AC**, Moncada-Vélez MA, Cardona LF, Muñoz S, Orrego JC, Franco JL. Evaluation of the T-dependent costimulation in B cells from patients with common variable immunodeficiency. *(In preparation)*